The Role of Prostate Cancer Small Extracellular Vesicles on the Bone Environment

Ben Lanning

Thesis submitted for the degree

DOCTOR OF PHILOSOPHY

Cardiff-China Medical Research Collaborative

School of Medicine
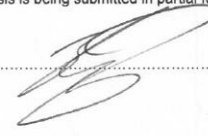
Cardiff University

January 2019

DECLARATION

This work has not been submitted in substance for any other degree or award at this or any other university or place of learning, nor is being submitted concurrently in candidature for any degree or other award.

Signed .... (candidate)   Date ... 22|3|19

STATEMENT 1

This thesis is being submitted in partial fulfillment of the requirements for the degree of PhD.

Signed .... (candidate)   Date ... 22|3|19

STATEMENT 2

This thesis is the result of my own independent work/investigation, except where otherwise stated, and the thesis has not been edited by a third party beyond what is permitted by Cardiff University's Policy on the Use of Third Party Editors by Research Degree Students. Other sources are acknowledged by explicit references. The views expressed are my own.

Signed .... (candidate)   Date ... 22|3|19

STATEMENT 3

I hereby give consent for my thesis, if accepted, to be available online in the University's Open Access repository and for inter-library loan, and for the title and summary to be made available to outside organisations.

Signed .... (candidate)   Date ... 22|3|19

STATEMENT 4: PREVIOUSLY APPROVED BAR ON ACCESS
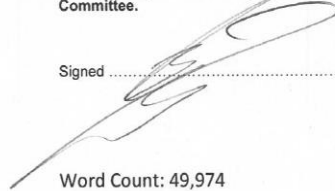
I hereby give consent for my thesis, if accepted, to be available online in the University's Open Access repository and for inter-library loans **after expiry of a bar on access previously approved by the Academic Standards & Quality Committee.**

Signed .... (candidate)   Date ... 22|3|19

Word Count: 49,974

Acknowledgements

Summary

Skeletal metastases are the most common form of secondary tumour associated with prostate cancer (PCa). Aberrant function of bone cells neighbouring these tumours leads to the development of osteolytic or osteoblastic lesions, with the latter being most commonly seen with PCa. Communication between PCa cells and bone cells at these secondary sites governs both the formation/development of the associated lesion, as well as growth of the secondary tumour.

We isolated small extracellular vesicles (sEVs), known to facilitate intercellular communication, from PC3 cells and examined their effect on cells of the bone microenvironment.

Using Next Generation Sequencing (NGS), we profiled the miRNA content of sEVs from PC3 cells, showing that miR-221-3p and miR-16-5p were highly expressed. We then showed these PC3 sEVs are able to stimulate increased differentiation of 7F2 osteoblast cells, with Ingenuity® Pathway Analysis (IPA®) revealing miR-16-5p as likely involved in this signalling.

Using the NGS data, miR-16-5p targets in 7F2 cells, possibly facilitating the increased osteoblastogenesis, were selected; AXIN2, PLSCR4, ADRB2 and DLL1. We then confirmed the targeting of these genes by sEV miR-16-5p, and subsequently developed 7F2 cell lines overexpressing them. Overexpression of PLSCR4, ADRB2 and DLL1 lead to decreased osteoblastogenesis, whereas AXIN2 overexpression lead to increased osteoblastogenesis.

We then examined the effect of PC3 sEVs on RAW 264.7 cells (osteoclast precursors), showing that the addition of PC3 sEVs decreased the osteoclastogenesis of RANKL treated RAW cells.

These results indicate that PC3 sEVs induce osteoblastogenesis and inhibit osteoclastogenesis, mirroring, and potentially partially explaining the tendency of PCa secondary tumours to produce osteoblastic lesions.

Publications and Presentations

- Non-Coding RNA Signalling in Cancer (Review) – Currently with Editor of Critical Reviews in Oncology/Haematology following peer review.

- Lanning, B. Clayton, A. Jiang, W.G. Dart, D. miRNAs in the Development of Prostate Cancer Related Bone Metastatic Lesions. Oral presentation, CUKC Beijing 2017

- Lanning, B. Clayton, A. Jiang, W.G. Dart, D. microRNAs in the Progression of Prostate Cancer - PCa Exsosomes as Mediators of Bone Remodelling. Oral presentation, Division of Cancer and Genetics Seminar, November 2017

- Lanning, B. Clayton, A. Jiang, W.G. Dart, D. Prostate Cancer Exosomes as Mediators of Bone Remodelling – Implications in Prostate Cancer Derived Bone Metastases. Oral presentation, Royal Society of Medicine Presidents Day 2017.

- Lanning, B. Dart, D. Sequencing MicroRNAs in Prostate Cancer Cell Lines: Comparing cellular and exosomal expression. Oral presentation, Next Generation Sequencing (NGS) Cyprus 2017.

- Lanning, B. Clayton, A. Jiang, W.G. Dart, D. PC3 Exosomal miR-16-5p Mediates Osteoblast Function - Implications in Prostate Cancer Derived Bone Metastases. Oral presentation, Travelling Surgical Society of Great Britain and Ireland Autumn Meeting 2018.

Abbreviations

ABX	Antibiotic antimycotic solution
ACP	Amorphous calcium phosphate
ACVR1	Activin A receptor, type I
ADAR	Adenosine deaminase acting on RNA
ADRB2	Beta-2 adrenergic receptor
ADT	Androgen deprivation therapy
Ago	Argonaute
AJCC	The American Joint Committee on Cancer
ALIX	ALG-2-interacting protein X
ALP/AP	Alkaline phosphatase
AMO	Anti-miRNA oligonucleotide
AR	Androgen receptor
ARS	Alizarin Red S
APS	Ammonium persulphate
ATCC	American Type Culture Collection
ATP	Adenosine triphosphate
BCA	Bicinchoninic acid (assay)
BCIP/NBT	5-bromo-4-chloro-3-indolyl phosphate/nitro blue tetrazolium
BLC	Bone lining cell
BMP	Bone morphogenetic protein
BMSC	Bone marrow stromal cell
BMU	Basic multicellular unit
BPH	Benign prostate hyperplasia
BSA	Bovine serum albumin
BSP	Bone sialoprotein
CAF	Chromatin assembly factor
CCR	Carbon catabolite repressed
CD	Cluster of differentiation
CFU-M	Colony forming unit-granulocyte monocyte cell
CIC	Capicua transcriptional repressor

COL1A1	Collagen Type I Alpha 1 Chain
CSDC2	Cold shock domain containing C2
CSF	Colony stimulating factor
cSRC	Proto-oncogene tyrosine-protein kinase Src
CT	Computerised tomography (scan)
CTHRC1	Collagen triple helix repeat containing 1
DC-STAMP	Dendritic cell-specific transmembrane protein
DDX5	Dead box protein 5
DEPC	Diethylpyrocarbonate
DGCR8	DiGeorge syndrome critical region gene 8
DLL1	Delta like canonical notch ligand 1
DLX5	Distal-less homeobox5
DMSO	Dimethyl sulfoxide
DNA	Deoxyribonucleic acid
DRE	Digital rectal examination
EBRT	External beam radiotherapy
EBV	Epstein-Barr virus
ECM	Extracellular matrix
EDTA	Ethylenediaminetriacetic acid
eIF4G	Eukaryotic translation initiation factor 4G
ELISA	Enzyme linked immunosorbent assay
EMT	Epithelial–mesenchymal transition
ER	Endoplasmic reticulum
ESCRT	Endosomal Sorting Complex Required for Transport
Ets	E26 transformation-specific or E-twenty-six
EV	Extracellular vesicle
FAS	Fatty acid synthase
FcR	Fc receptor
FGF	Fibroblast growth factor
FXR1	Fragile X mental retardation–related protein 1
GLD2	Germ line development 2
HA	Hydroxyapatite

HCl	Hydrochloric acid
HDL	High density lipoprotein
HDR-BT	High dose temporary interstitial brachytherapy
hFOB	Humna foetal osteoblast
HIF	Hypoxia-inducible factor
HLA	Human leukocyte antigen
hnRNP	Heterogenous nuclear ribonucleoprotein
HRP	Horseradish peroxidase
HSA	Human serum albumin
HSC	Heat shock cognate
HSP	Heat shock protein
IGF	Insulin-like growth factor
IL	Interleukin
ILV	Intraluminal vesicle
IPA	Ingenuity® Pathway Analysis
ISP	Ion Sphere™ Particle
lEV	Large Extracellular Vesicle
LB	Lysogeny broth
LFA1	Lymphocyte function associated antigen 1
LDR-BT	Low dose permanent interstitial brachytherapy
MAPK	Mitogen activated protein kinase
MCP-1	Monocyte chemoattractant protein 1
M-CSF	Macrophage colony-stimulating factor
MEM	Minimum Essential Medium
MHC	Major histocompatibility complex
miPDC	miRNA precursor deposit complex
miRNA/miR	microRNA
MITF	Melanocyte inducing transcription factor
MMP	Matrix metalloproteinase
MR(I)	Magnetic resonance (imaging)
MSC	Mesenchymal stem cell
MV	Microvesicle

MVE	Multivesicular endosome
NCP	Non-collagenous proteins
NFATc1	Nuclear factor of activated T cells, cytoplasmic, calcineurin dependent 1
NOT	Negative on TATA
NPC	Nuclear pore complexes
NSAID	Nonsteroidal anti-inflammatory drug
nSMase	Neural sphingomyelinase
NTA	Nanoparticle Tracking Analysis
OC-STAMP	Osteoclast stimulatory transmembrane protein
OCN	Osteocalcin
Oligo	Oligonucleotide
OM	Osteogenic media only
OMEV	Osteogenic media + small extracellular vesicles
ON	Osteonectin
OPN	Osteopontin
OPG	Osteoprotegrin
OSCAR	Osteoclast-associated immunoglobulin-like receptor
OSM	Oncostatin M
OSX	Osterix
P:P	Particles:Protein
PABP	Poly A binding protein
PAGE	Polyacrylamide gel electrophoresis
PBS	Phosphate buffered saline
PCa	Prostate cancer
PCR	Polymerase chain reaction
PDB	Pagets disease of bone
PDB-OS	Pagets associated osteosarcoma
PDGF	Platelet-derived growth factor
PET	Positron emission tomography
PI3K	Phosphoinositide 3 kinase
PKC	Protein kinase C
PLD	Phospholipase D

PLSCR4	Phospholipid scramblase 4
PM	Plasma membrane
pre-miRNA	Precursor microRNA
pri-miRNA	Primary microRNA
PSA	Prostate specific antigen
PTHrP	Parathyroid-hormone-related protein
PVDF	Polyvinylidene fluoride
Ran	Ras related nuclear protein
RanBP	Ran binding protein
RANKL	Receptor activator of nuclear factor kappa-B ligand
RBS	Radioisotope bone scintigraphy
RGD	Arginine-glycine-aspartic acid
RHA	RNA helicase A
RISC	RNA induced silencing complex
RLC	RISC loading complex
RNA	Ribonucleic acid
RNAi	RNA interference
RNase	Ribonuclease
ROS	Reactive Oxygen Species
RPKM	Reads per kilobase of transcript per million mapped reads
Runx2	Runt-related transcription factors 2
sEV	Small Extracellular Vesicle
S1P	Sphingosine-1-phosphate
SaOS	Sarcoma osteogenic
SATB2	Special AT-rich sequence-binding protein 2
SDS	Sodium dodecyl sulphate
SEM	Standard error of the mean
SNARE	Soluble NSF-attachment protein receptor
TBE	Tris/Borate/EDTA
TBS(T)	Tris buffered saline (Tween)
TGFβ	Transforming growth factor β
TNF	Tumour necrosis factor

TNM	Tumour, node and metastasis
TNRC6A	Trinucleotide repeat containing 6A
TRAIL	TNF related apoptosis-inducing ligand
TRAP	Tartrate-resistant acid phosphatase
TRF	Time resolved fluorescence
TRUS	Transrectal ultrasound
TSG101	Tumour susceptibility gene, protein 101
UGS	Urogenital sinus
uPA	Urokinase-type plasminogen activator
UTR	Untranslated region
VEGF	Vascular endothelial growth factor
Wnt	Wingless (signalling pathway)
XPO5	Exportin 5
XRN1	Exoribonuclease 1
β-GP	B glycerophosphate

Contents

List of Figures

List of Tables

Chapter I: General Introduction

1 <u>Introduction</u>

1.1 Prostate:

The prostate is a chestnut sized gland, belonging to the organs of the male reproductive system. The prostate surrounds the urethra immediately inferior to the bladder and is posterior in relation to the rectum, allowing its inspection rectally. The ducts of the prostate feed into the urethra, where prostatic secretions along with sperm from the testis make up roughly 1/3 of the fluid component of semen. The function of these secretions are to aid sperm survival and delivery to the ovum; for example, prostate specific antigen (PSA) thins the fluid to aid sperm motility, citrate acts as an energy substrate for sperm and zinc prevents the oxidation of citrate (Verze *et al.*, 2016).

1.1.1 Structure:

1.1.1.1 Microanatomy:

The prostate is comprised of three main cell types; exocrine glandular cells, smooth muscle cells and fibrous cells. The glandular tissues of the prostate are responsible for the production and secretion of the prostatic secretions found in semen. The fibrous component of the prostate provides support via large amounts of connective tissue, rich in dense, irregular collagen fibres. The expulsion of prostatic secretions is aided by the abundance of smooth muscle both within and around the prostate, which are strongly stimulated during ejaculation.

1.1.1.2 Zones:

The prostate is made of three zones (figure 1.1). The central lies furthest from the rectum whereas the peripheral zone is closest to the rectum and therefore is the area felt during a digital rectal examination (DRE). The transition zone lies between the central and peripheral zones and is commonly associated with an enlargement of the prostate known as benign

prostate hyperplasia (BPH). Some texts also refer to the stroma, a surrounding capsule of connective tissue and smooth muscle, as a zone of the prostate.
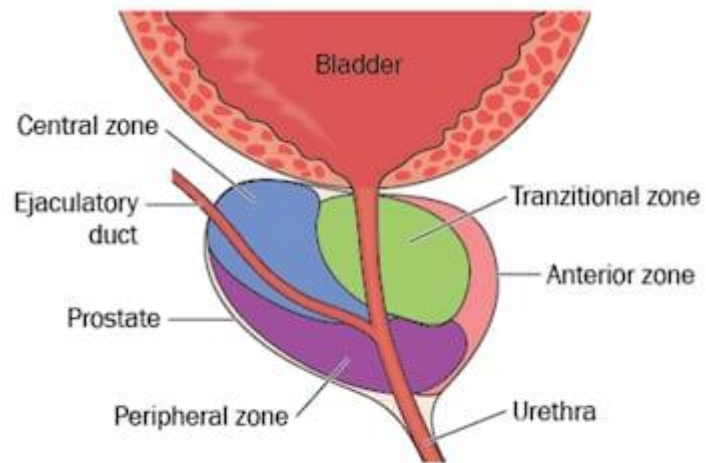
Figure 1.1: Anatomical diagram of the prostate showing distribution of the three zones: the central zone (red), the transition zone (green) and the peripheral zone (blue) (image curtesy of Shutterstock)

1.1.2 Lobes

Whilst zones are often used to describe the prostate in the context of pathology, the lobe description is often favoured in terms of anatomy. The prostate is made of 5 lobes; anterior lobe (lying in front of the urethra), median lobe (found between the two ejaculatory ducts), two lateral lobes (the lateral sections of the gland, together make up the majority of the gland) and posterior lobe (the posterior portion of the gland).

1.1.3 Prostate Morphogenesis

Prostate morphogenesis originates within the embryonic urogenital sinus (UGS), an area present during the early development of the urinary and reproductive organs. Here, interactions between the stroma and epithelia drive the development of the mature prostate gland. Androgen-dependant signals from the UGS mesenchyme guides the early prostatic epithelium to form buds from the UGS which elongate and form canals characterised by an epithelium rich in tall columnar luminal cells (Cunha *et al.*, 1983). The mesenchymal cells then form the adjacent smooth muscle, the patterning of which is determined by the interactions with the recently formed, adjacent epithelia (Hayward *et al.*, 1996).

1.1.4 Prostate Cancer

Prostate cancer (PCa) is the most common form of cancer to occur in men with around 382,000 cases in Europe a year. PCa is also the third leading cause of cancer related mortality in men behind lung and colorectal cancers (Ferlay *et al.*, 2010). Prostate cancer is unique due to its often slow growing nature and the fact it almost exclusively presents in men over 50. Over 95% of primary prostate cancers present as adenocarcinoma, with the remaining cases being rare tuours such as small cell, intralobular and ductal tumours (Nelson *et al.*, 2003). Although only 1 in 14 men will be diagnosed with prostate cancer at some point in their life, autopsy studies show that 50% of 50 year olds and 75% of 85 year olds present with prostate cancer related histological changes (Sakr *et al.*, 1993).

1.1.4.1   Symptoms

PCa symptoms are usually urinary in nature, due to the expansion of the prostate pressing on the urethra. These include difficulty urinating, urinating more frequently and the feeling that the bladder is not being fully emptied (NHS, 2014).

1.1.4.2   Risk Factors

As discussed PCa almost exclusively affects those over 50. A study by the American Cancer Society in 2007 found that incidence and mortality is higher in African-Americans compared to European Americans, and that conversely incidence is lower in Hispanic, Asian-American and Pacific Island men. Twin studies have shown that the genetic risk of PCa accounts for around 42% of total familial PCa risk (Lichtenstein *et al.*, 2000), higher than the genetic risk of any other cancer.

Lifestyle and dietary factors can also influence an individual's chances of developing PCa. Salem *et al.* (2011) found that a diet high in fat increases the chances of developing PCa whereas diets high in tomato or garlic negatively correlate with PCa risk. A review by Allott *et al.* (2013) showed that although obesity appeared to be linked to decreased incidence of PCa, it was also linked to higher incidence of aggressive PCa, PCa related death, biochemical failure following radical prostatectomy and external-beam radiotherapy and complications following androgen deprivation therapy.

Studies have also found that an increase in frequency of ejaculation, particularly between the ages of 20-30, can be linked to a decreased risk of developing prostate cancer (Giles *et al.*, 2003; Leitzmann *et al.*, 2004).

1.1.4.3   Diagnosis

Before a diagnosis can be made, biomarker levels are tested to determine a patient's likelihood of having PCa. The most frequently tested biomarker in PCa is prostate specific antigen (PSA), with a PSA level of >4ng/ml being indicative of PCa risk (Crawford & DeAntoni,

1993; Moore *et al.*, 1992; Pepe & Aragona, 2011). However PSA levels can be unreliable with an alarmingly high number of false negatives (15%) and false positives (66%) (Kang *et al.*, 2015).

A patient with a PSA level of >4ng/ml is often given a digital rectal examination (DRE), this often unpleasant procedure involves feeling the prostate via the rectum for any abnormalities in size or shape. In the early stages of prostate cancer DRE can be unreliable if tumours have originated in zones distal from the rectum i.e. the central or transition zones (Green, 1993).

If the PSA and DRE tests point towards an abnormality, a transrectal-ultrasound (TRUS) guided needle biopsy is performed. TRUS has been the guidance technique of choice since its discovery by Hodge *et al.* (1989). Again this procedure has a high false-negative rate, estimated at around 25% (Daneshgari *et al.*, 1995).

There are also a number of imaging techniques that can help in the diagnosis of PCa. TRUS has already been discussed, as a method of biopsy guidance rather than PCa imaging. TRUS can also be used to calculate the volume of the prostate for measuring PSA density (Terris & Stamey, 1991). Computerised tomography (CT) scanning has a limited role in prostate cancer, only being used in very advanced, high-grade, nodal tumours due to the fact CT scans can only pick up tumours of >1cm^3 (O'Dowd *et al.*, 1997). Magnetic resonance (MR) imaging can be effective if used at a high enough resolution, allowing the detection of PCa in zones of the prostate often missed by TRUS-biopsy such as the transition zone (Zakian *et al.*, 2003). PET scanning can also be useful in PCa, not in diagnosis of primary PCa but in the locating of bone metastases or recurrent disease (Vali *et al.*, 2015).

1.1.4.4   Staging

The most widely used staging system for prostate cancer is the The American Joint Committee on Cancer (AJCC) and International Union Against Cancer (UICC) tumour, node

and metastasis (TNM) system, where T= Primary tumour, N= Regional lymph nodes and M=

Distant metastasis (Cheng *et al.*, 2012).

1.1.4.5   Grading

PCa tumours are also given a grade based on how much of the biopsy looks like healthy or cancerous tissue. A grade of 1-5 is given, with 1 representing healthy tissue, and 5 representing the most poorly differentiated cancerous tissue. Gleason scores are given in two parts, one is the score for the largest representative area of the biopsy, and the second is for the second largest area. For example, if the largest part of the biopsy is grade 4, and the second largest is grade 3, the score is given as "4+3=7". Alternatively, these two scores can be the same.

1.1.4.6   Tumour frequency by Zone

The three zones of the prostate (see section 1.1.1.2) each have their own independent incidence of tumour development, shown in table 1.1:

Table 1.1: Frequency of prostate tumour development per zone displayed as a percentage of all tumours found in the study (Cohen *et al.*, 2008).

Zone	% of total Prostate tumours
Central	2%
Transitional	34%
Peripheral	64%

1.1.4.7   Tumour Characteristics by Zone

Tumours of the central zone have much higher rates of ejaculatory duct and seminal vesicle invasion than peripheral zone or transition zone tumours which is unsurprising given the close proximity of the central zone to these areas. Central zone tumours also displayed the highest Gleason score and were consistent with the worst outcomes with a considerably lower failure-free probability and shorter time to failure than peripheral or transitional zones. However central zone tumours are the rarest form, and failure-free survival and time to failure of peripheral and transitional zone tumours was similar (Cohen *et al.*, 2008).

1.1.4.8   Localised PCa

Localised PCa is defined as not extending beyond the capsule of the prostate (Akduman & Crawford, 2006).

1.1.4.9   Localised PCa Treatments

For low risk localised prostate cancers where the patient has a life expectancy in excess of 20 years, the primary course of action is "watchful waiting". This emphasises monitoring of the tumour with bi-annual or annual DRE and PSA testing with biopsies dependant on the results (Mohler *et al.*, 2014).

Localised PCa is relatively low risk, with the main treatment option being radical prostatectomy. This involves the complete removal of the prostate, seminal vesicles and pelvic lymph nodes. PSA should be undetectable 4-6 weeks post-surgery and levels of more than 0.2ng/mL can indicate a recurrence (Mohler *et al.*, 2014). (Bill-Axelson *et al.*, 2011) showed that radical prostatectomy can reduce "disease-specific mortality, overall mortality, and the risks of metastasis and local progression" in prostate cancer patients compared to watchful waiting. Since the discovery of the location of the cavernous nerves by Dr Patrick Walsh in 1981, nerve sparing radical prostatectomy has become common practice in order to maintain a patient's post-operative erectile function and quality of life. With the

development of nerve sparing radical prostatectomy came the concerns that this method would involve higher risks of positive surgical margins and biochemical progression. These concerns were tested by Alkhateeb *et al.* (2010) who found that in properly selected patients, the risk of positive surgical margins and biochemical progression was no greater in nerve sparing procedures compared to non-nerve sparing procedures.

Radiation therapy is also used in low risk patients in an attempt to stop tumour growth through the fatal damaging of malignant cell DNA. For prostate cancer, there are two radiation therapies commonly used; interstitial brachytherapy or external beam radiotherapy (EBRT). Interstitial brachytherapy involves inserting rods of radioactive isotopes such as palladium 103 or iodine 125. The rods are implanted under the perineum into the prostate gland via unltrasonograph guidance (Simmons *et al.*, 2011). Two main types of interstitial brachytherapy are currently in use; low-dose permanent (LDR-BT), a slow release system that sits within the prostate indefinitely and high-dose temporary (HDR-BT) which has a higher release of radioactivity but over a shorter period of time. LDR-BT is a more cost effective option and preferred in early prostate cancers (Skowronek, 2013). EBRT involves the delivery of ionising radiation from an external source using a linear accelerator (Vanneste *et al.*, 2016). Via the use of imaging and beam manipulation, EBRT can be used to target the prostate whilst minimising collateral tissue damage. Newer ERBT techniques involve the use of heavier particles such as protons which due to their ability to arrest within the target (in this case the prostate tumour), can deliver higher doses of treatment whilst minimising off target effects (Wisenbaugh *et al.*, 2014). The main benefits of ERBT are that it is non-invasive and painless. However, treatments last for several weeks and require multiple visits to a speacialist unit a week. For more advanced localised cases with higher risk, ERBT and brachytherapy can be combined (Zaorsky *et al.*, 2017).

However, these treatments can often be associated with significant morbidity and reduced quality of life. Furthermore, overtreatment is frequently seen in prostate cancer and often a close monitoring approach may avoid unnecessary treatments and allow more personalised treatment options at a later date (Klotz, 2013).

1.1.4.10   Metastatic PCa

Like all cancers, PCa can metastasise to distal sites. Cancers of different origins have individual metastatic tendencies, in the case of the prostate the most common metastatic locations (in order) are the bone (84%), distant lymph nodes (11%), liver (10%) and the thorax (9%) (Gandaglia *et al.*, 2014). Other less common metastatic sites include the brain, digestive system, kidneys and adrenal glands (Gandaglia *et al.*, 2014). Metastases are associated with considerably higher mortality rates (Sieh *et al.*, 2013; Tangen *et al.*, 2003).

Diagnosis of metastatic disease is dependent firstly on imaging techniques. For example, for the past 35 years the detection of bone metastases has been primarily done by radioisotope bone scintigraphy (RBS), with a technetium 99m- labelled diphosphonate (Pollen *et al.*, 1981). RBS works by visualising high metabolising areas, thus are most effective at detecting metastases that hypermetabolise the bone, which are commonly seen in PCa (Heindel *et al.*, 2014). X-rays are a simple way to view the damage caused by bone metastases and CT scans are useful for viewing bone metastases in cortical bone. Whereas CT scans are useful for viewing metastases of the cortical bone, MRI can be useful in detecting metastases within the bone marrow. PET scanning is used to detect areas of high metabolic activity, and can be used to detect multiple metastatic locations, including the bone with high accuracy (Fujimoto *et al.*, 2006).

Biopsy of the metastatic site can sometimes be extremely effective in diagnosis of primary tumour location. For example, case reports from Nakata *et al.* (2005) and Ueda *et al.* (2007) state that in their patients, no primary tumour could be found from two separate prostate

biopsies. However, biopsy of metastases in the pubic bones of these patients revealed poorly differentiated prostate cancer or general adenocarcinoma, likely to be of prostatic origin.

1.1.4.11 Bone Metastasis

As discussed, the most common secondary site of prostate cancer is the bone (Bubendorf *et al.*, 2000), this occurrence is known as metastatic bone disease. Common complications of metabolic bone disease include spinal compression which leads to paresis or hemiparesis, or an increase in mechanical/chemical activation of periosteal and endostial pain receptors leading to a constant sense of dull pain (Msaouel *et al.*, 2008).

1.2 Formation of Metastatic Bone Disease

PCa metastasis to the bone is a multi-step process (for overview of the process see figure 1.2) that begins with tumour formation within the prostate. Over time, growth of the tumour results in spreading to the prostate stroma, the first step in the development of an invasive tumour (Koutsilieris, 1993).
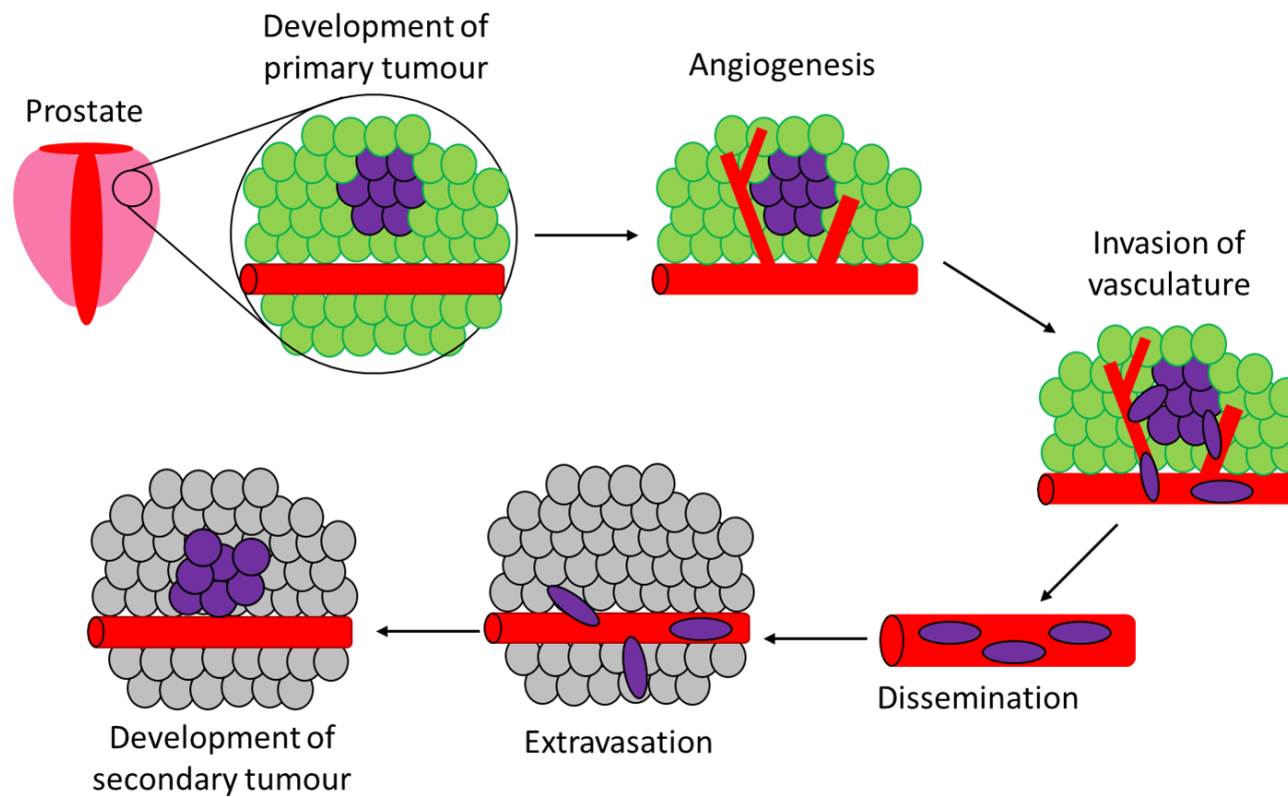
Figure 1.2: An overview of the metastatic process from the PCa to the bone. The primary tumour develops and induces angiogenesis, tumour cells then use this new vasculature to disseminate, eventually extravasating at the secondary site. Commonly for PCa this is the bone (adapted from de Groot *et al.*, 2017).

As the tumour becomes more advanced it invades the surrounding tissues such as the seminal vesicle and the bladder (Msaouel *et al.*, 2008). As the tumour becomes larger, simple diffusion is insufficient to supply all cancerous cells with enough nutrients, thus angiogenesis occurs to increase the blood flow to all parts of the tumour. Angiogenesis is the *de novo* formation of capillaries from post-capillary venules, stimulated by growth factors such as hypoxia-inducable factor (HIF)-1α which modulates the expression of vascular endothelial growth factor (VEGF), angiopoietin-2 and several others (Pugh & Ratcliffe, 2003). The development of this vasculature increases the chances of metastasis due to the now close proximity of malignant cells to the bloodstream. Furthermore, the vasculature at cancerous sites is highly permeable to cancer cell extravastation (Garcia-Roman & Zentella-Dehesa, 2013).

In order for cells to travel to distal sites, they must enter the bloodstream. The first hurdle in the process is a phenomenon known as 'Anoikis', a process of fatty acid synthase (FAS)-induced apoptosis that occurs in epithelial cells that detach from the extracellular matrix (Rennebeck *et al.*, 2005). In order to metastasise, cancer cells must develop Anoikis resistance.

A major hurdle in the migration of PCa cells is survival within circulatory systems, protection systems still pose threats to cancer cells after the evasion of Anoikis. Approximately 85% of tumour cells that enter the circulation will undergo a rapid phase of intravascular cell death (Msaouel *et al.*, 2008). A survival advantage can sometimes be gained by PCa cells by circulating withinin platelet aggregates, protecting them from the shear forces of the circulatory system. Furthermore PCa cells have been known to down-regulate major histocompatibility complex (MHC) class I molecules from their surface, resulting in a decrease in their degradation by cytotoxic T cell killing. Complete loss of human leukocyte antigen (HLA) I is seen in 34% of primary PCa tumours and 80% of prostate derived lymph

node tumours, wheras downregulation of HLA I is seen in 84% of primary tumours and 100% in the metastases (Blades *et al.*, 1995).

PCa cells show tendencies for metastasising to particular parts of the skeletal system. Notably, PCa cells frequently infiltrate trabecular bones of the axial skeleton such as the pelvis, ribs and lumbar spine as well as the proximal ends of the femurs (Msaouel *et al.*, 2008), although the reason for this preference is still under debate. Stephen Paget's "Seed and Soil" hypothesis states that distal sites (soil) contain/secrete factors that provide a habitable environment for a specific cell type (seed) (Paget, 1989). Another theory may be explained by the close relationship shared between the marrow of the vertebral column and a network of veins called the Batson plexus first detailed in 1967. These veins drain blood from the lower vertebral column which receives blood from the prostate (Batson, 1967).

PCa cells extravasate to the marrow, but bone metastases are found on the bone surface (Suva *et al.*, 2011). The first step in gaining entry to the bone marrow is the arrest of PCa cells in the microvasculature within. This occurs in the sinusoids of the skeletal vascular beds, here the large diameter and reduced velocity aid cell bedding (Msaouel *et al.*, 2008). Lehr and Pienta (1998) showed that PCa cells preferentially adhere to bone marrow endothelium compared to other endothelial cell types, at least partly through their interaction with epithelial galectin-3 and lymphocyte function associated antigen 1 (LFA-1) receptors. Here the cells secrete proteolytic enzymes which aid the traversal of PCa cells through the endothelial basement membrane and enables extravasation into the bone microenvironment (Koutsilieris, 1995). Once in the bone microenvironment, the PCa cells stimulate their own vascular supply via angiogenesis which facilitates their migration to the bone surface (Suva *et al.*, 2011). The bone surface is covered in lining cells, therefore when the PCa cells move to within close proximity of the endosteal bone surface they release

agents that stimulate the motility of lining cells and trigger bone resorption. This crucial step provides the PCa cells with access to the demineralised bone surface.

1.3   Bone

Bone is a dynamic tissue with many functional roles including providing structural support, protection of vital organs and permitting movement in conjunction with the muscular system. Bone also plays a role in the homeostasis of minerals such as calcium (Bronner, 1992). Roughly 80% of the human skeleton is cortical bone (Eriksen, 1994), dense bone that surrounds the marrow and forms the outer surface of bones, providing protection and strength. The remaining 20% of the human skeleton is trabecular (or cancellous) bone, located at the ends of long bones and within flat and irregular bones such as the spine, sternum and pelvis (Keaveny *et al.*, 2001). Trabecular bone is formed of open porous space, filled with bone marrow and cells. A directional grain within the porous structure of trabecular bone increases its load bearing strength, whilst still having a reduced weight compared to cortical bone.

1.3.1 Bone Matrix

Bone matrix represents the extracellular component of bone which consists of around 60% inorganic component, formed of primarily hydroxyapatite (HA), 10% water and 30% organic material, formed of various bone matrix proteins (Morgan *et al.*, 2013; Zhu *et al.*, 2008).

1.3.1.1   Inorganic Component

HA [$Ca_5(PO_4)_3(OH)$] is the major component of crystallised inorganic bone matrix (Fujisawa & Tamura, 2012). HA contains vast amounts of both calcium and phosphate, therefore formation and degradation of HA is key to the homeostasis of these minerals. Impurities within HA are common, such as the substitution of phosphate groups with carbonate ions, substitutions of calcium groups with potassium, sodium and magnesium and substitution of

chloride and fluoride with hydroxyl groups (Morgan *et al.*, 2013). The inclusion of these impurities into HA crystals means the inorganic bone matrix is also involved in the homeostasis of these minerals.

1.3.1.2   Organic Component

The organic component of bone matrix is made up of various proteins. Collagenous proteins make up 90% of the organic matrix, of which most is type I collagen (Viguet-Carrin *et al.*, 2006). However, small amounts of other collagens such as type III and V are also present in bone. Collagen provides much of the strength and load bearing qualities of bone. Collagen molecules are organised in the same orientation to form long fibrils, with overlapping collagen molecules to provide additional strength. These molecules are then crosslinked by lysyl oxidase enzymes to form collagen fibrils, which in turn group together to form collagen fibres. Collagen fibres are organised according to the load bearing direction of the bone and are responsible for the incredible directional strength seen in bones such as the femur (Martin *et al.*, 2015). Nudelman *et al.* (2010) implicated collagen I fibrils in the process of HA mineralisation, linking the functions of the organic and inorganic phases. In this study, they showed that the positive charge close to the C-terminal end of collagen molecules facilitates the invasion of negatively charged non-collagenous protein and amorphous calcium phosphate (ACP) complexes into the collagen fibril.

As well as collagens, a wide variety of non-collagenous proteins (NCPs) and growth factors also exist within the bone matrix. Proteins such as osteocalcin (OCN), bone sialoprotein (BSP), osteopontin (OPN), osteonectin (ON) and bone morphogenetic proteins (BMPs) are abundant within the matrix and are generally involved in guiding cells as well as modulating cellular functions and the mineralisation process as a whole (Al-Qtaitat, 2014). Similarly, numerous growth factors and cytokines are present within the bone matrix such as transforming growth factor β (TGFβ), fibroblast growth factors (FGFs), insulin-like growth

factors (IGFs), platelet-derived growth factors (PDGFss), colony stimulating factor (CSF), tumour necrosis factor (TNF) interleukin (IL) 1, 4, 6 and interferon-γ. Again the role of these growth factors is to tightly control cell function within the bone matrix, a process which is under constant, dynamic feedback modulation.

1.3.2 Bone Cells

Within bone, three principle cell types exist that perform tightly regulated roles; osteoblasts, osteoclasts and osteocytes. The cells arise from various stem cell lines and are involved in a number of processes such as bone remodelling and mineral homeostasis.

1.3.2.1   Osteoblasts

The primary role of osteoblasts is the creation and deposition of fresh bone matrix. This matrix deposition is key to maintaining skeletal integrity. Osteoblasts are cuboidal in shape and have very distinctive intracellular features such as basal PAS-positive granules containing bone matrix precursor glycoproteins (Del Fattore *et al.*, 2012) and membranes enriched in alkaline phosphatase (Morris *et al.*, 1992), an enzyme crucial for mineralisation (Sugawara *et al.*, 2002). Active osteoblasts also display a prominent Golgi apparatus and abundant rough endoplasmic reticulum (Caetano-Lopes *et al.*, 2007), typical of a high protein synthesising cell.

1.3.2.1.1   Osteoblast Function

As discussed, the primary function of osteoblasts is the deposition of bone matrix. The initial step in the process is the production of uncalcified matrix termed osteoid (Del Fattore *et al.*, 2012), which forms the organic phase of mature bone matrix. This is achieved through the secretion of a number of proteins, primarily type I collagen, but also contain non-collagenous proteins such as BSP, ON and osteocalcin as well as the proteoglycans biglycan and decorin. Osteoid is subsequently mineralised by osteoblasts. This process is partially mediated by the action of osteoblast associated matrix vesicles (Anderson *et al.*, 2005). Matrix vesicles are

around 50-200nm in size and bud from the osteoid-facing surfaces of osteoblasts. HA crystals initially form within the vesicles, which occur because of excessive concentrations of Ca^{2+} (Genge *et al.*, 1992) and PO_4 (Montessuit *et al.*, 1995), which leads to the deposition of $CaPO_4$ in the form of HA (Anderson *et al.*, 2005). These HA crystals are then released through the membranes of the matrix vesicles, which, due to high levels of local Ca^{2+} and PO_4, grow by a process of nucleation. These HA crystals can interact with collagen molecules as described earlier, and after continuous nucleation, are able to fill the gaps between collagen fibres within the skeletal matrix. The activity of non-collagenous proteins are also largely responsible for the overall process of mineralisation. For example, BSP is able to bind gap zones within the collagens, thus mediating mineral deposition from ions in solution (Glimcher, 1984). Some non-collagenous proteins, such as OPN contribute to the inhibition of matrix mineralisation (Yuan *et al.*, 2014), whereas others, such as MMP3 indirectly increase mineralisation by degrading inhibitory proteins such as OPN (Boukpessi *et al.*, 2008).

1.3.2.1.2 Osteoblast Differentiation

Osteoblasts differentiate from mesenchymal stem cells (MSCs). Commitment of MSCs towards an osteo/chondroprogenitor lineage is the first step in osteoblastogenesis (figure 1.3), a pathway under the control of BMP and Wingless (Wnt) signalling pathways (Grigoriadis *et al.*, 1988). Osteo/chondroprogenitors now have high expression of crucial osteoblast differentiation genes such as Runt-related transcription factors 2 (Runx2), the master osteoblast differentiation gene, as well as Distal-less homeobox5 (Dlx5) and osterix (Osx) (Capulli *et al.*, 2014; Ducy *et al.*, 1997). Osteoprogenitor cells then undergo a proliferative stage, during which Alkaline Phosphatase (ALP) activity increases, these cells are now deemed preosteoblasts and express Collagen Type I Alpha 1 Chain (COL1A1) which is upregulated by runx2 (Capulli *et al.*, 2014). From the immature osteoblast stage onwards, the function of runx2 becomes inhibitory (Komori, 2006). It is therefore believed that the function of runx2 lies in maintaining the supply of immature osteoblasts, at which point,

other genes may take over in driving maturation to mature osteoblasts. For example, maturation from preosteoblasts to mature osteoblasts is characterised by a further increase in the expression of Osx as well as the secretion of organic matrix proteins such as type I collagen, osteocalcin and BSP (as described in section 1.2.2.1.1) (Nakashima *et al.*, 2002). Furthermore, during this final stage, there is a morphological shift towards the large cuboidal shape characteristic of a mature osteoblast.

When osteoblasts reach the end of their lifespan, which in humans is up to 8 weeks (Sommerfeldt & Rubin, 2001), they have a number of potential fates; such as apoptosis, or becoming bone lining cells (BLCs). BLCs are quiescent osteoblasts displaying a flat morphology. As their name suggests, BLCs line the surface of bone and have a number of roles in bone physiology. Firstly the act as a physical barrier, preventing interactions between osteoclasts and bone matrix (Florencio-Silva *et al.*, 2015). BLCs also modulate the maturation of osteoclasts via differential expression of both receptor activator of nuclear factor kappa-B ligand (RANKL) and osteoprotegrin (OPG) (a decoy receptor for RANKL). Finally it is hypothesised that BLCs can regain an active osteoblastic phenotype and through this, extend their lifespan (Matic *et al.*, 2016).
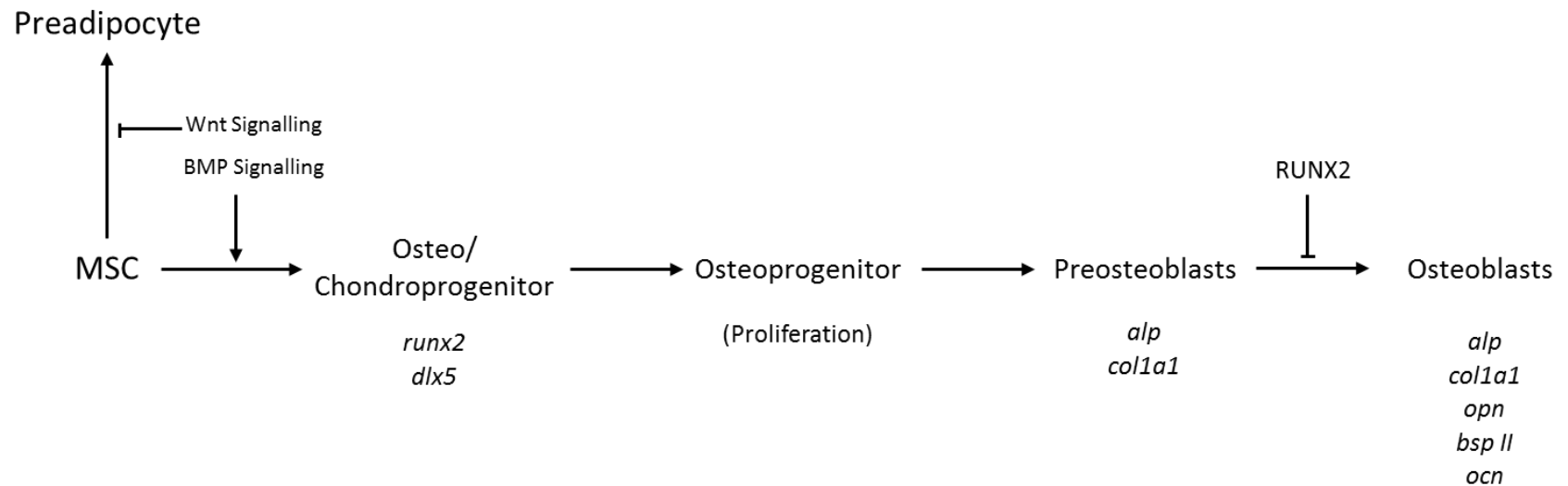
Figure 1.3: Differentiation of MSCs into mature Osteoblasts. BMP and Wnt signalling drives MSCs down the oseo/chondroprogenitor lineage, while Wnt signalling also prevents MSCs from maturing into preadipocytes. Expression of runx2, and dlx5 is crucial for driving further maturation of the osteo/chondroprogenitor cells. Osteoprogenitor cells then proliferate and mature into preosteoblasts, characterised by a rise in the expression of ALP and COL1A1. These cells then mature into osteoblasts, characterised by further increases in ALP and COL1A1 expression, increased secretion of matrix proteins such as BSP and OCN as well as a morphology change to a large cuboidal shape (adapted from Del Fattore *et al.*, 2012; Komori, 2006).

1.3.2.2   Osteocytes

Another potential differentiation avenue for osteoblasts occurs when they become trapped in the mineralised bone matrix and become osteocytes. Osteocytes make up 95% of the cells within bone (Dallas *et al.*, 2013). Osteocytes are found within lacunae, located within the mineralised matrix, and have a dendritic phenotype (Florencio-Silva *et al.*, 2015). Osteocytes have many dendritic processes (around 40-100 per cell) (Beno *et al.*, 2006) that spread through canaliculi within the bone, allowing communication with nearby osteocytes as well as the bone surface and surrounding vasculature (Dallas *et al.*, 2013). Osteocytes are also able to communicate with osteoblasts and osteoclasts, relaying mechanical loading and pressure information to orchestrate effective rebuilding of the local bone (Bonewald, 2007).

1.3.2.3   Osteoclasts

Osteoclasts are giant multinucleated cells responsible for the resorption of mineralised bone matrix. Osteoclasts are highly specialised cells, able to polarize and segregate plasma membrane domains for a more specific pattern of resorption (Szewczyk *et al.*, 2013).

1.3.2.3.1   Osteoclastogenesis

Osteoclasts originate from haematopoietic stem cells which become colony forming unit-granulocyte monocyte cells (CFU-M) upon initiation of osteoclastogenesis (figure 1.4). The initial commitment of a precursor cell to the osteoclast lineage is governed by PU.1, a transcription factor of the Ets (E26 transformation-specific or E-twenty-six) transcription factor family (Tondravi *et al.*, 1997). PU.1 is activated by M-CSF signalling, which along with RANKL signalling, upregulates another transcription factor; nuclear factor of activated T cells, cytoplasmic, calcineurin dependent 1 (NFATc1) (Asagiri & Takayanagi, 2007; Ishiyama *et al.*, 2015). A third transcription factor, Melanocyte Inducing Transcription Factor (MITF), is also involved in this stage of osteoclastogenesis. Initially, MITF was found to work with PU.1 to recruit NFATc1 into a complex able to promote osteoclastic genes (Sharma *et al.*, 2007),

although further work has since revealed a role for MITF downstream of NTFATc1 during RANKL signalling to further promote NTFATc1 dependent osteoclastogenesis (Lu *et al.*, 2014).

The next step in osteoclastogenesis is the fusion of mononuclear cells to form mature, multinucleated osteoclasts. Fusion of osteoclast precursors relies on a small subset of cells with a "fusion founder" competence (Levaot *et al.*, 2015), these cells generally represent <10% of a cell population *in vitro* and fuse with multiple "fusion follower" cells. Numerous molecules have been identified as being involved in osteoclast fusion such as cluster of differentiation (CD)47 (Han *et al.*, 2000), E-cadherin (Mbalaviele *et al.*, 1995) and Meltrin-α (Abe *et al.*, 1999). Two key molecules in osteoclast fusion are dendritic cell-specific transmembrane protein (DC-STAMP) and osteoclast stimulatory transmembrane protein (OC-STAMP). DC-STAMP is up-regulated by RANK-NFATc1 and knockdown of DC-STAMP completely abrogates osteoclast precursor fusion (Yagi *et al.*, 2005), indicating DC-STAMP as the master regulator of osteoclastogenesis. OC-STAMP, another transmembrane protein, also results in abrogated osteoclastogenesis when blocked (Chiu & Ritchlin, 2016). However the mechanism by which DC and OC-STAMP mediate osteoclastogenesis remains largely unknown due to the lack of characterised ligands.

Multinucleated osteoclasts are then recruited to the bone surface by the action of CSF-1 and RANKL, at which point the cells adhere to the bone and undergo cytodifferentiation to form bone resorbing osteoclasts. The activity of genes such as c-Src (Proto-oncogene tyrosine-protein kinase Src), capicua transcriptional repressior-7 (ClC-7) and cathepsin K are crucial for the development of a bone resorbing phenotype (Kornak *et al.*, 2001; Lowe *et al.*, 1993; Troen, 2004). Throughout differentiation, continuous RANKL stimulation is required for osteoclast survival (Park *et al.*, 2017).
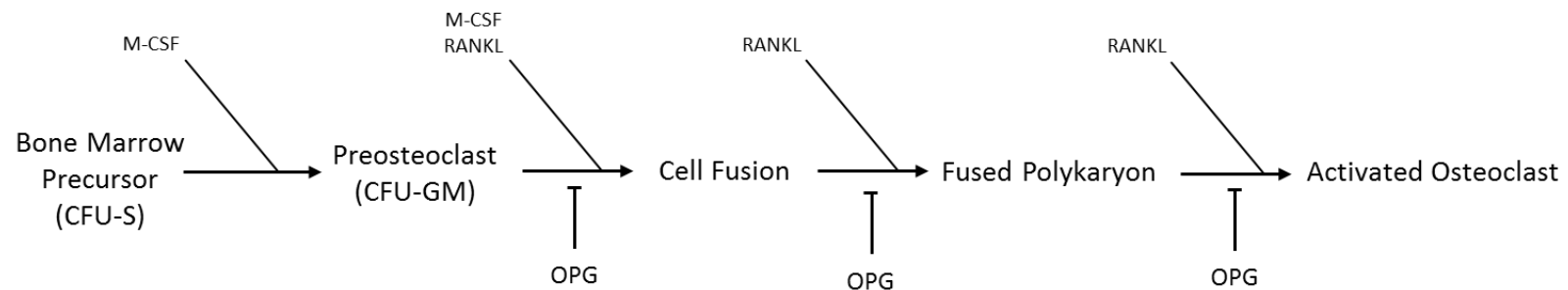
Figure 1.4: Osteoclast Differentiation Lineage and Affecting Factors: Osteoclasts originate as haematopoietic precursors which are stimulated to begin osteoclastogenesis by the PU.1 transcription factor, becoming CFU-GM cells. M-CSF and RANKL are crucial for driving further differentiation whilst OPG inhibits osteoclastogenesis at multiple stages. CFU-GM cells then fuse to form a polykaryon, termed a multinucleated osteoclast, which then mature and gain resorbing activity, becoming activated bone resorbing osteoclasts. Above and below the image are the genes of which mutations are known to increase and decrease osteoclastogenesis (respectively) (blue boxes refer to the effects of these genes in mouse overexpression models) (adapted from Boyle *et al.*, 2003).

1.3.2.3.2   Osteoclast Bone Resorption

For resorption to occur, polarisation of the osteoclasts is crucial. Once polarised, four distinct membrane domains can been seen. The "ruffled border" describes the plasma membrane domain facing the bone surface where bone resorption occurs, and is characterised by numerous membrane folds (Stenbeck, 2002). The adhesion domain describes the area immediately surrounding the ruffled border, responsible for attaching the osteoclast to the bone surface and creating a sealed off area for bone resorption to occur in, known as the "Howship's Lacunae" (Del Fattore *et al.*, 2012). The apical domain is located opposite the ruffled border and the basolateral domain is located between the adhesion and apical domains. These domains are responsible for ion transport and transcytosis of products internalised from the lacunae into the extracellular space.

As discussed, bone matrix has two main components; an organic phase, consisting of largely type 1 collagen and a HA containing inorganic phase. Breakdown of the bone is therefore a two-step process specifically designed for the degradation of each component. The first step involves acidification of the lacunae and is carried out by H^+ATPase pumps within the ruffled membrane (Blair *et al.*, 1989). This releases calcium and phosphate, leaving the organic component vulnerable to proteolytic degradation. The proteolytic enzymes utilised by osteoclasts are cathepsin K and Matrix metalloproteinase-9 (MMP9) (Reponen *et al.*, 1994; Troen, 2004). Cessation of osteoclast activity is primarily orchestrated by OPG, which can directly inhibit osteoclast activity (Hakeda *et al.*, 1998), cause detachment of osteoclasts from the bone surface (O'Brien *et al.*, 2001) and even promote osteoclast apoptosis (Liu *et al.*, 2015).

1.3.2.4   Bone Remodelling

Bone remodelling describes the dynamic process by which bone is simultaneously degraded and synthesised. Bone remodelling takes place within specialised units, called basic

multicellular units (BMUs), where various bone cell types including the crucial osteoblasts and osteoclasts, are active and cooperate in a coordinated manner. The bone remodelling process has 5 stages; activation, resorption, reversal, formation and termination (Raggatt & Partridge, 2010). An overview of the bone remodelling process is shown in figure 1.5.
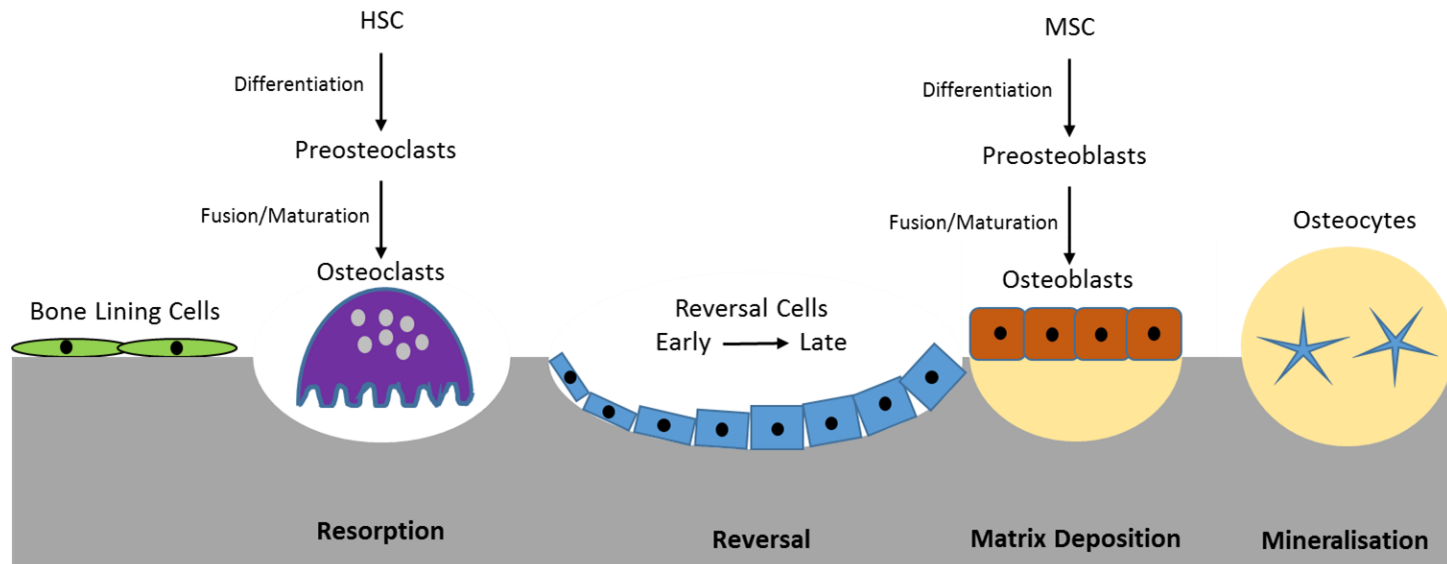
Figure 1.5: An overview of the bone remodelling process. Activation stimulates osteoclastogenesis, resorption involves osteoclastic degradation of the bone, the reversal phase terminates osteoclast function and stimulates osteoblastogenesis, the formation phase involves the osteoblastic deposition of new bone and the termination phase halts bone remodelling by suppressing osteoblast function (adapted from Abdelgawad *et al.*, 2016; Kapinas & Delany, 2011).

The activation phase begins with the detection of an initiating signal, such as mechanical strain, damage or hormone signalling. Bone damage causes nearby osteocyte apoptosis, resulting in a reduction in local TGF-β, an osteoclastic inhibiting hormone produced by the osteocytes (Heino *et al.*, 2002). Parathyroid hormone (PTH) is produced by the parathyroid glands in response to low serum calcium levels and binds PTH receptors on osteoblasts, which in turn activates pro osteoclastic signalling, resulting in osteoclastogenesis (Swarthout *et al.*, 2002).

The resorption phase is activated by pro osteoclastic signals, originating from osteoblasts as discussed, as well as from stromal and bone lining cells (Proff & Romer, 2009). Monocyte chemoattractant protein 1 (MCP-1) secreted by these cells acts as a strong chemotactant for osteoclast precursors. Osteoblasts also increase their expression of CSF-1 and RANKL whilst subsequently reducing their OPG expression, resulting in a heavily pro osteoclastic environment (Ma *et al.*, 2001). At this stage, osteoblasts also produce MMP-13, which degrades the fresh, unmineralised surface of the bone, revealing arginine-glycine-aspartic acid (RGD) adhesion sites (McHugh *et al.*, 2000). RGD adhesion sites act as anchoring points for osteoclasts by their interaction with osteoclastic $\alpha_v\beta_3$ integrin, creating the adhesion domain described previously. Once attached and fully differentiated, mature osteoclasts begin the process of bone resorption (described in section 1.3.2.3.2).

The reversal phase is primarily orchestrated by 'reversal cells', mononuclear cells of osteoblastic lineage (Andersen *et al.*, 2013). Reversal cells have a flat phenotype, similar to that of a bone lining cell, albeit less elongated (Delaisse, 2014). Their role is proposed to be smoothening of the reversal surface, the area of bone that remains post resorption before osteoblastic deposition (Andersen *et al.*, 2013). This smoothening is facilitated by the secretion of MMPs from reversal cells that degrade remaining collagens left over from resorption, and interestingly, blocking this demineralised collagen degradation can prevent

the deposition of fresh bone matrix, highlighting the importance of the reversal process (Everts *et al.*, 2002). Early reversal cells interact with neighbouring osteoclasts and perform smoothening of the reversal surface, as discussed, but as bone lining cells mature, they gain a more osteoblastic phenotype (Abdelgawad *et al.*, 2016).

The formation phase is the osteoblastic phase of bone remodelling, where new bone is synthesised in response to formation signals. The formation phase is key to maintaining skeletal density and integrity by replacing bone removed by osteoclasts. The signalling relationship between osteoclasts and osteoblasts is therefore crucial to maintaining bone homeostasis, and this signalling relationship is known as coupling. The exact origin of these coupling signals is still unclear although data suggests a multitude of potential signal sources. Matrix derived signals, released by the action of bone resorption, were originally thought to trigger formation (Howard *et al.*, 1981), specifically TGFβ and insulin like growth factors. However, in an environment containing functionally redundant osteoclasts, these formation signals still persist, suggesting a potential osteoclastic origin for these signals separate from resorption (Lotinun *et al.*, 2013). In this model sphingosine-1-phosphate (S1P) is the primary osteogenic signal, although studies have also implicated other coupling molecules such as collagen triple helix repeat containing 1 (CTHRC1) (Takeshita *et al.*, 2013) and afamin (Kim *et al.*, 2012). Formation signals can also arrive from other sources such as macrophage derrived oncostatin M (OSM) which can enhance osteoblast differentiation (Guihard *et al.*, 2012). Once signalled to differentiate, mature osteoblasts begin to deposit fresh bone matrix as described in section 1.2.2.1.1.

The termination phase concludes the remodelling process once the resorbed bone has been sufficiently replaced. Sclerostin, produced by local osteocytes suppresses osteoblastic activity and prevents matrix deposition (van Bezooijen *et al.*, 2004). To inhibit further bone

resorption, osteoblasts produce OPG through Notch and Wnt signalling (Matsuo & Irie, 2008).

1.3.3 Effects of Bone Metastases on Bone Remodelling

Interplay between cancer and bone cells drives both the progression of the tumour and modulates the remodelling of the surrounding bone. The effects of bone metastases on the remodelling of the bone can be broadly divided into two main categories; osteolytic and osteoblastic, representing the excess resorption and deposition of bone respectively. Breast and prostate cancer both commonly metastasise to the bone, with breast cancer predominantly forming osteolytic lesions and prostate cancer metastases forming predominantly osteoblastic lesions (Ye *et al.*, 2007).

1.3.3.1 Osteoblastic Lesions

As the name suggests, an osteoblastic bone metastatic lesion is characterised by a relative over activity of osteoblasts within the surrounding area. This results in nodules formed by excess bone deposition, often seen on X-rays as bright areas representing increased bone density. Osteoblastic lesions account for roughly 85% of PCa bone metastases with 12% being mixed lesions and only 4% being osteolytic (Charhon *et al.*, 1983; Roudier *et al.*, 2004). The most common complication with osteoblastic lesions is pain (Coleman, 2001), caused by either stimulation of the local nerves by tumour released cytokines or chemical mediators or by mechanical stimulation from the tumour mass itself (Selvaggi & Scagliotti, 2005). Epidural spinal cord compression is another complication of metastatic lesions, but is not specific to osteoblastic phenotypes. Compression of the spinal cord by the metastatic tumour causes demyelination and axon damage and leads to vascular compromise (Cole & Patchell, 2008), which becomes a significant source of pain.

1.3.3.1.1   Osteoblastic PCa Bone Metastasis

Upon the arrival of PCa cells to the bone there is an initial lytic stage, resulting in the debulking of the bone surface which subsequently aids the seeding of the PCa cells (Msaouel *et al.*, 2008), a process carried out by bone resorbing osteoclast cells. To initiate this osteoclastic stage, the tumour cells chemotactically recruit pre-osteoclasts whereupon their maturation is subsequently triggered. This maturation is initiated by local increases in osteoblastic factors, including RANKL, which triggers osteoclastogenesis as described in section 1.3.2.3.1 PCa cells themselves also express several factors capable of further regulation of osteoclastogenesis including M-CSF, parathyroid-hormone-related protein (PTHrP), interleukin (IL)-1/6 and TGF-β.

Osteoclastic activity then stimulates osteoblastic activity through the mechanisms described in the formation stage of bone remodelling (section 1.3.2.4). This triggering of osteoblast activity is a precursor to the following stage of PCa related metastatic bone disease, which displays as predominantly osteoblastic, favouring bone deposition (Ibrahim *et al.*, 2010). As discussed, during the early stages of bone metastasis, PCa cells secrete a number of factors that act on the bone microenvironment, such as IL-6 and PTHrP that can stimulate pro-osteoclastic pathways (Axmann *et al.*, 2009; Kudo *et al.*, 2003). However, in the later stages of bone metastasis, PCa cells express large amounts of OPG, thus reducing the activity of local osteoclasts via a reduction in RANK-RANKL signalling. Additionally, OPG acts as a pro-survival factor for PCa cells by binding to TNF related apoptosis-inducing ligand (TRAIL) and preventing TRAIL induced apoptosis (Holen *et al.*, 2002). Furthermore PCa cells also secrete factors such as BMPs, TGF-β and IGF (Logothetis & Lin, 2005). These bind a range of receptors on osteoprogenitor cells triggering a number of pathways such as the mitogen-activated protein kinase (MAPK), protein kinase C (PKC) and SMAD signalling pathways. These activate genes including RUNX2 and osterix, inducing osteoblastogenesis. Metastatic PCa cells are also responsible for a rise in local levels of urokinase-type plasminogen activator (uPA)

(Koutsilieris, 1993). uPA promotes osteoblastic activity in number of ways; firstly uPA is responsible for the lysis of IGF binding proteins (IGFBPs) . IGFBPs sequester IGFs, therefore uPA indirectly increased the activity of IGFs resulting in proliferation of osteoblasts and PCa cells via IGF-R (Koutsilieris & Polychronakos, 1992). uPA can also cleave and activate TGF-β as well as binding osteoblasts and triggering activation directly (Ibrahim *et al.*, 2010). This osteoblastic shift in signalling results in the formation of nodules , characteristic of PCa bone metastases.

In addition to the signalling network changes induced by PCa cells, excess bone deposition can occur directly from the action of PCa cells through a process called osteomimicry. This describes the ability of PCa cells within the metastatic niche to increase their expression of osteoblastic genes such as ALP, BMPs, COL1A1, OPN and OCN (Knerr *et al.*, 2004).
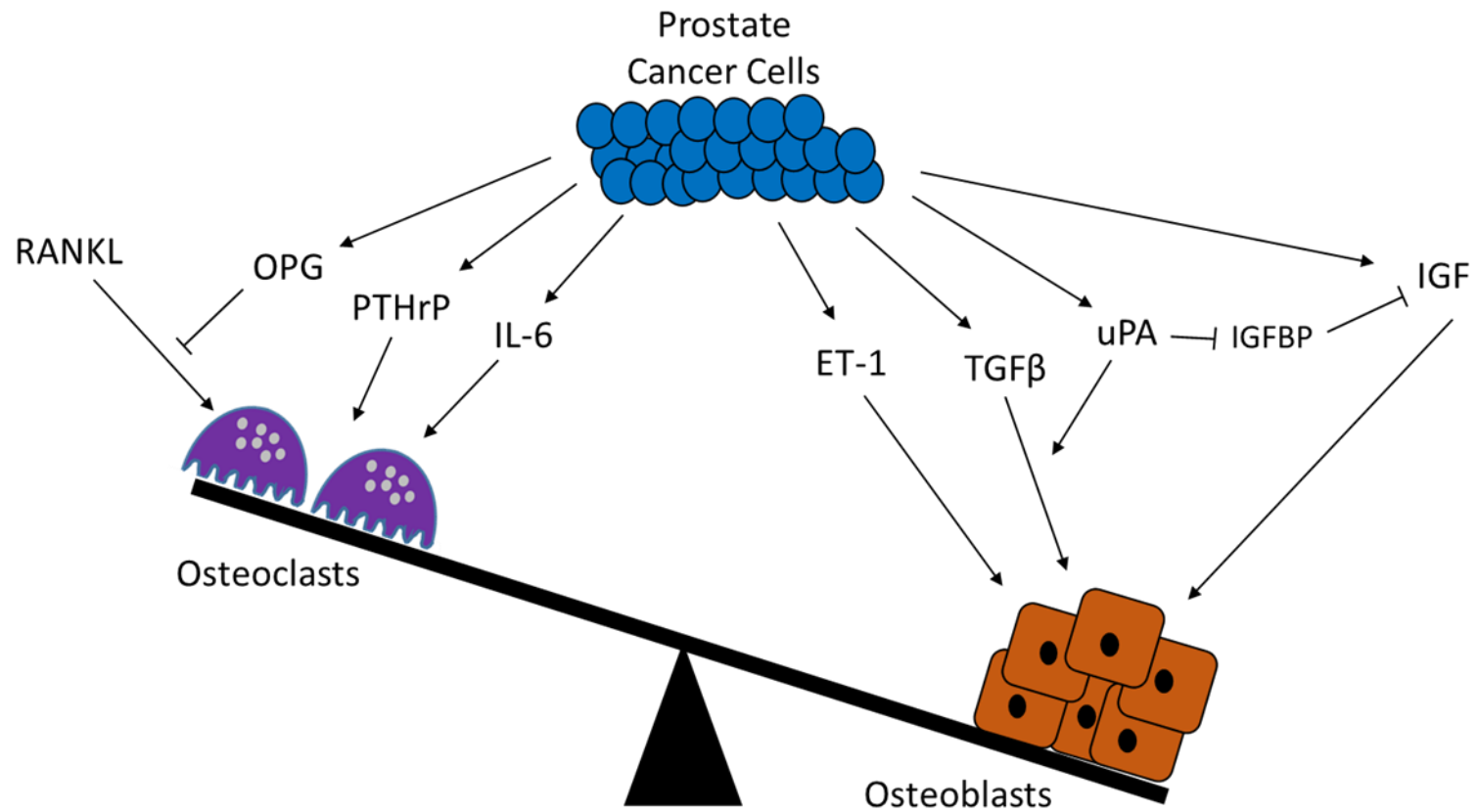
Figure 1.6: Signalling network shared between PCa and bone cells. PCa cells secrete factors that act to increase osteoclast function (PTHrP & IL-6), decrease osteoclast function (OPG) and increase osteoblast function (IGFs, TGF-βs, ET-1 & BMPs) (adapted from Msaouel *et al.*, 2008).

1.3.3.1.2   Osteolytic Lesions

Osteolytic lesions are characterised by a relative over activity of osteoclasts within the surrounding area of the metastasis. As discussed, osteolytic lesions only represent 4% of PCa related bone metastases. However, osteolytic lesions are markedly more common from lung and renal cancer metastases as well as breast cancer, where 48% of metastatic lesions present as osteolytic (Harvey, 1997). Osteolytic lesions appear on X-rays as dark areas within the bone representing reduced bone density as a result of the increased osteoclastic activity.

The increased osteoclast activity seen in osteolytic bone metastases are predominantly the result of increased osteoclast stimulation by RANKL (Boyce & Xing, 2008). This RANKL is produced by local osteocytes and osteoblasts and is upregulated in response to stimulation with PTHrP, produced by tumour cells (Soki *et al.*, 2012).

Pain is also a common complication of osteolytic lesions (Coleman *et al.*, 2014), this is again linked to mechanical stimulation from the tumour itself but is also stimulated in other ways such as a general increase in local acidity due to overproduction of hydrochloric acid (HCl) by osteoclasts (Yoneda *et al.*, 2015). Hypercalcaemia is another complication of osteolytic lesions, caused by calcium release during excessive bone resorption (Stewart, 2005). Hypercalcaemia can cause nausea and vomiting as well as impair cognition, and is also able to stimulate pain (Tsuzuki *et al.*, 2016). Unsurprisingly, bone fractures are common in patients with osteolytic bone metastases and usually appear within the long bones (Sarahrudi *et al.*, 2006). These fractures are painful and show poor healing, often requiring surgery (Harrington, 1995). This leads to a significantly reduced quality of life.

1.3.3.2   Treatment of metastatic PCa

The primary treatment option for metastatic PCa is androgen deprivation therapy (ADT). This involves reducing the circulating levels of testosterone, thus reducing androgen receptor (AR) activity, a prominent driver of PCa progression. The most abundant androgen in males is testosterone, which can be lowered in a two main ways; removal of the testis (the main site of testosterone production) known as surgical castration or pharmacological intervention leading to reduced function of the testis, known as medical castration. However in the majority of cases, advanced PCa develops an androgen independent phenotype, where growth and development can occur in the absence of testosterone. This process is thought to occur via multiple mutations including the acquisition of the 3q12-q13 and loss of the 6q24-qter and 21q chromosomal regions (Hyytinen *et al.*, 1997). For castration resistant metastatic prostate cancer, a breakthrough came in 2004 in the form of Docetaxel, a chemotherapy drug (Tannock *et al.*, 2004), which was followed over the next decade by sipuleucel-T (immunotherapy), cabazitaxel (taxane), abiraterone (CYP17 inhibitor), radium 223 (α-emitter), and enzalutamide (androgen receptor antagonist) (Park & Eisenberger, 2015).

Treatment options for bone metastases are also very limited. Currently, no curative options are available for bone metastases, instead treatment options look to reduce symptomatic issues associated with the tumour. For example, bisphosphonates are able to disrupt osteoclast function and are the standard treatment for tumour-induced hypercalcaemia (Body *et al.*, 1996). Denosumab, a monoclonal antibody able to inhibit RANKL signalling is also used to inhibit osteoclast function and prevent bone loss, and has been shown to improve the outcome of patients with castration-resistant PCa (Smith *et al.*, 2015). Bone metastasis associated pain is treated in a number of ways, with varying degrees of success. Radiotherapy provides pain relief, although the mechanism for this is not understood (Maisano *et al.*, 2001). Analgesia for bone metastases comes in a number of forms and

depends on the severity of the pain. These range from NSAIDs and paracetamol to mild opioids such as codeine and even stronger opioids such as morphine and oxycodone (Marras & Leali, 2016). Surgery is only indicated for the repair of fractured bones or relieving nerve compression (Selvaggi & Scagliotti, 2005).

1.3.3.3 The Importance of Cell Signalling in PCa Bone Metastases

As discussed in section 1.3.3.1.1 and in figure 1.6, the network of signalling molecules governing the function of bone cells within a PCa secondary site is extremely complex. Cell signalling can occur in a number of ways, including paracrine, autocrine endocrine and synaptic signalling. Frequently, in cancer, cellular signalling pathways become dysregulated. For years, cell signalling was focussed on the release of ligands, commonly proteins or hormones and their interactions with receptors on the target cell. However, the recent discovery of several small nucleic acid molecules has challenged the definition of what is/is not a signalling molecule (Cech & Steitz, 2014). Nucleic acid signalling functions without the need for receptors and can deliver/alter genetic information within the target cell. One of these recently discovered groups of nucleic acis are the microRNAs.

1.4   miRNAs:

MicroRNAs (miRNAs, miRs) are 19-25nt single stranded RNAs that regulate gene expression at the post-transcriptional level, targeting the 3'untranslated region (UTR) of protein coding mRNAs utilising a complementarity dependant mechanism.

1.4.1 miRNA Biogenesis

miRNA biogenesis is a complex multistep process, of which certain aspects are still not fully understood. miRNA synthesis has two main processing stages; the nuclear and cytoplasmic stages (figure 1.7).
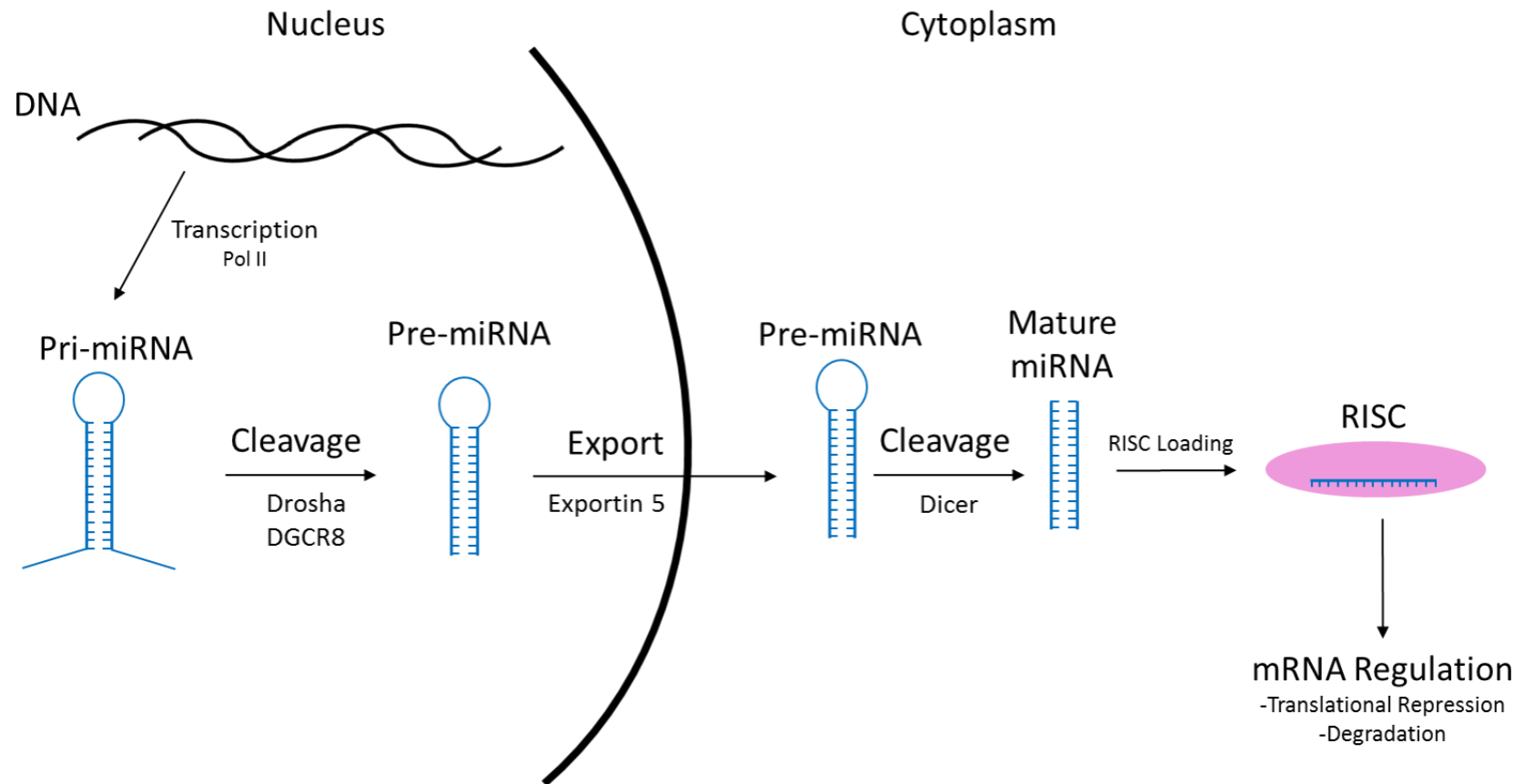
Figure 1.7: miRNA biogenesis pathway showing both the nuclear and cytoplasmic stages. (Nuclear stage) Pri-miRNAs are transcribed from DNA by RNA Polymerase II. Pri-miRNAs are cleaved to pre-miRNAs by the enzyme drosha. Pre-miRNAs are exported out of the nucleus by exportin 5. (Cytoplasmic stage) premiRNAs are cleaved by the enzyme dicer to form mature miRNAs, which associate with RNA-induced silencing complexes (RISCs) which fascilitate their mRNA regulatory effects (adapted from Ryan *et al.*, 2015).

1.4.1.1   Nuclear Processing

In terms of processing pathways, two types of miRNA exist; intergenic (exonic) miRNAs and coding-intronic miRNAs. The most commonly documented pathway of miRNA synthesis follows the lineage of intergenic miRNAs. Intergenic miRNAs are transcribed by RNA polymerase (pol) II or III. The resulting RNA product is a primary miRNA (pri-miRNA), a hairpin structure several kilobases (sometimes >10 kilobases) in length that features lower stem, miRNA duplex, upper stem and terminal loop sections (Han *et al.*, 2006) (figure 1.8). Within the nucleus, pri-miRNAs undergo a cleavage process known as "cropping", catalysed by the ribonuclease (RNase) III member; Drosha (Lee *et al.*, 2003a). For cropping to occur, Drosha requires the activity of a cofactor; DiGeorge syndrome critical region gene 8 (DGCR8) which binds Drosha to form a complex known as the microprocessor (Denli *et al.*, 2004). The stem of a pri-miRNA (the total section between the basal single stranded tails and apical terminal loop) contains 3 helical turns (Han *et al.*, 2006). The microprocessor recognises the basal single stranded segment junction and facilitates cleavage of pri-miRNAs on the stem ~11bp (roughly one helical turn) away from this, forming precursor miRNAs (pre-miRNAs). Occasionally, cleavage can also occur ~11bp from the apical junction on a pri-miRNA, resulting in cleavage of the miRNA sequence, a process known as "unproductive processing" or "abortive processing".

Although also transcribed by RNA pol II, coding-intronic miRNAs are processed differently within the nucleus. Due to their location within the intron of a protein coding gene, these miRNAs are transcribed as part of a pre-mRNA (Rodriguez *et al.*, 2004). From here two main hypotheses exist as to how miRNAs are excised from these pre-mRNAs. The first involves splicesomal components that excise and debranch the introns from the pre-mRNAs (Lin *et al.*, 2003). Within this a number of potential sub steps may occur, the exact nature of which is still unclear. The splicesome may release pri-miRNAs, which subsequently acquire a stem loop structure and are processed by Drosha and DGCR8 as intergenic miRNAs do. Conversely

they may produce pre-miRNAs directly. Furthermore a third molecule may be produced, a small 50-200nt intronic section able to support hairpin formation, termed a mirtron (Macfarlane & Murphy, 2010). Although the subsequent pathway of mammalian mirtrons have not yet been studied, it is suggested based on invertebrate mirtrons that they bypass microprocessor cleavage and are exported similar to pre-miRNAs (Ruby *et al.*, 2007). The second hypothesis is that the microprocessor directly liberates pre-miRNAs from pre-mRNAs (Kim & Kim, 2007), these pre-miRNAs follow the same lineage as pre-miRNAs produced from pri-miRNA cleavage from both intronic and exonic sources.
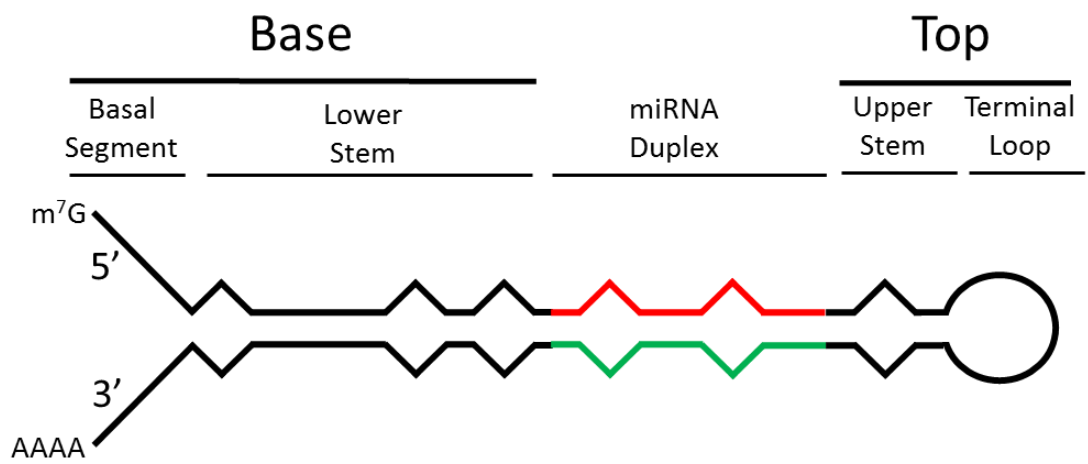
Figure 1.8: Pri-miRNA structure. Structure of pri-miRNA showing two mature miRNA strands (green & red) released during later processing (adapted from Zhu *et al.*, 2013)

1.4.1.2 Nuclear Export

Further processing of pre-miRNAs occurs within the cytoplasm and thus pre-miRNAs must translocate the nuclear envelope. This translocation occurs through nuclear pore complexes (NPCs). NPCs are tube like structures that connect the nucleoplasm to the cytoplasm and are around 100-150nm in diameter, with an internal diameter of 9nm and a cut off weight for free diffusion of 60-100kDa (Wang & Brattain, 2007). Pre-miRNA export through NPCs is mediated by the nucleocytoplasmic transport factor; Exportin 5 (Exp5) in a RanGTP dependent manner. Exp5 recognises the 3' 2nt overhangs on pre-miRNAs (Wang *et al.*, 2011), however in free solution, the inner surface of Exp5 is distorted and residues within Exp5 "lock" the entrance of the 3' overhang binding site. Binding of Ras-related nuclear protein (Ran)GTP rigidifies the Exp5 in a tight curved conformation, aiding pre-miRNA binding (Wang *et al.*, 2011). Binding of the pre-miRNAs to Exp5 begins with the pre-miRNA 3' 2nt overhang adopting a fully closed state, which reduces steric barriers, allowing easier entry of the pre-miRNA into the Exp5 pocket. As the pre-miRNA reaches the bottom of the pocket, the Exp5 facilitates the movement of negative phosphodiester groups on the 3' end of the pre-miRNA forming an extended state. This extended state eases the binding of the pre-miRNA to the Exp5 pocket. Widening of the minor groove within the double helix stem of the pre-miRNA also aids Exp5 binding. Furthermore, phosphate residues within the pre-miRNA major grooves form H-bonds with the basic area of Ran, increasing the stabilisation of the Exp5/GTP/RNA complex.

The Exp5/GTP/RNA complex then translocates through the NPC utilising weak interactions between the complex and FG repeats within the NPC lumen (Katahira & Yoneda, 2011).

After reaching the cytosol, Ran binding protein (RanBP1) binds the molecule causing the dissociation of RanGTP and RanBP1 from the remaining Exp5 whilst also releasing the pre-

miRNA (Bischoff & Gorlich, 1997). Once removed from the complex, RanGTP is hydrolysed by RanGAP to form RanGDP, which then dissociates from RanBP1.

1.4.1.3   Cytoplasmic Processing

Cytoplasmic processing of miRNAs is centred around the removal of the hairpin loop from pre-miRNAs by the RNase III Dicer. This process occurs in conjunction with the loading of the pre-miRNA onto the RNA induced silencing complex (RISC).

1.4.1.4   RISC Loading

The process of mRNA regulation by miRNAs is facilitated by the guiding of an associated group of proteins known as the RISC. RISC is the term given to a family of heterogeneous molecular complexes capable of silencing a multitude of genes (Pratt & MacRae, 2009). The minimal requirements of a RISC capable of gene recognition and silencing are an Argonaute (Ago) protein and a small RNA (Rivas *et al.*, 2005), with the RNA providing the guidance and specificity, and the Ago protein exerting the silencing effect. However RISC isolations display vast variability due to the extensive list of potential Ago protein binding partners. The human genome encodes four different Ago proteins, of which only Ago2 is capable of catalytic RNA slicing (Liu *et al.*, 2004). Ago proteins have four distinct domains; the N-terminal, PAZ, Mid and PIWI domains. The PAZ domain recognises the 3' end of miRNAs and siRNAs and is able to bind these in a sequence independent manner (Lingel *et al.*, 2004; Ma *et al.*, 2004). The PIWI and Mid domains are responsible for binding and anchoring the 5'-phosphate, which binds to a divalent cation at the interface between the two domains (Ma *et al.*, 2005; Parker *et al.*, 2005).

RISC assembly in mammals is still relatively unclear, *Drosophila* RISC assembly is characterised much more clearly and early mammalian RISC hypotheses were often based on this. Early work from Maniataki and Mourelatos (2005) suggested the requirement of a RISC loading complex (RLC) consisting of Ago, Dicer and TRBP. They hypothesised the binding

and cleavage of pre-miRNAs was carried out by Dicer in association with Ago and that the cleaved product was then oriented by DICER-TRBP heterodimers and transferred to Ago. However miRNA mediated RNA interference (RNAi) still takes place in Dicer KO cells transfected with small RNA duplexes, indicating the role of Dicer is at least cleavage *and* handover based rather than being involved in small RNA delivery to Ago alone (Kanellopoulou *et al.*, 2005). Subsequent work by Liu *et al.* (2012) has since shown that expression of non-functional Dicer mutants causes a build-up of RLC, indicating that Dicer processing of pre-miRNAs and loading may trigger the dissociation of Ago from the RLC. The findings of Liu *et al.* (2012) are consistent with those of Maniataki and Mourelatos (2005) suggesting Dicer is involved in the handover of cleaved small RNA duplexes from pre-miRNAs to Ago proteins, but at the same time do not exclude the possibility of Dicer independent loading of small RNA duplexes shown by Kanellopoulou *et al.* (2005).

Cleavage of pre-miRNA begins with the recognition of the 3' 2nt overhang on pre-miRNAs by the PAZ domain of Dicer, which initiates binding (Zhang *et al.*, 2004). Intermolecular dimerisation of two RNase III domains within Dicer create a catalytic centre that cleaves the pre-miRNA using the distance between the PAZ and RNase III domains as a guide (Zhang *et al.*, 2004).

As discussed, after processing by Dicer in the RLC, miRNAs exist as duplexes consisting of the guide strand; which is essential for guiding the RISC, and the passenger strand; which is degraded once released from the guide strand. These duplexes have characteristic 5' monophosphates and 3' 2-nucleotide overhangs, crucial for Ago loading as discussed (Nakanishi, 2016). These characteristic 5' and 3' groups aid the docking of the RNA duplex within the Ago protein at the PAZ and PIWI domains as mentioned previously. Furthermore the 'seed' region of the guide strand, located between nucleotides 2 and 8, is recognised by the nucleic acid binding channel via the 2' hydroxyl groups and phosphate backbone (Schirle

& MacRae, 2012). The loading of RNA duplexes into the Ago proteins is an ATP-dependant process requiring the action of chaperone machinery consisting of Heat shock cognate (Hsc)70/90 (Iwasaki *et al.*, 2010). The energy from adenosine triphosphate (ATP) hydrolysis is used to 'stretch' the Ago protein so as to allow entry of the bulky RNA duplex, often referred to as the "rubber band model" (Kawamata & Tomari, 2010). It is suggested that unwinding of the duplex RNA is performed by RNA helicase A (RHA), a DEAH-box protein capable of unwinding RNA duplexes with 3'overhangs (Robb & Rana, 2007).

Interestingly, pre-miRNAs can also directly bind Ago2 without prior processing. The pre-miRNA-Ago complex is termed the miRNA precursor deposit complex (miPDC). Ago2 cleaves the middle of the 3' strand, generating a small "ac-pre-miRNA" fragment (Diederichs & Haber, 2007), a process that is believed to aid in removal of the 3' passenger strand. Furthermore, pre-miR-451 actually bypasses Dicer-dependant biogenesis altogether (Cheloufi *et al.*, 2010). Instead, pre-miR-451, which is shorter than other pre-miRs, binds Ago2, upon which its 3' strand is cleaved. From here a process of uridylation and trimming of the 3' end produces a mature 23nt miRNA bound to Ago2, capable of acting as a functional RISC.

1.4.2 miRNA Mediated Gene Regulation

1.4.2.1   miRNA Binding

miRNA mediated gene regulation is achieved through binding of the miRNA and the RISC to protein coding mRNAs. These interactions are thought to be dependent on the level of complementarity between the two strands. Metazoan miRNA targets often show a high level of complementarity to a 6-8 nucleotide section at the 5' end of the miRNA, known as the 'seed region (Brennecke *et al.*, 2005). miRNAs can bind to a number of areas on a target mRNA (figure 1.9) The main mechanism for this interaction is the binding of the miRNA/RISC to the 3' UTR of its target mRNA. In animals this interaction generally results in the

translational repression or degradation of the target mRNA, however in some rare cases it can result in the endonucleolytic cleavage of the mRNA (reviewed by Ameres & Zamore, 2013).

As well as binding the 3' UTR of their mRNA targets, miRNAs are able to bind the 5' UTR (figure 1.9). miRNAs binding to the 5' UTR of their mRNA targets also leads to translational repression (Lytle *et al.*, 2007) but binding here can also enhance translation of the gene in some cases (Orom *et al.*, 2008). Tay *et al.* (2008) showed an additional ability of miRNAs to bind to the coding sequence of an mRNA target (figure 1.9) whereupon translational repression again occurred.
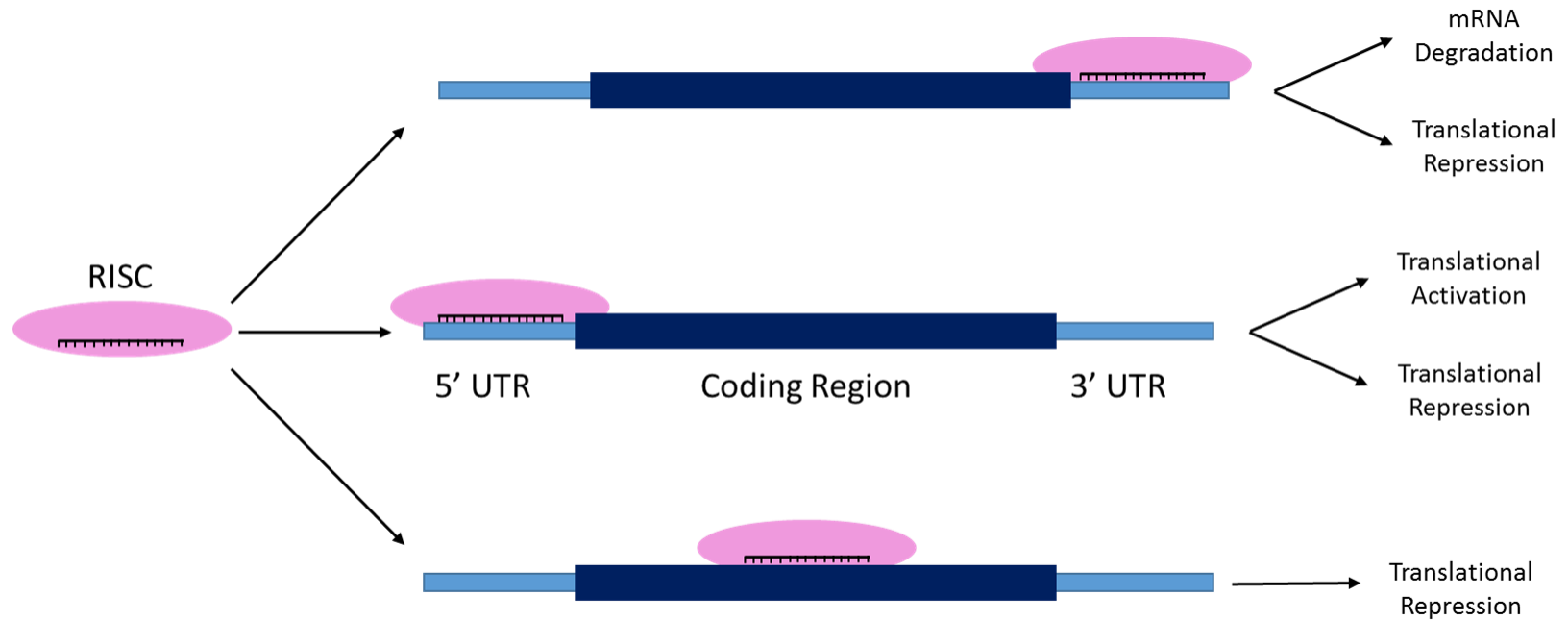
Figure 1.9: Mechanism of miRNA and RISC binding to target mRNAs and the associated outcome. miRNA/RISC can either bind to the 3'UTR, resulting in mRNA degradation or translational repression, the 5'UTR, resulting in translational repression of translational activation, or to the coding sequence, resulting in translational repression (adapted from Ling *et al.*, 2013).

1.4.2.2   Non-Cleavage Mediated Regulation

The majority of human miRNA gene regulation is carried out in a non-cleavage mechanism. This is due to, amongst other factors, the fact that of the four human Ago proteins, only Ago2 is capable of catalysing mRNA cleavage (Liu *et al.*, 2004). Non-cleavage mechanisms of gene regulation are namely translational repression and miRNA degradation.

1.4.2.2.1   Translational repression

Translational repression is described as an observation of decreased protein that is greater than the decrease in the level of the associated mRNA. Translation consists of three main steps; ribosome initiation, elongation and termination (Gu & Kay, 2010). Initial studies were conflicting on which stage of translation the repression occurred at, with some arguing it occurred at the post initiation stage (Petersen *et al.*, 2006) and some arguing it occurred during translation initiation (Mathonnet *et al.*, 2007). Furthermore, multiple molecules such as translation initiation factors were proposed as being crucial (Chendrimada *et al.*, 2007; Kiriakidou *et al.*, 2007). These findings, along with reports suggesting that the protein GW182 is crucial for miRNA mediated translational repression (Eulalio *et al.*, 2008; Iwasaki *et al.*, 2009), lead Gu and Kay (2010) to propose a model for translational repression (figure 1.10 A-D). This model suggests translational repression may occur in multiple different ways, mediated by GW182. These include;

- GW182 and poly a binding protein (PABP) competing with eukaryotic translation initiation factor-4G (eIF4G) to prevent circularisation of the mRNA required for translation (figure 1.10A)

- Preventing association of 60s and 40s ribosomal subunits (figure 1.10B

- Slowing of ribosomes along the mRNA (Figure 1.10C)

- Initiating premature termination of translation (Figure 1.10D)
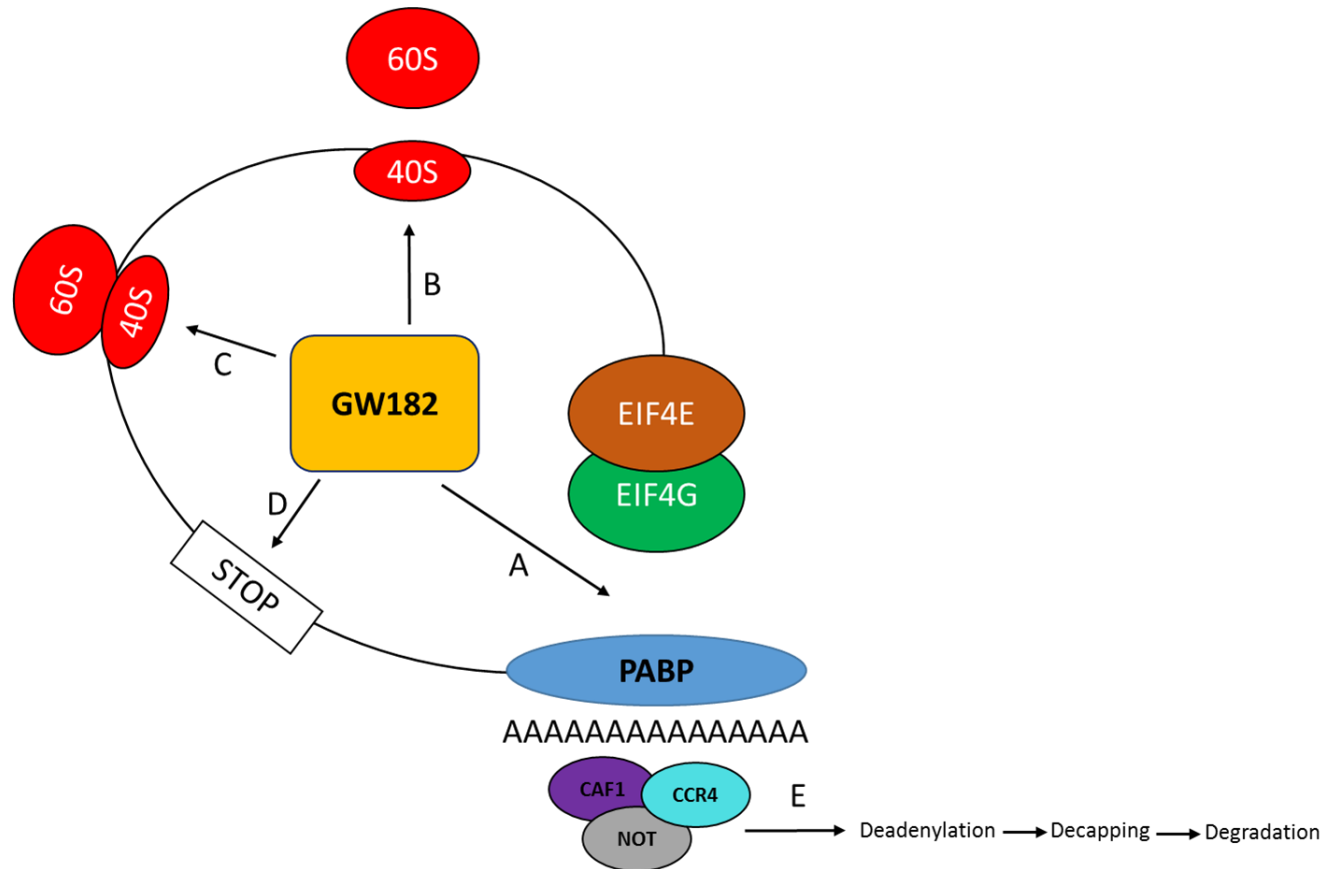
Figure 1.10: Proposed mechanisms for miRNA mediated translational repression. (A) GW182 and PABP competing with eIF4G to prevent circularisation of the mRNA required for translation, (B) Preventing association of 60s and 40s ribosomal subunits, (C) Slowing of ribosomes along the mRNA, (D) Initiating premature termination of translation. (E) Mechanism of mRNA degradation (Gu & Kay, 2010).

mRNA degredation, in a mechanism separate from endonucleolytic cleavage, represents >84% of miRNA mediated mRNA repression in mammals (Guo *et al.*, 2010). mRNA degradation is also mediated by GW182. GW182 first mediates deadenylation of the mRNA followed by de-capping before negative on TATA (NOT)/ carbon catabolite repressor 4 (CCR)4/ chromatin assembly factor-1 (CAF1) complexes degrade the mRNA (figure 1.10E) (Gu & Kay, 2010).

Djuranovic *et al.* (2012) and Bazzini *et al.* (2012) have subsequently shown that translational repression may actually precede mRNA degradation. This balance between repression and degradation of the mRNA is dependent on the interactions of the miRNA with 3' UTR proteins as well as local translational regulators/mRNA decay machinery (Hu & Coller, 2012).

1.4.2.3   Endonucleolytic Cleavage

Endonucleolytic cleavage of target mRNAs is rare in animals. As discussed, only AGO2 has cleavage capability whereas Ago1, Ago3 and Ago4 do not (Liu *et al.*, 2004). For cleavage to occur, complementarity must be extremely high between the miRNA and its target mRNA. One example of this is miR-196a and its ability to cleave HoxB8 mRNA (Yekta *et al.*, 2004). miRNA-196a and HoxB8 are complementary on 20/22 base pairs, and as frequently occurs in plants, cleavage of the mRNA occurs opposite nucleotides 10 and 11 on the miRNA (Ameres & Zamore, 2013). This cleavage then leaves the mRNA open to exonucleic degradation from both 5'-3' and 3'-5' directions by exoribonuclease 1 (XRN1) and the exosome complex respectively.

1.4.2.4   Translational Activation

As discussed, although miRNAs are generally known as repressors of gene expression, they are also able to activate genes. Usually this activation occurs in an indirect manner, via the repression of a gene repressor, thus increasing the expression of a particular gene. miR-128

for example, targets nonsense-mediated decay machinery in the brain during mammalian neuronal differentiation, therefore increasing the amount of local mRNAs involved in neuron and brain function (Bruno *et al.*, 2011).

Interestingly Place *et al.* (2008) showed that miR-373 is able to directly induce expression of its target genes, namely E-cadherin and cold shock domain containing C2 (CSDC2). This activation is triggered by miR-373 binding to a complementary site within the promotor of these gene and functioning similar to a transcription factor.

The action of some miRNAs appears to be dependent on cell cycle status. In proliferating cells miR-369-3 represses tumour necrosis factor alpha (TNFα). However, during G_1/G_0 arrest miR-369-3 activates TNFα translation by recruiting fragile X mental retardation–related protein 1 (FXR1) and Ago2 to AU-rich elements within the 3'UTR of the TNFα mRNA (Vasudevan *et al.*, 2007). This change in miR-369-3 function at different cell cycle states is thought to be dependent on differential subcellular localisations of Ago2-FXR1 complexes during different stages of cell cycle (Vasudevan & Steitz, 2007).

1.4.3   GW-Bodies

Many components of the RNAi pathway such as Ago proteins are concentrated in GW-bodies, distinct foci within eukaryotic cytoplasm (Jakymiw *et al.*, 2005). Furthermore, knockdown of GW182, another crucial component of RNAi prevented the formation of GW-bodies (Yang *et al.*, 2004), further emphasising a link between RNAi and GW-bodies. miRNA induced RNAi is therefore believed to occur within these bodies (Jakymiw *et al.*, 2005) however there is still an abundance of non GW-body associated RNAi components (Leung *et al.*, 2006). miRNA function is now believed to occur not only in GW-bodies, but in other cellular compartments such the nucleus and mitochondria (Leung, 2015).

1.4.4 miRNA Isoforms

It is now known that many miRNAs may comprise multiple isoforms (Westholm *et al.*, 2012). These isoforms, or isomiRs have mostly the same sequence as the original miRNAs, with modifications at either the ends or to internal nucleotides, allowing them to be identified as isomiRs and not different miRNAs. Three main mechanisms exist for generating isomiRs; internal A to I editing, 5' modifications and 3' modifications.

1.4.4.1   Internal miRNA Isoforms

Internal A to I editing is rare and is carried out by adenosine deaminase acting on RNA (ADAR) (Hundley & Bass, 2010). Editing of miRNAs in this way can affect RISC loading (Iizasa *et al.*, 2010) and if editing occurs within the seed sequence, can also affect target recognition/binding (Gandy *et al.*, 2007).

1.4.4.2   3'miRNA Isoforms

3' modifications to miRNAs can be either trimming (removing nucleotides) or tailing (adding nucleotides). Because the seed region, used for target recognition, is measured from the 5' end of the miRNA, adaptations to the 3' end are proposed to produce miRNAs with the same targets but different repression capabilities. Trimming in *Drosophila* requires the 3'-5' Exoribonuclease Nibbler (Liu *et al.*, 2011) which removes 2nt from the 3' end of 24nt Ago1 loaded miRNAs. A similar process of 3' trimming of Ago bound miRNAs in mammals has been seen (Juvvuna *et al.*, 2012) although as yet the protein that facilitates this remains unknown.

The monouridylation of pre-miRNAs by the terminal nucleotidyl transferases (TNTases) ZCCHC11 and ZCCHC6 can enhance Dicer activity on miRNAs (Heo *et al.*, 2012), and if uridylation occurs on the 3' arm, this will be propagated into the mature miRNA. Addition of an adenosine to a mature miRNA by Germ line development 2 (GLD2) can also occur, increasing miRNA stability (Katoh *et al.*, 2009).

1.4.4.3   5' Isoforms

As discussed, the seed region of miRNAs is measured from the 5' end, therefore any alteration to the length of the 5' end will result in a change in the seed sequence and subsequently alter the miRNAs targeting. 5' isomiRs can be formed from the processing of different paralogous pre-miRNAs or from the imprecise trimming of pre-miRNA 5' extensions (Chiang *et al.*, 2010).

1.4.5   Regulation of miRNA Expression

DNA methylation is a substantial mechanism of miRNA regulation. Methylation predominantly occurs within the promotor of miRNAs and is correlated with decreased expression of the associated miRNAs (Deneberg *et al.*, 2014; Jimenez-Wences *et al.*, 2016; Qin *et al.*, 2015). In these cases, aberrant methylation and subsequent changes in miRNA expression are associated with poor prognosis in multiple forms of cancer.

Regulation of miRNA levels can also occur through changes in the levels of miRNA processing proteins. For example, Dicer and Drosha are both elevated in the dorsolateral prefrontal cortex of Schizophrenia patients, resulting in an overall increase in miRNA levels (Santarelli *et al.*, 2011).

Other factors such as hormone levels and exposure to xenobiotics such as carcinogens, including cigarette smoke and even alcohol can alter miRNA levels (Most *et al.*, 2016; Shi *et al.*, 2016; Zhang *et al.*, 2012). Furthermore, due to the global expression of miRNAs and their role in a multitude of signalling pathways, it is likely that countless additional regulators of miRNA function will discovered in the future.

1.4.6   miRNAs in Prostate Cancer

miRNAs play a role in most biological functions and their aberrant expression is linked to numerous diseased states, including multiple forms of cancer (Ardekani & Naeini, 2010; Li & Kowdley, 2012).

In PCa, alterations to miRNA biogenesis machinery are common. However, these alterations tend to show a pattern of increased expression, with the opposite being rarely seen in PCa. Table 1.2 details the findings of a review by Kumar and Lupold (2016) linking overexpression of miRNA processing machinery to PCa:

Table 1.2 The effect of miRNA processing protein overexpression on PCa.

Gene/Protein Overexpressed	Details	Reference
DGCR8 (Drosha Cofactor)	DGCR8 is overexpressed in primary tumours, knockout of DGCR8 caused decreased PCa progression	(Ambs *et al.*, 2008; Belair *et al.*, 2015)
DEAD box protein 5 (DDX5) (helicase component of Drosha complex)	Overexpressed in PCa, related to AR signalling and possible hormone-refractory disease.	(Clark *et al.*, 2008; Clark *et al.*, 2013)
EXP5	Up-regulated in metastatic vs organ-confined PCa	(Chiosea *et al.*, 2006)
Dicer*	Up-regulated in metastatic vs organ-confined PCa and correlated to PCa staging	(Chiosea *et al.*, 2006)
AGO1	Up-regulated in metastatic vs organ-confined PCa	(Chiosea *et al.*, 2006)
AGO2	Not present in prostate gland basal or alveolar cells but present in 57% of prostate carcinoma samples	(Yoo *et al.*, 2010)
Trinucleotide Repeat Containing 6A (TNRC6A) (GW body component, involved in RISC induced mRNA silencing)	Not present in prostate gland basal or alveolar cells but present in 64% of prostate carcinoma samples	(Yoo *et al.*, 2010)

*Although Dicer is upregulated in human PCa samples, lower Dicer levels are seen in recurring primary PCa tumours compared to non-recurrent tumours (Zhang *et al.*, 2014). This indicates multiple roles of Dicer in PCa development and sustenance, a relationship that is not yet understood.

1.5   miRNA Therapeutics

miRNA based therapeutics can be split into two main forms; treatments that utilise miRNA based gene silencing such as exogenous miRNAs and miRNA mimics, and treatments that decrease miRNA based gene silencing such anti-miRNA oligonucleotides (AMOs). The crux of miRNA therapeutics is centred around the simple idea of attempting to reduce the effect of tumour promoting miRNAs, or increasing the activity of tumour suppressive miRNAs.

One of the biggest hurdles in the development and use of RNA based cancer therapies is the effective delivery of the RNA to target cells. Methods including conjugation of small RNAs to cholesterol or association with polymers (to create nanoparticles) are effective in increasing the delivery of RNA therapies and have been utilised in mouse studies (Hu-Lieskovan *et al.*, 2005; Krutzfeldt *et al.*, 2005).

Currently there is one miRNA based therapeutic in clinical trials. Phase I clinical trials of the miR-34 mimic MRX34 are underway after animal studies using MRX34 were able to show safety and reduced tumour growth (Daige *et al.*, 2016). In Phase I trials, MRX34 showed several adverse effects (AEs) (Beg *et al.*, 2017), most likely due to the multitude of downstream miR-34 targets. However these AEs are tolerable under dexamethasone pre-treatment. Responses to MRX34 were mixed but some anti-tumour activity was seen in particular subsets of patients (Beg *et al.*, 2017; Hong *et al.*, 2016).

1.6   Extracellular Transport of miRNAs

1.6.1 Free transport

Ribonucleases (RNases) are abundant in circulation and are elevated further in certain pathologies including cancer (Reddi & Holland, 1976). Therefore, it was hypothesised that miRNAs are not exported as naked RNA molecules. This was confirmed by Tsui *et al.* (2002)

who showed that >99% of synthetic RNA in plasma was degraded within 15 seconds. Since then, a number of molecules have been discovered that are known to shuttle extracellular miRNAs. Arroyo *et al.* (2011) showed that Arganaut2 (Ago2), the catalytic component of the miRNA RISC is present in human serum and is associated with miRNAs. Vickers *et al.* (2011) found that purified HDL contained miRNA and that the level of miRNA associated with HDL changes during a diseased state. They also showed that HDL molecules can associate with exogenous miRNA in culture and are capable of delivering miRNAs to co-cultured cells.

1.6.2 Vesicular Transport

miRNAs are also exported in extracellular vesicles (EVs). Three types of EV are involved in exportation; microvesicles (MVs), exosomes and apoptotic bodies. miRNAs within EVs may be considered more likely signalling molecules than non-vesicular miRNAs due to the protective effects of vesicle encapsulation (Turchinovich *et al.*, 2013). Exosomes and MVs are formed as a part of regular cell processes, although their production can be stimulated under the influence of stress and/or exogenous stimuli. Converesely, apoptotic bodies, as their name suggests, are only formed during programmed cell death (Akers *et al.*, 2013). Thus MVs and exosomes often attract more attention in terms of their ability as signalling molecules.

Although biological definitions exist for individual vesicle subtypes, the increasingly apparent difficulty in isolating specific vesicle subtypes has prompted a shift in vesicle nomenclature. When referring to isolated vesicles throughout this thesis, intracellular/endosomal vesicles, including exosomes, as well as some smaller membrane derived vesicles, will be referred to as small extracellular vesicles (sEVs). Conversely, larger membrane derived vesicles, such as microvesicles and apoptotic bodies, will be referred to as large extracellular vesicles (lEVs). This is except for when referencing papers which specifically refer to exosomes, microvesicles or apoptotic bodies by name.

1.6.3 MVs

MVs are around 100-1000nm in size. MVs are formed by a process known as membrane blebbing, where membrane budding and fission occurs to release cytosolic contents into the extracellular space (Cocucci *et al.*, 2009). This fission resembles that of the abscission step of cytokinesis where contractile machinery brings opposing membranes together and cuts within the cleavage furrow (Schweitzer & D'Souza-Schorey, 2004). MVs are abundant within the circulation of healthy individuals, with the majority of these MVs being platelet derived (Horstman & Ahn, 1999). Furthermore it is now well known that MV levels are often elevated in diseased states (Galindo-Hernandez *et al.*, 2013; Harms *et al.*, 2015; VanWijk *et al.*, 2003).

1.7   Exosomes

Exosomes are 40-100nm lipid-bilayer vesicles first described in 1981 (Trams *et al.*, 1981) as extracellular vesicles with 5'-nucleotidase activity. Shortly after, Harding *et al.* (1983) redefined exosomes as vesicles of an endosomal origin released during rat reticulocyte maturation as a method of releasing transferrin receptors.

1.7.1 Exosome Biogenesis

Exosome biogenesis begins with the invagination of the plasma membrane (PM), budding to form endosomal compartments in a clathrin-dependent manner or by clathrin-independent pathways such as calveolae or lipid raft endocytosis (figure 1.11) (Doherty & McMahon, 2009). These endosomes are then directed to the sorting endosomes (SEs); highly specialised comparements that act to accept and sort internalized cargo from the PM (Gruenberg *et al.*, 1989). SEs are responsible for sorting cargo destined for a variety of cellular destinations such as late endosomes or recycling to the PM. Within SEs, vacuolar regions exist, where inward budding of the limiting membrane generates intraluminal vesicles (ILVs) of around 50nm in size (Mari *et al.*, 2008). Generation of ILVs depends on the actions of a number of proteins

such as Endosomal Sorting Complex Required for Transport (ESCRT) proteins and ESCRT associated proteins such as ALG-2-interacting protein X (ALIX) and tumour susceptibility gene 101 protein (TSG101) which are involved in cargo sorting as well as membrane budding and abscission (reviewed by Kowal *et al.*, 2014). Other non-ESCRT proteins are also involved in ILV generation such as phospholipase D2 (PLD2) and CD63 (Laulagnier *et al.*, 2004; van Niel *et al.*, 2011) as well as the sphingolipid ceramide (Trajkovic *et al.*, 2008). These vesicle rich regions of the SE can either mature or detach to form multivesicular endosomes (MVEs) (Bissig & Gruenberg, 2013). If the content of these ILVs is destined for degradation, MVEs can mature into lysosomes or interact with lysosomes already present in the cytosol (Luzio *et al.*, 2007).

1.7.2 Exosome Secretion

If the ILV cargo is destined for extracellular release, the MVE must fuse with the PM. The process of MVE trafficking to the PM is complex and is known to involve multiple proteins including the Rab family of small GTP-ases. Rab proteins are involved in multiple steps of membrane organisation including budding, trafficking, docking and fusion (figure 1.11). Rab11 and Rab35 are both believed to be involved in the sorting of early ILV containing endosomes (Kowal *et al.*, 2014). In more mature MVEs, Rab27a and Rab27b are responsible for extracellular exosome release. Ostrowski *et al.* (2010) showed that silencing of Rab27a or Rab27b resulted in a build-up of intracellular MVEs indicating that both are involved in PM docking. However differing MVE size and subcellular clustering proved that RAB27a and Rab27b are responsible for different aspects of MVE trafficking and PM docking. Ostrowski *et al.* (2010) also showed that Rab2b, Rab5a and Rab9a were involved in exosome secretion.

Release of the exosomes requires the fusion of the PM and MVE membrane. This process is mediated by another GTPase; RAL-1 (Hyenne *et al.*, 2018), which activates complexes consisting of the target soluble NSF-attachment protein receptor (t-SNARE) protein syntaxin

5 (Syx5) and vesicle (v)-snares on the surface of the MVE. Vaculolar H^+-ATPases (V-ATPases) are also involved in MVE-PM tethering and fusion (Liegeois *et al.*, 2006), knockdown of VHA-5, part of the transmembrane V0 subunit of the V-ATPase resulted in a decrease in MVE tethering/fusion and subsequent exosome release. However whether V-ATPases affect membrane fusion by creating a H^+ gradient or creating a fusion pore remains unknown (Maxson & Grinstein, 2014).

Although knowledge of these factors and pathways has grown dramatically in recent years. The full repertoire of endogenous factors responsible for exosome biogenesis, trafficking and exocytosis are still completely understood and may indeed be prone to change by external stimuli.
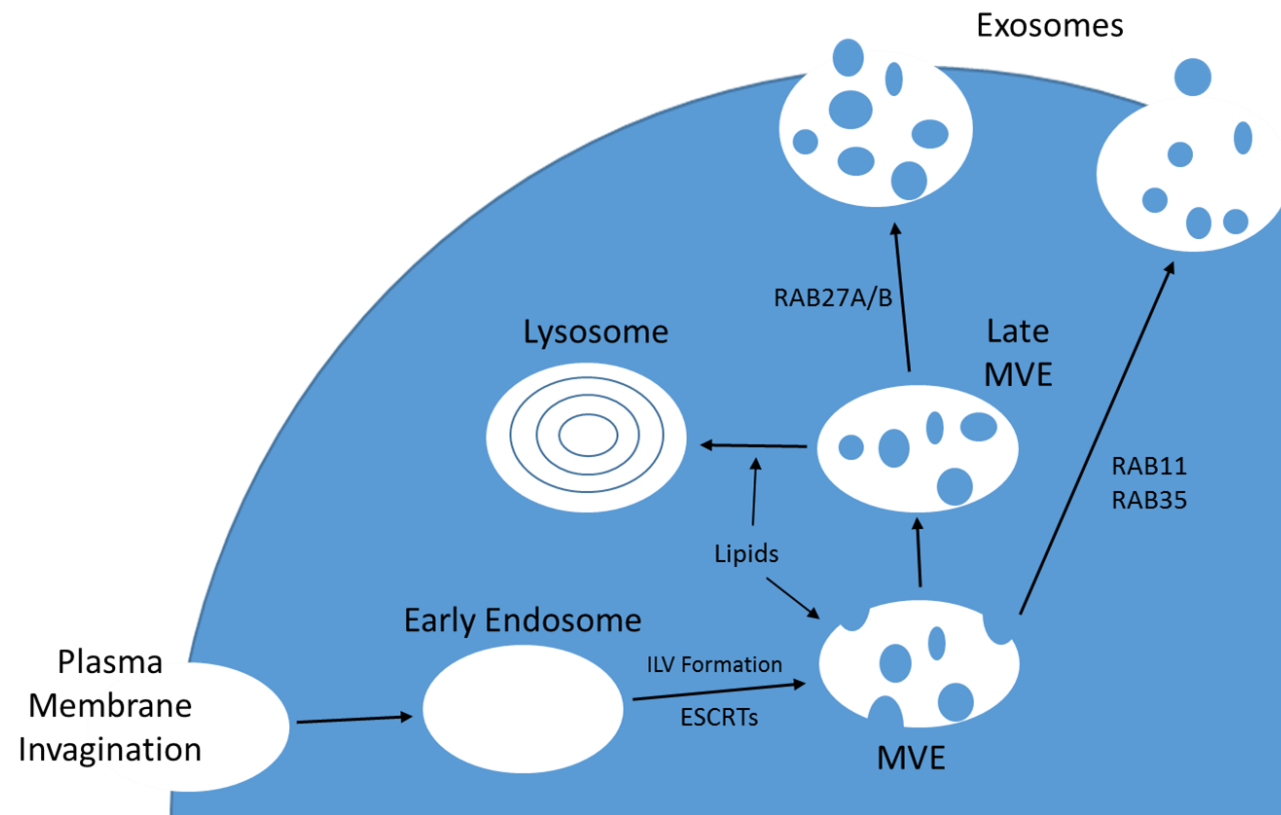
Figure 1.11: Intracellular exosome trafficking pathways. ESCRT proteins, lipids (including ceramide) and tetraspanins are involved in ILV formation. RAB11 and RAB35 are involved in sorting early ILV containing endosomes. RAB27a and RAb27b are involved in the extracellular release of MVEs (adapted from Kowal *et al.*, 2014).

1.7.3 Exosome Content

Exosomal contents have been widely studied and a plethora of molecules have been found both internally and within exosomal membranes. Full characterisation of exosomal molecules is difficult due to the differential expression of molecules between exosomes of different cell types (Griffiths *et al.*, 2017). This characterisation is further complicated by variation in exosomal molecules between cells of the same type. For example exosomes released from apical or basolateral surfaces of the same cell can even exhibit differences in the expression of exosomal molecules (van Niel *et al.*, 2001; Willms *et al.*, 2016).

Whilst exosomes vary dramatically in the levels of certain molecules, there are a set of molecules associated with what is currently believed to be most, if not all exosomes (highlighted in figure 1.12). Of the ~2,400 proteins found in exosomes (Mathivanan & Simpson, 2009) heat shock protein (Hsp)70, Hsp90 and MHC molecules are present in most (Blanchard *et al.*, 2002; Thery *et al.*, 2002). The tetraspanins CD9, CD63, CD81 and CD82 are the proteins most commonly associated with exosomes, and as a result are often used in the characterisation of exosomal isolations (Jorgensen *et al.*, 2013). Other proteins such as ALIX and TSG101, involved in exosome biogenesis (see section 1.7.1) are also present in exosomes.

As well as proteins, a number of nucleic acids are present within exosomes. Vast quantities of tRNA, rRNA and mRNAs are present along with a number of small non-coding RNAs (Huang *et al.*, 2013; Li *et al.*, 2014). Of all the small RNAs, miRNA is the most abundant in exosomes, making up around 76% of all sequences in exsosomal short RNA libraries (Huang *et al.*, 2013).
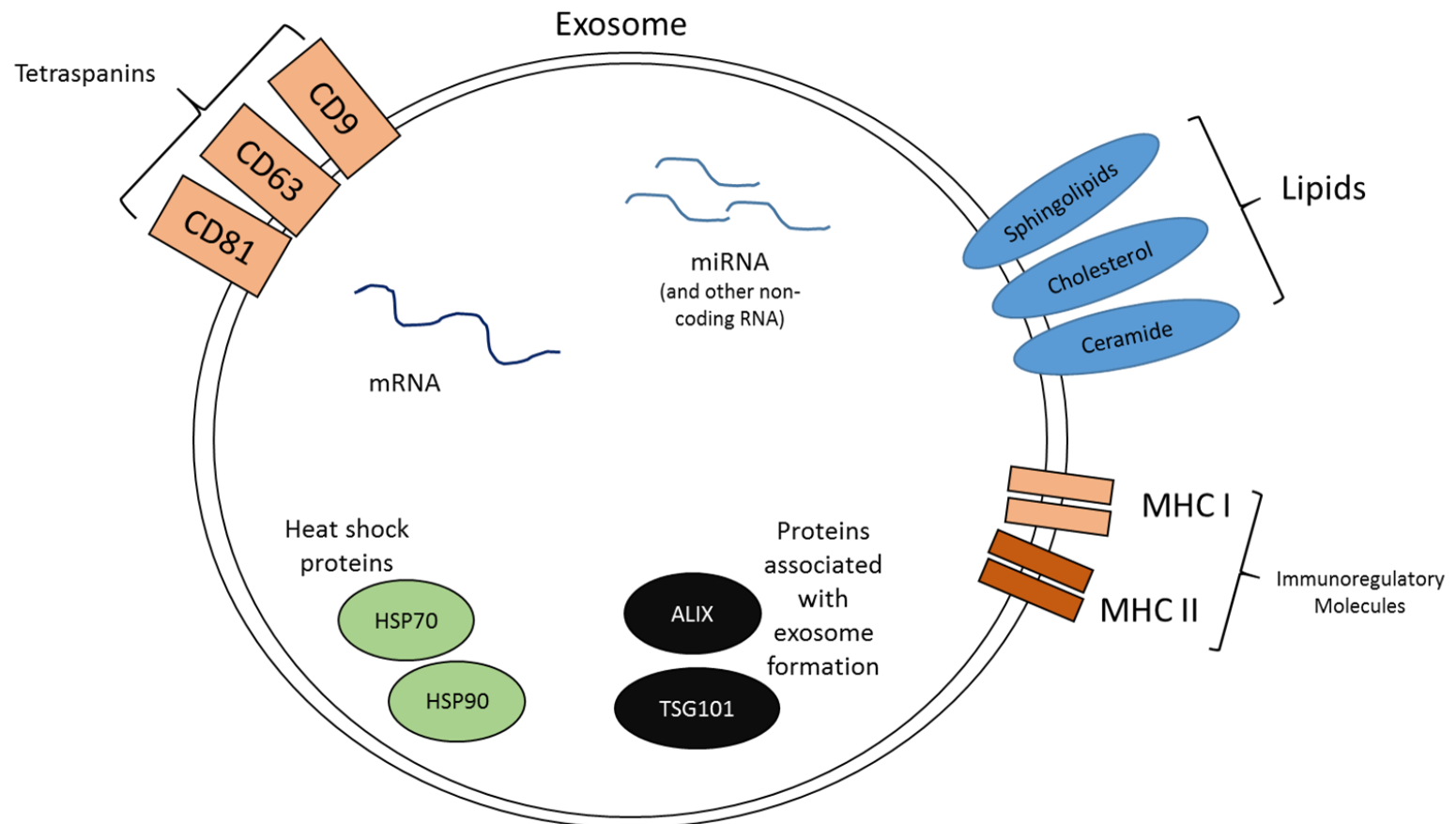
Figure 1.12: Exosomal intracellular and surface contents. Exosomes contain crucial surface molecules such as the tetraspanins, lipids such as ceramide and MHC molecules. Exosomes also contain a wide range of intracellular cargo such as miRNAs, mRNAs, HSPs as well as proteins such as ALIX and TSG101 involved in MVE formation (adapted from Gupta & Pulliam, 2014).

1.7.3.1 Sorting of Exosomal miRNAs

Due to the way exosomes are synthesised, by inward budding of the endosomal membrane, it could easily be assumed that they simply randomly sample the nearby cytoplasm. However, studies have subsequently found that concentrations of molecules such as miRNAs are found at different levels in exosomes than in whole cells (Montecalvo *et al.*, 2012; Valadi *et al.*, 2007) These stoichiometric differences suggest a selective packaging mechanism for exosomes, further indicating their potential as dedicated signalling molecules.

Current evidence points toward four potential methods for miRNA packaging into exosomes (outlined by Zhang *et al.*, 2015):

1. Kosaka *et al.* (2013) showed that overexpression of neural sphingomyelinase 2 (nSMase2) increased the quantity of exosomal miRNA and conversely, inhibition of nSMase2 had the opposite effect.

2. Heterogenous nuclear ribonucleoprotein (hnRNP)A2B1 recognises a GGAG motif in the 3' end of the miRNA. This recognition targets specific miRNAs for exosomal packaging (Villarroya-Beltri *et al.*, 2013).

3. Koppers-Lalic *et al.* (2014) demonstrated a role for 3' end motifs in the sorting of miRNAs. Adenylated miRNAs were predominantly found in RNA samples from whole B cells, whereas uridylated miRNAs were found to be overexpressed in isolated B cell exosomes.

4. Ago2 has also been linked to exosomal miRNA sorting. Knocking out Ago2 resulted in a decrease in the abundance of miRNAs that are preferentially exported in EVs by HEK294T cells such as miR-451, mIR-150 and miR-486 (Guduric-Fuchs *et al.*, 2012).

1.7.4 Exosome Internalisation

A number of exosome internalisation mechanisms have been described in the literature. Some result in cellular responses whilst others result in exosome degradation and a termination of any signalling potential. Internalisation can occur in four main ways; fusion, phagocytosis, micropinocytosis and receptor/raft mediated endocytosis (figure 1.13) (McKelvey *et al.*, 2015; Mulcahy *et al.*, 2014).
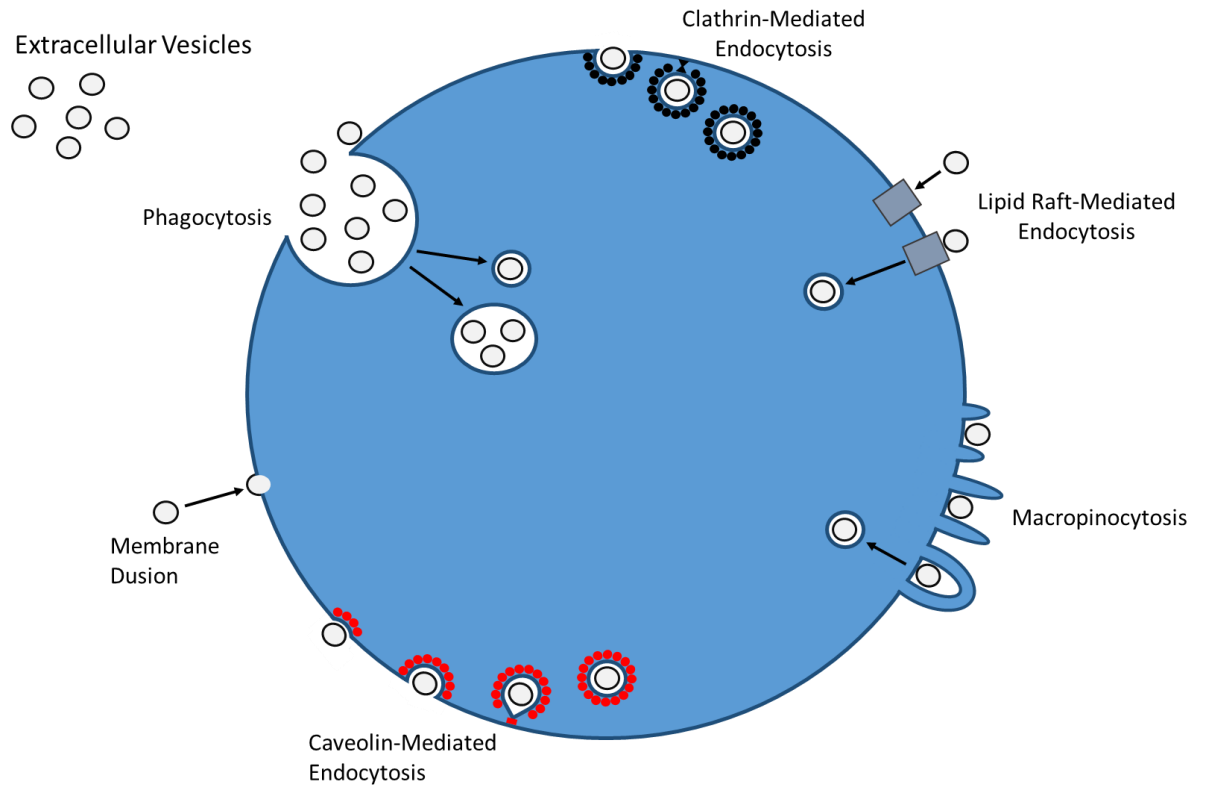
Figure 1.13: Mechanisms of EV uptake. The main mechanisms of EV uptake are fusion, phagocytosis, micropinocytosis and receptor/raft mediated endocytosis (Mulcahy *et al.*, 2014).

Fusion of exosomes with target cells has been seen in the uptake of exosomes by melanoma cells, and is mediated by the lipid composition of the target cell membrane (Parolini *et al.*, 2009). Internalisation of exosomes by phagocytosis has also been proven (Feng *et al.*, 2010). Phagocytosis of exosomes requires the action of opsonin receptors such as Fc receptor (FcR) and complement receptors, and subsequently this process occurs more efficiently in phagocytic cells. Phagocytosis is primarily a mechanism of lysosomal clearance, however, whether this can also be a route of exosomal genetic transfer remains unclear. Macropinocytosis, stimulated by phosphatidylserine on the surface of exosomes is a method of internalisation for non-antigen-presenting cells (Fitzner *et al.*, 2011). This process is often mediated by NA^+ and phosphoinositide 3-kinase (PI3K) within the target cell (Tian *et al.*, 2014). Finally, receptor/raft mediated endocytosis can internalise exosomes by utilising interactions between exosomal ligands and cellular receptors. These interactions result in in clathrin mediated endocytosis, whereas caveolae mediated endocytosis is not involved in exosome uptake (Svensson *et al.*, 2013; Tian *et al.*, 2014).

Internalisation of exosomes represents the majority of mechanisms that allows transfer of internal exosomal genetic material such as miRNAs, along with direct fusion of the vesicle and cell membranes. However, non-internalisation based signalling of exosomes can occur via interactions between target cell receptors and membrane bound or soluble exosomal ligands (McKelvey *et al.*, 2015). FasL and TRAIL can all be cleaved from exosome surfaces to form soluble ligands and can also interact with target cells in their membrane bound form. Exosomal MHC molecules can also interact with target cell plasma membrane receptors, triggering signalling pathways (McKelvey *et al.*, 2015).

1.8 Study Aims

In this study we look to uncover the signalling relationship between PCa cells and bone cells, hopefully uncovering some of the mechanisms at play in the development of PCa bone metastases. Cancer cell sEVs have shown an ability to educate pre-metastatic sites including the bone, even in cancers with low bone metastatic tendencies (Peinado *et al.*, 2012). Furthermore, sEV miRNAs have displayed an ability to alter key processes involved in bone metastatic development (Valencia *et al.*, 2014). Osteoclast sEV miRNAs have also shown an ability to alter the function of bone cells, a crucial factor in the development of metastatic lesions (Sun *et al.*, 2016).

As discussed, sEVs and their associated miRNAs can have a multitude of effects on metastatic sites and the function of the cells within. Therefore, our hypothesis is as follows:

Prostate cancer cells use small extracellular vesicles to deliver miRNAs to cells within the bone microenvironment during the development of bone metastases, thus altering the delicate balance of bone remodelling.

To do this, our aims are:

- To assess the miRNA content of PCa sEVs, looking at which are most abundant and whether miRs are being selectively packaged
- To explore the effect of sEV treatment on the function of cells of the bone microenvironment
- To implicate the sEV miRNAs in any changes seen in sEV treated bone cells

Chapter II: Materials and Methods

2 <u>Methods</u>

2.1 Cell Lines

The PC3, DU145 and LNCaP prostate cancer cell lines, the PZ-HPV-7 prostate epithelial cell line and the 7F2 osteoblast cell line used throughout this research project were all obtained from the American Type Culture Collection (ATCC, Middlesex, UK). Origin, characteristics and culture medium for all cell lines used are detailed in table 2.1.

Table 2.1 Cells, Characteristics and Culture medium

Cell Line	Species	Morphology	Origin	Additional Information	Culture Medium
Prostate Cell Lines					
PC-3	*Homo sapiens*	Epithelial	Caucasian male, aged 62	Derived from bone metastasis from grade IV prostate adenocarcinoma.	DMEM/F12
DU145	*Homo sapiens*	Epithelial	Caucasian male, aged 69	Derived from prostate cancer brain metastasis.	DMEM/F12
LNCaP	*Homo sapiens*	Epithelial	Caucasian male, aged 50	From metastatic site; left supraclavicular lymph node	RPMI-1640
PZ-HPV-7	*Homo sapiens*	Epithelial	Caucasian male, aged 70	Derived from prostate epithelial cells harvested from the peripheral zone of the prostate. HPV-18 Transformed.	keratinocyte media + bovine pituitary extract and human recombinant epidermal growth factor
Bone Cell Lines					
7F2	*Mus musculus*	Fibroblast (Osteoblast)	Male mouse, aged 5-6 weeks	Isolated from p53$^{-/-}$ mouse.	MEM + 10mL 200mM L-Glutamine
RAW 264.7	*Mus musculus*	Macrophage	Adult male mouse	Abelson murine leukaemia virus transformed	DMEM/F12

2.2   Primers

Both Taqman® and SYBR® Green quantitative polymerase chain reaction (qPCR) was performed during this research project. Taqman® primers used are detailed in table 2.2 and SYBR® Green primers used are detailed in table 2.3.

2.3   Antibodies

2.3.1 Primary Antibodies

Primary antibodies used throughout this research project are detailed in table 2.5 including supplier, host species and dilution used.

2.3.2 Secondary Antibodies

For western blot, secondary antibodies were used to match primary antibody species and were either horseradish peroxidase (HRP) conjugated anti-mouse IgG (A5278) or anti-rabbit IgG (A6154) antibodies (Sigma-Aldrich, Dorset, UK).

Table 2.2 Taqman® primers used

Primer	Species	Assay ID
HPRT	Mouse	Mm03024075_m1
β-Actin	Mouse	Mm02619580_g1
AXIN2	Mouse	Mm00443610_m1
ACP5 (TRAP)	Mouse	Mm00475698_m1
miR-16-5p	Human	477860_mir
miR-423-3p	Rat	rno478327_mir
miR-423-5p	Human	478090_mir
miR-221-3p	Rat	rno481005_mir
mIR-93-5p	Human	478210_mir
miR-222-3p	Human	477982_mir

Table 2.3 SYBR® Green primers used

Primer	Sequence
ACVR1	F: TCTCCCTTGGAGCAGTCAGT
	R: CCTGGATCCATTCATCCCTGT
MMP3	F: TAAAGACAGGCACTTTTGGCG
	R: GGAGACCCAGGGTGTGAATG
COL1A1	F: GAGAGGTGAACAAGGTCCCG
	R: AAACCTCTCTCGCCTCTTGC
DLX5	F: TATGGCAAAGCGCTCAACCC
	R: TTCTTTCTCTGGCTGGCTGGT
GAPDH	F: TGCACCACCAACTGCTTACG
	R: GGCATGGACTGTGGTCATGAG
RPL-19	F: AGCGAGCTCTTTCCTTTCG
	R: GAGCCTCTTCTGAAGCCTGA
DLL1	F: ACCAAGTGCCAGTCACAGAG
	R: TCCATCTTACACCTCAGTCGC
PLSCR4	F: AAATGTCAGGTCTGGTCCCCA
	R: ACAAGGAGAGGCAACTGGTC
ADRB2	F: TGGTGGGCTACGTCAACTC
	R: TCCGTTCTGCCGTTGCTATT
OSCAR	F: TCGCTGATACTCCAGCTGTC
	R: CTAGGGGCGCTGTTGGTG

Table 2.4 Primers used for amplifying coding regions

Primer	Sequence
AXIN2	F: ATGAGTAGCGCCGTGTTAGTG
	R: TCAGTCGATCCTCTCCACTTTG
DLL1	F: ATGGGCCGTCGGAGCG
	R: TTACACCTCAGTCGCTATAACAC
PLSCR4	F: ATGTCAGGTCTGGTCCCCA
	R: CTATCTTGACATACGTCGCGG
ADRB2	F: ATGGGGCCACACGGGAAC
	R: TTACAGTGGCGAGTCATTTGTACTA

Table 2.5 Primary Antibodies used for Western Blot and Immuno-Phenotyping

Antibody	Code	Company	Dilution
ALIX	3A9	Cell Signalling	1 in 1000
CALNEXIN	C5C9	Cell Signalling	1 in 1000
AXIN2	Ab109307	abcam	1 in 1000
RANKL	Sc9073	Santa-Cruz	1 in 1000
GAPDH	6C5	Santa-Cruz	1 in 500
CD9	MAB1880	R&D Systems	1µg/mL
CD63	MCA2142	AbD Serotec	1µg/mL
CD81	MCA1847EL	BioRad	1µg/mL

2.4 Reagents and Solutions

2.4.1 Solutions for General Laboratory Work

2.4.1.1 Diethylpyrocarbonate (DEPC) water

500μL of DEPC was topped up to 500mL using distilled water and left for 24 hours at RT before being autoclaved.

2.4.1.2 Phosphate-Buffered Saline (PBS)

A 10x PBS stock (Sigma-Aldrich) was diluted to a 1x solution using distilled water. PBS was then aliquoted and stored at room temperature.

2.4.2 Solutions for Tissue Culture

2.4.2.1 Trypsin-Ethylenediaminetriacetic Acid (EDTA)

10x Trypsin-EDTA stock (Sigma-Aldrich) was diluted to a 1x solution with PBS.

2.4.2.2 Antibiotic Antimycotic Solution (Abx)

A 100x antibiotic antimycotic solution (10,000U/mL penicillin, 10mg/mL streptomycin, 25μ/mL amphotericin B) (Sigma-Aldrich) was diluted to a 1x solution with distilled water.

2.4.3 Solutions for Western Blot

2.4.3.1 Lysis Buffer

For 100mL 0.87g 150mM NaCl + 0.19g 5mM EGTA + 0.61g 50mM Tris + 1mL 1% (v/v) Triton X-100 was combined with dH_2O. For use, one protease inhibitor tablet (Roche) was added. The solution was then aliquoted and stored at -20°C.

2.4.3.2 Tris-Buffered Saline (TBS)

10X TBS (Sigma-Aldrich) was diluted to a 1x soltuion using dH_2O.

2.4.3.3 10% w/v Ammonium Persulphate (APS)

1g of APS (Melford Laboratories Ltd, UK) was dissolved in 9mL dH$_2$O. The solution was the aliquoted and stored at -20°C. Once opened, APS was stored at 4°C for no longer than 2 weeks.

2.4.3.4 0.1% v/v TBS/Tween (TBST)

1mL of Tween20 (melford Laboratories Ltd, UK) was added to 1L of TBS and mixed thoroughly.

2.4.3.5 Running Buffer

1L of 10x Tris Glycine SDS Buffer (Sigma-Aldrich) was added to 9L dH$_2$O

2.4.3.6 Transfer Buffer

1L of 10x Tris/Glycine Concentrate Buffer (Sigma-Aldrich) and 2L of Methanol (Fisher Chemical) was added to 7L of dH$_2$O.

2.4.3.7 10% Sodium Dodecyl Sulfate (SDS)

10g of SDS (Melford Laboratories Ltd, UK) was dissolved in 100mL of dH$_2$O.

2.4.4 Solutions for Bacteriology

2.4.4.1 Lysogeny Broth (LB)

8g of low salt LB (Melford Laboratories Ltd, UK) was added to 400mL dH$_2$O and mixed until fully dissolved. The solution was then autoclaved. Before use and once cooled, 400µL of 100mg/mL ampicillin (Sigma-Aldrich) was added.

2.4.4.2 LB-Agar Ampicillin Plates

8g of low salt LB (Melford Laboratories Ltd, UK) was added to 400mL dH$_2$O and mixed until fully dissolved. 5g agar (Melford Laboratories Ltd, UK) was added, prior to sterilisation by

autoclaving. Once cooled, but still liquid, 400μL of 100mg/mL ampicillin (Sigma-Aldrich) was added. The solution was then poured into $10cm^2$ dishes to cool and solidify.

2.4.5 Specialised Solutions

2.4.5.1 RANKL

Recombinant mouse RANKL (R&D Systems) was diluted to 10μg/mL in sterile PBS + 0.1% (w/v) bovine serum albumin (BSA).

2.4.5.2 1x Reporter Lysis Buffer

5x reporter lysis buffer (Promega) was diluted to a 1x solution with dH_2O and stored at room temperature.

2.5 Cell Culture

2.5.1 Cell Culture Medium

Keratinocyte Serum Free Medium (Gibco) was supplemented with bovine pituitary extract and human recombinant EGF (Gibco). Mimimum essential medium eagle (MEM) (Sigma-Aldrich) was supplemented with 1% v/v Abx, 2mM L-glutamine (Sigma Aldrich), 1mM sodium pyruvate (Thermo Fisher Scientific, Massachusetts, USA) and 10% (v/v) Foetal Bovine Serum (FBS). Dulbecco's Modified Eagle's Medium DMEM/F12 with L-glutamate (Sigma-Aldrich) was supplemented with 1% v/v Abx. RPMI-1640 was supplemented with 1% (v/v) antibiotics (penicillin-streptomycin 10,000U/mL) and 10% (v/v) FBS.

2.5.2 Cell Passaging

Cells were grown in $25cm^2$ or $75cm^2$ tissue culture flasks (Greiner Bio-One Ltd, Gloucestershire, UK), incubated at 37°C with 5% CO_2 and 95% humidity. All tissue culture was performed using aseptic techniques within a class II laminar flow cabinet using autoclaved

equipment. Cells were passaged upon reaching 80-90% confluency, gauged visually using a light microscope. Once 80-90% confluency was met, medium was removed and cells were washed with PBS. 1-2mL of Trypsin:EDTA (0.01% trypsin and 0.05% EDTA in PBS buffer) (depending on cell type and flask size) was added to the cells and flasks were left at 37°C for 5 minutes. Once detached, 5mL of serum containing medium was added to neutralise the effects of the trypsin. Cells were decanted into a universal container and pelleted by centrifugation at 1700xg for 5 minutes. The Trypsin:EDTA and medium mixture was aspirated and cells were resuspended in pre-warmed media. The required amount of cells were then placed in a fresh tissue culture flask to continue growing.

2.5.3 Cell Counting

10μL of cells in suspension were added to a 0.100mm depth haemocytometer (Neubauer). Cells were counted within the squares of the haemocytometer a minimum of 3 times before an average was taken.

2.5.4 Freezing Cells

Cells were trypsinised and pelleted according to section 2.2.3. Cell pellets were resuspended in 1mL FBS + 10% (v/v) dimethyl sulfoxide (DMSO) (Sigma-Aldrich). Cell suspension was then transferred to a Cryo-tube (Grenier Bio-one), wrapped in tissue and stored at -80°C overnight before being transferred to liquid nitrogen.

2.5.5 Revival of Cells

Cells were thawed quickly using a 37°C water bath. Cell suspension was transferred to a sterile universal container and 5mL of fresh medium was added. Cells were pelleted at 1700xg for 5 minutes and supernatant was removed. Cells were resuspended in fresh medium, transferred to fresh cell culture flasks and placed in a 37°C incubator.

2.5.6 Mycoplasma Test

Cells were checked for mycoplasma using an EZ-PCR Mycoplasma Test Kit (Biological Industries). Media from cell culture flasks was centrifuged for 5 minutes at 250xg. Supernatant was removed and centrifuged again for 10 minutes at 15000xg. Supernatant was discarded and the pellet was resuspended in 25µL of buffer solution and heated to 95°C for 3 minutes. A 35 cycle specific PCR was conducted using the supplied reaction mix, including supplied positive controls and results were visualised on a 2% agarose gel (positive product= 270bp).

2.5.7 Co-Culture

0.4µm pore size 24 well inserts (Sigma-Aldrich) were used for co-culture experiments. 7F2 cells were seeded at 80% confluency and left overnight to settle. The following day, the media was changed to 1mL of control or osteogenic media. Inserts were added above the 7F2 cells and PC3 cell pellets, containing the required cell number were resuspended in 200µL of control or osteogenic media and added into the inserts. 7F2 cells were then left to mineralise.

2.6   sEV Isolation

For collection of sEVs PC3 cells were cultured in Bioreactor Flasks; CELLine AD 1000 (Integra). Bioreactor flasks are dual chamber flasks, allowing large quantities of cells to grow in a compartment separated by a 10kDa membrane. This compartment holds a maximum of 20mL of media, allowing for extremely concentrated media to be collected. Above the cell compartment, a media compartment holds 0.5-1L of medium. These two chambers ensure delivery of fresh nutrients to the cells through the semi-permeable membrane, whilst

allowing a build-up of larger molecules within the cell compartment, in this case, sEVs. An overview of these compartments and their surrounding membranes is shown in figure 2.1.
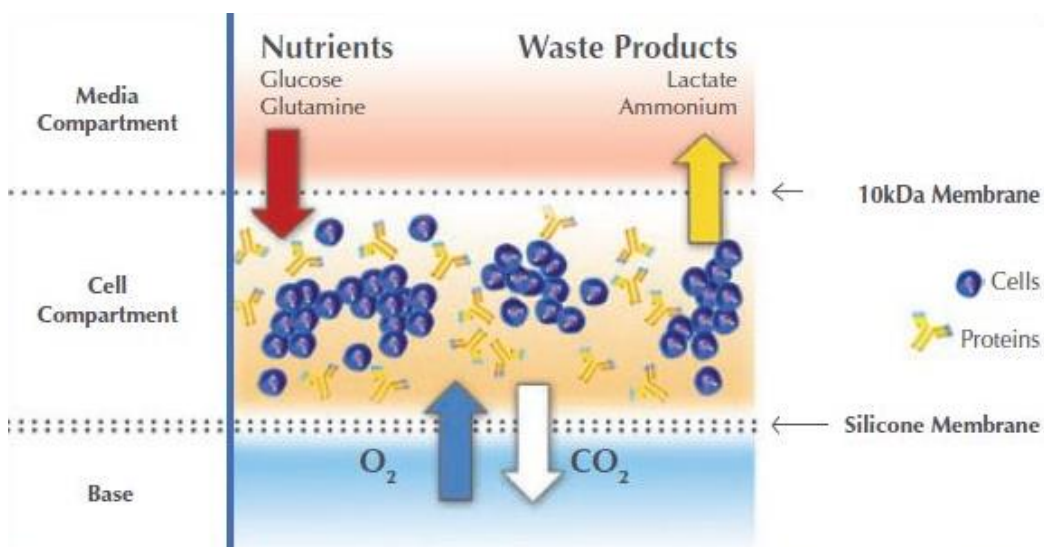
Figure 2.1: Overview of the chambers within the bioreactor flask. The cell compartment holds large quantities of cells. The 10kDa membrane above allows free movement of nutrients from the media above and smaller waste products from the cells. The 10kDa limit of this membrane traps large products produced by the cells, such as sEVs. The lower silicone membrane allows efficient gas exchange between the cells and the surroundings (The Lab Depot, 2018)

2.6.1 Bioreactor Flask Setup

1% (v/v) antibiotics (penicillin-streptomycin 10,000U/mL) was added to a fresh bottle of medium. 15mL was removed and 5% (v/v) FBS was added to the remaining medium. 50mL of this medium was added to the inside of the bioreactor flask for 5 minutes to wet the semi-permeable membrane and allow it to equilibrate. According to the protocol, $25x10^6$ cells were collected from T75 flasks and resuspended in the 15mL of serum free medium decanted prior. 5% (v/v) exosome depleted FBS (Thermo Fisher Scientific, Massachusetts, USA) was added to the cell suspension and all 15mL was added to the cell compartment using a serological pipette. The remaining media (roughly 500mL) was then added to the media compartment and cells were left for 10 days.

2.6.2 Media Collection

Cell compartment media was collected weekly. Outer chamber media was also changed weekly in coordination with collection chamber media.

For collection of inner chamber and changing of outer chamber media, a fresh bottle of DMEM/F-12 was pre-warmed to room temperature. All media from the collection chamber was removed using a 20mL serological pipette and added to a sterile 20mL universal container. 1% (v/v) antibiotics (penicillin-streptomycin 10,000U/mL) was added to the bottle of medium and 45mL was decanted into a sterile 50mL falcon tube. Ten millilitres of this was then used to wash the inner chamber 3 separate times using a fresh 20mL serological pipette, leaving 15mL. 5% (v/v) of exosome depleted FBS (Thermo Fisher Scientific, Massachusetts, USA) was added to the remaining 15mL of media. A final fresh 20mL serological pipette was used to add this 15mL of media into the collection chamber. The outer chamber was then emptied and discarded. 5% (v/v) of regular FBS was added to the remaining 455mL of media.

This media was then carefully poured into the outer chamber of the bioreactor flask, and both lids were tightened.

The universal container, containing the collected media was span twice at 2000xg for 5 minutes, and finally at 4000xg for 15 minutes to remove debris, pouring into fresh universal containers between each centrifugation. The media was then filtered through a 0.8μm filter and subsequently a 0.22μm filter using a 20mL syringe under sterile conditions and stored in a universal container at -80°C.

For the sEV isolation, media was defrosted in a 37°C water bath and the ultracentrifuge (Beckmann Coulter, Optima LE-80K) was cooled to 4°C. Media was then transferred to QuickSeal 33mL centrifuge tubes (Beckmann Coulter). 3-5mL of 30% sucrose/D_2O cushion consisting of 7.5g sucrose and 22.5g D_2O was carefully added to the bottom of the QuickSeal 33mL centrifuge tubes using a spinal needle pouring under gravity, underneath the media, being careful not to disturb the separate layers. Once all air was removed from the tube, the tips of the tube were sealed using a soldering iron and casting dye to create a uniform, air-tight seal. Media then underwent ultracenrifugation at 100,000xg for 60 minutes on a Beckmann Coulter SW32 swing arm rotor at 4°C. The sucrose cushion was then removed from the ultracentrifuge tubes using a syringe and spinal needle and diluted in enough PBS to fill another ultracentrifuge tube. The sucrose cushion/PBS mix was then added to a fresh ultracentrifuge tube using a spinal needle under gravity. Media was then ultracentrifuged again at 100,000xg for a further 60 minutes at 4°C on a 70Ti fixed arm rotor to pellet the sEVs. The sEV pellet was then resuspended in 500μL of PBS.

2.6.3 sEV Validation

2.6.3.1   Nano Particle Analysis

Nanoparticle Tracking Analysis (NTA) is a technique used to measure nanometre sized particles of 10-2000nm in liquids, under flow. NTA uses a high powered 488nm LM14 laser module which is scattered by nanoparticles flowing through the sample chamber in suspension. This scattering is recorded by a highly sensitive digital camera (OrcaFlash 2.8, Hamamatsu C11440, Hamamatsu City, Japan). NTA (Malvern Instruments, Malvern, UK). utilises the scattering of this light to determine the size of the nanoparticle over multiple frames as well as Brownian motion; the random motion of nanoparticles in suspension dependant on the temperature and viscosity of the liquid. The NanoSight^{TM} NS300 machine was calibrated using 100nm latex nanobeads (Malvern Instruments, Malvern, UK). For NTA, particles were suspended in particle free water (Fresenius Kabi, Runcorn, UK) to a concentration of $2x10^8$ and $9x10^8$ particles/mL. Samples were administered under a constant speed using a NanoSight syringe pump set to 50, and temperatures were kept at a constant 25°C. Tracking videos of 30 seconds were used and each sample had a total of 6 replicates. Videos were analysed using NTA software (version 3.1), with the camera sensitivity and detection threshold set to 14-16 and 1-3 respectively.

2.6.3.2   Protein Concentration Assay

The protein concentration of sEV samples was assessed using a Bio-Rad DC^{TM} Protein Assay kit (Bio-Rad Laboratories, Hemel-Hempstead, UK). Samples were diluted 1:8 in PBS and compared to a standard curve from 0-2000μg/mL of BSA. (see section 2.11.2 for assay details).

2.6.3.3   Immuno-Phenotyping Assay

SEVs were diluted in PBS and 1µg was added to each well of a High Protein Binding enzyme linked immunosorbent assay (ELISA) Strip 96 well plate (Greiner Bio-One, Germany). SEVs were incubated in the wells at 4°C overnight. Wells were washed 3 times using TRIS-wash buffer (Kaivogen, Finland). 1% BSA (w/v in PBS) blocking solution was added for 2 hours at room temperature and wells were subsequently washed 3 times. Primary antibodies (1µg/mL) were added and incubated for 2 hours at room temperature and subsequently washed 3 times. Bioatinylated secondary antibody (Perkin Elmer, USA) was diluted to 200ng/mL in 0.1% BSA (w/v in PBS) and incubated in wells for 1 hour at room temperature. Wells were washed again 3 times and a Europium-Streptavidin conjugate (Perkin Elmer) in assay buffer (Kaivogen) was added and incubated at room temperature for 45 minutes. Well were finally washed 6 times and enrichment intensifier (Kaivogen) was added and incubated at room temperature for 5 minutes. Time-resolved fluorescence (TRF) was measured using a PHERAstar FS Microplate Reader (BMG Labtech, UK)

2.6.3.4   Western Blot

PC3 sEV lysate (20µg) was analysed alongside PC3 cellular lysate (20µg) via western blot. See section 2.11 "methods for protein detection".

2.7   Methods for Gene Expression Detection

2.7.1 RNA Extraction

2.7.1.1   Cellular RNA

RNA extraction was carried out following the TRI Reagent protocol from Sigma-Aldrich as detailed below. When cells were ready, media was aspirated and washed with PBS before TRI Reagent was added (1mL per $5\text{-}10\text{x}10^5$ cells). TRI Reagent was mixed around the

well/flask thoroughly and passed multiple times through a pipette to ensure all cells were lysed. Cell lysate was then transferred to a sterile 1.5mL microcentrifuge tube and left at room temperature for 5 minutes. Two hundred microlitres of 1-bromo-3-chloropane is added to each tube and samples are vortexed for 15 seconds to ensure thorough mixing. Samples were then left for 15 minutes at room temperature before being centrifuged at 12,000g for 15 minutes at 4°C. The upper aqueous, RNA containing layer was carefully removed and 500μL of 2-propanol was added (500μL per mL of TRI Reagent). The mixture was vortexed and left to stand at room temperature for 10 minutes before centrifugation at 12,000g for 10 minutes at 4°C. The supernatant was discarded and RNA pellets were washed in 75% (v/v) ethanol before being centrifuged at 7,500xg for 5 minutes at 4°C. The ethanol was then removed and pellets were resuspended in 20μL of DEPC water.

2.7.1.2 RNAs in Media

For RNA extraction, 1mL of media was transferred to a sterile 1.5mL microcentrifuge tube and centrifuged at 2,000g for 5 minutes at 4°C. Eight hundred microlitres of media was taken from the top of the centrifuged media and transferred to a fresh 1.5mL microcentrifuge tube. This was then centrifuged at 16,000g for 15 minutes at 4°C. Five hundred microlitres was taken from the top of the newly centrifuged media and placed in a final 1.5mL sterile microcentrifuge tube and stored at -80°C until required.

RNA harvested from media was often too dilute to accurately quantify by Nanodrop (Thermo Fisher Scientific, Massachusetts, USA). Because of this, for media RNA extractions, *C. elegans* miR-39 was used as a housekeeping gene to control for changes in RNA extraction efficiency between samples. A constant volume was added before RNA extraction and samples were normalised to this C. *elegans* miR-39 level at the qPCR stage. Sufficient Trizol® LS (Thermo Fisher Scientific, Massachusetts, USA) for all current samples was added to a universal container along with a C. *elegans* miR-39 spike in control (1μL/mL of Trizol® LS). Seven

hundred and fifty microlitres of Trizol® LS was added to 250μL of media (prepared as described in section 1.3.2) in a sterile 1.5mL microcentrifuge tube and vortexed to mix thoroughly. Two hundred microlitres of 1-bromo-3-chloropane was then added and the reagents were vortexed again and left at room temperature for 2 minutes. The homogenate was then centrifuged at 12,000g for 15 minutes at 4°C. Three hundred microlitres of the upper aqueous, RNA containing layer was then carefully removed and transferred to a fresh sterile 1.5mL microcentrifuge tube and 2μL of Glycoblue (Thermo Fisher Scientific, Massachusetts, USA) was added to allow greater visualisation of the RNA pellet later. Five hundred microlitres of 100% 2-propanol (Fisher Chemical) was added to each tube, and the samples were left to incubate at room temperature for 10 minutes. Samples were then centrifuged at 12,000g for 25 minutes at 4°C. At this point a very small blue pellet was visible. All supernatant was carefully removed and the pellet was washed with 100μL of 75% ethanol:DEPC water. Samples were then centrifuged again at 12,000g for 5 minutes at 4°C and the supernatant was carefully removed. Samples were centrifuged briefly at 12,000g for 1 minute at 4°C and the remaining supernatant was very carefully removed with a 10μL tip and pipette. The pellet was then air dried for 2-5 minutes, dissolved in 20μL of DEPC water and stored at -80°C until use.

2.7.2 RNA Quantification

RNA quantity and purity was measured using an Implen Nanophotometer (Implen, Munich, Germany) set to detect single strand RNA. Absorbance was measured at 260nm and compared to a DEPC water blank.

2.7.3 Reverse Transcription

2.7.3.1   Advanced miRNA Reverse Transcription

Reverse transcription was carried out using the TaqMan® Advanced MicroRNA Assay kit following the supplied protocol (Thermo Fisher Scientific, Massachusetts, USA) as detailed below. The TaqMan® Advanced MicroRNA Assay is a 4 step process involving 4 separate mastermixes and thermal cycling runs (protocol dictates that all mastermixes contain an extra 10% to account for "variations in pipetting").

Guidelines dictated a maximum of 10ng of total RNA per reaction. Therefore RNA was diluted to a maximum of 5ng/µL, as 2µL of sample was to be used.

Step 1 Poly(A) Tailing Reaction:

The following mastermix was prepared in a sterile 1.5mL microcentrifuge tube;

Component	Per Reaction
10X Poly(A) Buffer	0.5µL
ATP	0.5µL
Poly A Enzyme	0.3µL
RNase-Free Water	1.7µL
Total Volume	**3µL**

The mastermix was vortexed and 3µL was combined with 2µL of sample in a sterile PCR tube (5µL total). The tube was then sealed, vortexed and centrifuged briefly to spin down the contents before being placed in a SimpliAmp Thermal Cycler (Thermo Fisher Scientific, Massachusetts, USA) under the following conditions:

Step	Temperature	Duration
Polyadenylation	37°C	45 minutes
Stop Reaction	65°C	10 minutes

We then proceeded immediately to the Ligation Reaction.

Step 2 Ligation Reaction:

The following mastermix was prepared in a fresh sterile 1.5mL microcentrifuge tube;

Component	Per Reaction
5X DNA Ligase Buffer	3µL
50% PEG 8000	4.5µL
25X Ligation Adaptor	0.6µL
RNA Ligase	1.5µL
RNase-Free Water	0.4µL
Total Volume	**10µL**

The mastermix was vortexed thoroughly and 10µL was combined with all 5µL from the Poly(A) Tailing reaction (15µL total). Tubes were vortexed briefly and centrifuged to spin

down contents. Tubes were then placed in a SimpliAmp Thermal Cycler (Thermo Fisher Scientific, Massachusetts, USA) under the following conditions.

Step	Temperature	Duration
Ligation	16°C	60 minutes

We then proceeded immediately to the Reverse Transcription Reaction.

Step 3 Reverse Transcription Reaction:

The following mastermix was prepared in a fresh sterile 1.5mL microcentrifuge tube;

Component	Per Reaction
5X RT Buffer	6μL
dNTP Mix (25mM each)	1.2μL
20X Universal RT Primer	1.5μL
10X RT Enzyme Mix	3μL
RNase-Free Water	3.3μL
Total Volume	**15μL**

The mastermix was vortexed and 15µL was combined with all 15µL from the Ligation Reaction (30µL total). Tubes were vortexed briefly and centrifuged to spin down contents. Tubes were then placed in a SimpliAmp Thermal Cycler (Thermo Fisher Scientific, Massachusetts, USA) under the following conditions.

Step	Temperature	Duration
Reverse Transcription	42°C	15 minutes
Stop Reaction	85°C	5 minutes

We then proceeded immediately to the miR-Amp Reaction.

Step 4: miR-Amp Reaction

The following mastermix was prepared in a fresh sterile 1.5mL microcentrifuge tube;

Component	Per Reaction
2X miR-Amp Master Mix	25µL
20X miR-Amp Primer Mix	2.5µL
RNase-Free Water	17.5µL
Total Volume	**45µL**

The mastermix was vortexed and 45µL was combined with 5µL of the reverse transcription reaction in a fresh PCR tube. Tubes were vortexed briefly and centrifuged to spin down contents. Tubes were then placed in a SimpliAmp Thermal Cycler (Thermo Fisher Scientific, Massachusetts, USA) under the following conditions.

Step	Temperature	Duration	Cycles
Enzyme Activation	95°C	5 minutes	1
Denature	95°C	3 seconds	14
Anneal/Extend	60°C	30 seconds	
Stop Reaction	99°C	10 minutes	1

Samples were then diluted 1:10 and stored at -20°C until use.

2.7.3.2 Standard miRNA Reverse Transcription

miRNA Reverse Transcription was carried out using a TaqMan MicroRNA Reverse Transcription Kit (Thermo Fisher Scientific, Massachusetts, USA) following the manufacturers protocol as detailed below. The protocol recommends using a maximum of 10ng of RNA per reaction, and as each reaction contains 5µL the RNA was diluted to a maximum of 2ng/µL.

All components were thawed and kept on ice throughout. The following mastermix was prepared:

Component	Per Reaction
100mM dNTPs (with dTTP)	0.15μL
MultiScribe™ Reverse Transcriptase, 50U/μL	1μL
10X Reverse Transcription Buffer	1.5μL
RNase Inhibitor, 20U/μL	0.19μL
Nuclease-Free Water	4.16μL
Total Volume	**7μL**

In a sterile PCR tube 7μL of mastermix was combined with 3μL of primer and 5μL of RNA sample. The solution was gently pipetted up and down to mix. Tubes were centrifuged to spin down contents and then placed in a SimpliAmp Thermal Cycler (Thermo Fisher Scientific, Massachusetts, USA) under the following conditions:

Temperature	Duration
16°C	30 minutes
42°C	30 minutes
85°C	5 minutes

cDNA samples were then stored at -20°C until use.

2.7.3.3   mRNA Reverse Transcription

RNA was diluted to 500ng in 10μL of PCR water to be reverse transcribed into cDNA. 10μL of

GoScript^{TM} Reverse Transcription Mix, Oligo(dT) (Promega) was added to the RNA in a sterile

PCR tube (20μL total). The mixture was vortexed and briefly centrifuged before being placed

in a SimpliAmp Thermal Cycler (Thermo Fisher Scientific, Massachusetts, USA) under the

following conditions:

Temperature	Duration
25°C	5 minutes
42°C	60 minutes
70°C	15 minutes

At this point samples were diluted 1:5 with PCR water and stored at -20°C until use.

2.7.4 Quantitative (q)PCR

All qPCR reactions were prepared in MicroAmp Fast Optical, barcoded, 96 well plates

(Thermo Fisher Scientific, Massachusetts, USA) using clear optical adhesive seals

(PrimerDesign, Southampton, UK).

2.7.4.1   SYBR® Green qPCR

SYBR® Green qPCR was performed on mRNA generated from the mRNA reverse transcription (section 2.7.3.3). For each reaction, 2µL of cDNA (diluted 1:5 as detailed in section 2.7.3.3) was combined with 8µL of mastermix containing the following components:

Component	Per Reaction
Sybr® Green PCR Master Mix	5µL
2.5pmol Primer Mix*	1µL
Nuclease-Free Water	2µL
Total Volume	**8µL**

*Primer Mix was a pre-made mix of 1µL forward primer, 1µL reverse primer and 38µL nuclease free water

Plates were placed in a StepOnePlus™ Real-Time PCR System Cycler (Thermo Fisher Scientific, Massachusetts, USA) under the following cycling conditions:

Stage	Temperature	Duration
Enzyme Activation	95°C	10 minutes
Cycling (50 cycles)	95°C	15 seconds
	60°C	60 seconds

CT values were recorded and gene expression was then quantified using the ΔΔCT method normalised to GAPDH and RPL-19 housekeeping genes for human cells and HPRT and β-Actin for mouse cells.

2.7.4.2   Taqman® qPCR

Conventional Taqman qPCR

Taqman® qPCR was also performed on mRNA generated from the mRNA reverse transcription (section 2.7.3.3). For each reaction, 2μL of cDNA (diluted 1:5 as detailed in section 2.7.3.3) was combined with 8μL of mastermix containing the following components:

Component	Per Reaction
Precision Fast 2x qPCR MasterMix	5μL
20x Primer	0.5μL
Nuclease-Free Water	2.5μL
Total Volume	**8μL**

Plates were placed in a StepOnePlus^{TM} Real-Time PCR System Cycler (Thermo Fisher Scientific, Massachusetts, USA) under the following cycling conditions:

Stage	Temperature	Duration
Enzyme Activation	95°C	20 seconds
Cycling (50 cycles)	95°C	1 second
	60°C	20 seconds

CT values were recorded and gene expression was then quantified using the ΔΔCT method normalised to GAPDH and RPL-19 housekeeping genes for human cells and HPRT and β-Actin for mouse cells.

Advanced miRNA Taqman® qPCR

Taqman® qPCR was also performed on cDNA reverse transcribed using the Taqman® Advanced miRNA Assays kit (section 2.7.3.1).

For each reaction, 5µL of cDNA (diluted 1:10 as described in section 2.7.3.1) was combined with 15µL of mastermix containing the following components:

Component	Per Reaction
Precision Fast 2x qPCR MasterMix	10µL
20x Primer	1µL
Nuclease-Free Water	4µL
Total Volume	**15µL**

Plates were placed in a StepOnePlus™ Real-Time PCR System Cycler (Thermo Fisher Scientific, Massachusetts, USA) under the following cycling conditions:

Stage	Temperature	Duration
Enzyme Activation	95°C	20 seconds
Cycling (50 cycles)	95°C	1 second
	60°C	20 seconds

2.7.5 Gel Electrophoresis

DNA fragments were separated based on their size using agarose gel electrophoresis. Samples were loaded onto a 0.5-2% w/v agarose gel, dependant on the size of the DNA fragment. Agarose gels were prepared by measuring 50 or 150mL of 1x Tris/Borate/EDTA (TBE) (depending on the size of the gel tank used) into a flask and adding an appropriate weight of agarose (Melford Chemicals, Suffolk, UK) depending on the % of the gel. The mixture was then heated in a microwave until the agarose was completely dissolved. The agarose solution was allowed to cool slightly before 10-20μL of SYBR safe (Abnova, Taiwan) was added, depending on the gel volume. Gels were then poured into the tanks which contained plastic combs (SCIE-PLAS, Cambridge, UK), allowing the formation of loading wells within the gel. Once the gels had cooled to room temperature and solidified, they were submerged in 1x TBE and the combs were removed. Five microlitres of ladder (either PCR ranger or high ranger depending on expected fragment size) was added to the first well and 8-20μL of sample was added to the remaining wells. Gel tanks were then connected to EV243 power consorts (Topac Inc., Cohasset, USA) and run using electrophoresis conditions of 100V, 150mA and 50W for 30 minutes to 2 hours to separate DNA fragments sufficiently.

Gels were visualised using a U: Genius 3 Gel Doc system (Syngene, Cambridge, UK), which was also used to capture images of the gels.

2.7.5.1 Gel Purification

DNA bands are located using the U: Genius 3 Gel Doc system (Syngene, Cambridge, UK) following the manufacturers protocol. Gel bands are then excised using a scalpel and added to 1.5mL microcentrifuge tubes before being weighed. For DNA extraction, a Wizard® SV Gel and PCR Clean-Up System kit (Promega, Wisconsin, USA) was used. Ten microlitres of Membrane Binding solution per 10mg of gel was added to each tube. Tubes were incubated at 50-65°C until the gels had completely dissolved. One SV Minicolumn per gel was inserted

into a fresh tube and the dissolved gel solutions were added. Tubes were incubated at room temperature for 1 minute and centrifuged at 16,000xg for 1 minute, flowthrough was discarded. SV Minicolumns were reinserted and 700µL of Membrane Wash Solution was added to each column. Tubes were centrifuged again at 16,000xg and flowthrough was again discarded. The wash step was then repeated with 500µL and tubes were centrifuged at 16,000xg for 5 minutes. Flowthrough was discarded and the empty SV Minicolumns were centrifuged at 16,000xg for 1 minute with lids open to remove residual ethanol. SV Minicolumns were transferred to fresh 1.5mL microcentrifuge tubes and 50µL of nuclease-free water was added to the membrane of each column. Columns were incubated for 1 minute at room temperature centrifuged at 16,000xg for 1 minute to elute the DNA. SV Minicolumns were discarded and microcentrifuge tubes containing eluted DNA were stored at -20°C.

2.7.6 Bioanalysis

Bioanalysis displays the size and quantity of RNAs within the population you are measuring using micro-capillary based electrophoresis. For RNA destined for sequencing or digestion by RNase, bioanalysis was used to visualise the isolated RNA population. An agilent RNA 6000 Nano Kit was used for sequencing library visualisation or the Agilent RNA 6000 Pico Kit for sEV RNA digest visualisation. As per the manufacturer's instructions, running gel was added to the analysis chip along with ladder and the RNA sample and samples were analysed using a 2100 Bioanalyser (Agilent, Santa Clara, CA, USA).

2.8   Methods for Plasmid Cloning

2.8.1 Preparation of Over Expression Plasmids

Coding regions of genes were amplified from original plasmids or cDNA by PCR using primers detailed in table 2.4. For amplification, the following mix was combined in a fresh PCR tube:

Component	Amount
GoTaq®G2 Green Master Mix	15µL
PCR Water	12.5µL
15ng/µl cDNA/Plasmid	2µL
10pmol Forward Primer	0.25µL
10pmol Reverse Primer	0.25µL
Total Volume	**30µL**

The mixture was then placed in a StepOnePlus™ Real-Time PCR System Cycler (Thermo Fisher Scientific, Massachusetts, USA) under the following cycling conditions:

Step	Temperature	Duration	Cycles
Initial Denaturation	95°C	5 minutes	1
Denaturation	94°C	30 seconds	
Annealing	55°C	40 seconds	25
Extension	72°C	1 minute per kb	
Final Elongation	72°C	10 minutes	1
Hold	4°C	∞	1

DNA was inserted into the pEF6/V5-His TOPO vector for over expression. This vector ligates the PCR product directly into the plasmid backbone. For insertion, the following components were combined in a fresh PCR tube and incubated at room temperature for 5 minutes, before being placed on ice ready for use:

Component	Amount
10ng/µl pEF6/V5-His TOPO	1µL
DNA (neat from amplification step)	4µL
Salt Solution*	1µL
Total Volume	**6µL**

*Salt solution: 1.2M NaCl, 0.06M $MgCl_2$

Overexpression plasmids were now ready for transformation into E. *coli*.

2.8.2 Preparation of miRNA Luciferase Reporter Plasmid

2.8.2.1 Annealing miRNA Oligos

Forward and reverse miRNA oligos (Eurofins Scientific, Luxembourg) were annealed by combining the following components in a fresh PCR tube:

Component	Amount
1µg/µl Forward Oligo	1µL
1µg/µl Reverse Oligo	1µL
Annealing Buffer*	46µL
Total Volume	**50µL**

*Annealing Buffer: 10mM Tris-HCl pH7.5-8, 50mM NaCl, 1mM EDTA.

The mix was then vortexed and centrifuged briefly to combine and placed in a StepOnePlus^{TM} Real-Time PCR System Cycler (Thermo Fisher Scientific, Massachusetts, USA) under the following cycling conditions:

Temperature	Duration
90°C	3 minutes
37°C	15 minutes

Oligos were then diluted 1:10.

2.8.2.2 Cutting pmirGLO Vector for Insertion

The pmirGLO vector was then cut twice using restriction enzymes ready for insertion as follows:

The following components were combined in a fresh PCR tube and heated at 37°C for 1 hour:

Component	Amount
300ng/µl pmirGLO Plasmid	30µL
5U/µl PME1	2µL
10X Buffer*	5µL
Nuclease-Free Water	13µL
Total Volume	**50µL**

*PME1 requires buffer B (Thermo Fisher)

The vector was then purified using a Wizard® SV Gel and PCR Clean-Up System kit (Promega, Wisconsin, USA) as detailed in section 2.7.6.1 (treating 50µL as 50µg of gel) and eluted in 30µL of RNase free water.

The purified vector was then combined with the following components and heated to 37°C for 1 hour again:

Component	Amount
Purified pmirGLO Plasmid (cut 1 time)	30µL
10U/µl XBAI	1µL
10X Buffer*	4µL
Nuclease-Free Water	4µL
Total Volume	**40µL**

*XBAI requires SH buffer (Sigma)

The vector, now cut twice, was run on a 1% agarose gel. A band within the gel at 7.3Kb, representing the cut vector, was extracted and purified using a Wizard® SV Gel and PCR Clean-Up System kit (Promega, Wisconsin, USA) as detailed in section 2.7.6.1, and quantified (16.5ng/µL).

2.8.2.3   Ligating miRNA Insert and Cut pmirGLO Vector

For ligation, the following components were combined in a fresh PCR tube and left at 16°C overnight:

Component	Amount
Purified pmirGLO Plasmid (cut 2 times) (50ng*)	3µL
Annealed Oligos (neat from annealing reaction)	1µL
400U/µl T4 DNA Ligase	1µL
10X T4 DNA Ligase Buffer	1µL
Nuclease-Free Water	4µL
Total Volume	**10µL**

*50ng total= ~3µl of 16.5ng/µl (from previous reaction)

pmirGLO reporter was now ready for transformation into E. *coli.*

2.8.3 Transformation of Chemically Competent E. *coli*

Transformations were performed using One Shot® TOP10 Chemically Competent *E. coli* (Thermo Fisher Scientific, Massachusetts, USA) following the manufacturers protocol as detailed below.

Per transformation, one vial (~60µL each) of One Shot® TOP10 chemically competent cells were thawed on ice. One to five microlitres of DNA (10pg-100ng) was added per vial and

mixed gently (not via pipetting). A control was included by adding 10pg of pUC19 to an extra vial of One Shot® TOP10 chemically competent cells, to show transformation efficiency. Vials, now containing E. *coli* and DNA, were incubated on ice for 30 minutes and heat-shocked at 42°C for 30 seconds before returning them to ice for another 2 minutes. In a sterile class II laminar flow cabinet, 250μL of room temperature S.O.C Medium was aseptically added to each vial. Vials were tightly capped and shaken horizontally at 37°C for one hour at 225 rpm. After one hour 100μL and 50μL from each vial was spread onto two room temperature selective plates made from LB-agar (see section 2.4.4.2) with 1μL/mL Ampicillin (plating two volumes gives a greater chance for one plate to have well-spaced colonies for picking). For the pUC19 control, the transformation mix was diluted 1:10 in LB (2.4.4.1 which was then plated the same way as the sample vials. Plates were inverted and stored upside down at 37°C overnight. The following day, individual colonies were carefully picked using an inoculation loop and shaken at 225 rpm at 37°C in 5mL of LB for a further 24 hours.

2.8.4 Plasmid Extraction

Plasmid extraction was done using a GenElute™ Plasmid Miniprep Kit (Sigma-Aldrich) following the manufacturers protocol as described below. All centrifugations were performed at 12,000g unless stated otherwise.

Five millilitres of overnight cultured plasmid containing cells was pelleted in a sterile 2mL microcentrifuge tube and supernatant was discarded. Samples were centrifuged at a maximum volume of 2mL due to the maximum volume of the microcentrifuge tubes, therefore for any volumes over 2mL cells were centrifuged multiple times with supernatant being discarded in between. Cell pellets were then resuspended in 200μL of Resuspension Solution by vortexing or pipetting. Two hundred microlitres of Lysis Solution was added to each tube and mixed gently by inversion before allowing to clear for 5 minutes. Three hundred and fifty microlitres of Neutralisation Solution was added and tubes were inverted

4-6 times to mix thoroughly. Neutralisation of the solution created a cloudy precipitate within the tube which was pelleted at 14,000g for 10 minutes. Whilst the neutralised mixture was pelleting one GenElute Miniprep Binding Column per sample was placed in a fresh 2mL collection tube. The table below details the remaining solutions added to each column for the plasmid washing and elution. Between the additions of each solution, the columns were centrifuged for 1 minute and the flow through collected in the 2mL collection tube was discarded.

Component	Amount
Column Preparation Solution	500µL
Clear Lysate from Neutralisation Step	All Supernatant
Optional Wash Solution	500µL
Wash Solution	750µL

Following the discarding of the flowed through Wash Solution, tubes were placed back in the centrifuge and centrifuged for a further minute to dry the columns. Columns were then transferred to a fresh 2mL collection tube and 50µL of Elution Solution was carefully added onto the membrane within the column. Tubes were then centrifuged for a final time for 1 minute to collect the purified plasmid, which was stored at -20°C until use.

2.8.5 Plasmid Quantification

Plasmid quantity and purity was measured using an Implen Nanophotometer (Munchen, Germany) set to detect DNA. Absorbance was measured at 260nm and compared to unused Elution Solution from the GenElute™ Plasmid Miniprep Kit (Sigma-Aldrich) as a blank.

2.8.6 Plasmid Verification

Further restriction enzyme digestion of plasmids was used to verify insertion of DNA sequences was successful. Successfully inserted plasmids were then sent for sequencing to determine whether orientation of the inserts was correct and that mutations had not occurred.

2.8.7 Large Scale Plasmid Extraction

Once sequencing had confirmed the positive insertion of the DNA sequence, E. *coli* were re-transformed and the plasmid was extracted on a larger scale using a PureYield™ Plasmid Maxiprep System (Promega). 200mL of E. *coli* was pelleted at 5,000xg for 10 minutes at room temperature, 50mL at a time, in a 50mL falcon tube. Pellets were resuspended in 12mL of Cell Resuspension Solution and another 12mL of Cell Lysis Solution was added and mixed. 12mL of Neutralisation Solution was then added and mixed thoroughly. Neutralised solution was centrifuged at 7,000xg for 30 minutes at room temperature. Plasmid purification was performed using a vacuum pump and PureYield™ Clearing/Maxi-Binding Columns. All supernatant from the centrifuged neutralised solution was filtered and washed with 5mL Endotoxin Removal Wash and 20mL of Column Wash. Once dry, the plasmid was eluted from the filter using 1mL f nuclease free water, quantified and stored at -20°C until use.

2.8.8 Plasmid Transfections

Cells were transfected using a Lipofectamine[TM] 3000 kit (Thermo Fisher Scientific, Massachusetts, USA) following the manufacturers protocol. Cells to be transfected were seeded and allowed to reach ~80% confluency. Transfections were prepared in two separate tubes, the components of which are described as following (per transfection):

Component	Tube A	Tube B
Opti-MEM® Medium	6 Well: 125µL 24 Well: 25µL 96 Well: 5µL	6 Well: 125µL 24 Well: 25µL 96 Well: 5µL
Lipofectamine® 3000 Reagent	6 Well: 3.75µL 24 Well: 0.75µL 96 Well: 0.15µL	n/a
Plasmid	n/a	6 Well: 5µg 24 Well: 1µg 96 Well: 0.2µg
P3000[TM] Reagent	n/a	6 Well: 10µL 24 Well: 2µL 96 Well: 0.4µL

The two tubes were then combined and incubated for 15 minutes at room temperature. The mixture was then added to medium of the plated cells and cells were incubated for 2 days.

Cells were then selected with antibiotic media depending on the resistance gene found within the plasmid, and single colonies collected and expanded.

2.9 Methods for Oligo Transfection

miRNA oligos were transfected using a Lipofectamine™ 3000 kit (Thermo Fisher Scientific, Massachusetts, USA) following the manufacturers protocol for RNA. For RNA transfection, P3000 reagent is not used. Cells to be transfected were seeded and allowed to reach ~80% confluency. Transfections were prepared in two separate tubes, the components of which are described as following (per transfection):

Component	Tube A	Tube B
Opti-MEM® Medium	6 Well: 125µL 24 Well: 25µL 96 Well: 5µL	6 Well: 125µL 24 Well: 25µL 96 Well: 5µL
Lipofectamine® 3000 Reagent	6 Well: 3.75µL 24 Well: 0.75µL 96 Well: 0.15µL	n/a
Oligo (10pmol/µL)	n/a	6 Well: 12.5µL 24 Well: 2.5µL 96 Well: 0.5µL

The two tubes were then combined and incubated for 15 minutes at room temperature. The mixture was then added to medium of the plated cells and cells were incubated for 2-3 days.

2.10 Methods for Sequencing

Two forms of sequencing were performed during this research project; miRNA sequencing and mRNA sequencing. The preparation of these two libraries is different, as detailed below. However, prepared libraries are sequenced using a common protocol, detailed after the library preparation sections.

2.10.1 Preparation of cDNA Libraries

2.10.1.1 Preparation of small RNA cDNA Library

RNA was extracted from cells and sEVs using TRI Reagent (Sigma) as detailed in section 2.7.1.1. RNA was then filtered to remove any RNA >200nt using a mirVana miRNA Isolation Kit (LifeTechnologies) following the manufacturers protocol. miRNA cDNA libraries were then prepared using a NEXTFlex^{TM} Small RNA-Seq Kit v3 (Bioo Scientific, Texas, USA) following the manufacturers protocol. Library sizes were analysed by bioanalysis.

2.10.1.2 Preparation of mRNA cDNA Library

PolyA mRNA was isolated from total RNA using a Dynabeads mRNA DIRECT Kit (Life Technologies). mRNA cDNA libraries were then prepared using the Total RNA-seq kit (Life Technologies) following the manufacturers protocol. Briefly, mRNAs were fragmented using RNase III to produce a library of <200bp.

2.10.2 Common Library Generation and Templating Steps

Once a library of <200nt RNA was generated, either by filtration in the case of miRNA or fragmentation in the case of mRNA, there are a number of common steps used to generate cDNA libraries ready for sequencing. The first step is the ligation of adaptors onto the RNA to allow for reverse transcription, generating cDNA. cDNA is then amplified using unique barcoded primers and attached to the surface of Ion Sphere^{TM} Particles (ISPs) using an Ion

PI^{TM} Template OT2 200 Kit v3 (Life Technologies) performed on an Ion OneTouch^{-TM} Instrument (Life Technologies). Attachment of cDNA to ISPs is performed in a 1:1 ratio with the aim of attaching a single cDNA strand to each bead. An emulsion PCR was used to amplify this single cDNA strand up to coat the surface of the bead. Template positive ISPs were loaded onto a P1 chip and sequenced using an Ion Proton Sequencer (Life Technologies).

An overview of this final common process, from adapter ligation to sequencing is shown in figure 2.2.

1) Ligation of 3' Adenylated Adapter and 5' Adapter

NNNN — NNNN
5' Adapter — RNA — 3' Adenylated Adapter

2) Reverse Transcription

1st strand synthesis product — RT Primer
NNNN
5' Adapter — RNA — 3' Adenylated Adapter

3) PCR and Size Selection

1st strand synthesis product
Universal Primer
Barcode Primer 1

4) Attachment of cDNA to Ion Sphere™ Particles

5) Sequencing of cDNA

A G T G A C T A T G

Figure 2.2: Overview of Common Library Preparation and Templating Steps for Sequencing. Adapted from Bioo Scientific and Life Technologies kits.

2.10.3 Bioinformatics

2.10.3.1   Partek Genomics Suite

Sequencing produced BAM files which were processed using Partek Genomics Suite. Raw data was processed according to the following flow diagram (figure 2.3):

```
┌─────────────────────────────┐
│        Base Calling         │
│ (Determining bases based on │
│   the pH signals from the   │
│          sequencer)         │
└─────────────────────────────┘
              │
              ▼
┌─────────────────────────────┐
│      Adapter Trimming       │
│ (Removal of adaptor         │
│  sequences ligated as part  │
│  of library preparation)    │
└─────────────────────────────┘
              │
              ▼
┌─────────────────────────────┐
│     Barcode Deconvolution   │
│ (Sorting of reads into      │
│  samples based on           │
│  individual barcodes)       │
└─────────────────────────────┘
              │
              ▼
┌─────────────────────────────┐
│  Alignment of Reads to      │
│  Human Genome 19            │
└─────────────────────────────┘
              │
              ▼
┌─────────────────────────────┐
│     Map to Reference Genes  │
│ (map reads to genomic       │
│  locations and determine    │
│  which RNA the read         │
│  corresponds to)            │
└─────────────────────────────┘
              │
              ▼
┌─────────────────────────────┐
│ Reads per Kilobase per      │
│ Million Mapped Reads (RPKM) │
│ Normalisation               │
│ Normalises reads based on   │
│ the length of the RNA and   │
│ the number of overall reads │
└─────────────────────────────┘
```

Figure 2.3: Brief overview of Partek Genomics Suite processing of sequencing data.

2.10.3.2   Ingenuity Pathway Analysis (IPA)

IPA was used for pathway analysis, in the prediction of both upstream regulators and downstream affected pathways. P values for gene changes between treated and untreated cells were uploaded and a "bone cell" downstream pathways were predicted, along with upstream regulators, including miRNAs.

2.11 Methods for Protein Detection

2.11.1 Protein Extraction

Flasks were washed 3 times with PBS and scraped into lysis buffer (150mM NaCL, 50mM Tris, 0.02% Sodium azide, 0.5% Sodium deoxycholate, 1.5% Triton X-100 and a protease inhibitor tablet) (250μL for T25 and 500μL for T75 flasks). Lysate was then transferred to a 1.5mL microcentrifuge tube and placed on a Labinoco rotating wheel (Wold Laboratories, York, UK) for at least 1 hour at 25rpm and 4°C. Lysates were then centrifuged at 16,000xg for 15 minutes and the supernatant was transferred to a fresh 1.5mL microcentrifuge tube.

2.11.2 Protein Quantification

A Bio-Rad DC^{TM} Protein Assay kit (Bio-Rad Laboratories, Hemel-Hempstead, UK) was used to determine protein concentrations of samples. A standard curve was made using BSA serially diluted 12 times (1:2) in lysis buffer from 50mg/mL to 0.024mg/mL. 5μL of samples and standards were added to a 96-well plate. 25μL of reagent A' (2% (v/v) reagent S in reagent A) was added to each sample, followed by 200μL of reagent B. After 15 minutes, absorbance was read at 750nm using an ELx800 plate reading spectrophotometer (Bio-Tek, Wolf Laboratories, York, UK). A standard curve was generated from the serially diluted BSA. All samples were performed in duplicate and protein concentration was extrapolated from the standard curve using a third-order polynomial equation.

Protein samples were the diluted to the same concentrations and combined 1:1 with 2x Laemmli Buffer (Sigma-Aldrich). Samples were then boiled at 100°C for 10 minutes and frozen at -20°C until use.

2.11.3 Sodium Dodecyl Sulfate–Polyacrylamide Gel Electrophoresis (SDS-PAGE)

Separation of protein by SDS-PAGE was done using a 2-part gel system, consisting of 5% stacking gel and 10% resolving gel (for components and volumes see tables 2.6 and 2.7 respectively). Proteins were separated using a polyacrylamide gel; stacking gel – 5% (v/v), running gel 10% (v/v).

Table 2.6 Components and volumes for 5% stacking gel

Component	Volume (mL)
H_2O	2.7
30% Acrylamide/Bis-Acrylamide Solution	0.67
1.5M Tris (pH 8.8)	0.5
10% SDS	0.04
10% Ammonium Persulfate	0.04
TEMED	0.004

Table 2.7 Components and volumes for 10% resolving gel

Component	Volume (mL)
H_2O	5.9
30% Acrylamide/Bis-Acrylamide Solution	5
1.5M Tris (pH 6.8)	3.8
10% SDS	0.15
10% Ammonium Persulfate	0.15
TEMED	0.006

Once prepared, the resolving gel was loaded between glass plated held in place by a loading cassette, and left to polymerase at room temperature. When set, the stacking gel was prepared and loaded on top of the resolving gel. A well forming Teflon comb was added to the stacking gel whilst still liquid. Once set, the loading cassette was transferred to an electrophoresis tank and filled with running buffer. Combs were removed and samples were loaded along with 8µL of BLUeye Prestained Protein Ladder (Geneflow Ltd., Staffordshire, UK). Electrophoresis was run at 120V, 60mA, 50W for 2 hours.

2.11.4 Transfer of Protein onto Polyvinylidene Fluoride (PVDF) Membrane

PVDF membranes were first activated in 100% methanol, before being washed in H_2O and finally in transfer buffer. 2 pieces of filter paper were also soaked in transfer buffer. Filter paper was placed on the bottom part of the semi-dry transfer tank and the PVDF membrane was added on top. Gels were removed from the glass plates and placed on top of the membrane, followed by the second piece of filter paper. Air bubbles were removed with a roller and the top section of the semi-dry transfer tank was placed on top. Semi-dry transfer was run at 15V, 500mA, 50W for 50 minutes.

2.11.5 Immuno-Blotting

Membranes were blocked using 5% (w/v) powdered milk (Marvel) in TBS-Tween (TBS-T) for 1 hour. Membranes were incubated with primary antibody overnight in TBS-T with 3% (w/v) powdered milk solution and 0.1% (v/v) Tween-20, under rotation at 4°C (for primary antibody dilutions see table 2.4). The following day, membranes were washed 3 times with 0.1% (v/v) TBS-T, under rotation at RT for 10 minutes. Membranes were then incubated with secondary antibodies, diluted 1:1000 in TBS-T with 3% (w/v) powdered milk solution, under rotation at RT for 1 hour. Membranes were then washed 2 times with 0.1% (v/v) TBS-Tween-20 and a final time with TBS, under rotation at RT for 10 minutes. Membranes were developed for 3

minutes in EZ-ECL solution (Biological Industries) prepared by mixing equal parts solution A and B. Images were captured using the G-BOX (Syngene). Semi-quantitative analysis was performed using Image J software (National Institute of Health, NY, USA).

2.12 Methods for Cellular Assays

2.12.1 Calcium Staining

Quantification of calcium staining was performed using a 2 part method, staining calcium with Alizarin Red S and subsequently normalising to cell number using a crystal violet assay.

2.12.1.1   Alizarin Red S Stain

Calcium staining was performed to visualise the level of mineralisation in cultured bone cells. Alazarin Red (2% w/v, pH 4.2) was used to stain for calcium. Cells were grown in 6, 24 or 96 well plates. Once ready for staining, cells were removed from the incubator and media was carefully aspirated. Cells were then gently washed with PBS, and enough 10% formalin was added to cover the cells for at least 30 minutes (1mL for 6 wells, 500µL for 24 wells, 100µL for 96 wells). After at least 30 minutes, the formalin was aspirated and cells were washed with the same volume of distilled water. After allowing the plate to dry, the same volume of Alizarin Red S was added to each well to completely cover the cells and wells were incubated for 45 minutes at room temperature in the dark. The stain was them aspirated and cells were washed 4 times with the same volume of distilled water. Cells were then imaged using a light microscope. For stain quantification, Alizarin Red S stain was eluted in 10% acetic acid (1mL for 6 wells, 500µL for 24 wells and 200µL for 96 wells), using an oscillating plate for at least 15 minutes to completely dissolve the Alizarin Red S. 200µL was then transferred to a clear 96 well plate and absorbance was calculated at 450nm using a GloMax plate reader (Promega).

2.12.1.2   Crystal Violet Assay

Crystal violet assays were performed on wells following Alizarin Red S staining to visualise and quantify cell density. Acetic acid remaining from Alizarin Red S staining was removed and wells were carefully washed with water 3 times. After washing, plates were placed upside down on tissue to dry completely. Enough crystal violet solution to cover the cells was then added and left for 15 minutes. Crystal violet was then aspirated and wells were washed 4 times with water. 10% acetic acid was then added (5mL for 6 well, 1mL for 24 well, 200μL for 96 well) and left on an oscillating plate for at least 15 minutes to completely dissolve the crystal violet. 200μL was then transferred to a clear 96 well plate and absorbance was calculated at 600nm using a GloMax plate reader (Promega).

2.12.2 Additional Osteoblast Staining

2.12.2.1   Alkaline phosphatase (AP) Stain

One SigmaFast^{TM} 5-bromo-4-chloro-3-indolyl phosphate/nitro blue tetrazolium (BCIP/NBT) tablet (Sigma Aldrich) was dissolved in 10mL dH$_2$O. Media was removed and cells were washed with PBS. Cells were fixed in 10% formalin for 60 seconds and washed with dH$_2$O. Enough BCIP/NBT solution to cover the cells was added and incubated in the dark for 10 minutes. BCIP/NBT solution was then removed and cells were washed with PBS. Cells were then visualised under a light microscope to observe alkaline phosphatase staining.

2.12.2.2   Von Kossa Stain

Media was removed from cells and cells were washed with dH$_2$O. 1% aqueous silver nitrate (w/v in dH$_2$O) was added to cells and incubated for 1 hour in UV light. Silver nitrate was then removed and cells were washed with dH$_2$O. Excess silver nitrate was removed by covering cells with 5% sodium thiosulfate (w/v in dH$_2$O) for 5 minutes. Cells were then washed for a

final time in dH$_2$O. Cells were then visualised under a light microscope to observe Von Kossa staining.

2.12.3 Luciferase Assay

Luciferase assays were performed using the Dual-Glo® Luciferase Assay System (Promega) Cells were grown on 96 well plates. After treatment, media was removed, 20μL 1x reporter lysis buffer was added and plates were frozen at -20°C for 1 hour to allow full lysis. Plates were then defrosted, 100μL of Dual-Glo® Reagent was added and after 15 minutes, 100μL was transferred to a white 96 well plate and firefly luminescence was analysed. 100μL of Dual-Glo® Stop & Glo® Reagent was then added, and after 15 minutes, *Renilla* luminescence was analysed. For calculating relative luminescence, firefly luciferase was divided by *Renilla* luciferase for each sample. (Luminescence was analysed using a GloMax Plate Reader (Promega)).

2.12.4 MTT Assay

Cells were plated on clear 96 well plates. 100mg of Thiazolyl Blue Tetrazolium Bromide (MTT) (Sigma Aldrich) was diluted in 20mL of PBS and filtered through a minisart 0.2 μm sterile filter (Sartorius Stedim Biotech) to sterilise. MTT was added 1:10 to the media (11μL added to 100μL media) and incubated at 37°C or 4 hours. Media was subsequently aspirated and the purple precipitate was dissolved in 200μL DMSO. Absorbance was quantified at 600nm using a GloMax Plate Reader (Promega).

2.12.5 Cell Death Assay

Cell death assay was performed using a CellToxTM Green Cytotoxicity Assay (Promega). 1000x CellTox^{TM} Green Dye was diluted 500x in Assay Buffer to make a 2X Reagent. This was then combined 1:1 with media (100μL + 100μL) and incubated for 15 minutes at room

temperature in the dark. Fluorescence was then measured at 490nm excitation and 510-570 emission using a GloMax Plate Reader (Promega).

2.12.6 ROS Production Assay

ROS production assay was performed using the ROS-Glo^{TM} H_2O_2 Assay (Promega). Reconstitution buffer and lyophilised Luciferin Detection Reagent were combined to make the Reconstituted Luciferin Detection Reagent. Before use, 10μL of D-Cysteine and Signal Enhancer Solution was added to 1mL Reconstituted Luciferin Detection Reagent to make the ROS-Glo^{TM} Detection Solution. After treatment, 20μL of H_2O_2 Substrate Solution was added to 80μL of media and cells were incubated at 37°C for 6 hours. 100μL of ROS-Glo^{TM} Detection Solution was then added and cells were incubated for 20 minutes at room temperature. Luminescence was then analysed using a GloMax Plate Reader (Promega).

2.12.7 Osteoclast Pit Formation Assay

RAW 264.7 cells were seeded in a 24 well Corning® Osteo Assay Surface plates (30,000 cells/well) and left to seed overnight. Cells were then treated for 7 days, after which media was removed and cells were removed by incubation with 10% bleach for 5 minutes. Bleach was then removed and wells were washed 3 times each with dH_2O. Wells were then covered with Alizarin Red S for 45 minutes, which was then removed and washed with dH_2O. After drying, wells were imaged using a bright field microscope.

To determine resorbed area, images were grouped and ImageJ software was used to highlight the resorption pits. A colourimetric threshold was chosen that highlighted resorption pits and differentiated them from unresorbed calcium. This same threshold was applied to all grouped images to maintain consistency. Once highlighted, combined pit area for each image was calculated using the same ImageJ software.

2.13 Statistical Analysis

SigmaPlot 11.0 (Systat, San Jose, USA) was used for all statistical analysis, with the exception of sequencing IPA. Experiments were repeated at least 3 times (unless otherwise stated), showing the mean of all repeats, with error bars showing either standard deviation (SD) or standard error of the mean (SEM) as stated in the figure legends. An unpaired T-test or one-way ANOVA were performed to test statistical significance. For ANOVA analysis, post hoc tests are described in the figure legend. Mann-Whitney Rank Sum test was used on non-normally distributed data. Significance symbolised by asterisk (*), $*p<0.05$, $**p<0.01$ and $***p<0.001$.

Chapter III: Characterisation of the Mineralising 7F2 Osteoblast Cell Line

3 Characterisation of the Mineralising 7F2 Osteoblast Cell Line

3.1 Introduction

The metastases of PCa cancer are associated with considerably higher rates of morbidity and mortality than localised PCa (Sieh *et al.*, 2013; Tangen *et al.*, 2003). The most common metastatic site of PCa is the bone, which represents around 84% of secondary tumours (Gandaglia *et al.*, 2014). Although several hypotheses exist, the exact nature of this preferential tendency of PCa to metastasise to the bone is not fully understood. Furthermore, once the cancer cells reach the bone there are several stages associated with the progression of a secondary tumour. These include invasion of the bone marrow via the vasculature, an initial osteoclastic stage of localised bone debulking to allow PCa cell entry and finally the development of a secondary tumour (metastatic deposit) and its associated bone lesion. These lesions can be either osteolytic or osteoblastic depending on whether the osteoclasts or osteoblasts (respectively) dominate. Roughly 84% of lesions caused by PCa secondary tumours are osteoblastic (Charhon *et al.*, 1983; Roudier *et al.*, 2004), thus the hypotheses of this chapter and thesis are primarily focused on osteoblast function.

PCa metastases are associated with considerably higher mortality rates (Sieh *et al.*, 2013; Tangen *et al.*, 2003) and lead to a heavily reduced quality of life. For example, the local cells within an osteoblastic lesion produce a number of pro-hyperalgesic (pain sensitising) mediators (Muralidharan & Smith, 2013) and can also influence the sprouting of new pain sensing nerves known as nociceptors (Jimenez-Andrade *et al.*, 2010), resulting in significant pain. The debilitating nature of PCa bone metastases, along with decreased survival, highlights why a greater understanding of the pathophysiology is crucial.

The signalling network that governs the balance between osteoclast and osteoblast function is complex and features a wide range of molecules. These factors promote an environment in which osteoblastogenesis and osteoblast function are increased.

Osteoblasts produce bone in a two-step process, firstly through the production of an organic bone matrix, consisting of type I collagen and other proteins such as bone sialoprotein (BSP), osteonectin and proteoglycans (Del Fattore *et al.*, 2012). Subsequently, osteoblasts produce vesicles containing HA crystals, forming the mineralised component that surrounds the previously produced matrix proteins. Crucially, osteoblast mineralisation, in the form of mineralised matrix deposition can be induced *in vitro* (Guo *et al.*, 2014) and visualised/measured using an Alizarin Red S (ARS) calcium stain.

An understanding of the process of osteoblast mineralisation, and the genes that control it, will be crucial as we aim to understand how PCa cells may influence it. Therefore, in order to conduct molecular studies of how PCa cells may influence osteoblasts, a robust but simple model of osteoblast mineralisation is required. Several cell lines exist, which would provide such models including 7F2, human foetal osteoblast (hFOB) and sarcoma osteogenic (SaOS2). However, we used the 7F2 mouse bone marrow cell line as a simplified *in vitro* model of osteoblast mineralisation, as inducing these cells to mineralise, as well as the ability to manipulate this mineralisation with treatments is well characterised (Hwang *et al.*, 2016; Yeh *et al.*, 2015). Human prostate cancer cell lines grown as xenografts readily form bone metastases in mice, therefore indicating that this process is common across species and that the factors controlling the complex bone remodelling process share sufficient homology. In this chapter we look to characterise the 7F2 mineralising osteoblasts at both the functional and gene expression level. Characterisation of mineralising cells in this way will provide insight into the mechanisms of mineralisation as well as providing a basis to allow analysis of the effects of external factors i.e. PCa cells or factors secreted from them.

3.2   Chapter Aims

The aim of this chapter is to characterise the 7F2 osteoblast cell line used in this thesis. Characterisation of this cell line will provide a model of osteoblastogenesis, in which the effects of PCa cells and various treatments can be tested. Therefore, the specific aims of this chapter are:

- To show that osteoblasts can be induced to mineralise *in vitro* and determine the kinetics of this mineralisation

- To show that mineralisation of osteoblasts *in vitro* can be reliably quantified

- To determine the key genes that change during osteoblast mineralisation

3.3   Results

Morphology of 7F2 Cell Line

The 7F2 cell line was purchased from the ATCC and cells were frozen in low passage stocks. Cells were cultured up to a passage number of 20, at this point cells were discarded and low passage cells were defrosted. 7F2 cells are an immortalised *Mus musculus* osteoblast cell line isolated from femoral bone marrow from p53$^{-/-}$ mouse. A 7F2 monolayer was visualised using a brightfield microscope (figure 3.1). The cells displayed a flattened, irregular, star shaped morphology (fibroblast-like) with multiple processes, consistent with images from the ATCC and the literature (Mayer-Kuckuk *et al.*, 2005).

Stimulating Mineralisation in 7F2 Cells Using Osteogenic Media

7F2 cells were stimulated to mineralise over a 14 day period by treating with osteogenic media (MEM + 5x10^{-3} Mmol/L β-glycerophosphate, 0.1g/L ascorbic acid, 10^{-8} mol/L menadione and 10^{-7} mol/L 1, 25(OH)$_2$D$_3$) (Guo *et al.*, 2014), and were collected at daily intervals for mineralisation staining. Cells were compared with untreated 7F2 cells cultured for an equivalent time. Mineralisation was assessed by ARS staining from day 8 onwards in an attempt to catch the initiation of the mineralisation process, as the literature suggests mineralisation occurs shortly after this time point (Gharibi *et al.*, 2016). From day 8, plates were taken daily, fixed in 10% formalin and stained using ARS to measure calcium deposition. Whole well images were taken on each day immediately following staining (figure 3.2A) and the same wells are imaged at 10x magnification using a brightfield microscope (figure 3.2B). 7F2 cells treated with osteogenic media began to show calcium deposition (in the form of HA) at day 10 as evidenced by the appearance of faint ARS staining at both the whole well and magnified level. This calcium deposition increased from days 10-12 at which point whole well staining appears to plateau. However, magnified images show subsequent increases in

calcium deposition up to day 14. ARS is a stain capable of reacting with free calcium. Other stains are available for monitoring changes associated with osteoblast mineralisation. BCIP/NBT is an alkaline phosphatase (AP) substrate, able to form a blue precipitate in the presence of the active enzyme. AP activity is greatly increased during osteoblastic mineralisation. Another calcium stain, Von Kossa's stain, reacts with calcium phosphate produced by mineralising osteoblasts resulting in a dark brown/black precipitate. BCIP/NBT and Von Kossa's stain was added to cells mineralised for 1 or 10 days (figure 3.2C). The presence of AP and calcium phosphate, both seen as dark coloured deposits was confirmed in mineralising 7F2 cells.

Quantification of ARS staining is crucial for accurately measuring changes in mineralisation. A method of quantification was used whereby ARS staining for each well was quantified and normalised using a crystal violet stain on the same well. Staining in this way allowed for normalisation of ARS staining in the event of cell monolayer disturbance, which occasionally occurred during washing steps. To show how this method accounts for this, 6 7F2 cell containing wells were mineralised for 14 days. Cells were stained with ARS, and excess staining was removed by washing 3 times in distilled water. At this point, half of the cells in 3 wells were removed by scraping (figure 3.3A). ARS staining was then dissolved in 10% acetic acid and quantified by measuring the absorbance of this solution at 450nm. This showed that ARS staining was stronger in whole wells compared to half wells (figure 3.3B). Wells were then washed 3 more times in distilled water and stained with crystal violet (figure 3.3C). Crystal violet staining was dissolved in 10% acetic acid and quantified by measuring the absorbance of this solution at 600nm, also showing that whole well staining was greater than that of half wells (figure 3.3D). Finally, the quantified ARS stain was divided by the quantified crystal violet stain for each well, which showed a similar level of normalised staining across the two groups (figure 3.3E). This showed that staining in this way is able to normalise ARS

intensity depending on cell monolayer integrity, allowing for comparison of ARS intensity across wells regardless of monolayer condition.

7F2 cells cultured over 14 days in regular or osteogenic media were stained daily with ARS from days 8-14. ARS staining was quantified and normalised as described above (figure 3.4). Quantification confirmed that deposition of calcium initiated at day 10, evidenced by an increase in absorbance for the cells grown in osteogenic media compared to day 10 control cells grown in regular media. However, calcium quantification in the osteogenic media group appeared to plateau after 11 days and remained relatively constant up to day 14 ($p < 0.001$ from day 11-14). This plateau in calcium staining may be a result of either an inability of cells to further mineralise, or may reflect the upper limits of the dynamic range of our assay. Furthermore, at day 14, spontaneous mineralisation occurred in the control group.
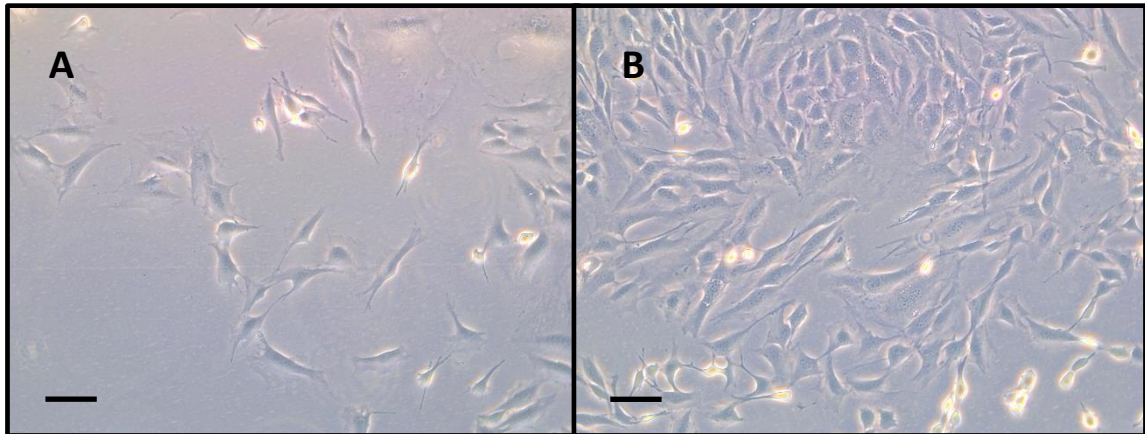
Figure 3.1. Morphology of 7F2 cells. Brightfield microscopy images of 7F2 cell monolayers, grown on plastic in cell culture flasks. (A) Low density (~10% confluency), (B) High density (~90% confluency). Scale Bar: 100μm.
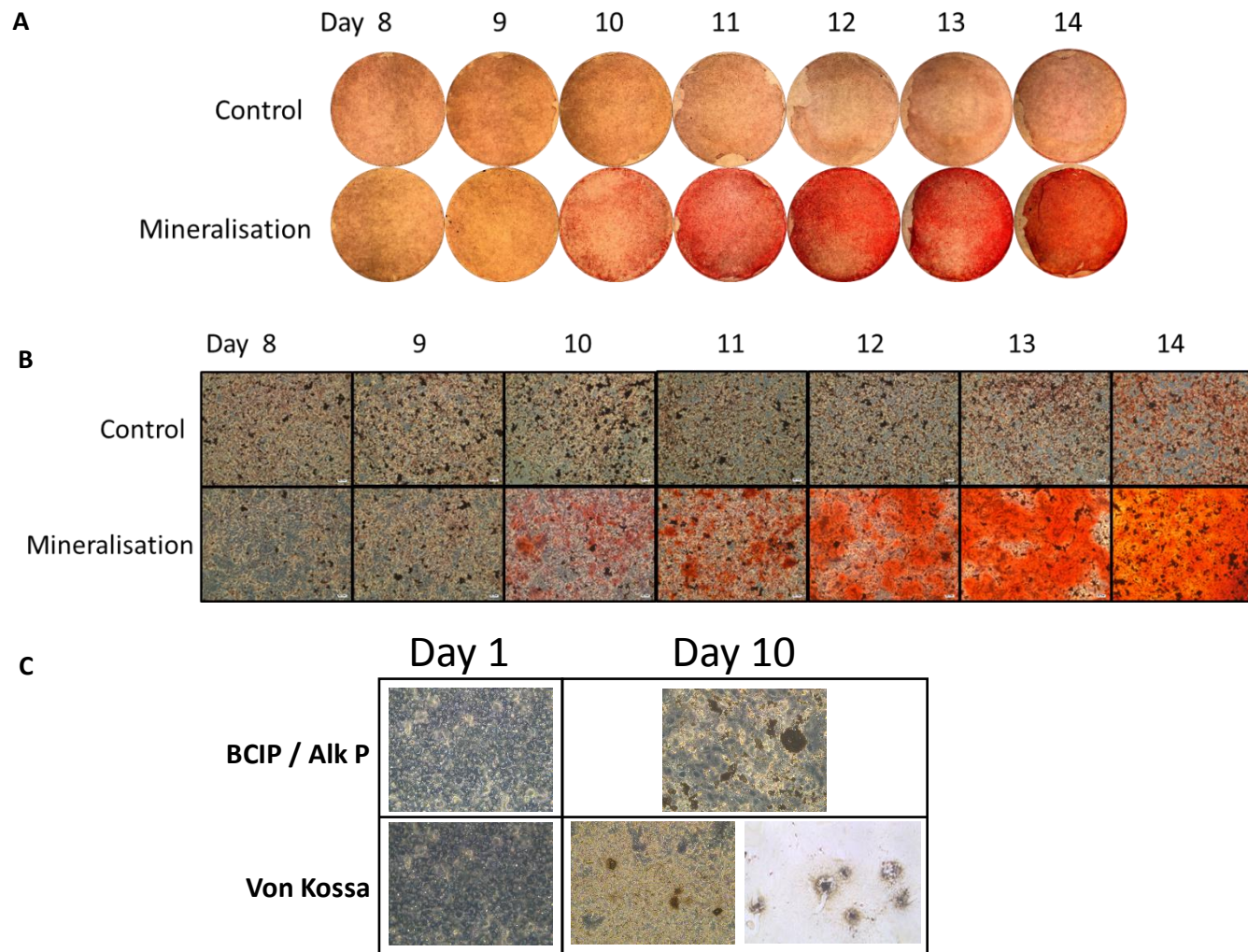
Figure 3.2. Staining of 7F2 cells grown in regular or osteogenic media. ARS staining of 7F2 cells over a 7 day period from days 8-14. (A) Whole well images. (B) 10x magnified images. (C) Magnified images of BCIP/Alk Phos Von Kossa stained 7F2 cells grown in osteogenic media for 1 or 10 days.

133
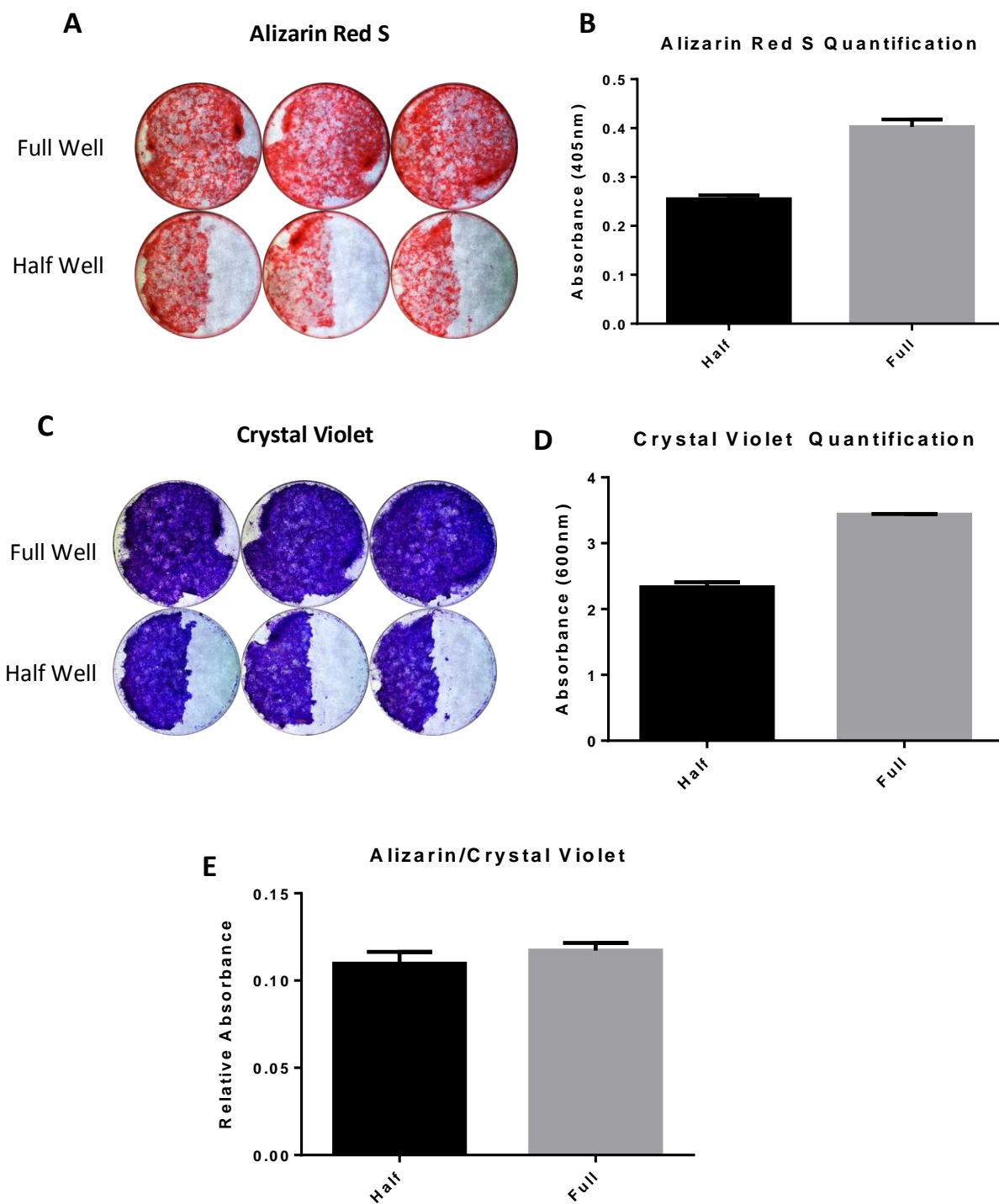
Figure 3.3. Example of Alizarin Red S and Crystal Violet staining method. (A) ARS stained wells, (B) Quantification of the ARS staining for full and half wells, (C) Crystal violet stained wells, (D) Quantification of the ARS staining for full and half wells. (E) Quantified alizarin staining divided by quantified crystal violet staining. (Graphs show absorbance +SEM for triplicate wells).
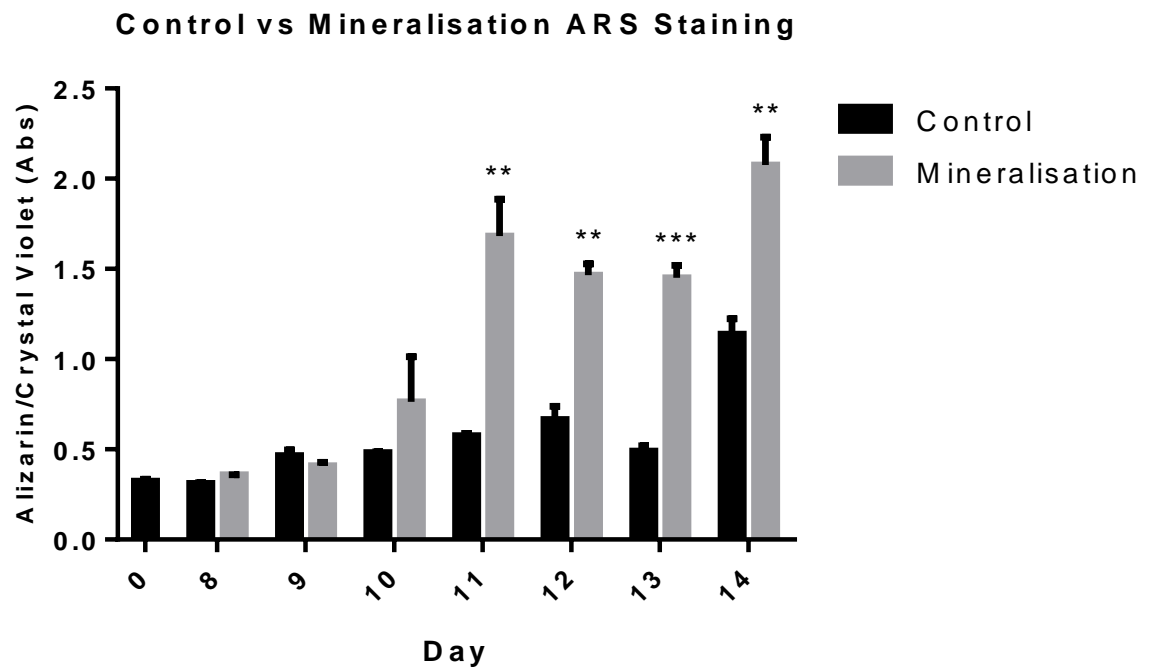
Figure 3.4. Quantification of ARS staining over a 7 day period from days 8-12 for mineralising 7F2 cells grown in osteogenic media and control 7F2 cells grown in regular media. (Graph shows ARS stain normalised to crystal violet staining, +SEM, statistical significance assessed by unpaired ttest at each time point, **p<0.01, ***p<0.001, n=3).

Gene Changes in Mineralising 7F2 Cells

The mineralisation and calcification of the 7F2 cells is a very complex process involving both rapid gene expression changes and slower physiological changes e.g. collagen deposition and consequent mineralisation. To get a more specific idea of the genetic changes that are associated with mineralisation, qPCR was done on mineralising 7F2 cells every 3 days from 0-12 days. A number of documented osteoblast differentiation genes were tested relative to 2 housekeeping genes (HPRT & β-actin), of these, 4 were selected based on the degree and direction of change compared to control cells; Activin A receptor, type I (ACVR1), Matrix metalloproteinase-3 (MMP3), distal-less homeobox 5 (DLX5) and Collagen type 1 alpha 1 (COL1A1). As stated, other osteoblast differentiation genes were also tested, such as RUNX2, SP7 and BGLAP (see appendix 1). However, these genes showed expression patterns in treated vs control cells that were contrasting from their well-established patterns shown in the literature and were therefore not included.

ACVR1 is a key receptor of bone morphogenetic protein (BMP) 7. In mineralising 7F2 cells, ACVR1 peaked at day 3 (figure 3.5A) compared to control cells, although this failed to reach significance. Expression then reduced greatly from day 3 to day 6 and continued to decrease up to day 12. However, although ACVR1 expression decreased after day 3, levels remained higher than control cells at both days 6 and 9, although not significant. By day 12, ACVR1 levels had returned to the same level as control cells. MMP3 is an enzyme responsible for the breakdown and remodelling of extracellular matrix proteins such as collagens, proteoglycans and elastin. In mineralising osteoblasts, MMP3 showed a significant increase in expression at day 3 compared to control cells with a further increase in expression seen at day 6 ($p<0.05$ for both) (figure 3.5B). A gradual decrease in expression was seen in mineralising cells between days 6 and 12 although expression was still greatly increased at all time points compared to control cells, albeit not significant. COL1A1 is a collagen protein

produced in large amounts by osteoblasts during the early stages of bone matrix formation. COL1A1 expression showed a sharp increase at day 3 in mineralising 7F2s (figure 3.5C), however this increase was not significant. Expression had returned to normal by day 6 and both mineralising and control cells showed a gradual decrease in expression between days 6 and 12. Of the genes selected, DLX5 was the only one to decrease in expression compared to control cells (figure 3.5D). Decreased DLX5 expression in mineralising cells compared to control cells was seen at all time points with a further gradual reduction in expression seen in mineralising cells up to day 12. However, DLX5 expression in mineralising cells failed to reach statistical significance compared to control cells. To confirm that these gene changes were occurring as a part of the mineralisation process, control and mineralising 7F2 cells were cultured alongside those destined for RNA extraction and were stained with ARS and quantified (figure 3.5E). ARS quantification confirmed that mineralisation was occurring in these cells, and therefore the gene changes witnessed were representative of different stages of the mineralisation process. A summary of the changes in expression of these 4 genes, adapted from figures 3.5 A-D is shown in figure 3.6.
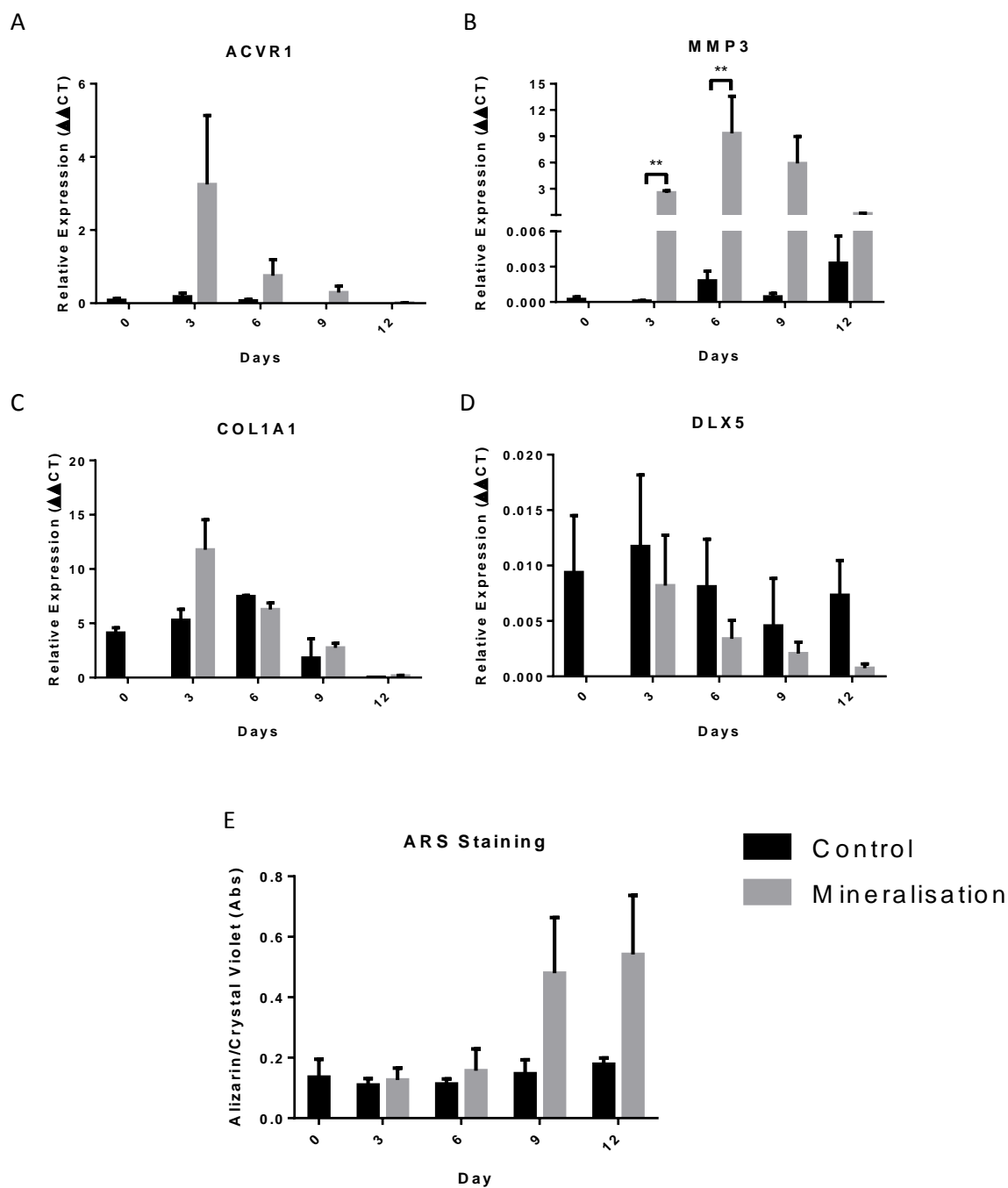
Figure 3.5. qPCR of Mineralising and Control 7F2 Cells Across a 12 Day Period. (A) ACVR1 expression, (B) MMP3 expression, (C) COL1A1 expression, (D) DLX5 expression. (Graphs A-D show ΔΔCT values normalised to housekeeping genes +SEM, significance between treated and control cells was assessed using Mann-Whitney U test, *=p<0.05, n=4). (E) Quantified ARS staining of cells cultured alongside those used for qPCR. (Graph shows ARS stain normalised to crystal violet staining, +SEM, n=2).
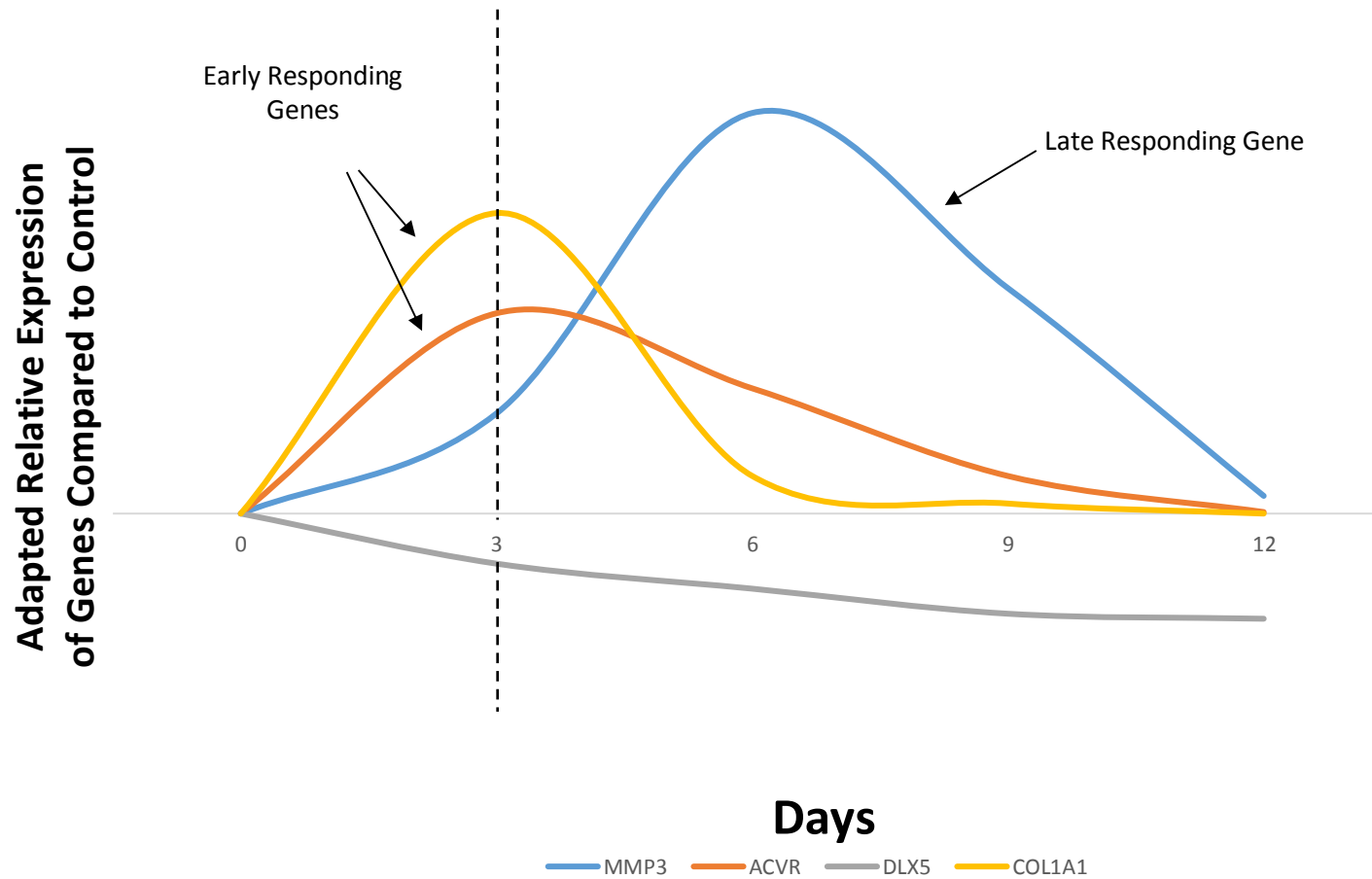
Figure 3.6. Summary of Gene Changes in Mineralising 7F2 Cells. Changes in gene expression in mineralising 7F2s relative to control cells adapted from data displayed in figure 3.5. Vertical dashed line represents the 3 day treatment period used in following experiments.

3.4 Discussion

Osteoblast overactivation, resulting in excess deposition of mineralised bone, is a hallmark of osteoblastic PCa bone metastases. Therefore, the aim of this chapter was to characterise an *in vitro* mineralising osteoblast model during different stages of mineralisation. By doing this, we would obtain a platform against which the effects of interactions with PCa cells or secreted factors can be compared.

For this study, 7F2 bone marrow osteoblast cells were used. This cell line was selected for its relative normality, non-disease related origin and ability to readily mineralise in osteogenic media. 7F2 cells showed a flattened, star shaped morphology (fibroblast-like) as expected, based on reference images from the ATCC.

Osteoblastic bone deposition is a two-step process, as discussed in section 1.3.2.1.1. The first step in this process is the secretion of uncalcified matrix, consisting of primarily type I collagen. This collagenous structure is then mineralised by the osteoblasts via the deposition of $CaPO_4$ in the form of HA (Clarke, 2008). ARS is a commonly used stain in osteogenic studies, favoured for its ease of quantification. ARS reacts with calcium within the hydroxyapetite via the following chemical equation to form a red precipitate (shown in bold) (Misra, 1992):
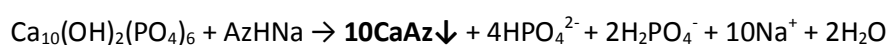
$Ca_{10}(OH)_2(PO_4)_6 + AzHNa \rightarrow \textbf{10CaAz} \downarrow + 4HPO_4^{2-} + 2H_2PO_4^{-} + 10Na^{+} + 2H_2O$

After the ARS solution is removed and cells are washed, this red precipitate remains visible, as shown in figure 3.2A and B. The steady increase in red staining of 7F2 cells grown in osteogenic media shown in figure 3.2A and B indicates a gradual deposition of calcium. Thus, we show that culture in osteogenic media is sufficient to induce 7F2 mineralisation and that the calcium deposition is detectable roughly 10 days after treatment. BCIP/NBT and Von Kossa staining showed that AP was increased and calcium phosphate was deposited after treatment with osteogenic media for 10 days. AP activity and calcium phosphate deposition

are increased during mineralisation, therefore these positive staining results further emphasise that complex mineralisation is occurring in these cells.

Reliable quantification of ARS staining is a crucial step that will allow for a more specific measurement of the effects of any subsequent treatments on 7F2 function. ARS staining features several washing steps, which, due to the extremely fragile nature of the 7F2 monolayer, occasionally results in the accidental removal of patches of 7F2 cells. To account for this, ARS staining was normalised to crystal violet staining for each well. A visual display of this process is shown in figure 3.3. The reduction of ARS staining seen in half full wells compared to full wells matched the reduction of crystal violet staining of the same wells, resulting in similar normalised ARS staining levels. Thus, we show that ARS staining can be accurately calculated and compared for all wells.

Figure 3.4 shows the quantified ARS staining for control and mineralising 7F2s, which correlates with the increase in ARS seen from visual inspection of cells in figure 3.2A and B. This graph confirms that increases in ARS staining are quantifiable and that any changes in mineralisation seen with subsequent treatments can be measured colourimetrically. Together, figures 3.2 A and B, and figure 3.4, indicate that subsequent treatments measured by ARS staining should have a treatment period of 10 days. This period of time is long enough to induce calcium deposition, whilst minimising the risk of reaching the limits of cell differentiation and/or the dynamic range of ARS staining seen at later days. BCIP/NBT and Von Kossa staining was effective in showing the presence of AP and calcium phosphates, two further markers of mineralisation. However, measuring the changes in BCIP/NBT and Von Kossa staining is qualitative and detecting subtle changes in staining levels between future treatments may not be possible. Therefore, ARS staining remained the principle measure of overall mineralisation.

Mineralisation, in the form of calcium deposition, represents the overall change (or end point) in the function of the osteoblasts compared to non-mineralising control cells. However, for a more specific idea of how the 7F2s change during this process, the gene expression changes in these cells were measured at 3 day increments from treatment through to complete mineralisation. Genes regulating osteoblast differentiation are well characterised, such as RUNX2, COL I, Alkaline phosphatase and Osteocalcin (Rutkovskiy *et al.*, 2016). However, in 7F2 cells, the gene changes that occur during mineralisation, either driving it or occurring as a result, have not been well characterised. Therefore, we tested a number osteogenic markers in 7F2 cells throughout the mineralisation process. From this panel, 4 genes showed an expression pattern indicative of an osteogenic marker across the treated and control time courses; ACVR1, MMP3, COL1A1 and DLX5. The expression of other well characterised osteoblast differentiation genes, such as RUNX2, SP7 and BGLAP were also tested. However, these genes showed reduced expression in mineralising cells vs control cells. As these genes are so well characterised as markers of osteoblastic differentiation, it was decided not to include them based on their unexpected results. The decrease seen in RUNX2 may reflect the inhibitory effect of RUNX2 in late osteoblasts (Komori, 2006). However, given the relative uncertainty of RUNX2 expression in differentiating 7F2 cells, it was decided not to use RUNX2 as a marker in this project.

ACVR1, is a BMP receptor belonging to the TGFβ family subgroup. ACVR1 has been linked to several aspects of musculoskeletal development. For example, *Acvr1* ablation resulted in hypotrophic craniofacial abnormalities and decreased ossification in mice (Dudas *et al.*, 2004). However, Kamiya *et al.* (2011) showed that osteoblast specific *Acvr1*-null mice had increased bone mass due to an increase in osteoblastic Wnt signalling, thus suggesting an inhibitory role of *Acvr1* in osteoblast function. These findings suggest that *Acvr1* has multiple and complex roles within bone development. Our data showed a strong increase in *Acvr1* expression early in mineralising 7F2s compared to control cells, peaking at day 3 where

expression in mineralising cells was over 18x higher than controls. As discussed, mineralising genes have not been well characterised in 7F2 cells and therefore *Acvr1* may play a different role in the differentiation of these cells.

MMP3 is an enzyme involved in the breakdown of extracellular matrix (ECM) proteins such as type III, IV and V collagens and fibronectin during tissue remodelling (Birkedal-Hansen *et al.*, 1993). Bauer *et al.* (2015) showed that mice lacking osteoblastic *Runx3* had decreased bone matrix formation and ossification. These Runx3-deficient cells also showed a >5-fold reduction in *Mmp3* expression compared to controls, suggesting either a functional role of *Mmp3* in osteoblastic bone deposition or a concurrent loss in expression with decreased osteogenesis. Our data agrees with these findings, with a substantial increase in *Mmp3* expression seen in mineralising osteoblasts compared to control cells. One reason for this could be that *Mmp3* may aid in remodelling collagen fibres for mineralisation.

The COL1A1 gene produces the pro-alpha1(I) chain, a key component of type I collagen along with the pro-alpha2(I) chain. Type I collagen is secreted by early differentiating osteoblasts and forms the majority of the organic phase of bone matrix (Del Fattore *et al.*, 2012), which is later mineralised by the osteoblasts. In our mineralising 7F2 cells, *Col1a1* expression peaked at day 3 compared to control cells before returning to control levels by day 6. This early pulse in *Col1a1* expression is expected based on the literature, which as discussed, states that type I collagen production occurs early and precedes matrix mineralisation.

Dlx5 was the only selected gene to show decreased expression in mineralising cells compared to controls. *Dlx5* is a homeobox transcription factor which forms a bigene cluster with *Dlx6*. DLX5 expression correlates with osteoblast differentiation and is suggested to induce differentiation through activation of other transcription factors such as *Runx2* and *Osx* (Osterix) (Laxman *et al.*, 2016; Ryoo *et al.*, 1997). *Dlx5/6*[-/-] mice show "severe limb, craniofacial and axial skeletal defects" including retarded axial skeletal growth (Robledo *et*

al., 2002). These findings seem to contradict our own, which actually suggests that *Dlx5* is lost during 7F2 differentiation and subsequent mineralisation. However, as discussed, data on *Dlx5* expression in 7F2 cells is limited. One study linking osteoblast differentiation and *Dlx5* in 7F2 cells showed that *Dlx5* is down regulated >3x in FGF2 treated cells compared to controls (Sugimoto *et al.*, 2016). Given that FGF2 is known to stimulate osteoblast differentiation and bone formation (Fei *et al.*, 2011), it's possible that decreased *Dlx5* expression either drives 7F2 differentiation or is lost as a result.

Although the selected genes showed a sizable difference in expression in mineralising vs control cells, this change failed to reach significance in 3 out of 4 genes. However, these gene expression patterns are used in combination with ARS staining to determine overall cell changes, and are therefore still viable markers able add a degree of certainty to any change in differentiation seen with future treatments. Furthermore, the lack of protein validation means that connections between the expression of these genes and a direct functional role in osteoblast mineralisation can not be made.

Although some of the gene expression patterns discussed appear to differ from the expected based on the literature, the data on 7F2 gene changes is poorly explored. The difference in differentiation stage between commonly studied osteoblast cell lines is just one of several factors that could explain variations in gene expression between these cells. Another factor that could explain the difference in gene expression compared to the literature could be differences in the contents of osteogenic medias. Many different formulations of osteogenic media have been described, containing a combination of β-glycerol phosphate, ascorbic acid, vitamin D and other chemicals such as dexamethasone (Olivares-Navarrete *et al.*, 2012). These various formulations may induce different changes in gene expression, making direct comparisons difficult.

The changes in expression of the selected genes compared to control cells is summarised in figure 3.6, using adapted data to show the general trends of expression for each gene. This summary also helps to outline why future treatments involving validation of osteoblast differentiation by gene expression involve 3 day treatment periods (represented by the vertical dashed line). This is because although some genes (ACVR1, COL1A1) are early responding and some (MMP3) are late responding, all genes were different to control cells at day 3, whereas the expression of some genes had returned to the level of control cells at later time points.

In conclusion, we showed that 7F2 cells can be stimulated to mineralise *in vitro* via treatment with osteogenic media, and that this mineralisation can be visualised with ARS staining. By subsequently showing that ARS staining can be quantified, we were able to provide a more accurate way for 7F2 mineralisation to be measured. Finally, by measuring the gene changes associated with 7F2 mineralisation we were able to gain a more in depth, specific idea of how mineralising 7F2 cells differ from their equivalent controls. By showing that mineralisation can be measured at the functional and gene expression level, we have successfully characterised mineralising 7F2 cells, thus providing a good osteoblastic bone model for future use in monitoring bone and prostate cancer cell interactions.

3.5   Summary of Key Points

Mineralisation of 7F2 cells *in vitro* was successful, and staining by ARS provides both a visual and measurable way to monitor this. Measuring gene changes in mineralising 7F2 cells provided a panel of 4 genes that are differentially expressed compared to control cells; ACVR1, MMP3, COL1A1 and DLX5. Analysis of time points shows that treatment periods should be 10 days for ARS staining and 3 days for gene expression quantification.

Chapter IV: The Effects of PCa Cell Signalling on Osteoblast Differentiation

4 <u>Effect of Prostate cancer cells on Osteoblasts</u>

4.1 Introduction

Within the last 30 years, multiple new forms of non-coding RNAs have been discovered (Cech & Steitz, 2014). The functions of most of these nucleic acids lies within their ability to alter the activity of other forms of RNA (Clouet d'Orval *et al.*, 2001; Darzacq *et al.*, 2002; Elbashir *et al.*, 2001; Hammond *et al.*, 2000). This information has drastically increased the understanding of a number of both physiological and pathophysiological pathways. miRNAs in particular have gathered much attention due to their widespread ability to regulate gene expression and alter a number of cellular processes (Esau *et al.*, 2006; Naguibneva *et al.*, 2006).

The activity of miRNAs has been linked to multiple facets of cancer development such as proliferation, evasion of apoptosis and have even been linked to metastatic processes such as epithelial–mesenchymal transition (EMT) (Peng & Croce, 2016). The aberrant expression of miRNAs has been noted in virtually all major cancers and numerous other diseases, indicating that their role in these cellular pathways may be significant (Ha, 2011; Wu & Lu, 2017).

A crucial discovery in the field of miRNAs came from Chim *et al.* (2008) who discovered the presence of miRNAs in extracellular biological fluids. This discovery that miRNAs are ubiquitous in bodily fluids has paved the way for a number of novel hypotheses centred around miRNAs being potential mediators of intercellular communication (Weber *et al.*, 2010).

Signalling between PCa cells and bone cells within the secondary tumour environment is extensive. This signalling involves a multitude of protein and growth factors, and many of

these factors are well characterised such as OPG, IGF and TGFβ. Within the context of bone metastatic lesions, miRNAs have been implicated in several aspects of development including osteotropism (Zoni *et al.*, 2015), regulation of angiogenic–osteogenic coupling (Li *et al.*, 2013) and even modulation of bone cell function (Eguchi *et al.*, 2013).

Models of human prostate cancer cells which metastasise to the bone, in mouse xenograft models, are available for study. The PC3 and VCaP (vertebral metastasis harvested PCa cell line) cell lines frequently metastasise to the bone, whereas LNCaP (lymph node harvested Pca cell line) cells have a lower propensity, but can do so more readily as aggressive subclones (Sobel & Sadar, 2005). In this chapter we looked to determine whether PCa cells are able to signal to osteoblasts *in vitro* via exported factors, examining what effect this has on their ability to differentiate and mineralise. By analysing PC3 cell conditioned media for the presence of miRNAs, we then attempted to ascertain whether miRNAs could function as intercellular communication between cancer cells and bone cells - in parallel or in combination with protein and other signalling mediators.

4.2   Chapter Aims

The aim of this chapter is to characterise the effects of communication between PCa cells and osteoblasts, using the bone model described in the previous chapter, and to discuss factors that may mechanistically explain this. To achieve this the specific aims of the chapter are:

- To analyse the effects of PC3 cell secreted signalling molecules on 7F2 mineralisation and differentiation using a co-culture system

- To determine whether this effect is specific to PC3 cells

- To analyse the miRNA content of PC3 cell conditioned media and use differential centrifugation to indicate which extracellular structures these miRNAs may be associated with

4.3   Results

Co-Culture of Osteoblasts with PCa Cells

To determine the effects of PCa cell signalling on osteoblast function, we set up a co-culture, where osteoblasts were seeded on the surface of a 24well plate, and 0.4μm pore size inserts containing increasing amounts of the highly aggressive PC3 PCa cells were added above (figure 4.1A). Osteoblasts and inserts were cultured in either regular or osteogenic media for 6 days and stained with ARS. In regular media, 7F2 cells cultured with increasing amounts of PC3 cells showed no change in their level of mineralisation. In osteogenic media, co-culturing 7F2s with PC3 cells increased mineralisation of the osteoblast cells in a PC3 cell number dependant manner. This dose dependent effect showed an increase in ARS staining reaching statistical significance at 40,000 PC3 cells ($p < 0.05$ for all) (figure 4.1A).

Additionally, it was observed that a more intense region of mineralisation staining was present in the immediate vicinity of the insert containing the PC3 cells (figure 4.1B). This pattern was noticeably absent in 7F2 cells cultured with empty inserts. Furthermore, crystal violet staining of these cells revealed a decrease in cell confluency below the PC3 containing insert, corresponding with the pattern seen with ARS staining. Again, this pattern was not seen in cells cultured with empty inserts.

To confirm that PC3 cells were inducing 7F2 differentiation at the gene expression level, the expression of 4 genes, characterised as part of the osteoblast model, were measured in 7F2 cells co-cultured with 20,000 and 40,000 PC3 cells, in regular and osteogenic media. In cells cultured in regular media, co-culture with PC3s had no effect on the expression of these genes. DlX5, which showed reduced expression during the model of osteoblast differentiation, was further decreased during co-culture with PC3 cells in osteogenic media in a cell number dependant manner. This reduction in DLX5 was significant for both 1x and

2x PC3 cells (p=0.011 and p=0.003 respectively). COL1A1, MMP3 and ACVR1 all showed increased expression during the 7F2 differentiation model. COL1A1 showed no change in expression during co-culture. However, MMP3 and ACVR1 both showed increased expression during co-culture in osteogenic media, in a cell number dependant manner, with ACVR1 showing a significant increase with 2x PC3 cells (p=0.009).

To validate that the induction of mineralisation seen in our co-culture model was specific to PCa cells and not simply a result of (unspecifc) cell number and the associated signalling molecules released, we mineralised 7F2 cells in the presence of a range of prostate cell line conditioned medias (figure 4.3). Non-cancerous, immortalised, prostate epithelial cell, namely PZ-HPV-7, conditioned media as well as conditioned media from three PCa cell lines was compared to osteogenic MEM. DU145 cells, another aggressive metastatic PCa cell line, as well as LNCaP, a less aggressive metastatic cell line, were included alongside PC3 cell conditioned media. Conditioned media was collected after 48 hours from equal numbers of cells and centrifuged twice, first at 2,000xg for 5 minutes and subsequently at 16,000xg for 15. All media contained the same concentrations of osteogenic supplements (described previously in section 3.3). Compared to osteogenic MEM, PZ-HPV-7 conditioned media had no effect on the level of 7F2 mineralisation. DU145 cell conditioned media was able to induce a 34% increase in 7F2 mineralisation, however, this change failed to reach statistical significance. PC3 cell conditioned media induced a 70% increase in 7F2 mineralisation (p<0.001). LNCaP cell conditioned media stimulated a minimal increase in mineralisation of around 15%.
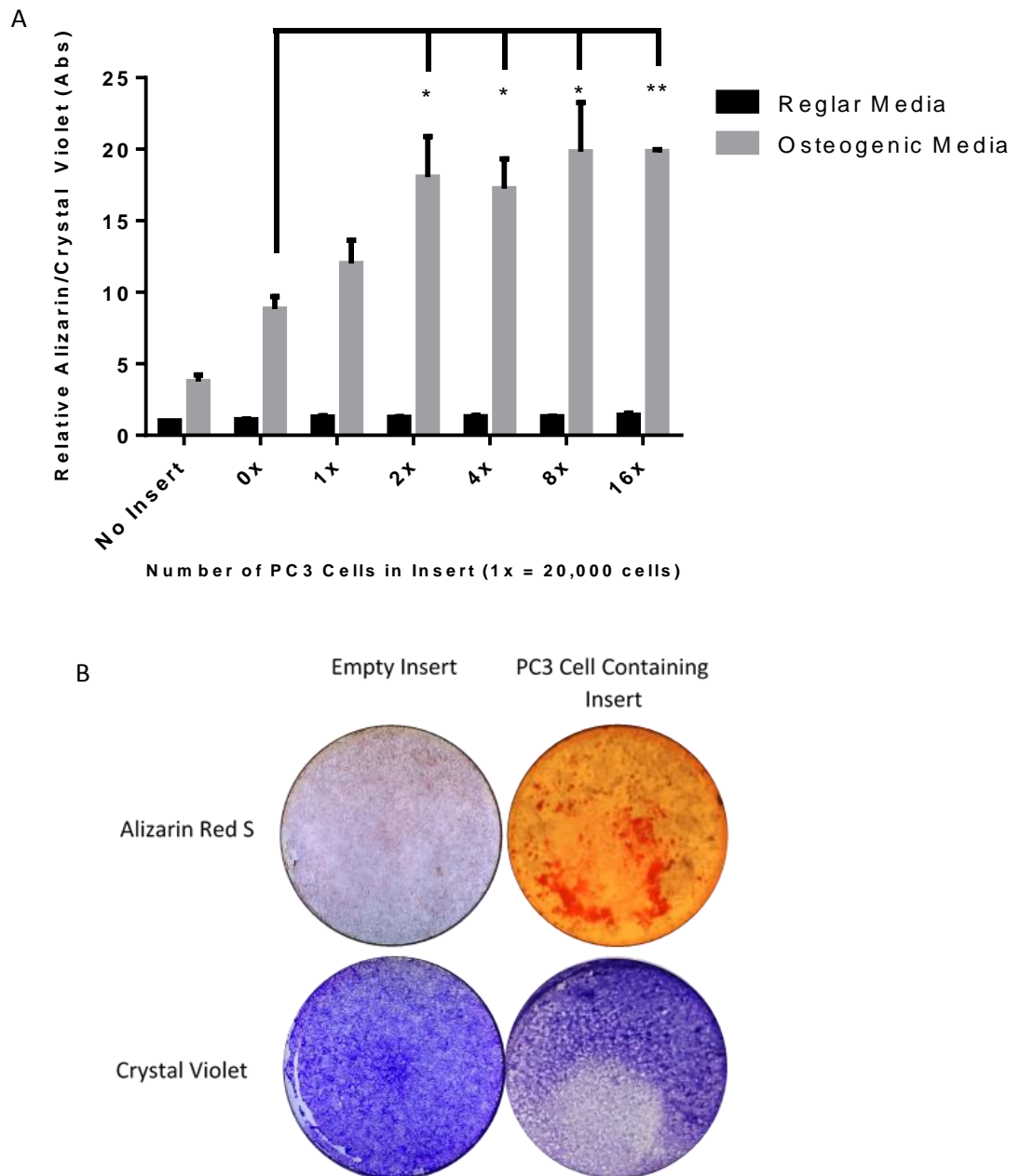
Figure 4.1: ARS staining of 7F2 cells co-cultured with increasing amounts of PC3 cells in either regular or osteogenic MEM. (A) Quantified ARS staining of co-cultured 7F2s, 1x = 20,000 PC3 cells seeded in the insert. (Graph shows average fold change compared to "no min, no insert" +SEM, n=3) (Statistical significance assessed by one-way ANOVA using Holm-Sidak multiple comparisons test between treatment and control (0x cell insert in mineralising media), *p<0.05, **p<0.01). (B) Representative whole well images of wells beneath either empty or PC3 cell containing inserts cultured in mineralising media, stained with ARS or crystal violet.
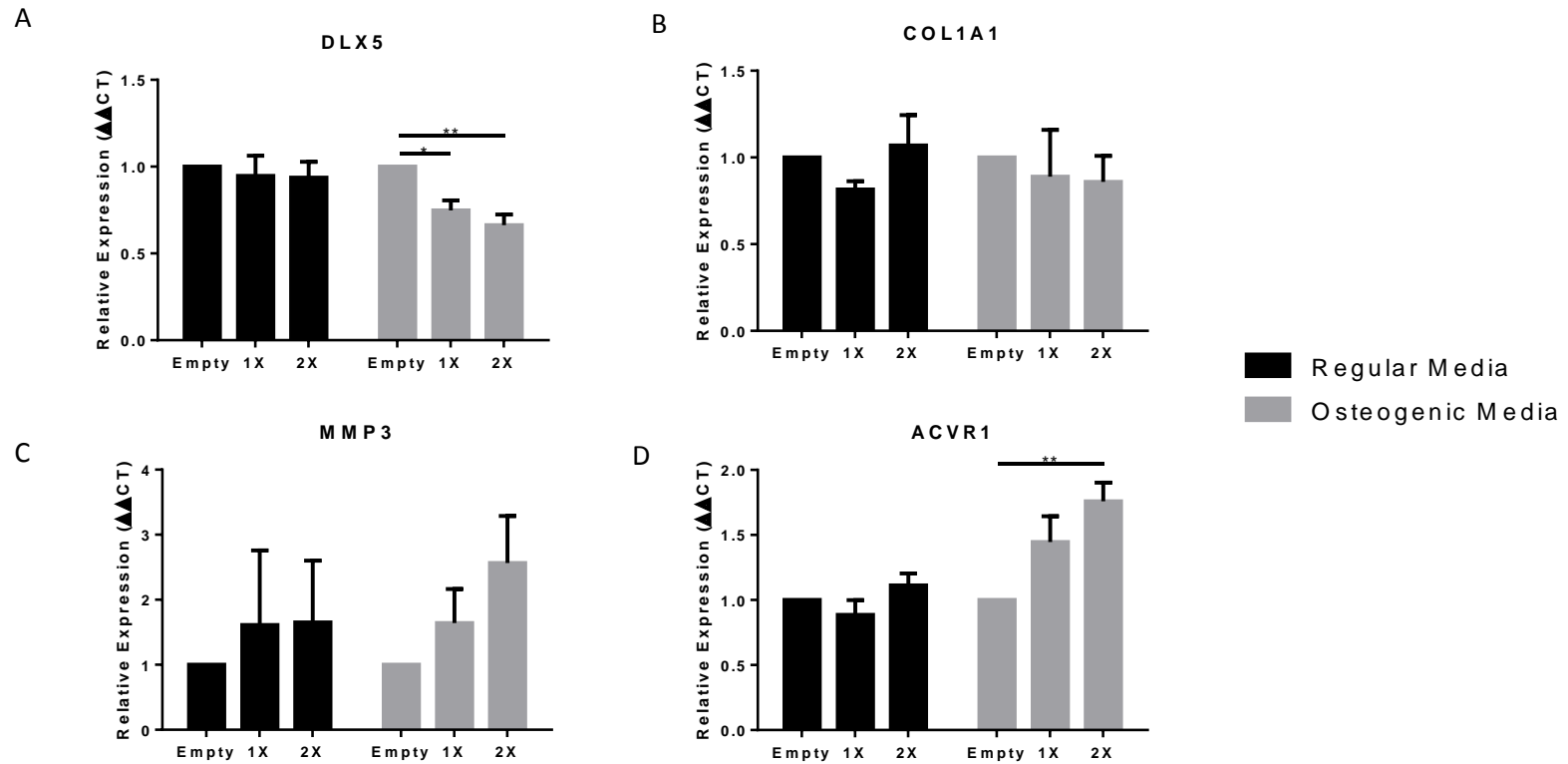
Figure 4.2: qPCR of osteoblast differentiation genes in 7F2 cells co-cultured with increasing amounts of PC3 cells in either regular or osteogenic MEM. (A) DLX5 expression, (B) COL1A1 expression, (C) MMP3 expression, (D) ACVR1 expression in 7F2 cells co cultured with PC3 cells 1x = 20,000 PC3 cells seeded in the insert. (Graphs show average fold change compared to empty controls +SEM, n=3) Statistical significance assessed by one-way ANOVA using Holm-Sidak multiple comparisons test, *p<0.05, **p<0.01.
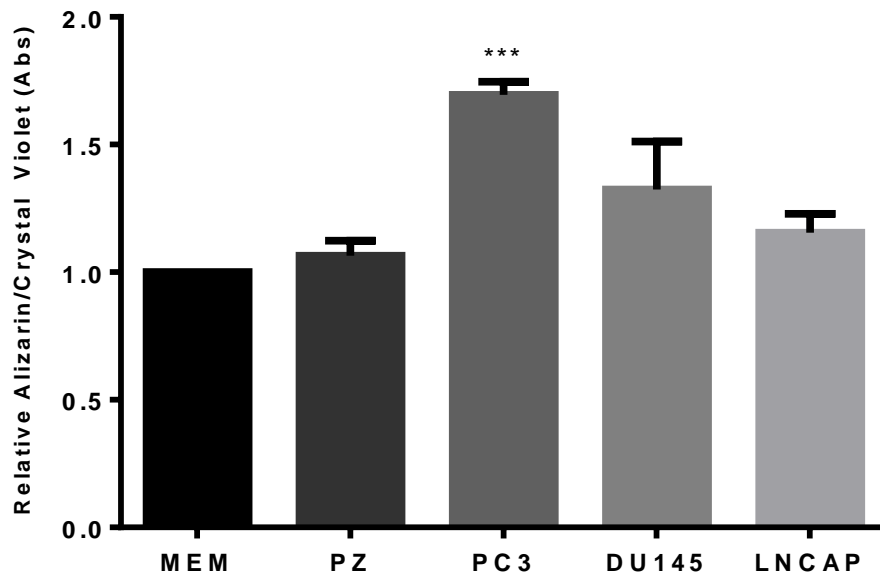
Figure 4.3: Effect of conditioned media from various prostate cell lines on 7F2 mineralisation. 7F2 cells were mineralised for 10 days in conditioned media from the prostate epithelial PZ-HPV-7 (PZ) and prostate cancer PC3 and DU145 cell lines with mineralisation supplements and compared to regular osteogenic MEM. (Graph shows average fold change compared to control +SEM, n=3). Statistical significance assessed between control and conditioned media groups by one-way ANOVA using Holm-Sidak multiple comparisons test, ***P<0.001.

Chapter IV: The Effects of PCa Cell Signalling on Osteoblast Differentiation

Analysing the miRNA Content of PC3 Conditioned Media

After showing that secreted signalling molecules from PCa cells can influence the activity of 7F2 cells, we looked to analyse the contents of PC3 cell conditioned media, for evidence of miRNAs. We hypothesised that PCa cells use secreted miRNAs to affect the gene expression in the recipient 7F2 cells and, therefore, their activity. We therefore looked to analyse the miRNA content of PC3 cell conditioned media.

PC3 cell conditioned media was centrifuged twice, first at 2,000xg for 5 minutes, and subsequently at 16,000xg for 15 minutes, to remove cells and cellular debris. RNA was extracted from the supernatant using Trizol-LS, analysed using a bioanalyser and compared to DMEM and DMEM + 10% FCS (figure 4.4). Bioanalysis revealed a population of small RNAs <150nt released by PC3 cells into the media.

To confirm that this population of small RNAs contains miRNAs, qPCR was performed on the PC3 conditioned media RNA (figure 4.5). The presence of 5 miRNAs; miR-16-5p, miR-423-3p, miR-222-3p, miR-93-5p and miR-221-3p, was analysed and compared to DMEM and DMEM + 10% FCS. All 5 miRNAs were found at significantly higher levels in PC3 conditioned media compared to DMEM + 10% FCS ($P<0.05$ for miR-93-5p, $p<0.01$ for all remaining miRs), indicating that these miRNAs are PC3 cell derived.

After confirming the presence of miRNAs in PC3 cell conditioned media, we looked to analyse how these are distributed. PC3 cell conditioned media was therefore centrifuged at increasing forces (xg), to remove various debris and other components, and the remaining supernatant was analysed to assess the concurrent loss in miRNA by qPCR (figure 4.6A-E). Centrifugation in this way removes different cellular contents at each stage; 2,000xg – cells, dead cells and apoptotic bodies, 16,000xg – cell debris and lEVs such as microvesicles, 100,000xg – sEVs such as exosomes and smaller microvesicles (Szatanek *et al.*, 2015). miRNAs were expressed at different levels in PC3 cell conditioned media, for example miR-16-5p and

miR-221-3p showed much higher expression than miR-423-3p, miR-222-3p and miR-93-5p. This matches the expression pattern seen in figure 4.5. However, although miRNAs were expressed at different levels, all tested miRNAs showed the same trends of depletion with increasing centrifugation, detailed as follows. Centrifuging cells at 2,000xg for 5 minutes resulted in no change in miRNA level. However, centrifugation at 16,000xg for 15 minutes removed an average of 12.5% of the miRNA found in uncentrifuged PC3 cell conditioned media. Centrifuging media at 100,000xg for 90 minutes resulted in a reduction in the levels of all tested miRNAs compared to media centrifuged at 16,000xg, This reduction in miRNA level failed to reach significance for individual miRNAs. Howver, the average miRNA loss between 16,000xg and 100,000xg centrifugation steps for the 5 miRNAs was >17% (p=0.006) (Figure 4.6E). Overall this shows that miRNAs are associated with various structures within conditioned media, and that the vast majority of miRNAs are likely not vesicle associated.
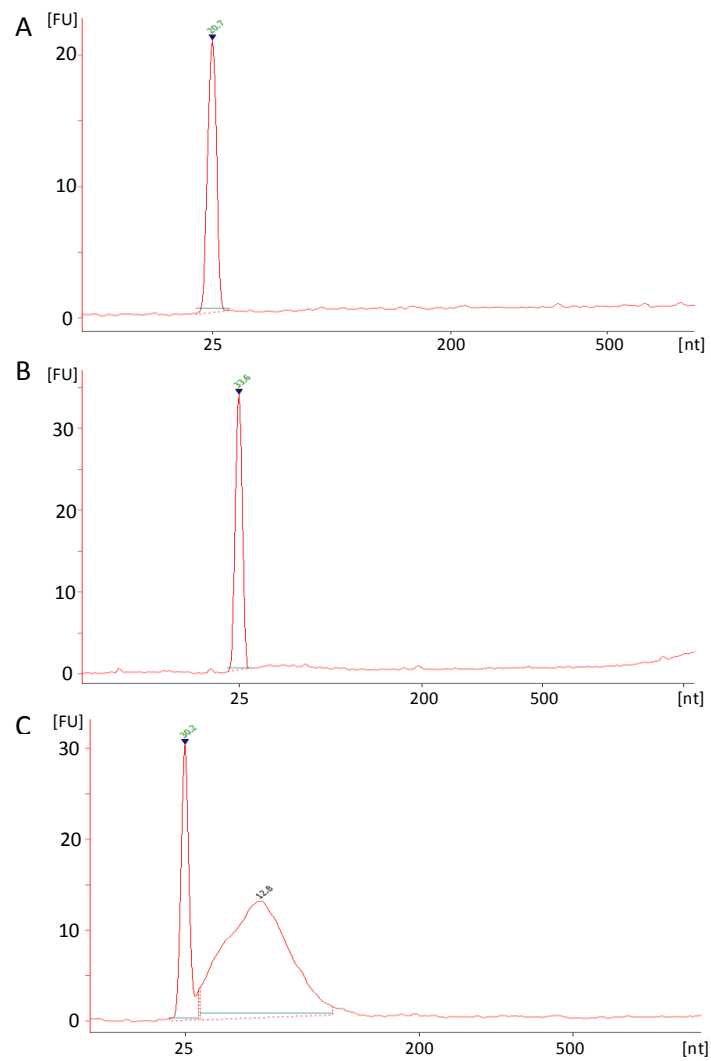
Figure 4.4: Bioanalyser Traces of Media Samples. Bioanalyser histograms showing levels of RNA in (A) Serum Free DMEM (B) DMEM + 10% FCS (C) DMEM + 10% FCS, conditioned with PC3 cells for 48 hours.
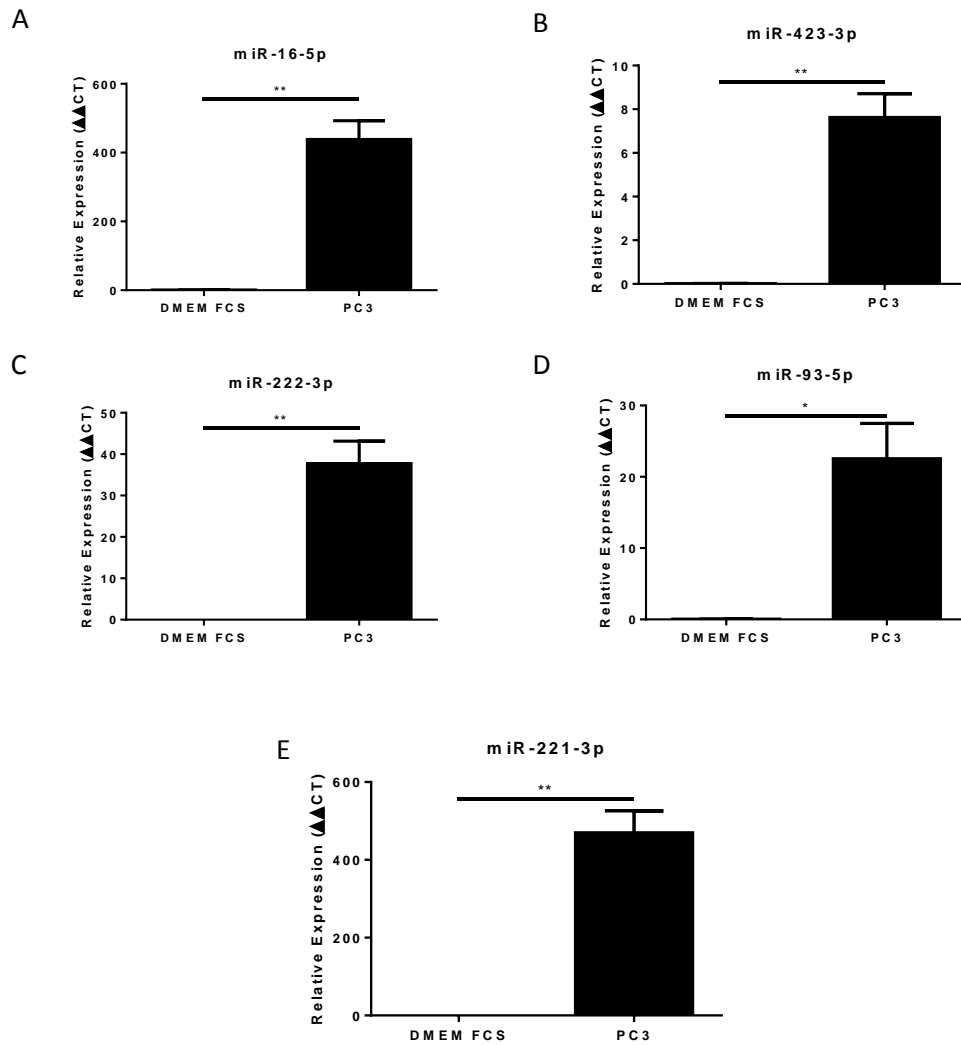
Figure 4.5: qPCR of miRNAs in PC3 Cell Conditioned Media. Levels of (A) miR-16-5p, (B) miR-423-3p, (C) miR-222-3p, (D) miR-93-5p, (E) miR-221-3p in DMEM + 10% FCS and PC3 conditioned DMEM. (Graph shows mean+SEM, n=3) (Statistical significance assessed by unpaired t-test, *p<0.05, **P<0.01)
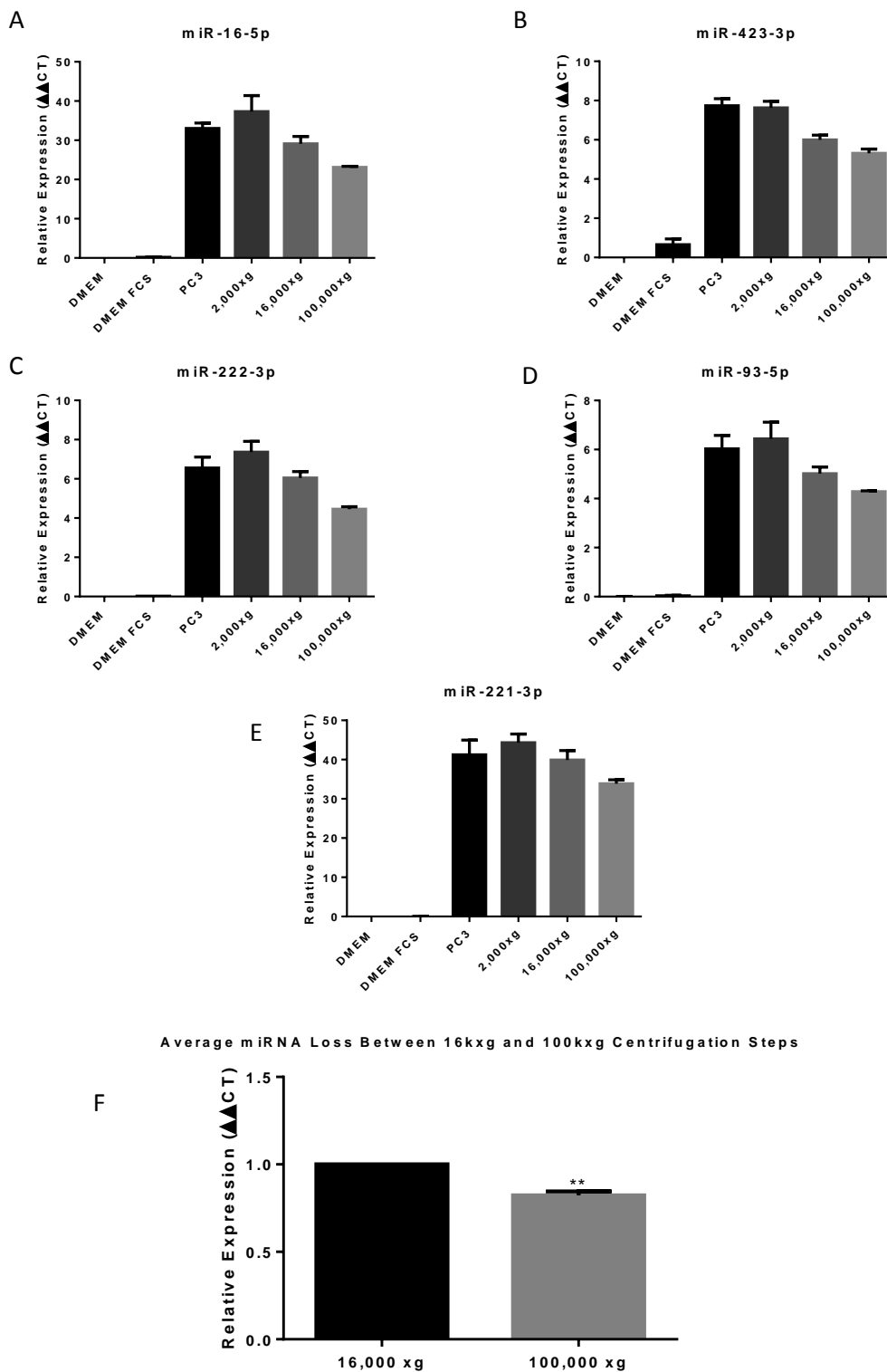
Figure 4.6: qPCR of miRNAs in PC3 Cell Conditioned Media Subjected to Increasing Force Centrifugation. Levels of (A) miR-16-5p, (B) miR-423-3p, (C) miR-222-3p, (D) miR-93-5p, (E) miR-221-3p in PC3 conditioned media after centrifugation at increasing forces) (F) Average of miRNA loss between 16,000xg and 100,000xg centrifugation steps (Graphs show mean+SEM, n=3, statistical significance assessed by one-way ANOVA for figures 4.6A-E and unpaired t-test for figure 4.6F, *p<0.05, **p<0.01)

4.4 Discussion

Cancer cell induced changes to the function of cells within the bone microenvironment drives the osteolytic/osteoblastic presentation seen in bone metastases. Metastases from PCa form predominantly osteoblastic lesions, characterised by increases in both osteoblastogenesis and osteoblast function (Ottewell, 2016; Ye *et al.*, 2007). Therefore, the aim of this chapter was to analyse the effect of local PCa cells on the osteoblastic bone model described in the previous chapter.

To test the effect of PCa cells on the osteoblastic model described earlier, we set up a co-culture experiment using 7F2 osteoblast cells and PC3 PCa cells. PC3 cells are PCa cells isolated from a bone metastasis. PC3 cells are androgen receptor negative and are often used for their aggressive nature compared to other PCa cell lines such as LNCaPs (Tai *et al.*, 2011). The 7F2 cells used in this co-culture were a gift from Dr Bronwen Evans, and mineralisation in these cells initiated at around day 6. These cells were later replaced with 7F2 cells from the ATCC, in which mineralisation initiated at around day 10, as shown in the previous chapter. These 7F2 cells were therefore mineralised in the presence of PC3 cells for 6 days. Using inserts with a 0.4µm pore size is a commonly utilised method of preventing cell migration whilst allowing the passage of small signalling molecules (Alexander *et al.*, 2015; Guo *et al.*, 2016). Crucially, a pore size of 0.4µm allows the passage of particular sEVs, such as exosomes, whilst limiting the passage of lEVs including MVs and apoptotic bodies. Mineralising osteoblasts in this way would allow us to determine whether communication between the two cell lines can affect mineralisation, and to what extent. Staining of co-cultured 7F2 cells revealed that PC3 cells had no effect on mineralisation in regular MEM, therefore indicating the PC3 cells do not produce factors that alone initiate mineralisation on this time scale. However, in osteogenic MEM, PC3 cells were able to enhance mineralisation in the 7F2 cells in a PC3 cell number dependant manner. Furthermore, visual

inspection of ARS stained co-cultured 7F2s revealed that areas of increased mineralisation were localised to the area directly beneath the insert. Crystal violet staining showed that these patches also displayed decreased cell confluence, likely a result of the cell cycle exit that occurs upon cell differentiation and as a precursor to matrix mineralisation (Rutkovskiy *et al.*, 2016). These staining patterns further indicate that differentiation is stimulated by secreted factors from the PC3 cells above. The osteoblastic model described in the previous chapter also detailed 4 genes that showed differential expression in mineralising vs control 7F2s. In this model, DLX5 showed decreased expression whereas COL1A1, MMP3 and ACVR1 all showed increased expression. 7F2 cells co-cultured with PC3 cells in regular media showed no change in the pattern of expression, an unsurprising result given that no increase in ARS staining was seen in this group. In mineralising media, co-culture with PC3 cells induced cell number dependant changes in these genes consistent with those seen in the mineralising 7F2 model in all genes bar COL1A1, which showed no change. The overall pattern seen in these gene changes supports ARS staining data suggesting that communication between the two cell lines has a pro-osteoblastic outcome in an environment that allows mineralisation.

As discussed, increased osteoblast function is characteristic of an osteoblastic lesion. However, PC3 cells are known to form osteolytic lesions (Akech *et al.*, 2010; Fradet *et al.*, 2013), and have been shown to have an inhibitory effect on the mineralisation of the osteosarcoma cell line SaOS-2 (Yuen *et al.*, 2010). Therefore, it was interesting to note that in this osteoblastic model, using 7F2 cells, that PC3 cells promoted mineralisation. PC3 cells do express a number of factors such as, TGF-β1 (Lee *et al.*, 2003b), BMP-4 and BMP-6 (Keller & Brown, 2004) that are known to induce osteoblast differentiation (Chen *et al.*, 2012; Yamaguchi *et al.*, 1996; Zhu *et al.*, 2012).

It could be argued that these pro-mineralising effects are not specific to PCa cells and are simply due to the presence of secreted signalling molecules from cells, regardless of origin. To test this, 7F2 cells were mineralised in osteogenic conditioned media from PCa cells as well as non-cancerous prostate cells. Compared to unconditioned osteogenic media, prostate epithelial PZ-HPV-7 conditioned media had no effect on the level of 7F2 mineralisation, whereas PC3 conditioned media induced a significant increase. Another PCa cell line, DU145, was also able to induce mineralisation, albeit to a lesser extent than PC3 cells. DU145 cells are also an aggressive metastatic PCa cell line, harvested from a brain metastasis. DU145 cells also form osteolytic lesions, again making their effect on osteoblasts surprising. LNCaP cells showed a minimal induction of mineralisation in the 7F2 cells, far less than seen with PC3 or DU145 cells. LNCaP cells are a PCa cell line harvested from a left supraclavicular lymph node metastasis. LNCaP cells are less aggressive than PC3 and DU145 cells with respect to their abilities to form metastases in mice, but do form mixed lesions, as opposed to the typically osteolytic lesions seen in PC3/DU145 metastases (Dai *et al.*, 2016). Together, the conditioned media results suggest that these pro-mineralising effects seen are specific to aggressive PCa cell lines, and do not correlate with the typical osteolytic/osteoblastic presentation seen in mouse bone lesions from the same cells.

As discussed, PCa cells produce a number of well characterised signalling molecules capable of inducing increased osteoblast function, such as BMPs, TGF-β, endothelin 1 (ET1), vascular endothelial growth factor (VEGF), platelet-derived growth factor (PDGF) and many more (Guise *et al.*, 2006; Logothetis & Lin, 2005). More recently, the role of miRNAs in the differentiation of osteoblasts has been investigated, with a number of miRNAs showing a propensity to either promote or inhibit this process (Peng *et al.*, 2016). For example, miR-27 promoted differentiation in hFOB1.19 cells via modulation of the Wnt signalling pathway (Wang & Xu, 2010) whereas miR-31 inhibited the differentiation of human mesenchymal

stem cells (hMSCs) by repressing special AT-rich sequence-binding protein 2 (SATB2) (Xie *et al.*, 2014).

To test whether the effects seen in our co-culture model may be mediated by miRNAs, we tested PC3 cell conditioned media for the presence of 5 miRNAs known to be expressed in PCa (Galardi *et al.*, 2007; Hellwinkel *et al.*, 2013; Luu *et al.*, 2017; Song *et al.*, 2017). All 5 miRNAs showed significantly higher expression in PC3 cell conditioned media compared to DMEM +10% FCS, indicating miRNA release from PC3 cells during culture. Interestingly, miR-16-5p and miR-221-3p showed roughly 20x higher expression in PC3 cell conditioned media than miR-423-3p, miR-222-3p and miR-93-5p.

Differential centrifugation of PC3 cell conditioned media from 2,000xg up to 100,000xg gave insight into which structures these miRNAs are associated with, within the conditioned media. Differential centrifugation showed no decrease in miRNAs at 2,000xg, which, given that miRNAs are known to be associated with apoptotic bodies (Zernecke *et al.*, 2009), and that apoptotic bodies are removed at 2,000xg (Szatanek *et al.*, 2015), indicates a potential lack of dead cells and apoptotic bodies within the conditioned media. This is unsurprising given cells were only cultured for 48 hours and exhibited the morphology of healthy cells. A decrease in miRNA was seen at 16,000xg indicating that a fraction of miRNAs within the conditioned media are likely associated with cell debris, or with microvesicles, which is well documented (Jansen *et al.*, 2014). Centrifugation at 100,000xg resulted in a further decrease in miRNA expression. Centrifuging at forces of ≥100,000xg is well known to pellet sEVs including exosomes (Li *et al.*, 2017; Webber & Clayton, 2013), as well as other sEVs and contaminants, therefore the loss in miRNAs seen at this stage likely reflects sEV associated miRNAs. As discussed, centrifugation at 16,000xg removes larger particles such as cell debris and microvesicles (Szatanek *et al.*, 2015). Therefore conditioned media centrifuged at 100,000xg was compared to conditioned media centrifuged at 16,000xg, as the difference

between these two reflects the loss of miRNAs from media containing only sEVs and other small contaminating molecules/proteins. Overall, the loss of miRNAs between these two groups was around 17%, indicating that this fraction of miRNAs are associated with small EVs or other co-pelleted contaminants. miRNAs are known to be exported from cells associated with argonaute proteins (Arroyo *et al.*, 2011), which likely reflects some of the miRNAs remaining after 100,000xg centrifugation, which as a whole, represents the majority of secreted miRNAs.

Combined, the results of the differential centrifugation give an idea of the mechanisms by which miRNAs are exported from PC3 cells, as well as indicating the relative amount of miRNAs that are exported in each way. Namely, miRNAs appear to be exported in three main groups, two smaller populations of miRNAs associated with microvesicles and smaller EVs, and a larger population of miRNAs associated with smaller molecules such as argonaute, that do not pellet at 100,000xg.

Overall, the results from this chapter show that PC3s are able to stimulate a pro-osteoblastic effect in mineralising 7F2 cells. Analysis of PC3 cell conditioned media confirmed the presence of miRNAs, of which a fraction were lost at 100,000xg. Together this suggests that miRNAs from PC3 cells may be mediating this pro-osteoblastic effect and that miRNAs associated with EVs are a possible mechanism by which this occurs.

4.5 Summary of Key Points

7F2 cells co-cultured with PC3 cells showed increased mineralisation in osteogenic media in a PC3 cell number dependant manner. This effect was seen at the gene expression level using genes characterised in the 7F2 differentiation model. The mineralising effects of various prostate cell conditioned media indicates that this process is specific to the more aggressive PCa cell lines. PC3 cells export miRNAs during culture which are detectable in conditioned

media. Differential centrifugation of this media indicates that a fraction of these miRNAs are

lost at 100,000xg, a force commonly used to pellet sEVs including exosomes.

Chapter V: Isolation of sEVs and Analysis of their miRNA Content

5   Isolation of SEVs and Analysis of their miRNA Content

5.1   Introduction

Cell signalling is one of the most studied aspects of cell biology. The majority of this time has been focussed on signalling through molecules such as secreted proteins or hormones. However, recently, the field of intercellular communication has shifted focus, with signalling through extracellular vesicles (EVs) becoming an exponentially growing research field (Lotvall *et al.*, 2014). EVs have gained much attention due to the variety of cargo they are able to transport, including proteins, DNA, mRNA and a wide variety of non-coding RNAs as well as the profound changes they drive in recipient cells.

As discussed, Chim *et al.* (2008) discovered the presence of miRNAs in extracellular biological fluids, indicating their potential as mediators of cellular communication. It is now known that miRNAs are exported from cells in two main ways; either attached to structures such as HDLs (Vickers *et al.*, 2011) and argonaute proteins (Arroyo *et al.*, 2011) or released associated with (or within) extracellular vesicles (Yu *et al.*, 2016; Zhang *et al.*, 2015). Previous data from Dr Alwyn Dart, using Sepharose CL-2B size exclusion chromatography of prostate cancer cell conditioned media, showed that miR-27 was released from PC3 cells in two distinct groups co-purifying with either smaller species in fractions 19-29 (*i*) or with larger species in fractions 7-13 (*ii*) (figure 5.1A). Previous chromatography work from Welton *et al.* (2015) on plasma samples showed a peak signal of CD9, an exosomal surface marker, in fractions 7-16 and a peak signal of albumin from fractions 20-30. The similar trends in peaks between the miRNA and the vesicles/free protein levels between these two figures further validates the idea that PC3 miRNAs are released associated with (or within) vesicles and other smaller non-vesicular molecules. This data is also consistent with findings from the previous chapter, which suggest

that PC3 exported miRNAs associate with both larger and smaller EVs, pelleted at 16,000xg

and 100,000xg respectively, as well as with lighter non-pelleted structures.
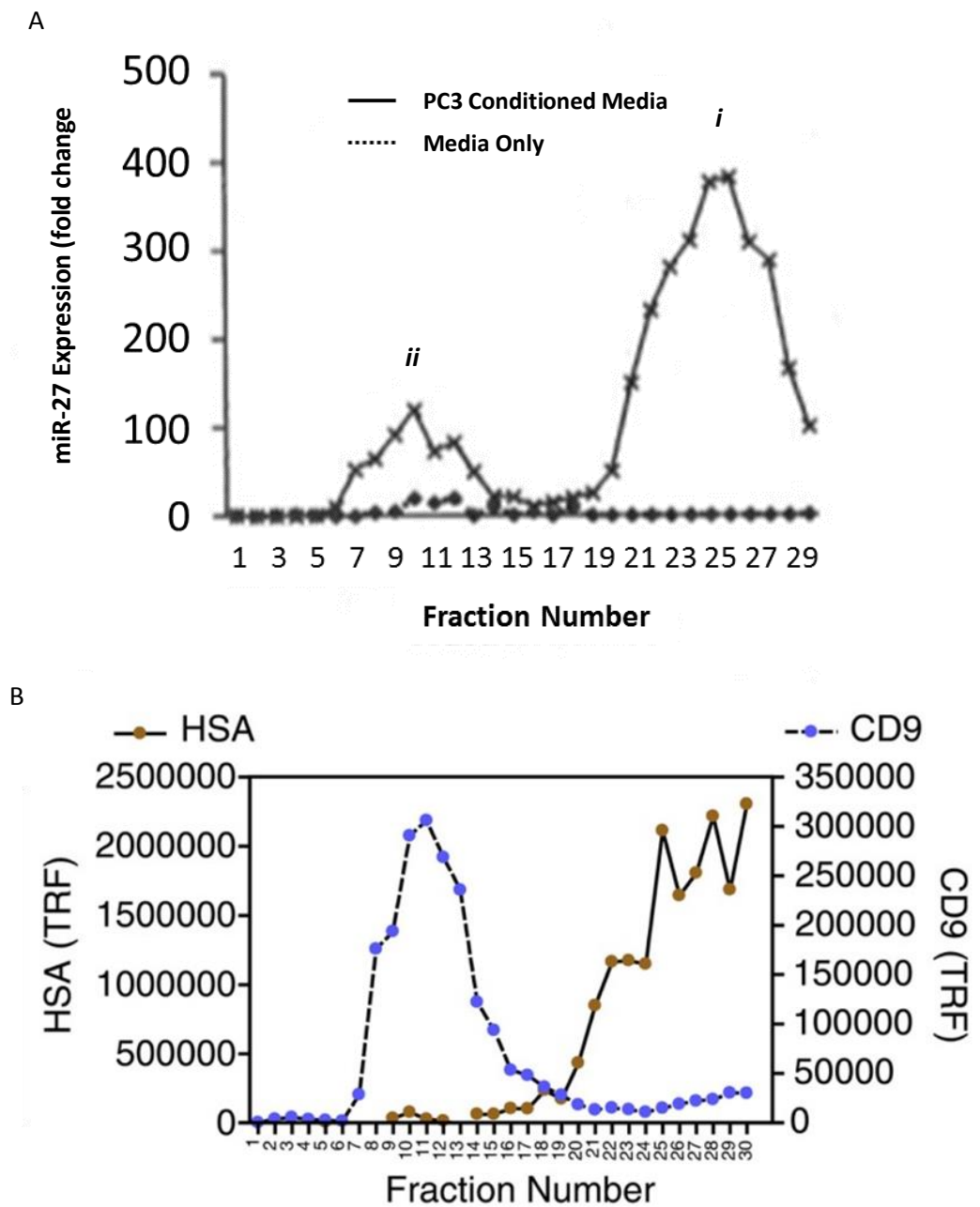
Figure 5.1: Size Exclusion Chromatography. (A) Data from Dr Alwyn Dart showing miRNA detection in fractionated PC3 cell conditioned Media using qPCR. *ii*: miRNAs associated with larger species. *i:* miRNAs associated with smaller species. (B) Fractionated plasma, tested for the presence of the exosomal surface marker CD9 and albumin (HSA) by ELISA (Welton *et al.*, 2015).

miRNAs can be exported from cells in both lEVs such as microvesicles and sEVS such as exosomes. Exosomes are roughly 40-150nm in size. Exosome biogenesis originates within endosomes, where inward budding of the endosomal membrane creates a multivesicular endosome (MVE) containing many exosomes (Huotari & Helenius, 2011). Subsequent fusion of the MVE with the cell membrane releases the exosome cargo into the extracellular space. This process involves a complex network of cargo sorting and release proteins such as ALIX (Baietti *et al.*, 2012), TSG101 (Nabhan *et al.*, 2012) and ESCRTs (Kowal *et al.*, 2014). This biogenesis pathway is significantly more complex than microvesicle biogenesis, which although also involving several protein families, is centred around budding from the cell surface. The complex biogenesis of exosomes could explain why the internal RNA population of sEVs appears more specialised than that of lEVs. For example, sEVs have a higher proportion of small RNAs than lEVs and are absent of ribosomal (r)RNA (Crescitelli *et al.*, 2013; Ji *et al.*, 2014).

Delivery of functional miRNAs by exosomes was first shown by Pegtel *et al.* (2010) between Epstein-Barr virus (EBV) infected B cells and Monocyte-Derived dendritic cells. Since then a number of studies have shown delivery of exosomal miRNAs in various bone related models, with varying results. Cui *et al.* (2016) showed that exosomes from mineralising osteoblasts induced osteoblastic differentiation in bone marrow-derived stromal cells, implicating exosomal miRNAs in this process. Li *et al.* (2016a) showed that osteoclast exosomal miR-214-3p was delivered to osteoblasts, resulting in decreased bone formation. Crucially, this process was rescued by treating osteoclasts with antagomiR-214-3p. Finally, Ye *et al.* (2017) showed that MDA PCa 2b cell derived exosomal miR-141-3p induced proliferation and mineralisation in osteoblasts. Furthermore, they showed that exosomal miR-141-3p promoted osteoblastic metastasis of PCa *in vivo*, with miR-141-3p inhibition resulting in decreased metastases and increased survival.

Based on the current literature, including the aforementioned studies, we believe sEV miRNAs from PCa cells to play multiple, crucial roles in the development and progression of bone metastases. Size exclusion chromatography and differential centrifugation of PCa cell conditioned media suggests that miRNAs exported by these cells may be associated with sEVs. Therefore, in this chapter we look to analyse the miRNA content of isolated sEVs from highly aggressive PCa cell lines using next generation sequencing. As a high quality sEV sample will be crucial for our experiments, the isolation and characterisation of sEVs is first discussed. Analysing cellular and sEV miRNAs from the same cells allows for direct comparison of miRNA concentrations. It has been shown that some miRNAs are selectively packaged into sEVs under certain conditions (Goldie *et al.*, 2014; Guduric-Fuchs *et al.*, 2012; Ohshima *et al.*, 2010). Thus, analysing cellular and sEV samples in this way and highlighting any selective packaging that may take place, will further validate the idea of miRNAs as mediators of intercellular communication.

5.2   Chapter Aims

The aims of this chapter are to characterise the sEVs used in this research project and analyse their miRNA content, thus providing an insight into how the PCa cells communicate with other cells, including cells of the bone microenvironment. Therefore, the specific aims of this chapter are:

- To assess whether that sEVs secreted and isolated from PCa cells are consistent with exosomes

- To analyse the miRNA content of these sEVs and their associated cells of origin, using next generation sequencing

- To identify whether miRNAs are being selectively or randomly packaged into PCa cell sEVs

5.3   Results

Isolation of SEVs from PC3 Conditioned Media

SEVs were isolated from conditioned media based on their density using ultracentrifugation and a 1.210g/mL sucrose cushion, a reliable, commonly utilised method (Lamparski *et al.*, 2002). Sucrose cushions were then washed in PBS and subsequently pelleted, before being resuspended in PBS.

The presence of exosome surface characterisation proteins, namely the tetraspanins CD9, CD63 and CD81, were analysed using an Immuno-phenotyping assay. SEVs were coated onto protein binding 96 well strips overnight and analysed for the presence of these common exosomal surface markers, measured by time-resolved fluorescence (TRF) (figure 5.2A). The expression of CD9, CD63 and CD81 was 1.82×10^5, 8.6×10^4 and 3.4×10^4 TRF respectively, after removal of isotype control background which was 2.7×10^3 TRF for IgG2B (CD9) and 986 TRF for IgG1 (CD63 & CD81).

A western blot was then performed on our isolated samples to probe for an exosome enriched protein as well as a protein known to be absent in exosomes. The ESCRT associated protein ALG-2-interacting protein X (ALIX), known to be present in exosomes was detected in both cell lysate and sEVs from PC3 cells (figure 5.2B). Calnexin, a chaperone protein exclusive to the endoplasmic reticulum (ER) was absent in the sEV sample but present in PC3 cell lysate protein. These results are consistent with those of a high purity exosome containing sEV sample (Aqil *et al.*, 2014), in that vesicles appear devoid of cell-derived contaminants.

Nanoparticle tracking analysis (NTA) was used to assess the size of the isolated particles. The mean sizes for the PC3 isolations were 116nm, 107nm and 118nm (figure 5.3A, B & C respectively), an expected size based on the literature (Webber & Clayton, 2013).

Furthermore, no particles >400nm were detected, indicating a lack of any larger contaminants such as larger MVs or apoptotic blebs.

NTA was also used to calculate a particle count for each sample, given in particles/mL. A BCA assay, a quantitative colourimetric protein assay, was then used to calculate total protein concentrations of the same samples. Combining these two values gives a particles:protein (P:P) ratio for the isolated sEV samples. Contaminating protein has been shown to reduce P:P values (Webber & Clayton, 2013), as a result, sEV samples with a P:P < $1x10^{10}$ are considered impure. P:P values were calculated for 3 isolated sEV samples, as a representative example of vesicle isolates used in this thesis. For the presented isolated PC3 sEVs, P:P values of $2.24x10^{10}$, $2.22x10^{10}$ and $2.06x10^{10}$ were calculated (Table 3.1), indicating a high level of purity.
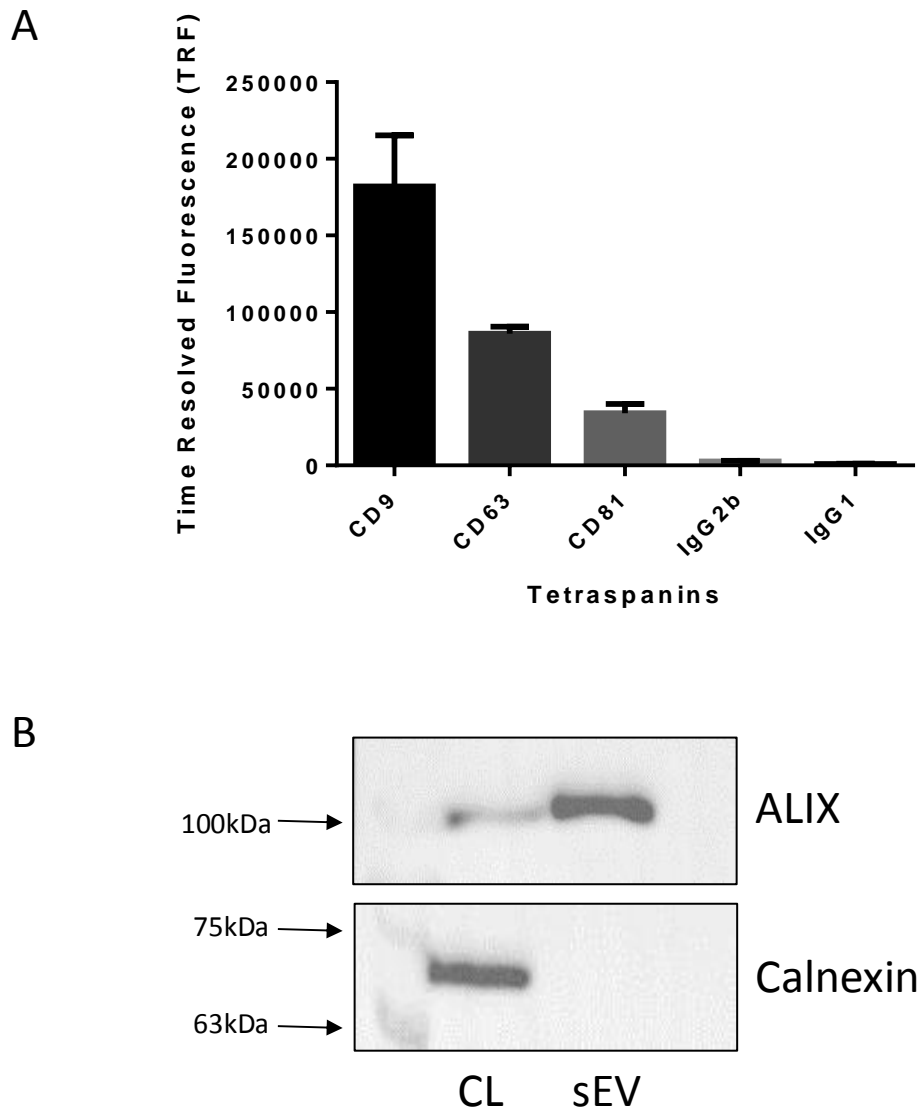
Figure 5.2: Characterisation of PC3 sEV protein. (A) Immuno-phenotyping assay of PC3 sEVs (1μg/well) for exosome associated tetraspanins; CD9, CD63 and CD81 compared to isotype controls. Graph shows average, minus isotype control, for triplicate wells, +SD. (B) Western blot of exosome characterisation proteins; ALIX and Calnexin from PC3 whole cell lysate (CL) (20μg) and PC3 sEV lysate (EXO) (20μg).

A

Mean: 116.0+/-1.0nm

Mode: 98.0+/-6.9nm

B

Mean: 107.4+/-0.8nm

Mode: 86.3+/-5.4nm

C

Mean: 116.0+/-2.4nm

Mode: 108.8+/-5.0nm
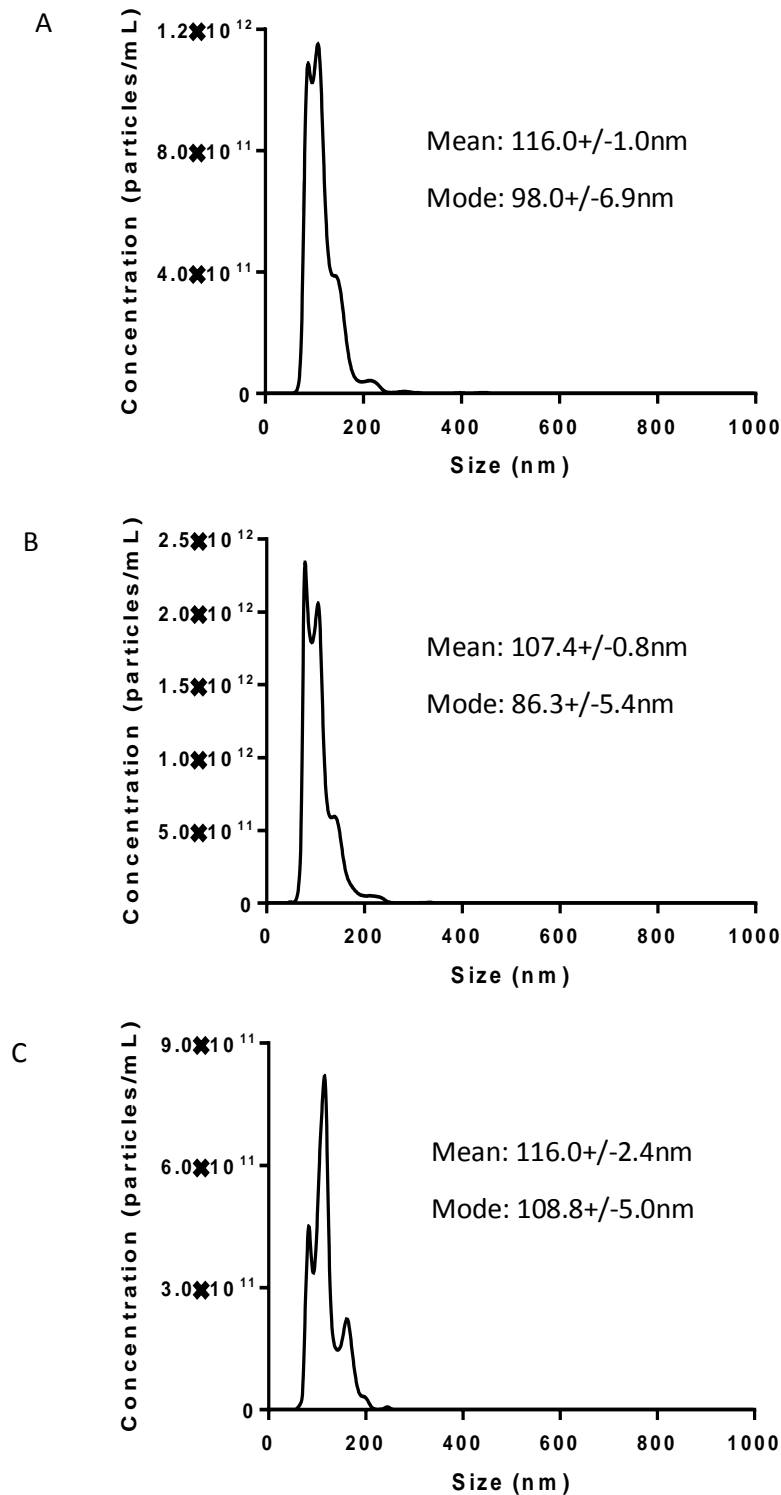
Figure 5.3: Size distribution of isolated vesicles. sEVs isolated from PC3 cell conditioned media using a sucrose cushion analysed by Nanosight[TM] NTA. Analysis was performed on sEVs isolated on 22/11/16 (A), 12/05/17 (B) and 29/01/18 (C). Histograms show average of 3 repeats, each taken from a 60 second video, for each isolation, displaying mean and mode of particle size.

Table 5.1: The purity of sEV isolations from PC3 cells was assessed using the particles:protein ratio. Particles:protein ratios were calculated by dividing particle concentration (determined by NTA) by the protein concentration (calculated using a BCA assay).

Isolation	Date	Particles/ml	Protein Conc (µg/ml)	Particles:Protein
1	22/11/16	6.7×10^{13}	2994.42	2.24×10^{10}
2	12/05/17	1.20×10^{14}	5412.98	2.22×10^{10}
3	29/01/18	3.76×10^{13}	1827.28	2.06×10^{10}

To determine the miRNA content of PCa sEVs, next generation small RNA sequencing was used. To get a better idea of the general trends of miRNA expression seen in PCa cells and sEVs, DU145 samples were also run. Running two aggressive PCa cell lines would allow for a comparison in the expression of miRNAs, adding validity to any trends found, and isolating any common miRs associated with aggressive PCa. For efficient sequencing of small RNAs, a filtration process was utilised to remove as much contaminating larger RNA as possible. RNA from PC3 cells and sEVs was used alongside RNA from DU145 cells and sEVs (DU145 sEVs were a gift from Prof Aled Clayton). Both sets of sEVs were isolated based on density using an ultracentrifugation sucrose cushion method (Webber & Clayton, 2013). RNA was extracted from all samples and filtered using a LifeTechnologies mirVana miRNA Isolation Kit. This separates the RNA into fractions greater than and less than 200nt using glass fibre filters. The larger RNAs captured within the filter, as well as the smaller RNAs found in the eluate were run along with unseparated RNA from the same samples on an Agilent Bioanalyser chip.

For PC3 samples (figure 5.4), the cellular unfractionated RNA sample included a peak for the small RNA population as well as large amounts of 18s and 28s rRNA. For the captured cellular RNAs, the rRNA still remains but the small peak at 25-30s has been removed. In the eluted cellular RNA, the rRNA has been completely removed and only a population of small RNAs remains. sEV unfractionated RNA also contained a population of small RNA but only a small amount of 18s rRNA. In the captured sEV RNA, the 18s rRNA is still present. The peak representing the smaller RNAs is still present, but the amount of RNA has reduced by over 50%. For the eluted sEV RNA, the small amounts of 18s rRNA has been removed, but the small RNA population remains.

For DU145 samples (figure 5.4), the cellular unfractionated RNA showed a peak for the small RNAs and substantial peaks for the 18s and 28s rRNAs. For the captured cellular RNAs, the peak at 25-30s has been filtered out but the rRNA still remains. For the eluted cellular RNA,

the rRNA has been completely removed and only the population of small RNAs remains. In the sEV total RNA, only a small amount of 18s rRNA is present. Small RNAs are present represented by a small peak at 25-30s. In the captured sEV RNA, the 18s rRNA is no longer present but almost all of the small RNA has also been removed. Finally, in the eluted sEV RNA, the small amounts of 18s rRNA have been removed, and the population of small RNAs still remains.

Overall, the results of the bioanalyser traces showed that RNA separation was successful as the larger rRNA appeared only in the unseparated and >200nt fractions and was absent in the <200nt sample. Small amounts of 18s rRNA were found in the sEV samples which is consistent with traces performed by Jenjaroenpun *et al.* (2013) on breast cancer exosomes. However, these were also successfully removed during the filtration process.

Figure 5.4: Bioanalyser Traces for PC3 Cell and sEV RNA samples. Traces on the left side are from PC3 cells whereas traces on the right side are from purified PC3 sEVs. The top row represents unfractionated RNA, the middle row represents RNAs captured within the RNA filter and the bottom row represents RNAs that were collected from the eluate from the filter.
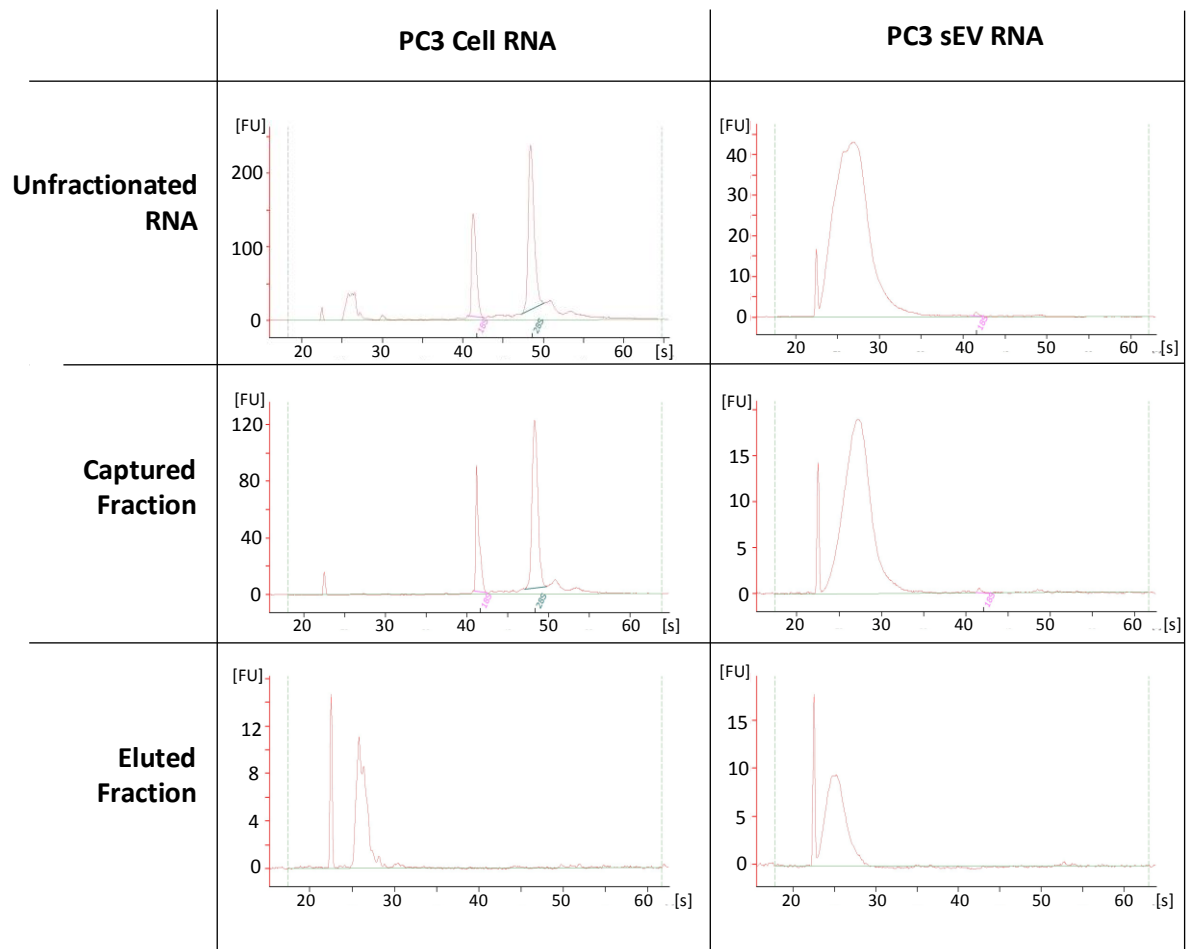
Figure 5.5: Bioanalyser Traces for DU145 Cell and sEV RNA samples. Traces on the left side are from DU145 cells whereas traces on the right side are from purified DU145 sEVs. The top row represents unfractionated RNA, the middle row represents RNAs captured within the RNA filter and the bottom row represents RNAs that were collected from the eluate from the filter (n=1).
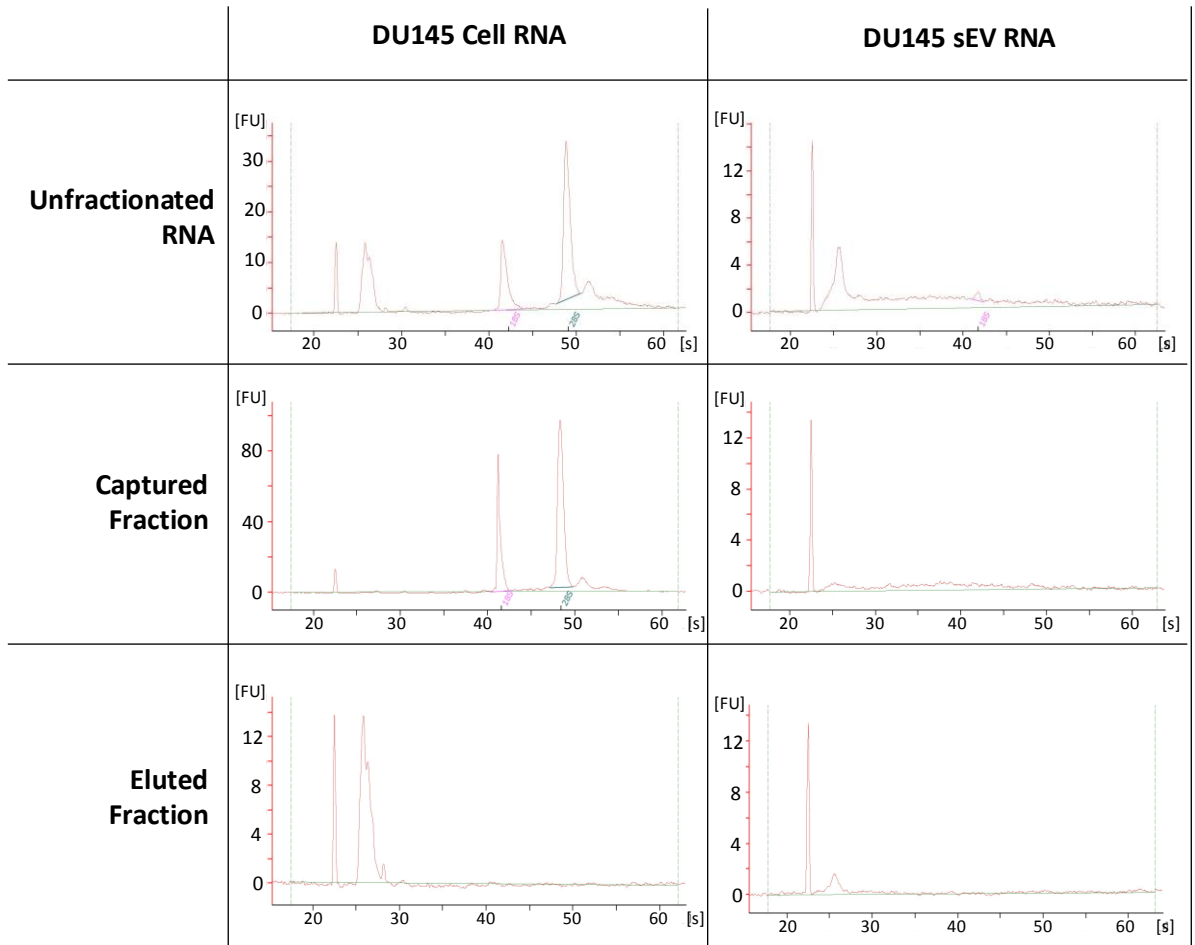
Filtered RNA samples of <200nt from PC3 cells and sEVs were sequenced using a Thermofisher Ion Proton™ Sequencer. Small RNAs were reverse transcribed into cDNA and amplified by PCR, during which time, individual barcode regions were added to the samples to allow post-sequencing sorting. cDNA is then loaded onto Ion Sphere™ Particles (ISPs) and amplified again using an emulsion PCR. These are then loaded onto the sequencing chip for analysis, with a single DNA coated bead filling each microscopic well within the sequencing chip, of which there are 150 million approx. Results from the summary of this sequencing run are shown in figure 5.6. Loading of the sequencing samples onto the sequencing chip was successful, with 83% loading achieved (figure 5.6A), producing a final sequencing library of over 67 million reads (figure 5.6B). The sequencing library showed no detectable reads above 200bp (figure 5.6C) and although the mean sequence length was 72bp, there was peak in reads at around 25-30bp indicative of a large miRNA population.

Sequencing data was assigned to each sample, and subsequently deconvoluted based on their barcodes, before being aligned to human genome 19. Here, sequences were aligned to chromosomal locations, and mapped onto a genomic reference for each gene / miR locus (RefSeq 2017 and miRBase version 20). An example of this can be seen in figure 5.7, showing the alignment of a sequence from the PC3 samples to the human genome using Partek Genomics Suite. In this case, based on alignment with chromosome Xp11.3, the reads aligned to miR-221.

A total of 218 miRNAs were detected in at least one sample. miRNA reads were normalised using a 'reads per kilobase of transcript per million mapped reads' (RPKM) method. Normalisation of reads in this way accounts for both gene size (per kilobase), usually more used in mRNA sequencing due to variable gene length, as well as read depth (per million mapped reads) for each sample. The RPKM values for the 5 highest expressed miRNAs were

recorded for each sample (figure 5.8). For reference, alongside these, the miRNA average is displayed, showing the average expression across all detected miRNAs for that sample.

Looking at all 4 samples, 3 miRNAs appear most highly expressed; let-7a-5p, miR-16-5p and miR-221-3p (figure 5.8). miR-221-3p was the 4th highest expressed miRNA in PC3 cells and the highest expressed miRNA in PC3 sEVs. However, miR-221-3p was not in the 5 highest expressed miRNAs for either the DU145 cellular or sEV samples and was actually expressed at levels below the miRNA average. miR-16-5p was the highest expressed miRNA in DU145 sEVs and was the second highest expressed miRNA in the remaining 3 samples. Let-7a-5p was the highest expressed miRNA in both cell samples and also featured in the top 3 highest expressed miRNA in both sEV samples.

Sequencing results were then validated by qPCR for PC3 and DU145 cellular samples. The levels of two highly expressed miRNAs from cellular sequencing samples; miR-221-3p and miR-16-5p were compared to three miRNAs that showed much lower expression; miR-423-3p, miR-423-5p and miR-93-5p. The results of these qPCRs are shown in figure 5.9B and 5.9D for PC3 and DU145 cells respectively and compared to sequencing results outlined in figures 5.9A and 5.9C. qPCR confirmed that in PC3 cells, miR-221-3p and miR-16-5p are expressed at much higher levels than other miRNAs ($p<0.001$ for all). However, although sequencing showed miR-16-5p to be expressed at a higher level than miR-221-3p, qPCR showed the opposite pattern, with miR-221-3p showing higher expression than miR-16-5p ($p<0.001$). In DU145 cells, qPCR confirmed that miR-16-5p was highly expressed compared to other miRNAs ($p<0.001$ for all). However, miR-221-3p, which showed low expression in DU145 sequencing, showed higher expression than other miRNAs in qPCR ($p<0.001$ compared to miR-423-3p and miR-423-5p) although miR-16-5p expression remained highest ($p<0.001$ compared to miR-221-3p).

Together, although there are minor differences between qPCR and sequencing, expression patterns largely show the same trends. miR-16-5p and miR-221 were confirmed as highly expressed in PC3 cells and miR-16-5p was confirmed as highly expressed in DU145 cells.

sEV RNA was limited, therefore qPCR validation on these samples could not be performed. However, miRNA qPCR of PC3 cell conditioned media showed that miR-221-3p and miR-16-5p were highly expressed compared to miR-222-3p (figure 5.10B). This pattern matches the expression of these miRNAs in sEVs from sequencing (figure 5.10A). Although direct comparison of miRNAs in conditioned media and sEVs should not be made, the similarities in expression patterns between the two goes some way to validate the sEV sequencing results.

To test whether the high expression of miRNAs such a miR-16-5p and miR-221-3p seen in sequencing and qPCR was specific to PCa cells, we analysed the expression of a range of miRNAs in both cell lines and the non-cancerous PZ cell line. qPCR of PZ cells revealed that miR-16-5p and miR-221-3p also show higher expression in these cells compared to other miRNAs. However, miR-16-5p showed significantly higher expression in PC3 and DU145 cells compared to PZ cells (p=0.004 & p=0.001 respectively). miR-221-3p showed significantly higher expression in PC3 cells compared to PZ cells (p<0.001), but showed no difference in expression between DU145 and PZ cells. For miR-93-5p, expression levels between PC3 and PZ cells showed no difference. For miR-423-3p and miR-423-5p, expression in DU145 and PC3 cells was higher than PZ cells for all three (p<0.01 for all).

A

4.8 G — Total Bases   **94** — Key Signal

83%
ISP Loading

ISP Density

B

67,456,671
Total Reads

57%
Usable Reads

ISP Summary

83% Loading	122,623,671	**17%** Empty Wells
100% Enrichment	122,441,879	**0%** No Template
68% Clonal	82,971,856	**32%** Polyclonal
81% Final Library	67,456,671	5% Test Fragments / 3% Adapter Dimer / 11% Low Quality

C

72 bp — Mean   **82 bp** — Median   **83 bp** — Mode
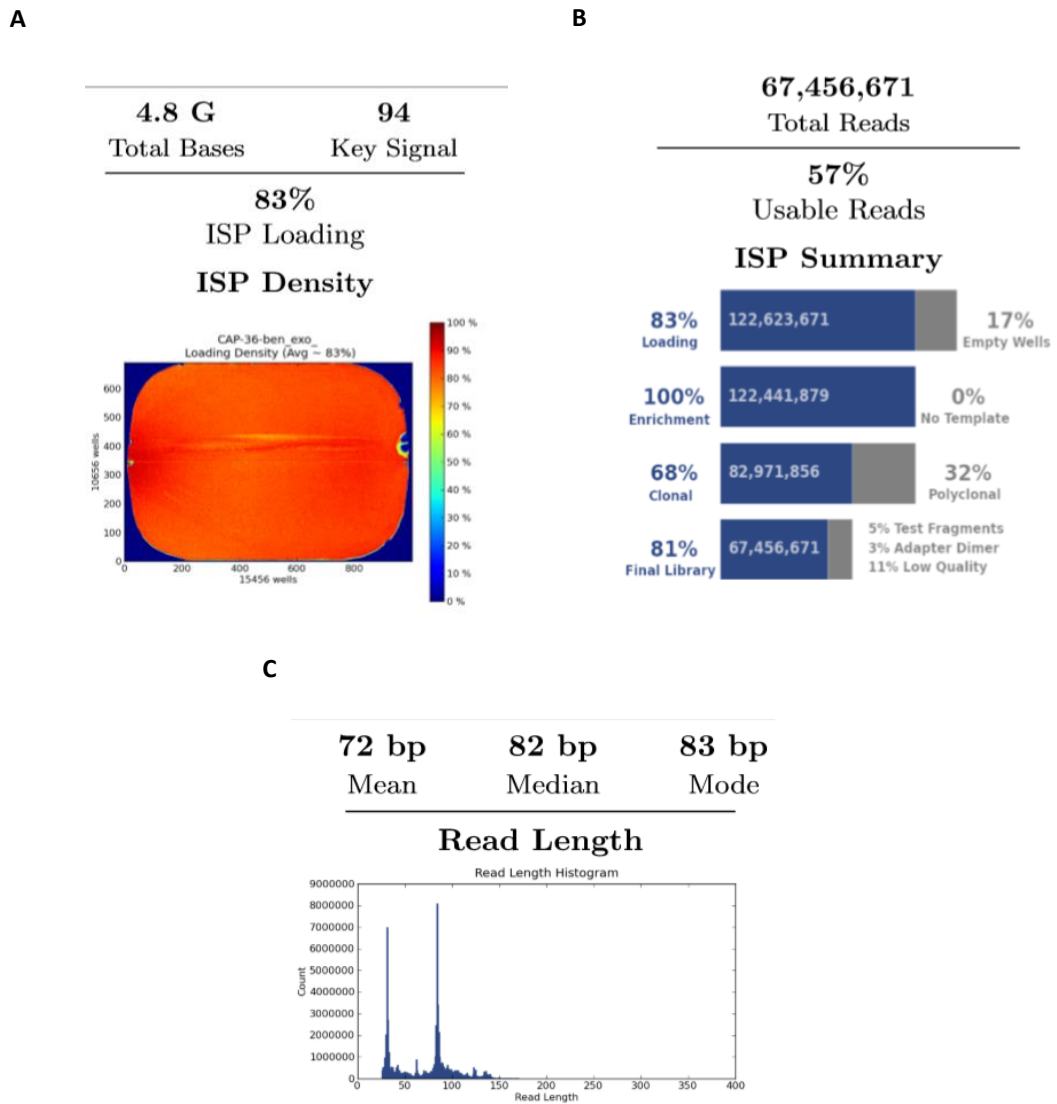
Read Length

Figure 5.6: Overview of Sequencing Run. (A) Heat map showing chip loading efficiency, of the Ion P1 chip. (B) Bar graph showing % usable reads from the sample once polyclonal or untemplated beads were removed. (C) Read length of sequences including mean, median and mode for all samples combined.
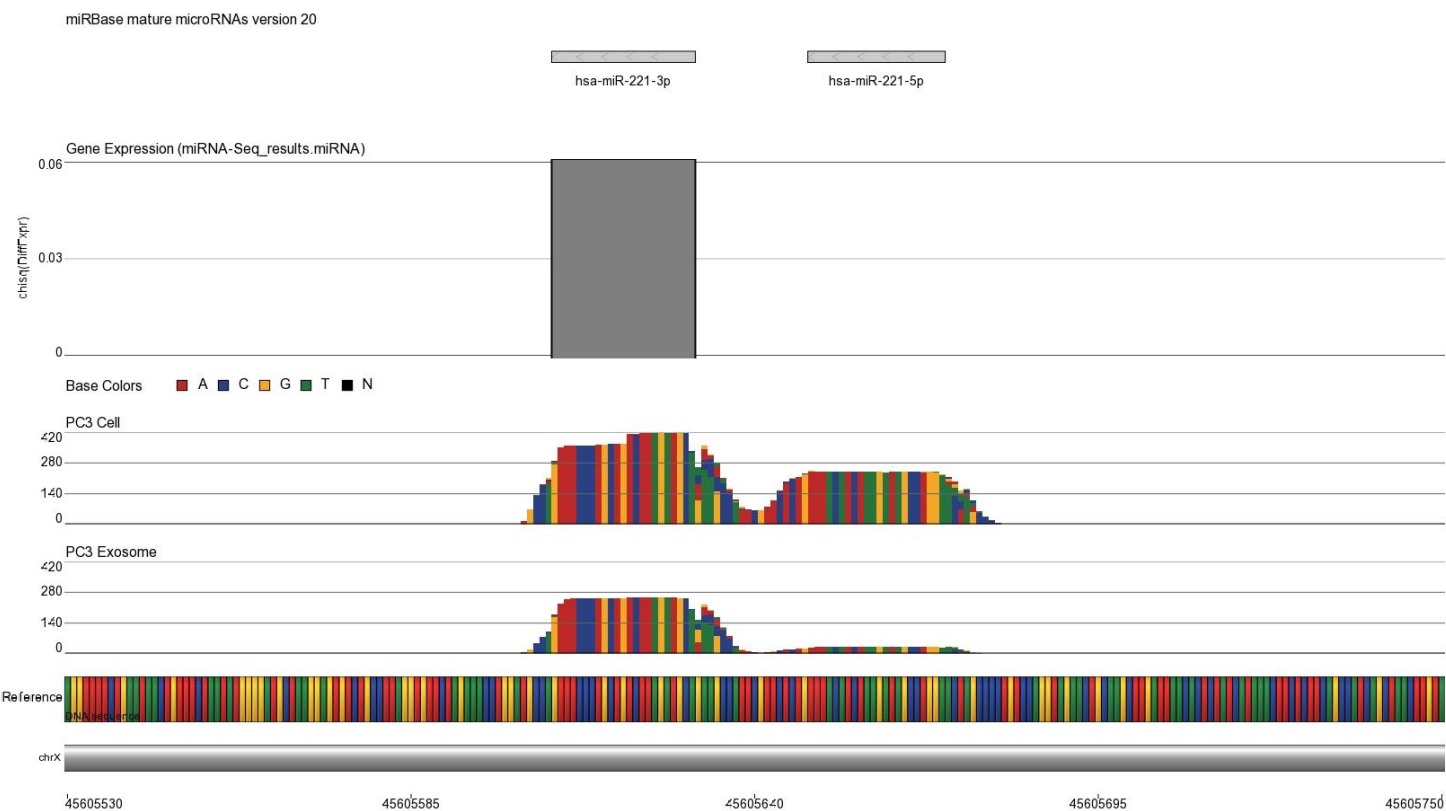
Figure 5.7 Mapping of miR-221-3p and miR-221-5p sequences from PC3 samples to human genome 19, generated using Partek Genomics Suite.
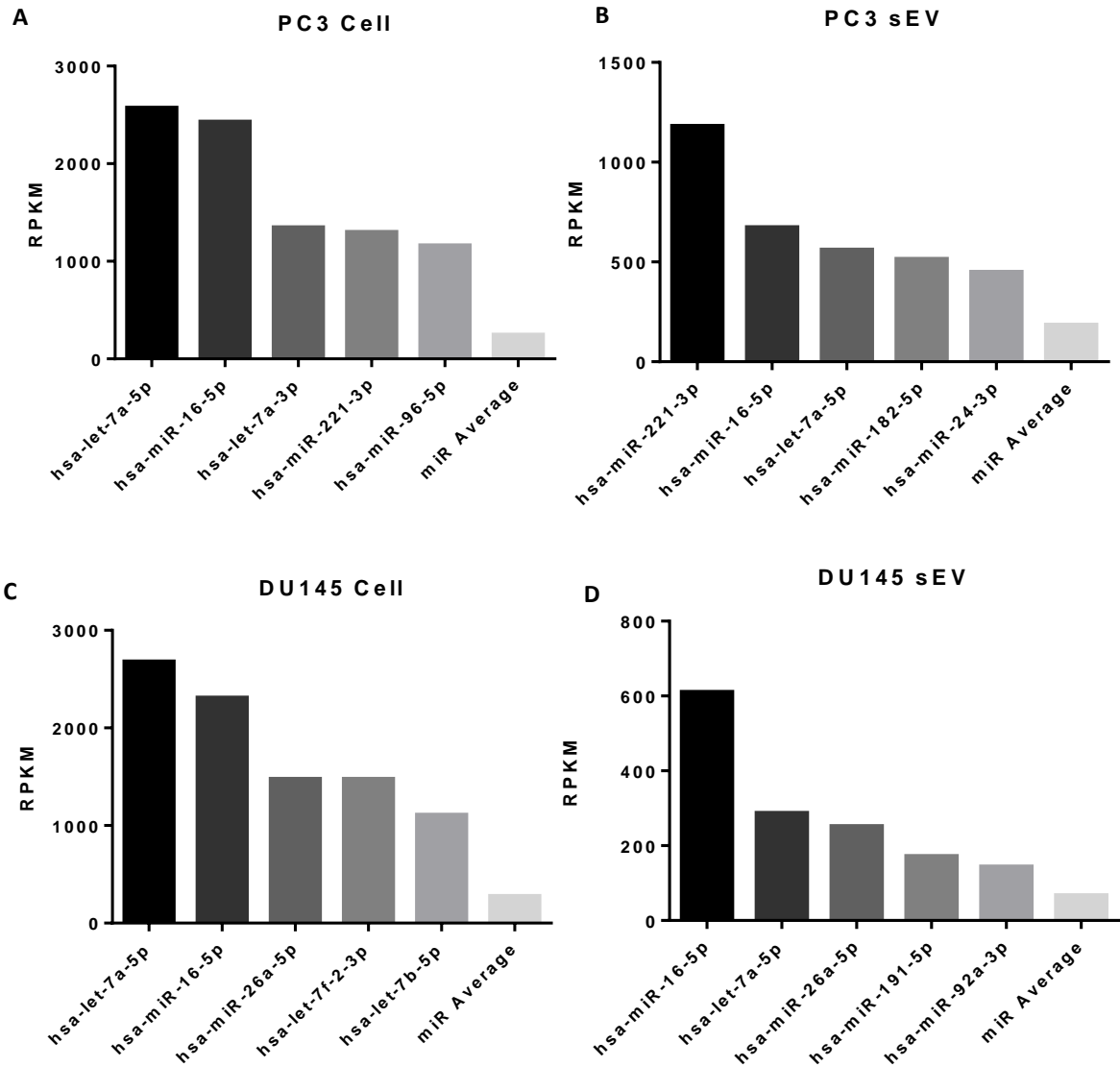
Figure 5.8 miRNA Expression in PC3 and DU145 Cell and sEV Samples from miR-Seq. The top 5 highest expressed miRNAs compared to the average miRNA level in (A) PC3 Cells, (B) PC3 sEVs, (C) DU145 Cells, (D) DU145 sEVs (n=1).
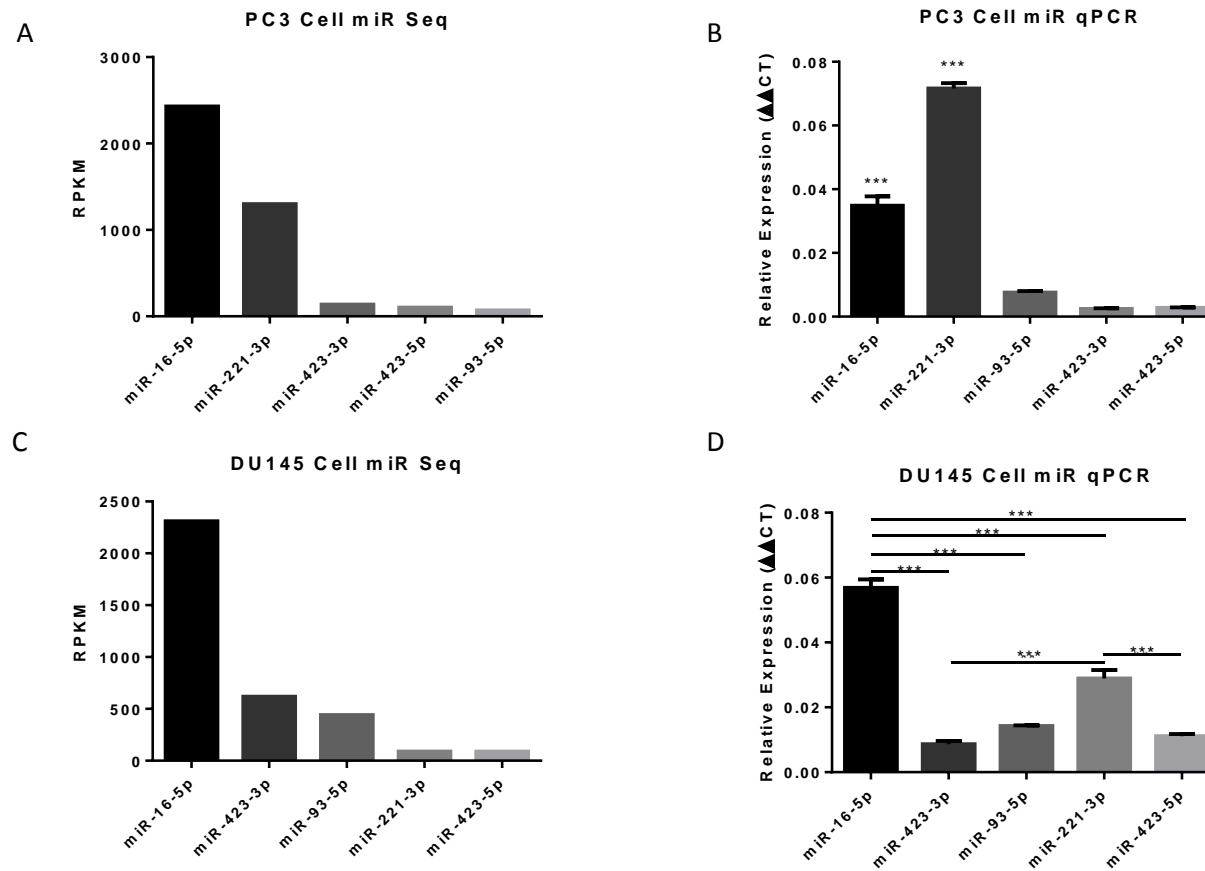
Figure 5.9. qPCR Validation of miRNA Sequencing Results in PC3 and DU145 Cells. High and low expression miRNAs from sequencing data in PC3 and DU145 cells (A & C respectively) were compared with qPCR of the same miRNAs in the same cell lines (B & D). Graphs B & D show average +SEM, n=3. Statistical significance assessed using one-way ANOVA with a Holm-Sidak multiple comparisons test, **p<0.01, ***p<0.001.

A

PC3 sEV miR seq

B

PC3 Conditioned Media miR qPCR
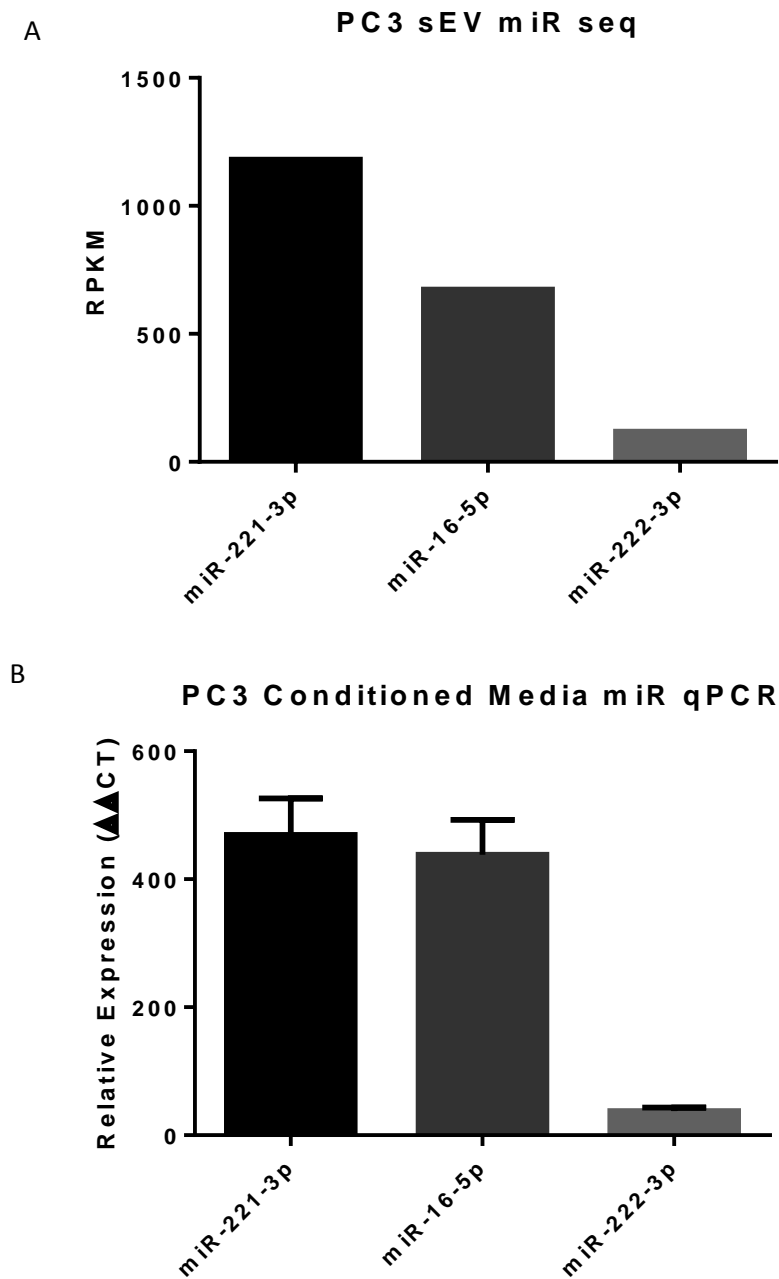
Figure 5.10. qPCR Validation of miRNA Sequencing Results in PC3 sEVs.
High and low expression miRNAs from sequencing data in PC3 sEVs (A) were
compared with qPCR of the same miRNAs in PC3 cell conditioned media (B).
Graph B shows average +SEM, n=3.
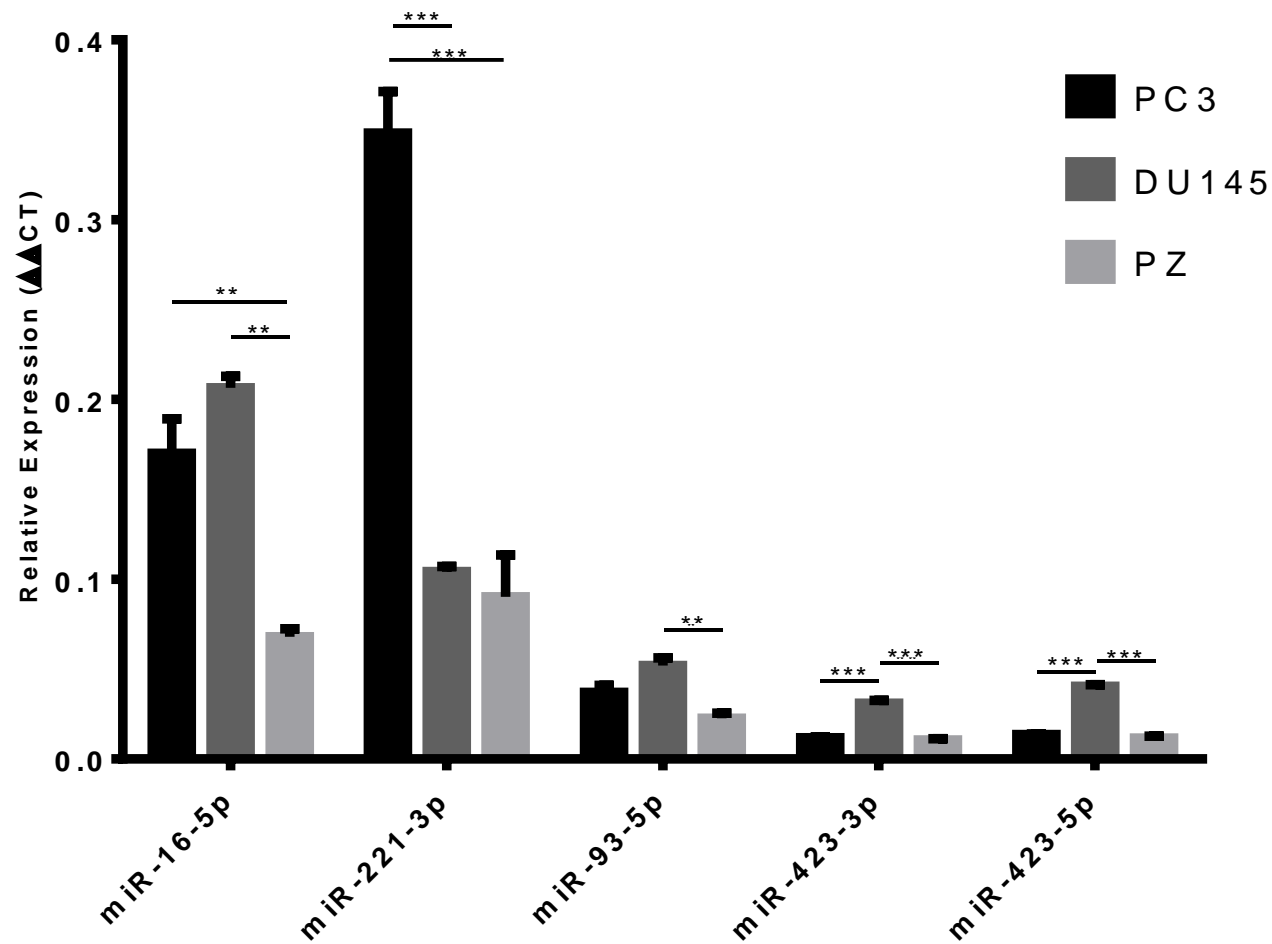
Figure 5.11: Comparison of miRNA Expression in PC3, DU145 and PZ-HPV-7 Cells. miRNAs with high and low expression in PCa cells selected from miRNA sequencing, analysed by qPCR in PC3, DU145 and PZ-HPV-7 cells. Graphs show average + SEM, n=3 (n=2 for PZ). Statistical significance assessed by one-way ANOVA for each miRNA using Holm Sidak multiple comparisons test, *p<0.05, **p<0.01, ***p<0.001.

The ratio of sEV:cellular miRNAs was calculated to determine whether miRNAs were being selectively packaged, excluded or randomly incorporated into sEVs. This was calculated by dividing the sEV RPKM value for each miRNA by its cellular RPKM value. For PC3 cells (figure 5.12) a total of 39 miRNAs were detected in both the cellular and sEV samples. A total of 14 miRNAs were found at higher concentrations in sEVs than in the cell and 19 were found at higher concentrations in the cell compared to the sEVs. Six miRNAs showed similar concentrations in both PC3 samples. miR-182-5p had the highest sEV to cellular ratio of all miRNAs at 1.96, indicating its selective inclusion into sEVs during biogenesis. miR-221-3p had a similar expression in PC3 cells and sEVs (ratio= 0.91). miR-16-5p and Let-7a-5p both had less than half the expression in PC3 sEVs as in cells (ratios= 0.28 & 0.22 respectively).

For DU145 cells (figure 5.13) 47 miRNAs in total were found in both cellular and sEV samples. Of these, 46 miRNAs were found at higher concentrations in cells compared to sEVs, with 1 miRNA, miR-181b-5p, showing marginally higher expression in sEVs than cells (ratio= 1.17). Although 98% of miRNAs were found at lower levels in sEVs than cells, there was a large degree of variability within these negative ratios. For example, miR-3184-5p had an sEV:cellular ratio of 0.58 whereas let-7b-5p had a ratio of 0.03, showing that exclusion from sEVs occurred at different extents for each miRNA, indicating a selective mechanism.

To partner the ratio analysis, an XY plot was constructed showing the cellular and sEV RPKM values for each miRNA found in both cells and sEVs (figure 6.14). A spearman rank order correlation test was performed to assess the link between cellular and sEV miRNA concentrations. Both PC3 and Du145 cells produced a correlation p value of <0.05 indicating a positive correlation. Combined with ratio analysis, these results suggest that miRNAs are packaged into sEVs largely based on cellular concentrations, but that some miRNAs may be selectively incorporated or excluded.
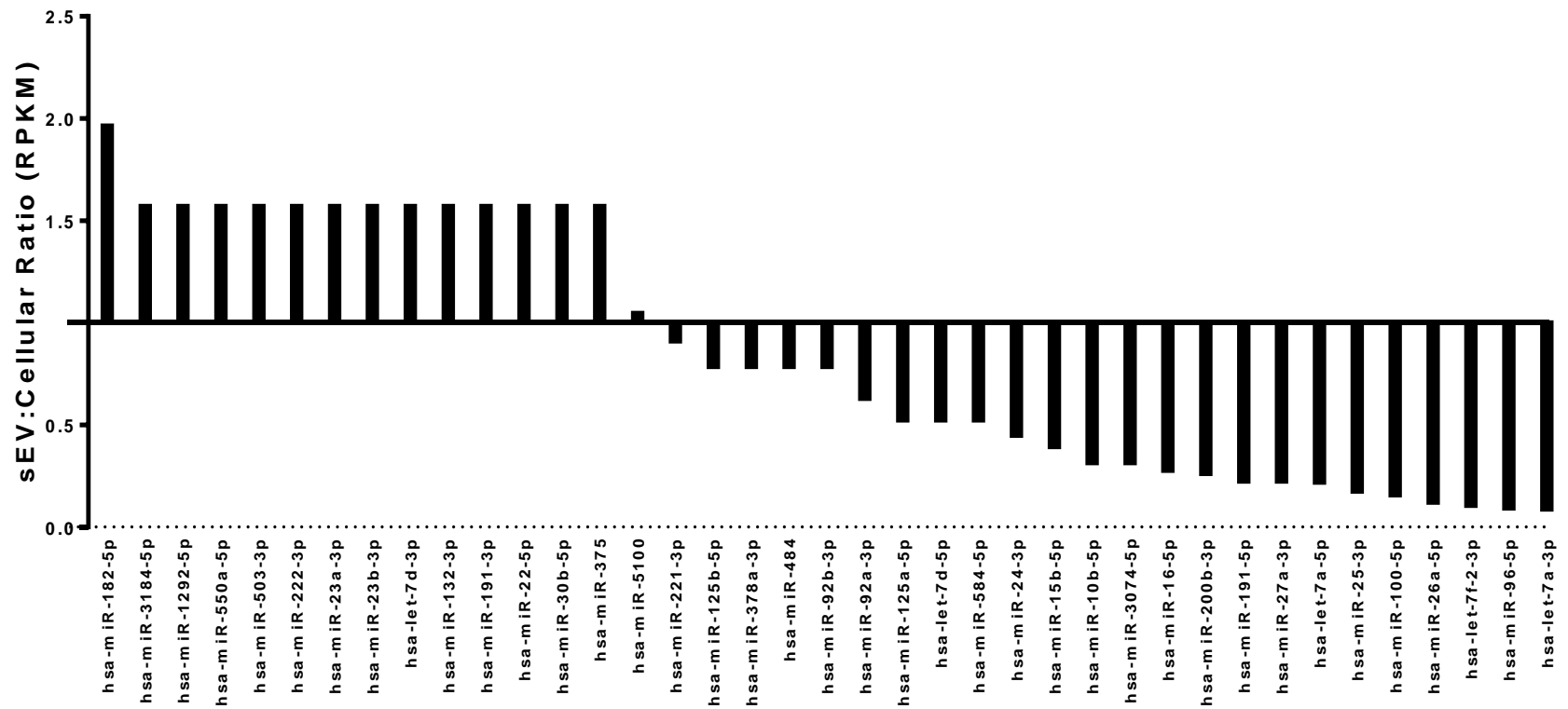
Figure 5.12: The ratio of sEV:Cellular miRNAs in PC3 samples. Ratio was calculated by dividing the RPKM for the sEV samples by the RPKM for the cellular samples for each miRNA (n=1).
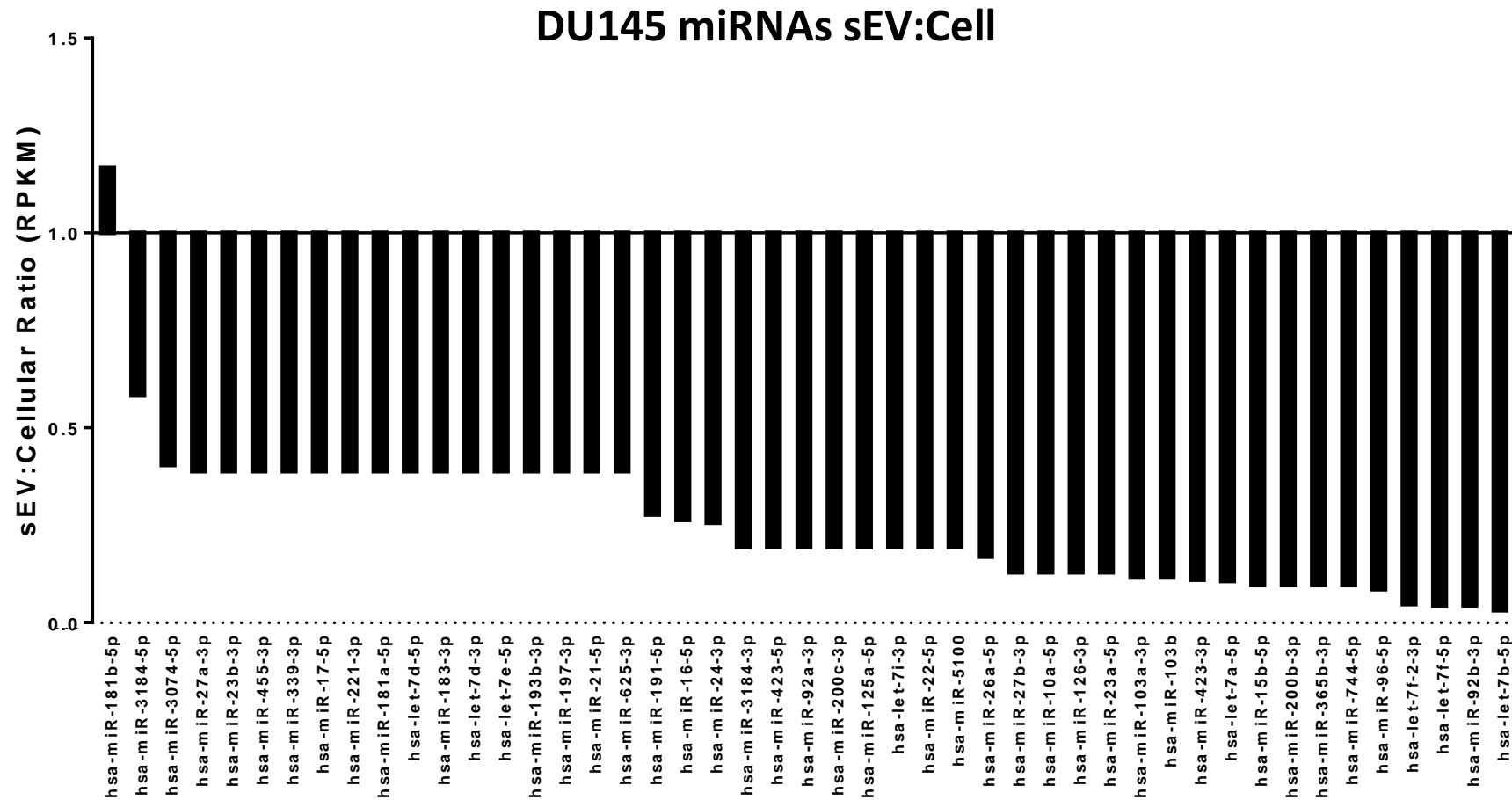
Figure 5.13: The ratio of sEV:Cellular miRNAs in DU145 samples. Ratio was calculated by dividing the RPKM for the sEV samples by the RPKM for the cellular samples for each miRNA (n=1).

A

PC3

Correlation Coefficient: 0.395
p=0.013

B

DU145

Correlation Coefficient: 0.504
p=0.0003
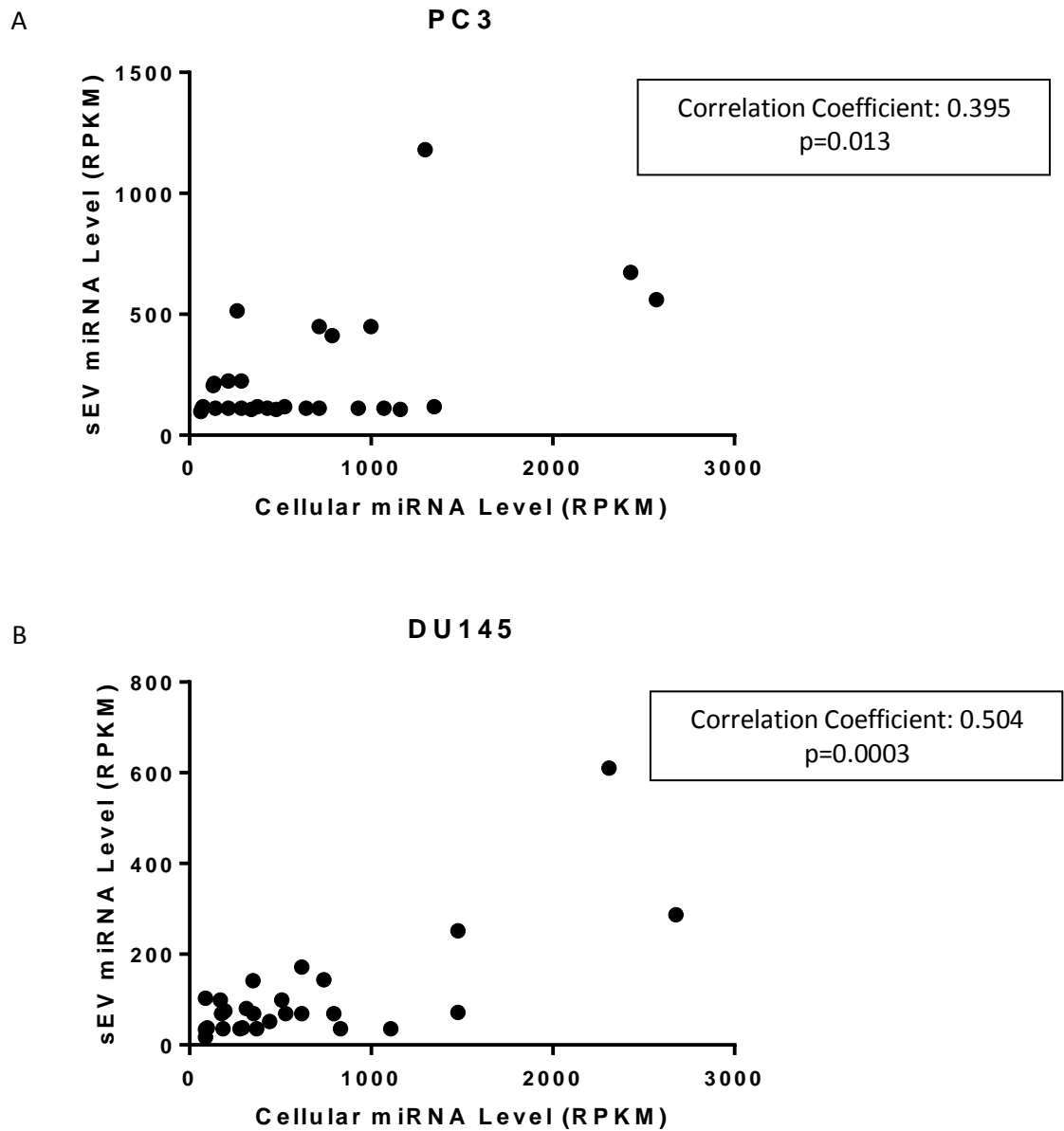
Figure 5.14: XY plot of cellular and sEV RPKM values. Cellular RPKM values for each miRNA were plotted against their sEV RPKM values in PC3 cells (A) and DU145 cells (B). Correlation assessed using Spearman Rank Order Correlation. Results are displayed as correlation coefficient and P value. (n=1).

Intravesicular miRNAs are naturally more protected from circulating RNases, as they are surrounded by a membrane envelope. These miRNAs would logically have the highest chance of survival, outside the cell e.g. in circulation, and therefore the highest chance of uptake in recipient cells. Thus, these miRNAs would have the greatest signalling potential. Vesicular protection of RNA from RNase activity has been shown previously (Cheng *et al.*, 2014). However, before the RNAs tested in this study can be considered as mediators of intercellular communication, their protection from RNase activity must also be demonstrated. An RNase digest of the PC3 sEVs was therefore performed (figure 5.15A). sEVs were incubated with proteinase K, to remove surface proteins, and subsequently with RNase. The RNA content of RNase digested and control (untreated) sEVs was analysed using a bioanalyser. RNase digest resulted in a 14% (approx.) reduction in RNA concentration indicating that around 86% of the RNAs are protected from RNAse activity. Furthermore, by pre-treating with proteinase K, we show that the remaining miRNAs are not attached to surface proteins, another mechanism that could offer protection from RNases. It should be noted that the lateral shift in peaks is likely a result of sub-optimal ladder recognition by the bioanalyser, rather than a reduction in the size of the individual RNAs. To show that the RNase used was able to efficiently degrade RNA, sEV RNA was treated with RNase following RNA extraction and visualised using agarose gel electrophoresis (figure 5.15B). Treatment of extracted RNA with RNase resulted in complete RNA degradation, exemplified by a complete removal of visible RNA seen in the untreated sample.
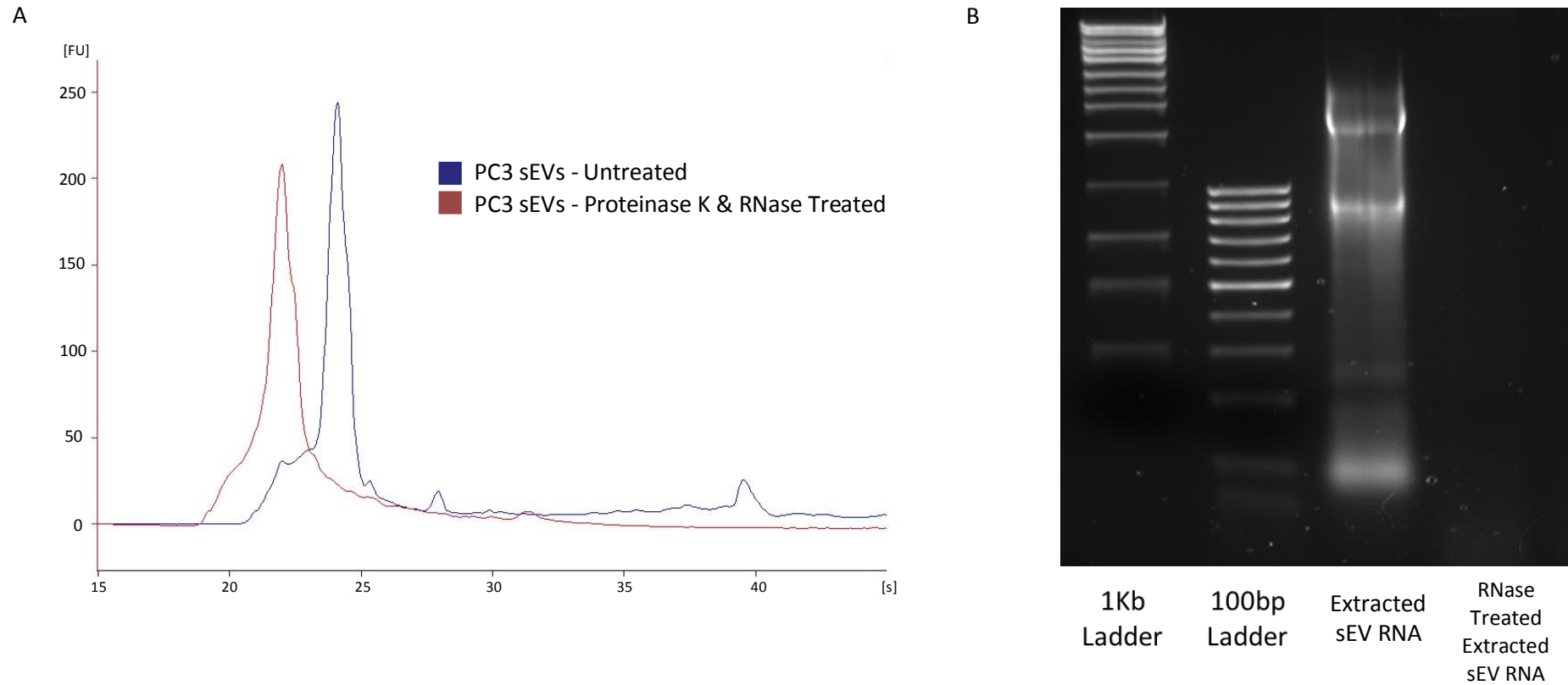
Figure 5.15: Bioanalyser trace of RNase treated PC3 sEVs. (A) sEVs isolated from PC3 cell conditioned media were treated with proteinase k and RNase to digest extravesicular RNA. Remaining RNA was assessed using a bioanalyser (representative image, n=2). (B) sEV RNA was extracted and treated with RNase to validate RNase activity.

5.4   Discussion

In the previous chapter, we showed that a miRNAs are released by PC3 cells into media. Furthermore, using differential centrifugation we showed that a population of these miRNAs are lost at 100,000xg indicative of miRNAs associated with small EVs such as exosomes. Interestingly, both differential centrifugation from the previous chapter and size exclusion chromatography from Dr Alwyn Dart suggest that the majority of miRNAs are non-vesicle associated. However, as discussed, the multiple sorting and uptake mechanisms of sEVs and their cargo make them interesting candidates for the delivery of miRNAs to near and distant target sites. Therefore, we focussed on the sEV population of miRNAs throughout this study.

In order to analyse the miRNA content of sEVs, a method of reliably isolating pure sEV samples must be utilised. Therefore, sEVs were isolated from PC3 cell conditioned media using a two-step ultracentrifugation method, involving an initial sucrose cushion flotation step followed by a pelleting step. The sucrose cushion, comprised of 30% sucrose/D_2O is known to have a density of 1.210 g/mL and is able to diffuse with H_2O at the interphase between the cushion and conditioned media. This diffusion creates a mini density gradient within the bottom of the centrifuge tubes of around 1.100-1.180g/mL, ideal for capturing sEVs which are known to have a density of around 1.120-1.160g/mL (Escola *et al.*, 1998). Recent data suggests that isolating sEVs from samples based on density alone may also result in the isolation of certain HDL species (Karimi *et al.*, 2018). However, separation based on size is also insufficient to remove these HDL species. This highlights the difficulty of sEV isolation, especially when high yield is required. Cells used for the production of conditioned media were cultured in bioreactor flasks, to facilitate the required scale of material required. Collecting sEVs this way is proven to give both high yield and purity, especially in combination with the sucrose cushion isolation method (Webber & Clayton, 2013).

Several techniques are used to measure sEV purity, including analysing protein content, size and particle count. Surface proteins can be utilised for sEV characterisation. For example, the tetraspanins CD9, CD63 and CD81 are enriched on the surface of exosomes (Andreu & Yanez-Mo, 2014). An Immuno-phenotyping assay of our purified samples showed high levels of these three tetraspanins compared to isotype controls, indicating the presence of exosomes within our sEV sample.

Western blot can also be used to characterise sEVs as well as assess sample purity, based on the expression of two proteins; ALIX, a protein responsible for exosomal cargo sorting (Willms *et al.*, 2016) and therefore abundant in exosomes, and Calnexin, a chaperone protein and marker of the ER, commonly used as a negative control and marker of exosome purity due to its absence in exosomes (Lasser *et al.*, 2012). Western blot confirmed the presence of ALIX in our sEV sample whilst also showing a lack of any contaminating ER specific calnexin, which was present in the PC3 cell lysate.

NTA revealed the particles within our sample to be a population of vesicles of around 60-150nm in size, consistent with the 40-100nm size of sEVs commonly documented in the literature. NTA measures vesicles in a fluid phase, representing a more natural state, and therefore giving more reliable measurement of vesicle size compared to conventional fixed or dehydration measurements. However, due to the poor refractive index of biological particles, the lower limit of detection for NTA is around 40nm (Shang & Gao, 2014). Thus, the smaller EVs within our population are likely underrepresented, which may explain the slightly larger population size compared to the literature. Measuring sEVs by cryo-electron microscopy (cryo-EM) can result in a smaller average particle size compared to NTA (Skliar *et al.*, 2018), reflecting the ability to detect smaller particles. However, using NTA is often favoured due to its high throughput and lower cost per sample. The lack of any detectable particles >400nm indicated an absence of larger contaminating extracellular particles such

as large microvesicles or apoptotic bodies (Crescitelli *et al.*, 2013). As discussed, NTA also calculates particle counts for each sample, which can be combined with the results of a BCA quantitative protein assay to give a P:P ratio for each sample. are another way of measuring sEV sample purity. Webber and Clayton (2013) showed that P:P ratios directly correlate to sample purity, stating that impure sEVs had a P:P $<1x10^{10}$. P:P values of $>2x10^{10}$ were calculated for all sEVs samples further indicating their high level of purity.

To determine the RNA content of sEVs, bioanalyser traces were performed on PC3 and DU145 cellular and sEV samples. Prior to analysis, RNAs were filtered into fractions of less than or greater than 200nt. The <200nt fraction would be used for sequencing as this would contain miRs but would minimise the presence of other larger RNAs such as mRNA and rRNA. By removing the larger RNA species that were not of interest, we could increase the efficiency of our sequencing run and ensure that wells within the sequencing chip contained RNA populations more likely to include miRs. Figure 5.4 shows that for the PC3 cellular and sEV samples, most large RNA species were removed during the filtration process. The same pattern is also shown for the DU145 samples in figure 5.5, meaning all 4 samples were largely free of contaminating RNAs and would have a higher efficiency when sequenced.

PC3 and DU145, cells and sEVs were sequenced using an Ion Proton™ sequencer. A summary of the sequencing run confirmed efficient loading of samples onto the sequencing chip with a final library of over 67 million reads. Within this, a large population of RNAs <50bp was sequenced. The filtering out of rRNA and other larger species resulted in an efficient miR sequencing run with read depths of over 200.

Overall 218 different miRs were detected across the four samples. For each sample, the 5 highest expressed miRs were recorded. miR-16-5p was in the 2 highest expressed miRs in all 4 samples. As both cell lines are aggressive, metastatic PCa cell lines, miR-16-5p overexpression may correlate with PCa severity and contribute towards the aggressive cell

phenotype. Furthermore, sEVs are known to pre-condition metastatic sites (Alderton, 2012; Peinado *et al.*, 2012), and as both cell lines have good metastatic potential it is possible that miR-16-5p enriched sEVs may also play a part in PCa metastasis. However, although some papers have shown an up-regulation of miR-16 in PCa (Lodes *et al.*, 2009), in most cases, miR-16-5p is actually down regulated in PCa samples compared to controls (Schaefer *et al.*, 2010). Furthermore, although miR-16-5p was found at high levels in sEVs, ratio analysis suggests that it may be selectively excluded to some extent, evidenced by its higher expression in cells than in sEVs. However, it remains that miR-16-5p is very highly expressed in PCa sEVs so will likely play a part in any communication between these cells and their environment.

miR-221-3p was found at high levels in both PC3 samples, consistent with data from Galardi *et al.* (2007) who also showed that miR-221-3p was overexpressed in PC3 cells. miR-221-3p targets p27^{KIP1}, a cyclin-dependent kinase inhibitor (le Sage *et al.*, 2007) which promotes cancer cell proliferation and is correlated with tumour grading (Guo *et al.*, 1997). The high expression of miR-221-3p may explain, in part, the aggressiveness of the PC3 cell line. miR-221-3p was not in the top 5 highest expressed miRNAs in DU145 cells, although another miRNAs, miR-26a-5p, was. miR-26a-5p targets Phosphatase and Tensin Homolog (PTEN) and downregulation of PTEN can lead to increased tumorigenesis through increased CXCR4 signalling (Chetram *et al.*, 2011).

Hessvik *et al.* (2012) have previously sequenced PC3 exosomal miRNAs, detailing the 20 highest expressed miRNAs. Surprisingly, the 5 miRNAs most highly expressed in our PC3 sEVs were not present in the 20 highest expressed sEV miRNAs presented by Hessvik *et al.* (2012). This indicates that packaging of sEV contents may vary depending on the specific handling of the cell lines, for example the cells used in this study were cultured for 24 hours in serum free medium, whereas our own cells were cultured for 1 week in sEV depleted FCS. miR-16 was however in the 20 highest expressed miRNAs in PC3 cells in this study. However, as miR-

16 was the 17th highest expressed miRNA in this study, this still reflects a sizable degree of variation between the two sequencing results.

miRNA sequencing results were validated in PC3 and DU145 cells using qPCR. qPCR confirmed that miR-16-5p and mir-221-3p were highly expressed in PC3 cells and that miR-16-5p was highly expressed in DU145 cells compared to other miRNAs. Although there were minor differences in the exact expression patterns of miRNAs between sequencing and qPCR, namely the apparent underrepresentation of miR-221-3p by sequencing, these results indicate that sequencing was effective in its ability to differentiate between high and low expression miRNAs in cellular samples.

As discussed, sEV RNA was limited, therefore direct validation of sEV miRNA expression by qPCR was not possible. However, qPCR of PC3 cell conditioned media showed the same pattern of miRNA expression as PC3 sEVs. Analysing conditioned media for miRNAs is not ideal for accurately estimating sEV miRNA levels, due to the fact that, as shown, sEV miRNAs make up only a small portion of extracellular miRNAs. However, miRNAs tested in both sequencing and conditioned media qPCR showed the same pattern of expression, with miR-16-5p and miR-221-3p showing high expression in both. This indicates that these miRNAs are exported to a greater extent than other miRNAs, which partially validates the fact that these miRNAs were seen at high levels in PC3 sEVs.

The levels of highly expressed miRNAs such as miR-16-5p and miR-221-3p were compared in aggressive PCa PC3 and DU145 cells and the non-cancerous PZ cell line. Comparing miRNAs in this way would allow us to determine whether the high expression of these miRNAs are exclusive to the aggressive PCa cells. Analysis of PZ miRNA qPCR revealed that miR-16-5p and miR-221-3p showed higher expression than other miRNAs such as miR-93-5p and miR-423-3p/5p, similar to the expression patterns seen in PC3 and DU145 cells. This suggests that higher expression of these two miRNAs may not be specific to PCa cells. However, although

these miRNAs show higher expression in all cell types compared to other miRNAs, the expression of miR-16-5p and miR-221-3p is significantly higher in PCa cells than in PZ cells whilst other miRNAs show generally more similar expression patterns to PZ cells. This suggests that although high expression of miR-16-5p and miR-221-3p is common at least among all the tested prostate cell samples, the expression of these miRNAs is over exaggerated in PCa cells and may reflect or contribute to their aggressive phenotype. As discussed, the high expression of miR-221-3p in PC3 cells has previously been shown (Galardi *et al.*, 2007) and may contribute to their cancerous properties. Thus, high expression of miR-221-3p in PC3 cells compared to PZ cells is expected. However, as also discussed, miR-16-5p shows mixed expression in PCa samples, but is widely regarded as a tumour suppressor, down regulated in PCa (Lodes *et al.*, 2009; Schaefer *et al.*, 2010). Thus by confirming high PCa cell miR-16-5p expression by qPCR and showing high expression compared to non-cancerous prostate cells, we validate miR-16-5p as playing a potential role in the aggressive cancerous phenotype seen in PC3 cells.

Figure 5.12 shows the sEV:cellular ratios of each miRNA found in both PC3 samples. The mix of both positive and negative ratios within this data indicates that a selective packaging mechanism may be at play for sorting PC3 cell sEV miRNAs. For DU145 samples (figure 5.13), all miRNAs, with the exception of one, miR-181b-5p, showed negative sEV to cellular ratios. However, within this, certain miRNAs such as let-7b-5p had drastically lower ratios than others, such as miR-3184-5p. Correlation analysis between cellular and sEV miRNA concentrations suggests that the incorporation of miRNAs into sEVs may be a largely passive process based on cellular concentrations. Together this indicates that the incorporation of miRNAs into sEVs is likely a largely passive process, with some miRNAs being potentially included/excluded within this. However, the lack of repeats means that conclusions cannot confidently be drawn at this stage.

From figure 5.7, it can be seen that the cellular expression of miR-221 3p and 5p was disproportionate, in favour of miR-221-3p expression. However, this ratio appears much more exaggerated in the sEV sample, with the 5p strand showing considerably lower expression than the 3p strand. This, therefore, suggests a mechanism of vesicular miRNA strand sorting. As opposing strands have different sequences and therefore different mRNA targets, this potentially acts as a mechanism of packaging miRNAs more advantageous in PCa signalling. This strand selectivity can also be seen in figure 5.12, where let-7d-3p appeared to be selectively packaged into sEVs whereas let-7d-5p was selectively excluded. Strand selectivity has been shown previously, for example in human colon carcinoma LIM1863 (Ji *et al.*, 2014) and cardiac fibroblast cells (Bang *et al.*, 2014). However, the reason for this selectivity, and the mechanism by which it occurs, is still poorly understood.

It should also be noted that although expression levels in sEVs vs cells for some miRNAs was drastically different, suggesting a selective packaging mechanism, there are clear links between the levels of miRNAs in both samples. For example, miR-16-5p, miR-221, has-let-7a-5p and several others all showed high expression in both the PCa cells and sEVs. This suggests that although a selective packaging mechanism may be at play, the process of miRNA loading into sEVs may also be a partially passive process, influenced by the concentrations of miRNAs in the cytoplasm.

Two cell lines were sequenced in this chapter to assess the commonality of miRNA expression in different PCa cell types. PC3 and DU145 cells are both aggressive PCa cell lines harvested from bone and brain metastatic sites respectively. Ratio analysis from both cell lines indicated that PC3 cells appear to have the more active selective packaging mechanism for sEV miRNAs, demonstrating that these may be more active signalling molecules. This was also demonstrated by a stronger correlation p value in DU145 cells than PC3 cells. Furthermore, in the wider context of the bone models used in this study, using a PCa cell line

harvested from a bone metastatic site will offer a more accurate representation of the communication between PCa cells and bone cells within the skeletal microenvironment. Therefore, subsequent sEV work will focus on PC3 sEVs, looking at the effects of transported miRNAs within this population.

Finally, if sEV miRNAs are to act as mediators of intercellular communication, they must be protected from RNase activity, which is prolific within the circulation (Koberle *et al.*, 2013; Tsui *et al.*, 2002). Therefore, after showing that miRNAs are present within our sEVs, we looked at the ability of sEVs to protect RNA from RNase degradation. RNase treated sEVs contained over 85% of the small RNA of untreated sEVs. This indicates that the vast majority of small RNA is intravesicular and therefore protected from external factors. This ability of sEVs to protect RNA is well documented (Cheng *et al.*, 2014; Koga *et al.*, 2011), indicating that sEVs are suitable carriers for both local and distant miRNA based signalling.

To conclude, in this chapter we looked to analyse the miRNA content of PCa sEVs. Characterisation of vesicles indicated a size and protein content consistent with those documented for sEVs. Sequencing of the miRNAs within these sEVs revealed a number of highly expressed miRNAs, which was later confirmed by qPCR. qPCR also revealed that these highly expressed miRNAs show differential expression in cancerous and non-cancerous prostate cell lines. Ratio analysis of sEV and cellular miRNAs revealed that miRNAs are differentially expressed in cells and sEVs, whereas correlation analysis suggests a link between cellular and sEV concentrations, suggesting both mechanisms may be at play. Furthermore, sEVs were able to protect this miRNA cargo from the effects of RNase treatment, thus suggesting that PCa cells may be using sEVs as mechanism of protecting miRNAs for extracellular transport. Regardless, the high expression of particular miRNAs in both cells and sEVs, indicates a possible functional role for these sEV miRNAs, which may include their use in extracellular communication.

5.5   Summary of Key Points

miRs secreted from PCa cells were present as both non-vesicle associated (bound to proteins, lipoproteins or as free molecules) and associated with EVs. Vesicles isolated from PCa cell conditioned media had an average size of just over 100nm and were abundant in the tetraspanins CD9, CD63 and CD81, key exosomal surface markers. Expression of the ESCRT protein Alix and absence of the cellular protein Calnexin confirmed effective isolation of vesicles from cellular contaminants. Together, this characterisation indicates the isolated vesicles are sEVs consistent with exosomes. Sequencing of PCa cellular and sEV miRNAs revealed a number of highly expressed miRNAs including miR-221-3p, miR-16-5p and Let-7a-5p. qPCR confirmed the high expression of miR-16-5p in DU145 cells and miR-16-5p and miR-221-3p in PC3 cells. qPCR also showed that these miRNAs show much higher expression in PCa cells compared to non-cancerous prostate cell lines. Ratio and correlation analysis revealed miRNAs are likely sorted into sEVs using a combination of selective packaging mechanisms and unselective incorporation based on cytoplasmic concentrations. Finally, RNase treatment showed that miRNAs are protected from external factors by sEVs.

Chapter VI: The Effects of PCa sEVs on Osteoblast Differentiation

6 The Effects of PCa sEVs on Osteoblast Differentiation

6.1 Introduction

Previously, we have shown an ability for PCa cells to communicate with osteoblasts via secreted factors, with a pro-osteoblastic outcome. Crucial advances in the field of sEV research, including the availability of easy to use isolation kits such as ExoQuick® (Tang *et al.*, 2017), as well as advances in characterisation of EVs (Lotvall *et al.*, 2014; Szatanek *et al.*, 2017), have allowed this research field to expand exponentially. Treatment of cells with sEVs in isolation has displayed their ability to induce functional changes in recipient cells, in the absence of any additional cellular signalling (Zhao *et al.*, 2018). As discussed, EVs are known to play a role in a multitude of biological processes and are implicated heavily in the progression of many cancers (Xu *et al.*, 2018b). Furthermore, sEVs have shown the ability to alter the function of cells within the bone microenvironment, including osteoblasts, a key factor in the development of debilitating osteoblastic lesions (Cui *et al.*, 2015; Li *et al.*, 2016c; Ye *et al.*, 2017).

In this chapter, we look to analyse the effect of PC3 cell sEVs in isolation, on the differentiation of 7F2 cells, and determine whether sEVs contribute to the pro-osteoblastic communication we have shown previously. Although the effects of sEV communication on osteoblast function have previously been analysed, expanding the range of both sEV producing cells and recipient bone cells used in this field will help build a more representative picture as to the effects of local sEV communication in the development and progression of metastatic bone lesions. By sequencing sEV treated 7F2s, we hope to uncover gene targets which are potentially modulated by miRNAs carried by PCa sEVs, thus uncovering novel pathways governed by this communication.

6.2 Chapter Aims

The aims of this chapter are to analyse if PC3 cell sEVs can alter 7F2 cell differentiation and function and explore if sEV miRNAs may be involved in these processes. To achieve this, the specific aims of this chapter are:

- To examine if isolated PC3 cell sEVs can alter 7F2 differentiation using the osteoblast differentiation model described previously.

- To use Next Generation Sequencing to identify changes in gene targets in recipient 7F2 cells.

- To select a miRNA (or miRNAs) of interest from this data and investigate its involvement in pro-osteoblastic sEV communication between PC3 and 7F2 cells, selecting specific mRNA targets.

6.3 Results

Mineralisation of 7F2 Cells Treated with PC3 Cell sEVs

To determine whether sEVs can induce osteoblast mineralisation, 7F2 cells were incubated with 50 µg/mL, 100 µg/mL and 200 µg/mL (µg of sEV protein based on protein concentration assay) of isolated PC3 sEVs in either regular or osteogenic media for 10 days, and stained with ARS. In regular media, sEVs (up to 200 µg/mL) had no effect on 7F2 mineralisation (figure 6.1A). In osteogenic media, 50 µg/mL and 100 µg/mL of sEVs also had no effect on 7F2 mineralisation, whereas 200 µg/mL of sEVs was able to induce a 90% increase in mineralisation (p=0.002) (figure 6.1B).

To assess the ability of sEVs to induce expression of genes involved in 7F2 differentiation, the expression of the 4 osteogenic genes, discussed previously, were measured in 7F2 cells treated with 200µg/mL of sEVs (or equivalent volume of PBS vehicle) in either regular or osteogenic media (figure 6.2). As expected, sEVs were able to induce changes in all 4 genes in osteogenic media compared to vehicle controls, mirroring the effects of the sEVs on the mineralisation of these cells. DLX5, MMP3 and ACVR1 all differed significantly in these cells compared to vehicle controls (p<0.05 for all) although the increase in COL1A1 expression failed to reach significance (p=0.343). However, sEVs also demonstrated an ability to significantly alter the expression of these genes in regular media (p<0.05 for all), especially MMP3, which showed a ~200x increase in expression. This result is surprising given that sEVs in regular media failed to induce mineralisation, and that co-culture with PCa cells in regular media in chapter IV failed to induce any changes in these genes.

The ability of sEVs to induce these gene changes, in the absence of any additional osteogenic supplements, lead us to re-think whether sEVs would be able to stimulate mineralisation in 7F2 cells in non-osteogenic media under certain conditions. In osteogenic media, vitamin D, and vitamin K induce osteoblast differentiation, and ascorbic acid induces collagen synthesis,

whereas β-glycerophosphate provides the crucial phosphate source required for HA formation. Therefore, 7F2 cells were treated with β-glycerophosphate (β-GP) alone with or without sEVs (figure 6.3). This would reveal whether sEVs are able to induce mineralisation in the absence of differentiation supplements. In these cells, sEVs were able to stimulate a 22% increase in mineralisation ($p < 0.001$).

.

A

sEV Treated 7F2 Mineralisation in Control Media

B

sEV Treated 7F2 Mineralisation in Osteogenic Media
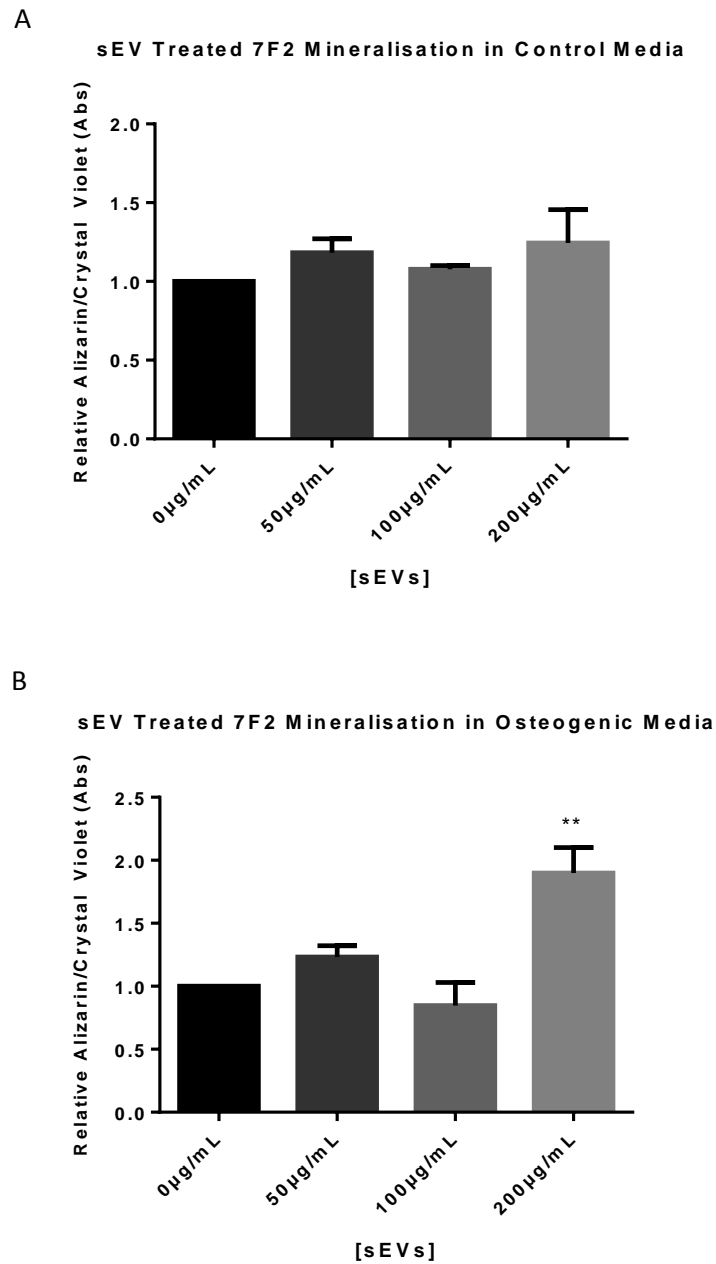
Figure 6.1: Mineralisation of sEV Treated 7F2 Cells. Mineralisation of 7F2 cells cultured with 0-200μg/mL of sEVs for 10 days in either regular media (A) or osteogenic media (B) assessed by ARS/Crystal Violet staining. (Graphs show average +SEM, n=3.) Statistical significance assessed using one-way ANOVA and Holm-Sidak multiple comparisons test, **p<0.01.
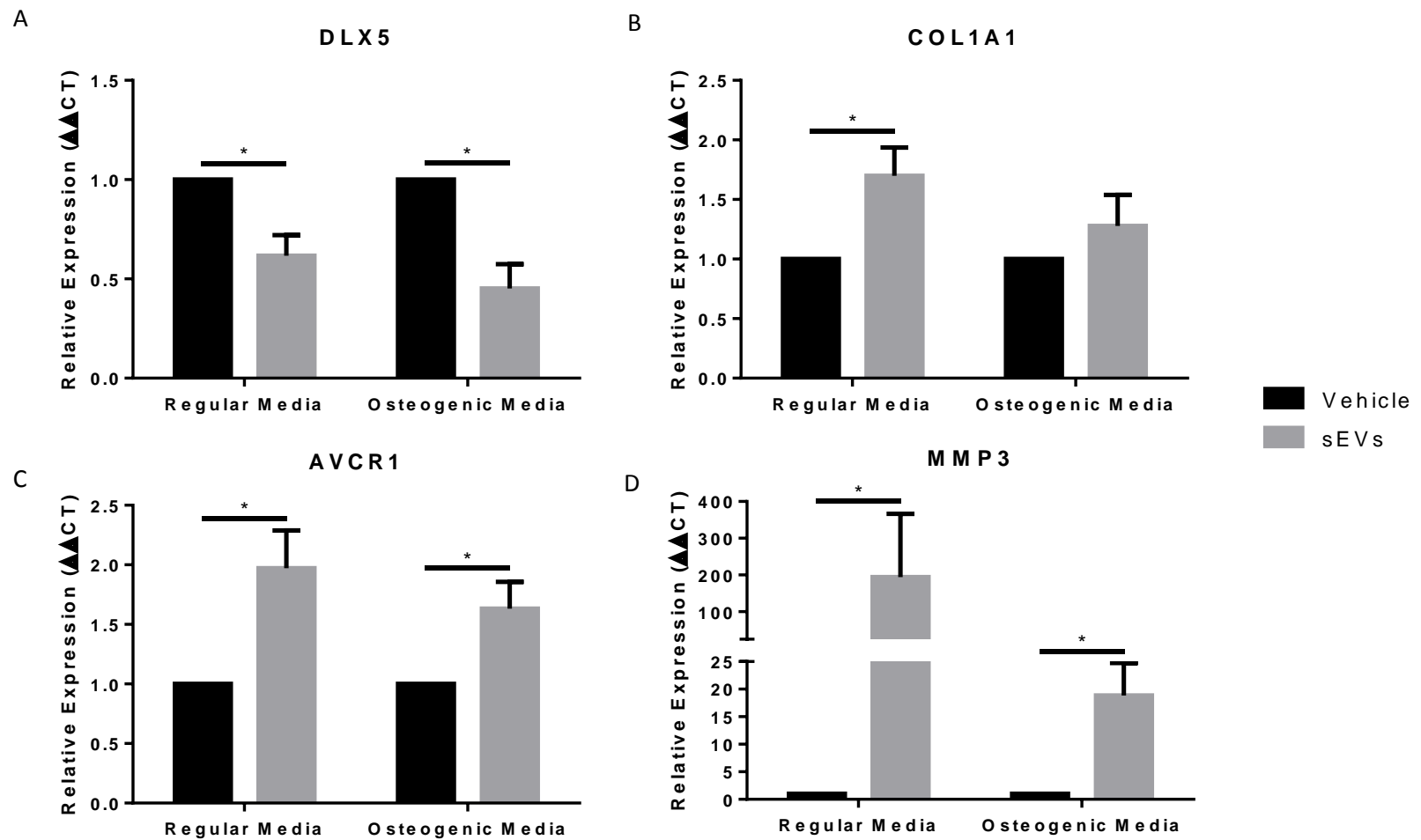
Figure 6.2: qPCR of osteoblast differentiation genes in 7F2 cells treated with sEVs in either regular or osteogenic MEM. (A) DLX5 expression, (B) COL1A1 expression, (C) ACVR1 expression, (D) MMP3 expression in 7F2 cells treated with sEVs or vehicle (PBS) in regular or osteogenic media. (Graphs show average fold change compared to vehicle controls +SEM, n=4) Statistical significance assessed by unpaired ttest between sEV and vehicle fold change control, *p<0.05.
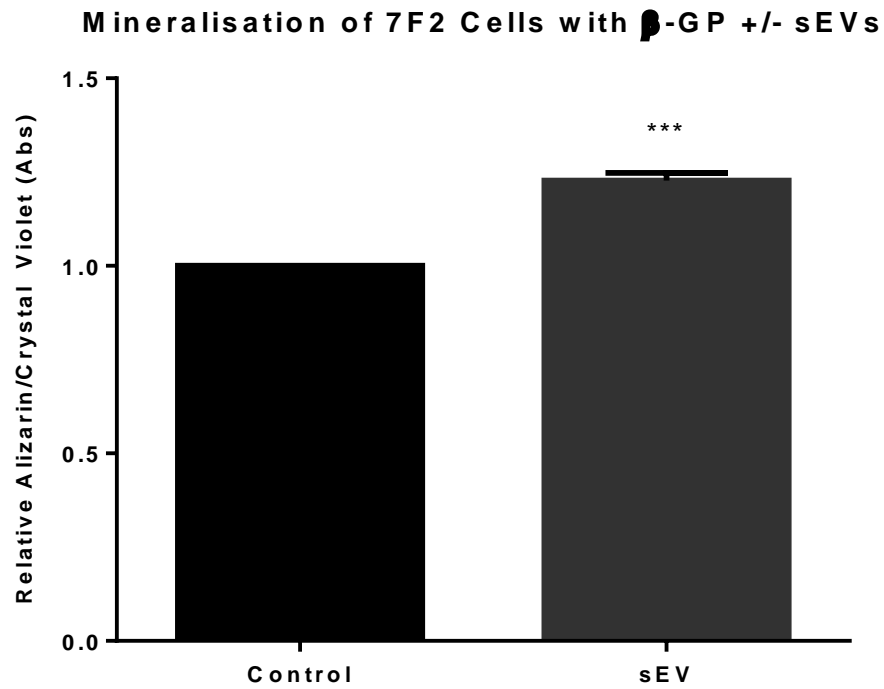
Figure 6.3: Mineralisation of sEV Treated 7F2 Cells with β-glycerophosphate. Mineralisation of 7F2 cells cultured with 200μg/mL of sEVs or vehicle (PBS) for 10 days in media supplemented with β-glycerophosphate only. (Graph shows average +SEM, n=3) Statistical significance assessed using unpaired ttest, ***p<0.001.

Sequencing of sEV Treated 7F2 Cells

Because the 7F2 cells seemed very responsive to sEV treatment in terms of their transcript changes, we decided to examine broadly the impact of sEV treatment on the recipient cell transcriptome. To test this, 7F2 cells treated with either osteogenic media + sEVs (OMEV) or osteogenic media only (OM) and were analysed by Next Generation Sequencing. RNA was extracted from 2 biological replicates of OM and OMEV treated 7F2s (4 samples total) and polyT beads were used to isolate the polyA mRNA fraction from this. The polyA mRNA library was then fragmented using RNase II, in order to achieve a library of smaller RNA fragments (<200 bases). The remaining stages of sequencing reflect those used in the previous chapter on the small RNA library; fragmented RNA strands were reverse transcribed to cDNA and unique oligo barcodes were added, cDNA was loaded onto ISPs and clonally amplified by PCR and finally cDNA coated beads were loaded onto a P1 chip for sequencing on an Ion Proton DNA Sequencer. Results from the summary of this sequencing run are shown in figure 6.4. 88% loading of ISPs onto the P1 chip was achieved (figure 6.4A). This resulted in a final usable library of over 90 million reads (figure 6.4B) with a mean and median read lengths of 125bp and 129bp respectively (figure 6.4C).

Reads were assigned to samples based on barcodes as previously stated and aligned to chromosomal locations within mouse (*Mus musculus*) genome 10 (mm10) (RefSeq 2017). Reads were subsequently normalised using the RPKM method (Mortazavi *et al.*, 2008) and a one way ANOVA was used to determine statistically differentially expressed genes between OM and OMEV treated 7F2 samples. Partek (Genomics Suite 6) software was used to generate a heatmap of our samples, with hierarchical clustering together of genes in order of change (figure 6.5A). The clustering together of replicates of OMEV and OM samples indicated good reproducibility of the gene changes seen between treatment groups. The total number of genes that were up or down regulated is shown in figure 6.5B and the

number of significantly up or down regulated genes (p<0.05) is shown in figure 6.5C. All available data indicates that a much higher proportion of genes were downregulated in the OMEV treated 7F2s compared to OM treated 7F2s than upregulated.

Ingenuity® Pathway Analysis (IPA) was used to determine the biological pathways most likely to be affected by sEV treatment in 7F2 cells. IPA utilises millions of manually assessed peer-reviewed findings, combined into a multitude of biological signalling networks, against which our own gene expression changes were mapped. Thus, a list of pathways most likely affected by the gene changes seen between our untreated and treated sequencing samples was generated. A bone cell specific analysis of the top 5 pathways most probably affected by sEV treatment are listed in table 6.1. Pathways including "skeletal development" or "skeletal disorders" featured in 4 of the top 5 most probably affected pathways, indicating that sEV treatment likely affects key osteogenic pathways and may reflect the dysregulation seen in osteoblasts neighbouring PCa bone metastases.

In a similar way, IPA was also used to predict upstream regulators, likely responsible for regulating the gene changes seen between untreated and treated cells. A Fisher's Exact Test is then used to generate an overlap p-value, a measure of the significance in the overlap between dataset genes and the genes regulated by particular transcriptional regulators. A total of 141 upstream regulators, including 7 miRNAs were indicated as statistically likely to be responsible for these gene changes. The miRNAs within this are listed in table 6.2. One of these miRNAs, miR-143 has been shown to reduce metastatic tendencies of PC3 cells (Huang *et al.*, 2012), and is therefore surprising as a mediator of communication between PC3 cells and cells of the most common PCa metastatic site. Another miRNA, miR-21 is the most commonly up-regulated miRNA in solid cancers (Volinia *et al.*, 2006). Interestingly, one of the miRNAs indicated by IPA was miR-16-5p (p=0.0469). miRNA sequencing and qPCR in the previous chapter showed miR-16-5p to be one of the most highly expressed miRNAs in PC3

cells and sEVs. Furthermore, miR-16-5p was significantly higher in 2 aggressive PCa cell lines compared to a non-cancerous prostate epithelial cell line. Combining this with the IPA data suggests that miR-16-5p may be a key mediator of the PC3 sEV induced changes in 7F2 cell differentiation and mineralisation.

A

B

C
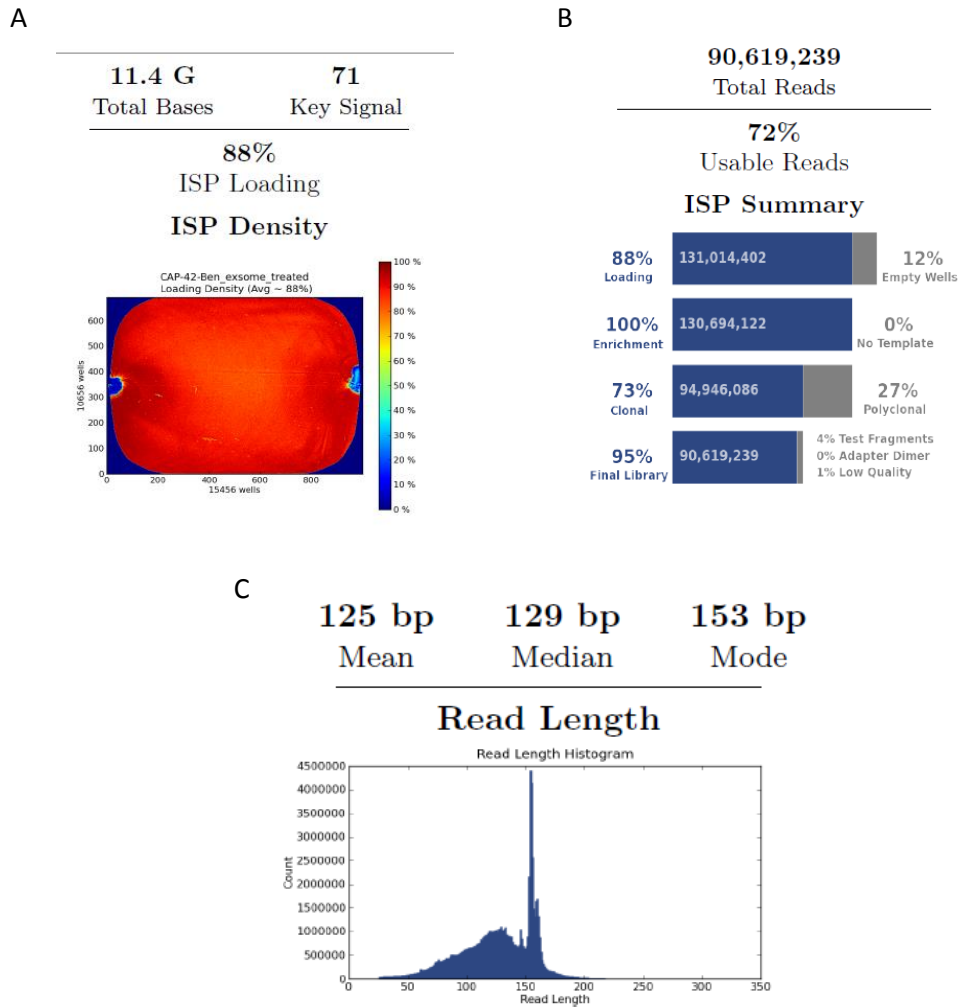
Figure 6.4: Overview of Sequencing Run. (A) Heat map showing chip loading efficiency, of the Ion P1 chip. (B) Bar graph showing % usable reads from the sample once polyclonal or untemplated beads were removed. (C) Read length of sequences including mean, median and mode for all samples combined.

A

B

Total Gene Changes OMEV vs OM

C

Significant (p<0.05) Gene Changes OMEV vs OM

■ Genes Up-Regulated   ■ Genes Down Regulated   ■ Genes Up-Regulated   ■ Genes Down Regulated
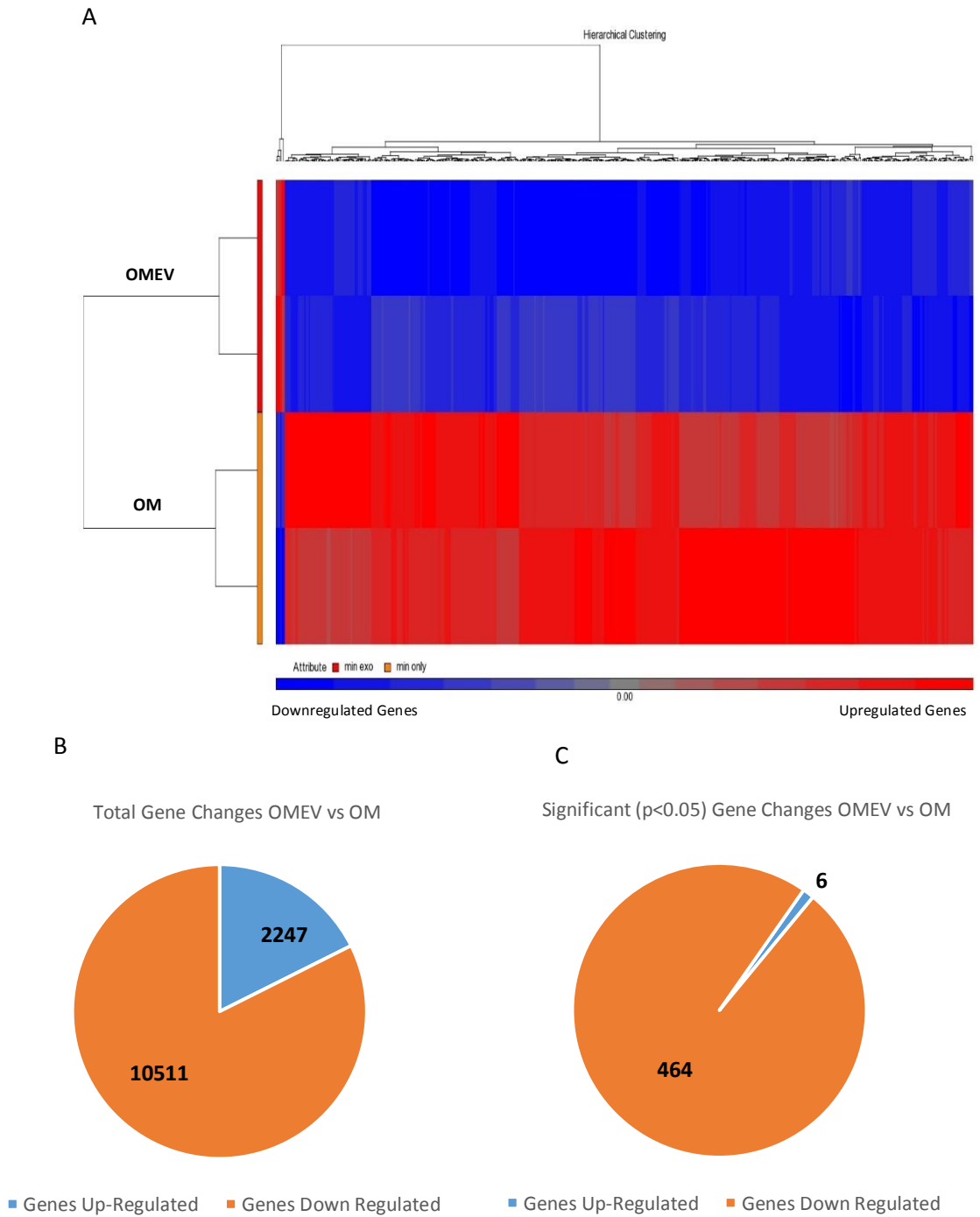
Figure 6.5: Gene Changes in 7F2s Treated with Osteogenic Media + sEVs (OMEV) vs Osteogenic Media Only (OM). (A) Hierarchical clustering of genes significantly (p<0.05) altered by treatment with OMEV vs treatment with OM. Red= upregulated genes, blue= down regulated genes. (B) Total up/down regulated genes in OMEV vs OM treated 7F2s. (C) Significantly up/down regulated genes in OMEV vs OM treated 7F2s. n=2.

Table 6.1. The top 5 pathways statistically likely to be affected by the gene changes seen between OMEV and OM treated 7F2 cells, according to IPA. n=2.

Rank	Disease and Function Pathways Most Correlated with Gene Changes	p-Value
1	Skeletal and Muscular Disorders	1.59×10^{-5}
2	Connective Tissue Development and Function, Organ Morphology, Skeletal and Muscular System Development and Function, Tissue Development, Tissue Morphology	2.04×10^{-5}
3	Organismal Development, Skeletal and Muscular System Development and Function	2.34×10^{-5}
4	Embryonic Development, Organismal Development	3.04×10^{-5}
5	Organismal Development, Skeletal and Muscular Disorders, Skeletal and Muscular System Development and Function	3.50×10^{-5}

Table 6.2. miRNAs statistically likely to have influenced the gene changes seen between OMEV and OM treated 7F2 cells, according to IPA. n=2.

Upstream Regulator	p-value of overlap
mir-143	3.18×10^{-3}
miR-1-3p	3.18×10^{-3}
mir-21	2.28×10^{-2}
miR-199a-5p	2.34×10^{-2}
mir-199	2.34×10^{-2}
mir-140	4.63×10^{-2}
miR-16-5p	4.69×10^{-2}

miR-16-5p Delivery by PC3 sEVs

As discussed, miR-16-5p showed high expression in PC3 cells and sEVs, and was also predicted to be involved in sEV communication between PC3 and 7F2 cells. Therefore, potential sEV delivery of miR-16-5p in communication between these cells was assessed.

To analyse whether miR-16-5p levels are increased in recipient cells following sEV treatment, 7F2 cells were treated with 200µg/mL of sEVs for 8 hours (figure 6.6). After 8 hours, excess sEVs were removed and cells were washed 3 times with PBS before RNA was collected. As a control, miR-30e-3p expression levels were also measured in vehicle and sEV treated 7F2 cells, as miR-30e-3p was undetectable in our PC3 sEVs by sequencing. Furthermore, Hessvik *et al.* (2012) also showed that miR-30e-3p was undetectable in PC3 sEVs analysed by sequencing. The data indicated that the expression of miR-16-5p was almost 30% higher in cells incubated with PC3 sEVs compared to PBS vehicle (p=0.007), whereas miR-30e-3p showed no increase in expression (figure 6.6).
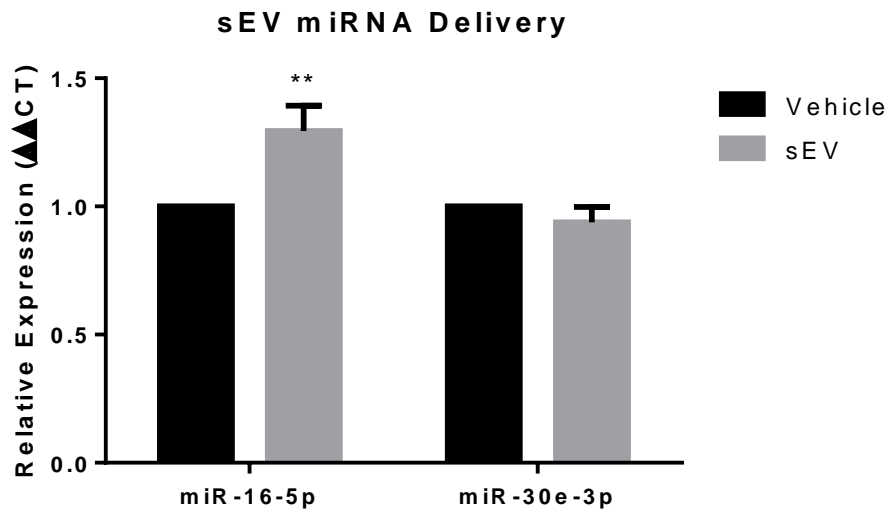
Figure 6.6: miR-16-5p and miR-30e-3p Expression in sEV Treated 7F2 Cells. qPCR of miR-16-5p and miR-30e-3p in vehicle (PBS) and sEV treated 7F2 cells. Graphs show average +SEM, n=3. Statistical significance assessed by unpaired ttest between sEV and vehicle fold change controls, **$p<0.01$.

Detection of miR-16-5p Functional Activity in Recipient Cells

To show that the miR-16-5p, increased as a result of sEV treatment, is functional, a 7F2 cell line with a stably integrated miR-16-5p pmirGlo reporter plasmid was created. Firstly, the pmirGLO plasmid (figure 6.7A) was cut with *PmeI* and *XbaI* restriction enzymes, producing a linear piece of DNA roughly 7.3Kb in size (figure 6.7B). Next, miR-16-5p forward and reverse oligonucleotides (oligos) were designed (figure 6.7C). Oligos contained the miR-16-5p binding site, as well as a NotI site, used for insertion check, and end sites complementary to *XbaI*/*PmeI* restriction sites on the cut plasmid. Oligos were then annealed and subsequently ligated into the cut plasmid using a T4 DNA Ligase enzyme, utilising the complementarity between the *PmeI*/*XbaI* end regions of the oligos and the cut plasmid. Insertion of the oligos was confirmed by performing a subsequent restriction enzyme step, using *NotI*. The pmirGLO plasmid contained a single *NotI* site, and the oligo insert contained an additional *NotI* site. Unsuccessful insertion would result in a single cut, producing a linear piece of DNA roughly 7.3Kb in size, whereas successful insertion would result in two cuts, producing an additional piece of DNA roughly 140bp in size (along with the 7.1Kb vector backbone). To check for insertion, E. *coli* were transformed with the ligated plasmid and spread on LB-ampicillin (LB-AMP) agar plates. 10 colonies were then picked and cultured in LB-AMP overnight. Plasmids were extracted from E. *coli* populations, digested with *NotI* and separated by agarose gel electrophoresis (figure 6.7D). Positive insertions can be seen in 3 of these 10 colonies, which were subsequently sent for sequencing for orientation confirmation.

Stably transfected 7F2 cell lines were created containing either the miR-16-5p pmirGlo reporter, or a negative control empty pmirGlo reporter. Stable transfection was confirmed by detection of both firefly and renilla luciferase. To confirm the functionality of the miR-16-5p reporter plasmid, 7F2 cells were first transfected with a miR-16-5p mimic oligonucleotide (oligo) using Lipofectamine 3000. qPCR of miR-16-5p transfected cells revealed significantly

higher levels of miR-16-5p compared to cells transfected with a negative control (scrambled) oligo (figure 6.8A) (p=0.003). 7F2 cells containing either the miR-16-5p reporter, or an empty pmirGLO reporter, were then transfected with scrambled and miR-16-5p oligos in the same manner. miR-16-5p transfection had no effect on luciferase activity in empty reporter 7F2 cells (figure 6.8B) compared to the scrambled oligo. However, in miR-16-5p reporter 7F2 cells, transfection of miR-16-5p oligo resulted in a significant decrease in luciferase activity compared to transfection with the scrambled oligo (figure 6.8C) (p=0.015).

After confirming the functionality of the miR-16-5p reporter, 7F2 empty and miR-16-5p reporter cell lines were treated with 200µg/mL of PC3 sEVs or equivalent volume of vehicle (PBS). In empty reporter 7F2 cells, sEV treatment had no effect on luciferase activity compared to vehicle treatment (figure 6.9A). In miR-16-5p reporter 7F2 cells, treatment with sEVs significantly reduced luciferase activity by 23% (figure 6.9B) (p=0.01). This is consistent with data showing a rise in miR-16-5p levels with sEV treatment, and demonstrates an ability of the sEV miR-16-5p to modulate complementary cytosolic targets.

To test the effect of isolated miR-16-5p on 7F2 cell mineralisation, cells were transfected with scrambled or miR-16-5p oligos and treated with osteogenic media. miR-16-5p transfection resulted in a 13% increase in mineralisation compared to scrambled oligo (figure 6.10A) (p=0.03). The effect of miR-16-5p transfection was also tested on the expression of osteoblast differentiation genes. Although miR-16-5p transfection had no effect on DLX5 or COL1A1 expression, ACVR1 and MMP3 were significantly increased compared to scrambled oligo transfected cells (p<0.01 for both). We therefore demonstrate that some transcripts, modulated by PC3 sEVs can also be modulated by exogenous delivery of miR-16-5p. Thus providing some evidence that vesicular miR-16-5p may be responsible for part of the biological response seen with sEV treatment.
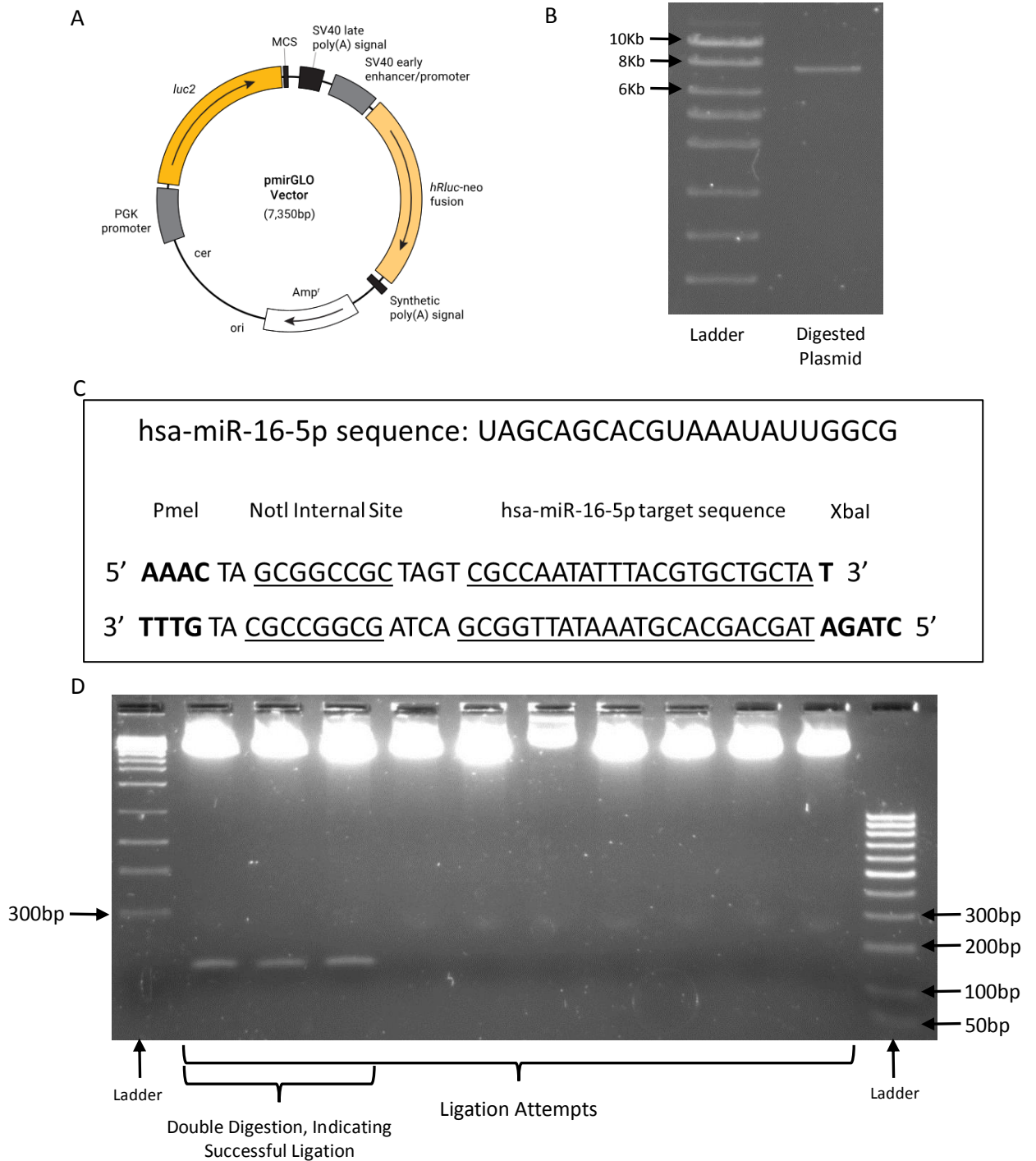
Figure 6.7: Synthesis of miR-16-5p pmirGLO Reporter. (A) pmirGLO Vector map showing multiple cloning site (MCS) (image from Promega). (B) Plasmid digested with *PmeI* and *XbaI*. (C) Design of miR-16-5p forward and reverse oligos to be annealed and inserted into the cut plasmid. Oligos contain internal *NotI* site, miR-16-5p binding site and complementary sites to *PmeI* and *XbaI* restriction sites on the cut plasmid. (D) Orientation check of ligated plasmid and oligos illustrating successful insertion of oligos (seen as ~140bp product).
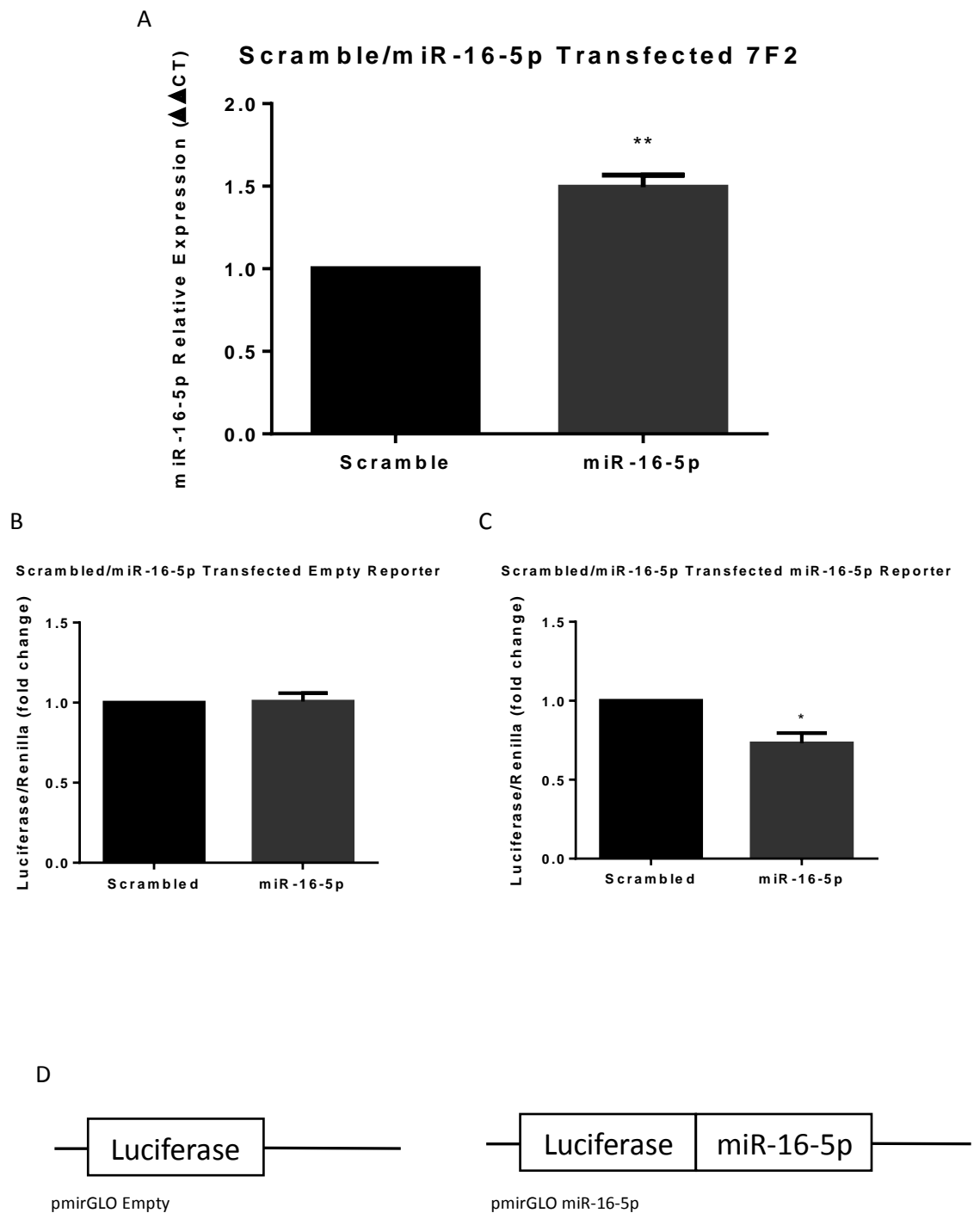
Figure 6.8: Testing of miR-16-5p Reporter with miR-16-5p Transfection. (A) qPCR of miR-16-5p in 7F2 cells transfected with scrambled or miR-16-5p oligo (5pmol). (B) Luciferase activity of empty reporter 7F2 cell line transfected with scrambled of miR-16-5p oligo (25pmol/mL). (C) Luciferase activity of miR-16-5p reporter cell line transfected with scrambled or miR-16-5p oligo (25pmol/mL). (D) Schematic representation of empty and miR-16-5p reporters used. Graphs show average +SEM, n=3. Statistical significance assessed by unpaired ttest, *p<0.05, **p<0.01.

A

Vehicle/sEV Treated Epmty Reporter

B

Vehicle/sEV Treated miR-16-5p Reporter

C

pmirGLO Empty

pmirGLO miR-16-5p
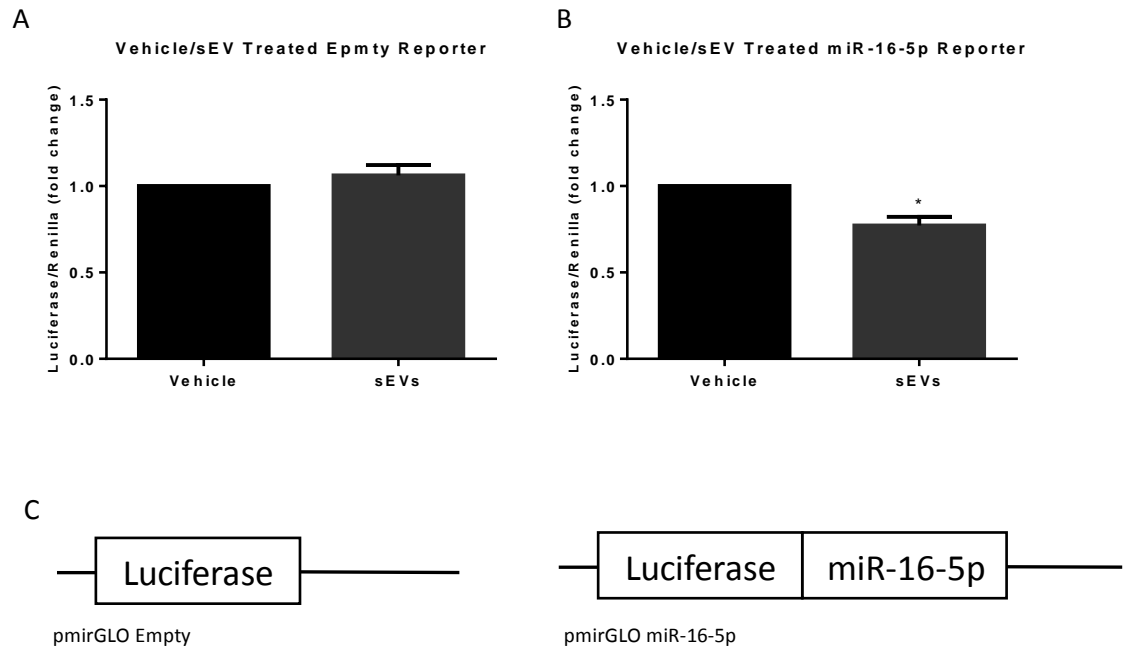
Figure 6.9: miR-16-5p Reporter Activity in sEV Treated 7F2 Cells. (A) Luciferase activity of empty reporter 7F2 cell line treated with vehicle (PBS) or sEVs (200µg/mL). (B) Luciferase activity of miR-16-5p reporter cell line treated with vehicle (PBS) or sEVs (200µg/mL). (C) Schematic representation of empty and miR-16-5p reporters used. Graphs show average +SEM, n=3. Statistical significance assessed by unpaired ttest, *p<0.05.

A

Scrambled/miR-16-5p Transfected 7F2 Mineralisation
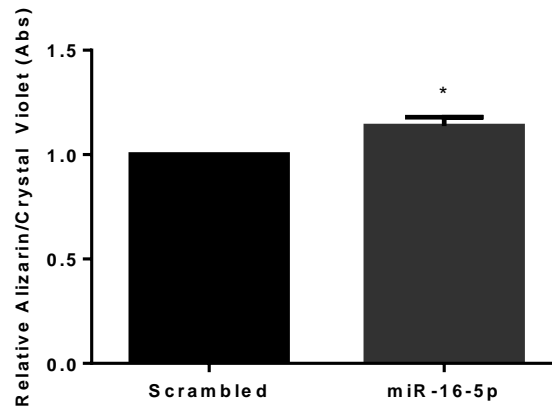
B
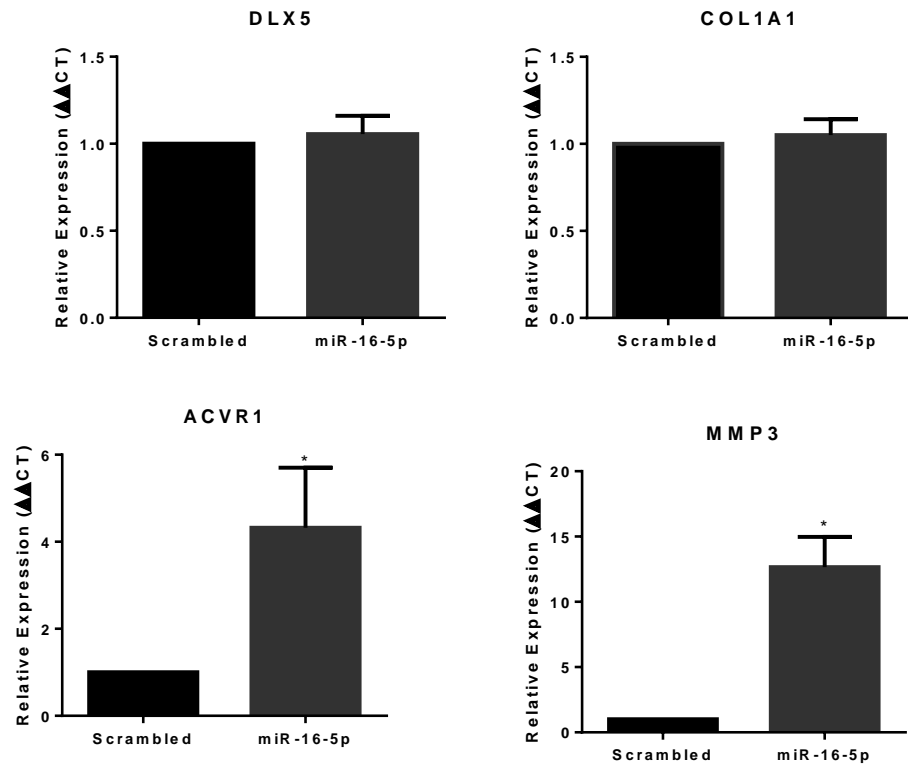
Figure 6.10: Mineralisation of 7F2 Cells Transfected with Scrambled or miR-16-5p Oligos. (A) ARS staining, (B) Osteoblast differentiation gene expression changes of miR-16-5p or scrambled oligo transfected 7F2 cells cultured in osteogenic media. Graphs show average +SEM, n≥3. Statistical significance assessed by unpaired ttest or Mann-Whitney U test, *p<0.05, **p<0.01.

Selection of miR-16-5p targets

After discovering that miR-16-5p was likely to be involved in the pro-osteoblastic sEV communication between PC3 and 7F2 cells, and confirming that miR-16-5p is likely transferred by PC3 sEVs to 7F2 cells, we looked for changes in miR-16-5p mRNA targets in sEV treated 7F2 cells that may explain this effect. Targets were selected in a step wise manner from sequencing data of PC3 sEV treated 7F2 cells, outlined in figure 6.11. Sequencing generated a list of over 12,000 detected genes, which was cross-referenced with predicted miR-16-5p targets from 3 independent databases (Targetscan, miRDB and microrna.org) using Microsoft Access, to generate a list of 616 miR-16-5p targets. From this list, genes that were increased or that had reduced by less than the arbitrary cut off of 1.5x were removed, leaving 95 genes. A manual literature search was performed on the remaining genes, of which 19 were found to have links to bone related studies. From this list of genes, 4 were found to be linked to osteoblast function, and were therefore selected as potential mediators of the increased osteoblast function seen with sEV treatment (table 6.3). The selected genes were delta like canonical notch ligand 1 (DLL1), AXIN2, phospholipid scramblase 4 (PLSCR4) and beta-2 adrenergic receptor (ADRB2) It is acknowledged that the final selection of the target genes based on their known function introduced a degree of bias.

To confirm the complementarity between miR-16-5p and the 4 selected targets, the genes were searched using TargetScan. TargetScan confirmed that miR-16-5p had complementarity based binding sites on all 4 selected genes, with two miR-16-5p binding sites on the DLL gene (figure 6.12). This search revealed that miR-16-5p binds via the 7mer-m8 sites on the target genes. This means that binding involves pairing of 7 bases, namely all 6 bases within the seed region of the miRNA (see introduction section 1.4.2.1 for details) including a 7th base at miRNA position 8, hence 7mer-m8.

Method of miR-16-5p
Target Selection

Remaining
Genes at
Each Stage

| Entire gene list from sequencing | 12,758 |

| Used Microsoft Access to merge gene expression data (from sequencing) and miR-16-5p target databases (Targetscan, microRNA.org and miRDB) and combined common genes | 616 |

| Selected genes that decreased >1.5 times | 95 |

| Manually searched genes for links to bone | 19 |

| Selected targets based on role in osteoblast function | 4 |

Figure 6.11: Schematic Representation of How Candidate miR-16-5p Targets Were Selected. Flow chart of how miR-16-5p targets in sEV treated 7F2 cells were selected. Figure shows method of selection at each stage as well as the number of genes remaining after each selection.

Table 6.3: Final 4 Selected miR-16-5p Targets

Gene	Fold Change	Log Change	Description	Reference
DLL1	0.029	-5.116	DLL1 increases the expansion of bone forming cells but reduces the maturation of osteoblasts. DLL1 is a ligand for Notch receptors. Notch signalling inhibits osteoblast differentiation.	(Muguruma *et al.*, 2017; Zanotti *et al.*, 2008)
AXIN2	0.203	-2.301	Osteoblast proliferation and differentiation was increased in AXIN2 ko mice	(Yan *et al.*, 2009)
			RUNX2 repressed AXIN2 in maturing osteoblasts	(McGee-Lawrence *et al.*, 2013)
			AXIN2 is linked to multiple aspects of Wnt signalling in osteoblastogenesis	(Huraskin *et al.*, 2016; Liu *et al.*, 2007)
PLSCR4	0.206	-2.277	PLSCR4 is downregulated in osteoblastic vs non osteoblastic osteosarcomas. Conversely, PLSCR4 is upregulated in high bone-forming vs low bone-forming hBMSC clones.	(Andersen *et al.*, 2015; Kubista *et al.*, 2011)
ADRB2	0.295	-1.760	ADRB2 signalling inhibits osteoblast proliferation and promotes osteoclast maturation	(Ma *et al.*, 2011)
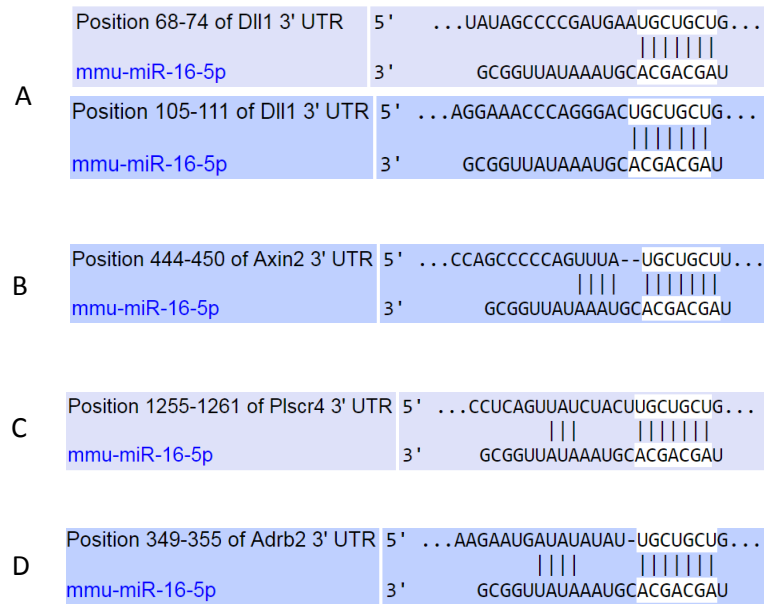
Figure 6.12: Confirmation of miR16-5p Complementarity to Selected Targets. Complementarity between miR-16-5p and DLL1 (A), AXIN2 (B), PLSCR4 (C) and ADRB2 (D) is shown, including the binding position on the target gene. Note; DLL1 has two miR-16-5p binding sites. Images from http://www.targetscan.org

Validation of miR-16-5p targets

To confirm that these targets are modulated by miR-16-5p, 7F2 cells were transfected with 25pmol/mL of either a scrambled or miR-16-5p oligos, and the expression of the 4 genes was analysed by qPCR (figure 6.13A). Transfection of miR-16-5p resulted in a significant decrease in the expression of all 4 genes compared to scrambled oligo transfected cells of 21-33% ($p < 0.05$ for all).

To test whether the increase in cellular miR-16-5p seen with sEV treatment is sufficient to modulate these genes, 7F2 cells were treated with 200µg/mL of sEVs or vehicle (PBS) and the expression of these genes was analysed by qPCR (figure 6.13B). The expression of all 4 genes was reduced in sEV treated cells compared to controls by 23-27%. However, whilst the reductions in the expression of DLL1, PLSCR4 and ADRB2 were all significant ($p < 0.05$ for all), the reduction AXIN2 narrowly failed to reach significance ($p = 0.08$).

The qPCR of sEV treated 7F2 cells highlights the modulation of gene expression seen in these cells. However, qPCR alone is unable to address the cellular mechanisms by which these regulatory effects may occur. To aid this, luciferase reporters were utilised. Mouse miTarget^{TM} 3'UTR reporters were purchased from GeneCopoedia (no *Mus musculus* PLSCR4 plasmid was available at the time of the study) and were transiently co-transfected with either scrambled or miR-16-5p oligos or with PC3 sEVs. Transiently transfected empty pmirGLO was again used as a control. When co-transfected with miR-16-5p, there was a significant reduction in the relative luminescence from the DLL1, ADRB2 and AXIN2 reporters compared to the scrambled oligo ($p < 0.05$ for all) (figure 6.14A). When co-treated with sEVs, there was again a significant reduction in the relative luminescence of the DLL1 and AXIN2 reporters ($p < 0.05$ for both) (figure 6.14B), whilst the reduction seen with the ADRB2 plasmid narrowly failed to reach significance ($p = 0.09$).
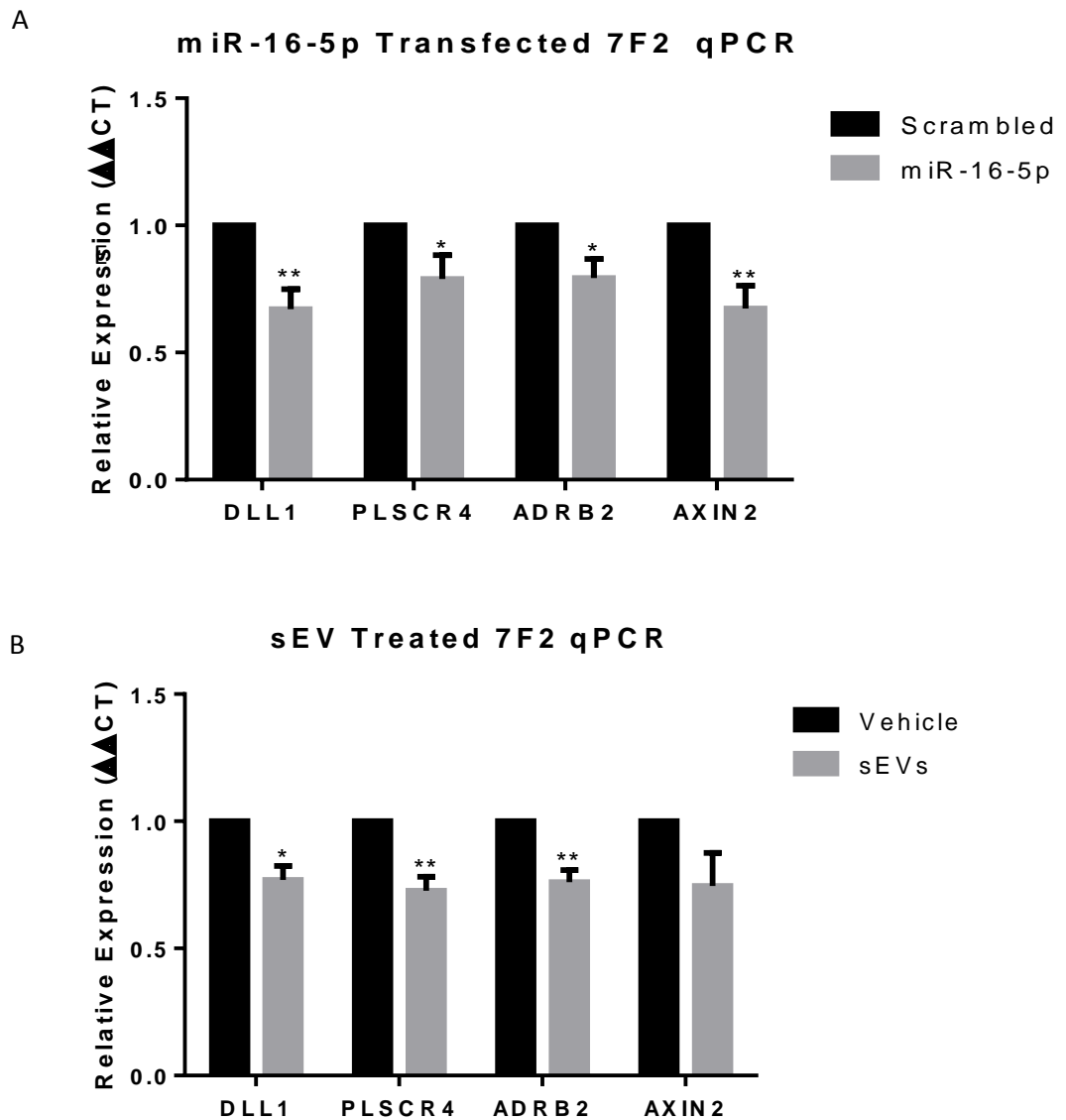
Figure 6.13: Changes in Expression of miR-16-5p Targets in Oligo or sEV Treated 7F2 Cells. (A) qPCR of miR-16-5p target genes in 7F2 cells transfected with scrambled or miR-16-5p oligos (25pmol/mL) (B) qPCR of 7F2 cells treated with vehicle or sEVs (200μg/mL). Graphs show average +SEM, n=3. Statistical significance assessed by unpaired ttest between treated and vehicle fold change controls, *p<0.05, **p<0.01.

A

B

C
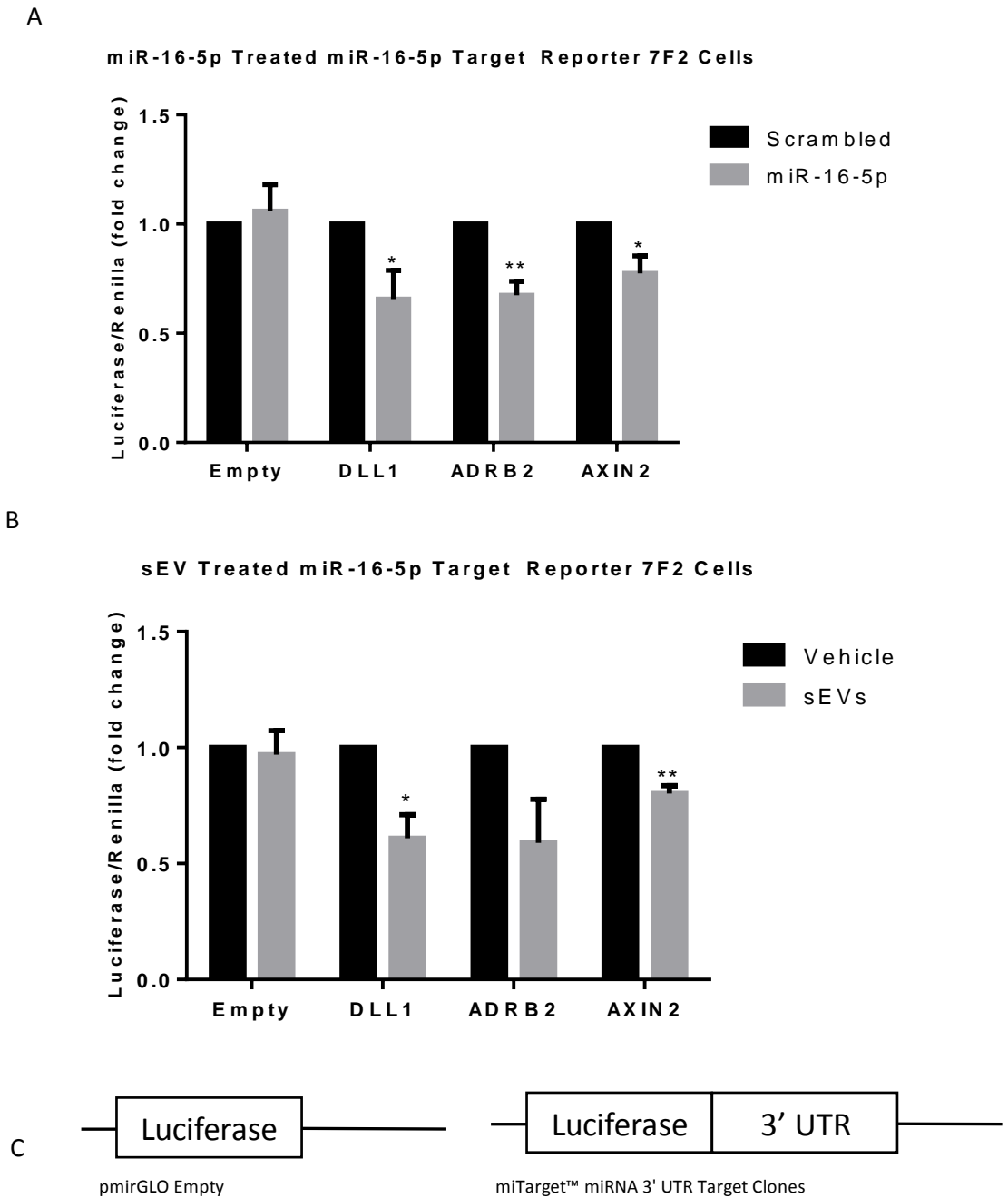
Figure 6.14: Validation of Gene Targeting Using Luciferase Reporters. (A) Luciferase activity in 7F2 cells co-transfected with target reporter (1μg/mL) and scrambled/miR-16-5p oligos (25pmol/mL). (B) Luciferase activity in 7F2 cells transfected with target reporter (1μg/mL) and treated with vehicle or sEVs (200μg/mL). (C) Schematic representation of empty and miR-16-5p target reporters used. Graphs show average +SEM, n=3. Statistical significance assessed by unpaired ttest between treated and vehicle fold change controls, *p<0.05, **p<0.01.

Overexpression of miR-16-5p targets

To test the effect of the overexpression of these miR-16-5p targets, pEF6 plasmids (figure 6.15) containing the coding regions of these genes were synthesised. Genes were amplified from 7F2 cDNA by PCR, with the exception of AXIN2, which due to its severely low expression, was amplified from the Myc-Axin2 plasmid (Addgene – 21279) (all primers for coding region amplification detailed in table 2.4). PCR products were then separated on an agarose gel, extracted and ligated with the pEF6 plasmid. E. *coli* were then transformed with the ligated plasmids, which were subsequently extracted and sequenced to confirm insertion and orientation. Finally, plasmids were transfected into 7F2cells using Lipofectamine 3000 (Thermo Fisher) and clones were selected using Blasticidin. Overexpression appeared to have little effect on 7F2 cell growth in culture.

Overexpression of the genes of interest was first validated at the gene expression level, by qPCR (figure 6.16). All genes showed a marked increase in expression, reaching significance for DLL1 ($p<0.05$) as well as PLSCR4 and ADRB2 ($p<0.001$ for both). The increase in gene expression seen in AXIN2 overexpression failed to reach significance ($p=0.1$), but did show >500x higher expression compared to empty pEF6 7F2 cells.

The next step was to assess, via western blot, whether overexpression was occurring at the protein level. Protein was extracted from all overexpression cell lines and compared to empty pEF6 7F2 cells. Unfortunately, even with multiple attempts at optimisation, clear protein bands in the expected region could not be seen for DLL1, and ADRB2, with multiple unspecific bands seen (data not shown). This likely reflects the poor quality of the antibodies, as GAPDH was easily detectable for these samples. Antibodies towards AXIN2 and PLSCR4 were able to generate specific bands (figure 6.17A and 6.17B) and were able to confirm protein overexpression. This overexpression was quantified using ImageJ software (figure

6.17C and 6.17D), which revealed a >3x in band density for AXIN2, although this narrowly failed to reach significance (p=0.089), and a >1.8x increase for PLSCR4 (p=0.03).

To test the functionality of the overexpression cell lines, cells were mineralised alongside empty pEF6 7F2 cells for 10 days. The level of ARS staining relative to crystal violet was then analysed. ADRB2 (figure 6.18A), PLSCR4 (figure 6.18B) and DLL1 (figure 6.18C) overexpression resulted in a decrease in mineralisation relative to control cells (p<0.05 for PLSCR4, p<0.01 for ADRB2 and DLL1). Conversely, overexpression of AXIN2 (figure 6.18D) resulted in an increase in mineralisation, although this increase failed to reach significance (p=0.22). We therefore conclude, that PLSCR4, ADRB2 and DLL1 may repress osteoblast differentiation, and that AXIN2 may augment differentiation.
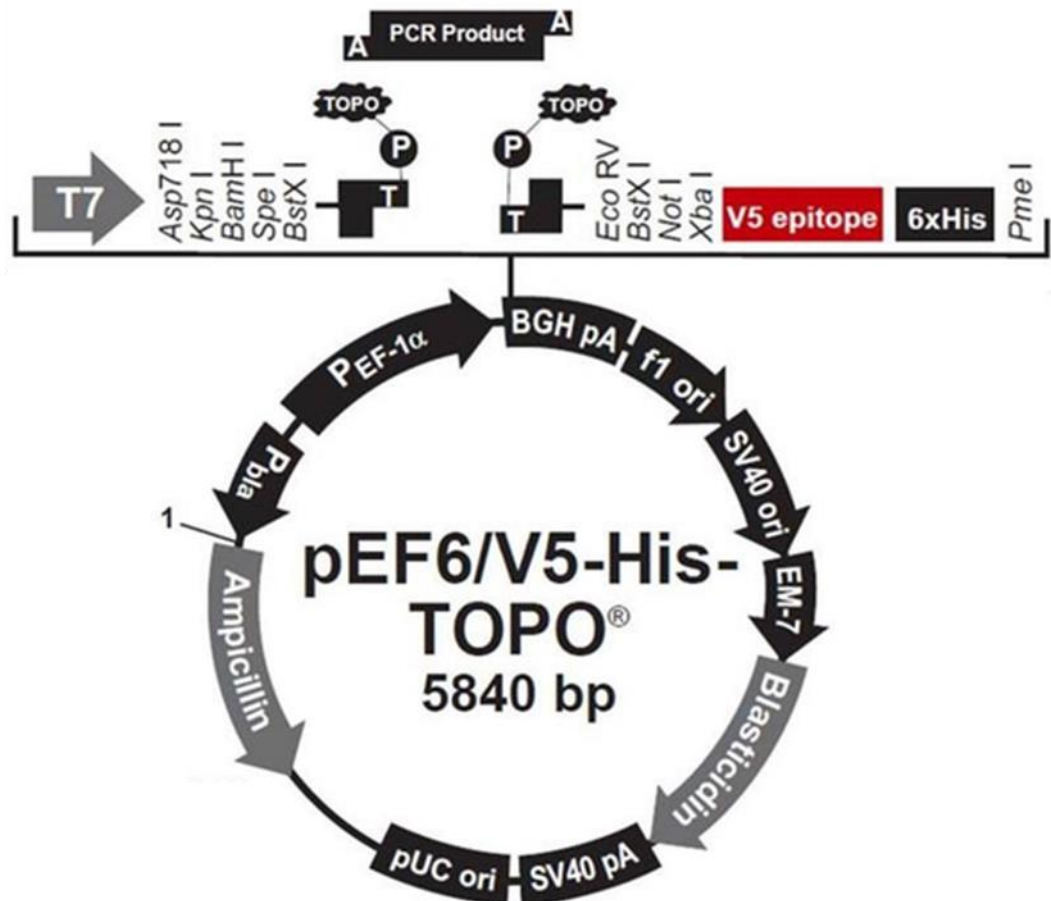
Figure 6.15: Plasmid Map of pEF6/V5-His-TOPO. miR-16-5p targets to be overexpressed were subcloned into the pEF6/V5-His-TOPO vector. Insertion and orientation were then confirmed by sequencing.

A

B

C

D
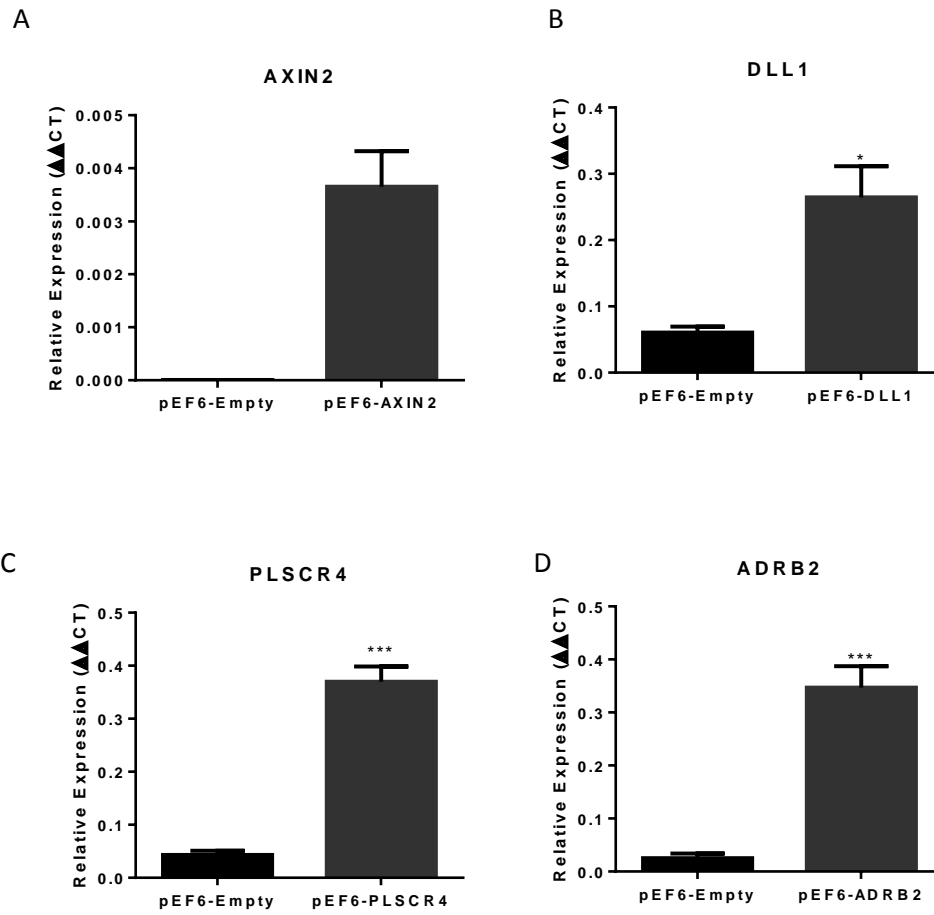
Figure 6.16: qPCR of Overexpression 7F2 Cell Lines. Expression of target genes in AXIN2 (A), DLL1 (B), PLSCR4 (C) and ADRB2 (D) overexpression 7F2 cell lines compared to empty pEF6 control cells. Graphs show average +SEM, n=3. Statistical significance assessed by unpaired ttest, *p<0.05, ***p<0.001.
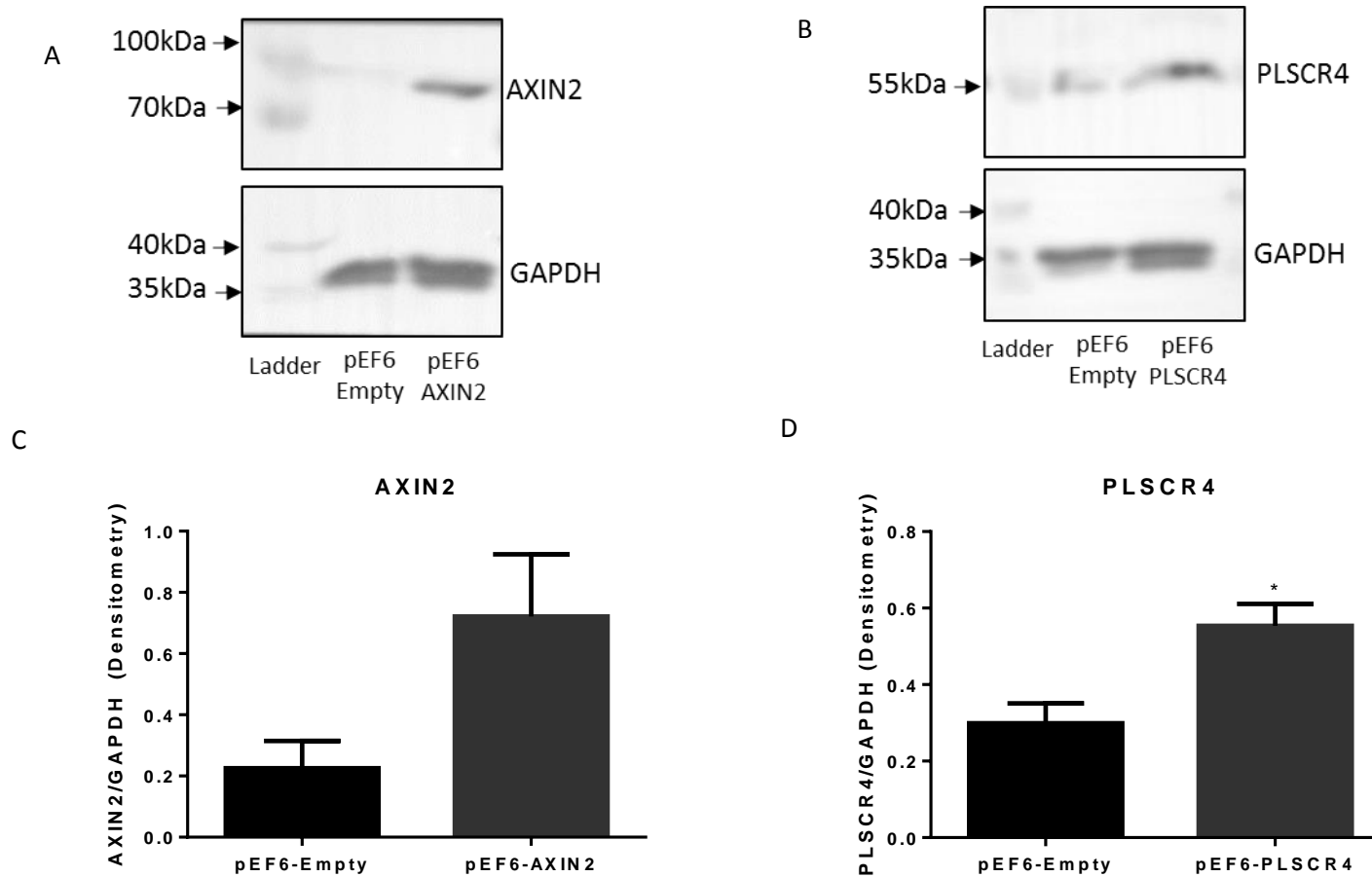
Figure 6.17: Western Blot of Overexpression 7F2 Cell Lines. Representative image showing expression of AXIN2 protein in AXIN2 overexpression 7F2 cells (A) and PLSCR4 protein in PLSCR4 overexpression cells (B) compared to empty pEF6 control cells analysed by western blot (20μg). Semi-quantification of band density using ImageJ software for AXIN2 (B) and PLSCR4 overexpression vs empty pEF6 cells. Graphs show average +SEM, n=3. Statistical significance assessed by unpaired ttest.
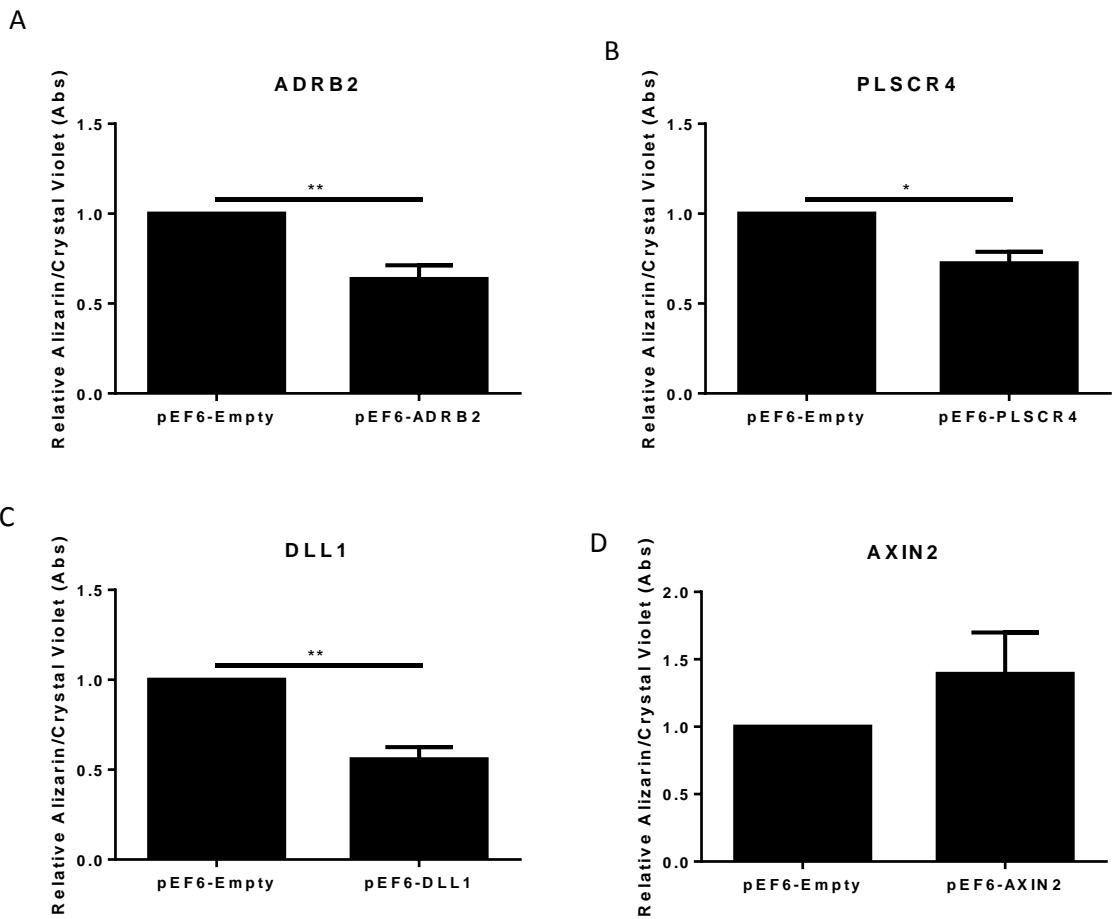
Figure 6.18: ARS Staining of Overexpression 7F2 Cell Lines. Quantified Alizarin Red S staining of (A) ADRB2, (B) PLSCR4, (C) DLL1 and (D) AXIN2 overexpression 7F2 cell lines relative to empty pEF6 control cells. Graphs show average +SEM, n=3. Statistical significance assessed by unpaired ttest, *p<0.05, **p<0.01.

6.4 Discussion

Cell to cell communication within bone metastatic sites drives a viscous cycle that ultimately leads to increased tumour growth and development of the metastatic lesion. We previously showed that PCa cells are able to stimulate increased osteoblast function *in vitro* and hypothesised that sEV miRNAs may be involved. After subsequently characterising the miRNA content of PCa sEVs, we looked to examine their effect on osteoblasts in isolation. We found that although PC3 cell sEVs were unable to stimulate mineralisation of 7F2 cells in regular media, 200µg/mL of sEVs was sufficient to enhance mineralisation of 7F2 cells grown in osteogenic media. Conversely, doses of 50µg/mL or 100µg/mL were unable to stimulate any enhancement of 7F2 mineralisation. However, it is acknowledged that leaving cells to mineralise for longer than 10 days may have yielded a more significant change in calcium deposition, although this was balanced by the risk of reaching the upper limit of the ARS assays dynamic range. Dosing of sEVs to match physiological levels found in and around tumours is inherently difficult due to an inability to accurately measure local sEV concentrations *in vivo*, with the exception of easily accessed fluids such as blood and urine (Li *et al.*, 2014). Dosages of sEVs vary drastically in the literature, from <10µg/mL (Ferguson *et al.*, 2018b) to >300µg/mL (Atay *et al.*, 2014; Li *et al.*, 2018a). Thus, a dose of 200µg/mL may be considered high. However, due to the close proximity of PCa cells and osteoblasts within a metastatic lesion (Shiirevnyamba *et al.*, 2011), and the fact that cancer cells may produce more sEVs than their non-cancerous equivalents (Riches *et al.*, 2014) and in a continuous manner, means that a high concentration of PCa cell sEVs in the localised tumour space surrounding the osteoblasts is feasible.

To confirm the increase in mineralisation seen with sEV was reflected at the gene expression level, 7F2 cells were treated with 200µg/mL of sEVs for 3 days in regular or osteogenic media, and the expression of the 4 osteoblast mineralisation genes outlined previously were

analysed. As expected, the expression of these genes was altered by sEV treatment in osteogenic media, reflecting the increase in mineralisation seen in these cells. However, surprisingly the expression of these genes was also significantly altered by sEV treatment in regular media. This change in gene expression but absence of mineralisation suggested these cells likely lack the ability to deposit HA as opposed to failing to respond to sEV treatment. Therefore, 7F2 cells were treated with β-glycerophosphate alone with or without sEVs. The increased mineralisation seen in sEV treated cells within this context, displays an ability of sEVs to induce differentiation of 7F2 cells, as opposed to only synergistically boosting differentiation when combined with osteogenic supplements. Although the ability of sEVs to modulate osteoblast differentiation has been demonstrated previously (Sun *et al.*, 2016), it was interesting to note that the dose of sEVs, able to stimulate an increase in mineralisation, was able to induce differentiation in regular media. Whereas PC3 cells used in a co-culture setup, able to stimulate similar levels of mineralisation, had little effect on differentiation in regular media. This suggests that sEVs have a greater potential to induce osteoblast differentiation compared to all combined secreted factors from their original cells.

Gene expression changes in sEV treated 7F2 cells were analysed by RNA sequencing, to gain a deeper understanding of the effects on gene expression and the associated cellular pathways. sEVs were given in addition to osteogenic media in order to assess the effects of sEV communication on top of regular mineralisation, as this closer reflects a biological environment, where vitamins and phosphate sources are readily available.

Sequencing revealed that >82% of genes detectable in both samples were down regulated following sEV treatment, with >98% of significantly changed genes showing down regulation. This unbalanced effect on gene expression may be the result of sEVs containing vast amounts of non-coding RNA, whose function generally lies in the down-regulation of other RNA species. When sequencing exosome vs PBS treated mesenchymal stem cells, Zhang *et al.*

(2016) showed that almost 80% of genes were down regulated following treatment, validating this unbalanced effect on gene expression. Together, this suggests that the effect of sEV treatment is primarily the downregulation of target cell genes. However, whether this is due to non-coding RNA delivery or via other signalling pathways remains to be seen.

IPA revealed that 4 skeletal development/disorder pathways were among the top 5 pathways most affected by sEV treatment, indicating that sEVs may target specific osteogenic pathways. IPA also revealed miR-16-5p as statistically likely to be involved as an upstream regulator of the gene changes seen in sEV treated cells. As previously discussed, although miR-16-5p is widely considered a tumour suppressor, it showed high expression in PC3 cells and sEVs. Green *et al.* (2017) showed that miR-16-5p is down regulated in Paget's disease of bone (PDB), which is characterised by over activity of osteoclasts. Conversely, miR-16-5p was shown to be overexpressed in Paget's associated osteosarcoma (PDB-OS) which presents as an osteoblastic lesion. Thus, miR-16-5p may regulate key genes within osteoblasts to promote differentiation and increase function. miR-16-5p was therefore selected as the primary miRNA candidate for future work looking at sEV communication between PC3 and 7F2 cells.

qPCR of sEV treated 7F2 cells confirmed a significant increase in miR-16-5p expression. By using foreign RNAs or RNA-dye based imaging, delivery of sEV RNA can be confirmed (Buck *et al.*, 2014; Li *et al.*, 2014). However, as mmu-miR-16-5p and hsa-miR-16-5p have the same sequence, it is not possible to determine, in this context, whether miR-16-5p is delivered by sEVs or upregulated by the target cell as a result of a separate signalling pathway. To give weight to the argument that miR-16-5p is delivered by sEVs, miR-30e-3p was also measured. miR-30e-3p was found to be absent in PC3 sEVs analysed by ourselves as well as by Hessvik *et al.* (2012). miR-30e-3p showed no increase in sEV treated cells, as expected. Thus, we show that sEV treatment does not result in global miRNA increases, and instead show that

increases are specific to certain miRNAs. However, again this does not disprove the fact that changes in miR-16-5p may be a result of alterations in target cell gene regulation, via another method of sEV stimulation, rather than sEV delivery.

A miR-16-5p pmirGLO reporter was synthesised, to show that the resultant increase in miR-16-5p following sEV treatment was associated with an increase in miR-16-5p function, as the plasmid accounts for the downregulation caused by endogenous miR-16-5p. Transfection of a miR-16-5p oligo was used to confirm the functionality of the reporter itself, which showed a significant reduction in luciferase activity. By also showing that miR-16-5p had no effect on the empty reporter, as well as showing that a scrambled oligo had no effect on the miR-16-5p reporter, we concluded that the miR-16-5p reporter was both functional and specific. The reduction in the miR-16-5p reporter seen with sEV treatment matches the increase in miR-16-5p levels shown by qPCR. However, again this also gives little insight as to the source of the miR-16-5p.

At this point, the combined findings suggest that sEV miR-16-5p is involved in communication between PC3 and 7F2 cells. Therefore, we looked to analyse the effects of miR-16-5p in isolation, on mineralisation. 7F2 cells transfected with miR-16-5p showed a small but consistent increase in mineralisation. Transfection of miR-16-5p had no effect on DLX5 or COL1A1 expression but was able to significantly increase the expression of ACVR1 and MMP3. The increase in only 2 of the 4 mineralisation genes may reflect the fact that mineralisation was only increased by 13%, as opposed to the 90% increase in mineralisation seen with 200μg/mL of sEVs. Furthermore, this also suggests, as expected, that whilst induction of mineralisation by sEVs likely involves miR-16-5p, the complete mechanism is multifactorial, and miR-16-5p only plays a part in the process. Nevertheless, the ability of miR-16-5p to increase mineralisation in the absence of any additional signalling molecules is novel, and thus, potential mechanisms for this interaction are hereby explored.

The gene expression changes, as analysed by RNAseq, in sEV treated 7F2 cells, was re-analysed in order to find miR-16-5p targets, modulated by sEV treatment. Targetscan, microRNA.org and miRDB databases were used to compile a conclusive list of miR-16-5p targets within the sequencing data. Of these, genes that reduced by >1.5x were selected, as these were considered to have shown a significant reduction. Although miRNAs have displayed an ability to induce target gene expression (Vasudevan *et al.*, 2007), their primary documented function lies in the repression of target genes. Therefore, for this study only genes showing reduced expression were considered. From the remaining genes, manual searches were performed to uncover links between them and any aspect of bone physiology or disease. Of these, 4 genes were documented to alter osteoblast proliferation, differentiation or function and were thus selected as candidate genes for further functional study. The 4 selected genes were; DLL1, AXIN2, PLSCR4 and ADRB2. Although selection of genes based on their documented function introduced a degree of bias, the time constraints of the project meant that functional analysis of all 19 bone related target genes was unachievable. But it should be considered that the remaining genes, also modulated by miR-16-5p, may have different functional roles in mineralisation.

After selecting gene targets, their modulation by miR-16-5p was assessed. All 4 genes showed a significant reduction in expression following transfection with miR-16-5p as expected. Furthermore, a reduction in all 4 genes was also seen following sEV treatment. However, as with the changes in miR-16-5p levels following sEV treatment, measuring gene expression reveals little of the mechanism by which the expression of these genes is reduced. To implicate miRNA-based modulation as a mechanism by which these genes are reduced, miTarget™ miRNA 3' UTR reporters were utilised. It should be noted that a reporter for mouse PLSCR4 was unavailable at the time of study. A reduction of luciferase activity was seen for all reporters with miR-16-5p transfection, confirming that direct modulation of these gene by miR-16-5p was occurring. A reduction in luciferase activity was also seen for

all reporters with sEV treatment. However, although this confirms that sEV miRNAs are able to modulate these genes, implicating the specific miRNA(s) responsible for this is not possible. For example, the 3' UTR region of DLL1 has 27 miRNA target sequences, of which only 2 are for miR-16-5p (Targetscan.org). A similar level of reduction in luciferase activity was seen between miR-16-5p transfected cells and sEV treated cells. miR-16-5p transfection was able to raise miR-16-5p levels by around 40% more than sEV treatment. This indicates that the reduction of luciferase activity seen in sEV treated cells is likely the result of the total miRNA population within the sEVs and not only miR-16-5p. An empty pmirGLO reporter was used as the control for these experiments, which consistently showed no change, but given the subtle differences in the luciferases between pmirGLO and miTarget^{TM} plasmids, an empty miTarget^{TM} plasmid should be used as a more accurate control for future work.

It should be noted, that although human and mouse miR-16-5p share the same sequence, their mRNA targets may not. Thus miR-16-5p may have slightly different signalling mechanisms depending on the species. However, both human and mouse DLL1, ADRB2, AXIN2 and PLSCR4 contain miR-16-5p binding sites, and therefore miR-16-5p can be assumed to have a similar effect on these genes in both species.

After linking a reduction in the expression of these genes to sEV miR-16-5p, we looked to analyse the effect of their overexpression. As a reduction in the expression of these genes was linked to increased osteoblast function, we hypothesised that overexpression would result in a mirrored decrease in osteoblast function. Reduced osteoblast differentiation and function would be beneficial in the management of osteoblastic lesions, the most common form of bone metastasis from PCa. Therefore, given the available time frame, overexpression of these genes was explored, as a potential reduction in osteoblast differentiation/function is a more clinically relevant outcome than that of a reduced expression model, which we hypothesised would further drive osteoblast differentiation/function.

All genes showed a substantial increase in expression at the transcript level, measured by qPCR, indicating that transfection and plasmid incorporation was successful. Furthermore, this demonstrates the ability of the plasmid to induce a high number of copies of the inserted gene. We then looked to analyse the overexpression cell lines at the protein level. For DLL1 and ADRB2, antibody issues meant that, within the given time frame, protein overexpression could not be confirmed. Multiple unspecific bands and a lack of bands at the expected size meant that further optimisation, or new antibodies would be required. However, the AXIN2 and PLSCR4 antibodies proved effective, giving a single band at the expected size. Furthermore, AXIN2 and PLSCR4 overexpression cells displayed a marked increase in target protein levels. Although protein overexpression could not be confirmed in all cell lines, confirmation of AXIN2 and PLSCR4 overexpression confirms that that the methodology, i.e. pEF6 plasmid containing a genes coding region, is able to induce protein overexpression.

Overexpression of ADRB2, DLL1 and PLSCR4 all resulted in a significant decrease in the mineralisation of 7F2 cells. This indicates a role for these genes in the repression of osteoblast differentiation. ADRB2 signalling has displayed an ability to both promote and inhibit osteoblast proliferation (Fu *et al.*, 2005). Given that osteoblast differentiation requires a cessation in proliferation (Raucci *et al.*, 2008), altering this pathway was expected to affect mineralisation levels. As ADRB2 overexpression resulted in a decrease in mineralisation, it is likely that ADRB2 activation in culturing osteoblasts may be promoting proliferation and therefore subsequently reducing differentiation.

PLSCR4 is poorly explored within osteoblast differentiation. However, studies have shown PLSCR4 expression changes in bone cell populations displaying different characteristics. Confusingly, the expression of PLSCR4 in two studies seems to be slightly conflicting, and means that hypothesising the function of PLSCR4 in osteoblasts is difficult. For example, Kubista *et al.* (2011) showed that PLSCR4 was downregulated in osteoblastic vs non-

osteoblastic osteosarcomas, whereas Andersen *et al.* (2015) showed that PLSCR4 was upregulated in high bone forming vs low bone forming human bone marrow stromal cells (hBMSC) populations. Our data shows that overexpression of PLSCR4 leads to decreased 7F2 mineralisation, therefore suggesting an anti-differentiation role of PLSCR4 in these cells.

DLL1 appears to have multiple roles in the physiology of osteoblasts. Muguruma *et al.* (2017) showed that DLL1 likely plays a dual role in the regulation of osteoblastogenesis, depending on the stage of differentiation. DLL1 was shown to positively regulate the expansion of bone-forming cells, whilst acting as a negative regulator of functional maturation in cells already committed to the osteoblast lineage. 7F2 cells appear to correspond to more mature osteoblasts, due to their AP expression and ability to secrete type I collagen (Thompson *et al.*, 1998). Therefore, the action of DLL1 in reducing their differentiation, seen here by a reduction in their mineralisation levels, is in keeping with the findings of Muguruma *et al.* (2017).

AXIN2 was the only gene whose overexpression resulted in an increase in the levels of mineralisation. Yan *et al.* (2009) showed that *Axin2* KO mice had increased osteoblast differentiation and function, leading to an increase in bone volume, bone mineral density and bone mechanical strength. McGee-Lawrence *et al.* (2013) showed that AXIN2 prevents Wnt signalling required for osteoblast differentiation, and that AXIN2 was negatively regulated by RUNX2, which is itself upregulated during osteoblast differentiation. Together, these studies show that RUNX2 reduces AXIN2 expression during its upregulation in osteoblast differentiation, and that this resultant loss in AXIN2 contributes to increased osteoblast differentiation and function through a reduced repression of Wnt signalling. However, during the characterisation of our mineralisation model (Chapter III), we found that RUNX2 was actually decreased in 7F2 cells grown in osteogenic media, which as discussed is likely due to the inhibitory role of RUNX2 on more mature osteoblasts. This link

between AXIN2, Wnt signalling and RUNX2 suggests that the inhibitory role of AXIN2 seen in these studies occurs at the early stages of osteoblastogenesis. It is therefore possible that this signalling interaction may have a different outcome in 7F2 cells. However, the increase in mineralisation seen in AXIN2 overexpressing 7F2 cells was still surprising given its direct functional link with osteoblast differentiation (Yan *et al.*, 2009).

In conclusion, the results of this chapter show that PC3 sEVs are able to induce differentiation of 7F2 osteoblast cells. By sequencing sEV treated cells, we showed that a number of molecules may be affecting these changes, including miR-16-5p, which was highly expressed in PC3 cells and sEVs. By overexpressing targets of miR-16-5p, we showed that these genes may have a functional role in the differentiation of osteoblasts.

6.5 Summary of Key Points

sEVs were able to induce an increase in the differentiation of 7F2 cells at both the functional and gene expression level when cultured in osteogenic media, or regular media with an appropriate phosphate source. Sequencing of sEV treated 7F2 cells revealed a number of upstream regulators, including miR-16-5p, which was shown by sequencing to be highly expressed in PC3 cells and sEVs. sEV treatment lead to a significant increase in the levels of miR-16-5p but not miR-30e-3p, a miRNA believed to be absent in PC3 sEVs. miR-16-5p reporters showed that sEV treatment lead to an increase in the functionality of miR-16-5p. Sequencing of sEV treated 7F2 cells was analysed again, and a number of significantly reduced miR-16-5p targets were found, from which ADRB2, AXIN2, PLSCR4 and DLL1 were selected, based on their links to osteoblast function. After confirming the reduction of these genes following sEV treatment, overexpression was performed. This revealed that overexpression of ADRB2, PLSCR4 and DLL1 results in a decrease in 7F2 mineralisation, whereas overexpression of AXIN2 results in increased 7F2 mineralisation.

Chapter VII: The Effects of PCa sEVs on Osteoclast Differentiation

7 The Effects of PCa sEVs on Osteoclast Differentiation

7.1 Introduction

Although PCa forms primarily osteoblastic lesions, the roles of osteoclasts in the pathophysiology of metastatic bone disease are vast. Osteolytic and mixed lesions, whilst rarer than osteoblastic lesions, still represent a significant proportion of metastatic PCa patients (Charhon *et al.*, 1983; Roudier *et al.*, 2004). Osteoclastic activity is also a precursor to bone metastatic site colonisation regardless of osteolytic or osteoblastic outcome (Msaouel *et al.*, 2008), where debulking of the bone surface aids PCa cell seeding. Furthermore, even within osteoblastic lesions, osteoclasts display increased activity (Keller & Brown, 2004), which results in an increased release of bone matrix derived growth factors, further driving the development of the secondary tumour.

Given the multiple roles of osteoclasts in various forms of bone metastases, and that bone remodelling is a balance of osteoclast and osteoblast activity, it was felt important to also consider the effects of PCa cell sEV signalling on osteoclast activity. PCa sEVs have displayed an ability to both induce and decrease osteoclast differentiation (Bijnsdorp *et al.*, 2015; Karlsson *et al.*, 2016), indicating the signalling relationship and associated outcome is likely dependant on both the PCa and osteoclast cell type as well as environmental factors. Thus we looked to test the effect of the PC3 sEVs, which have displayed an ability to induce osteoblastogenesis, on the osteoclastic differentiation of RAW 264.7 murine macrophage cells. Osteoclasts develop from both immature cells of the monocyte-macrophage lineage, as well as mature macrophages In the presence of RANKL (Huang *et al.*, 2017; Udagawa *et al.*, 1990). By using sEVs from the same PCa cell line, we hope to more accurately model the effects of sEV communication from the same tumour on different cell types within the bone microenvironment, and how these effects may contribute to metastatic lesion development.

7.2   Chapter Aims

The aims of this chapter are to examine the effects of PC3 cell sEVs on the differentiation and function of RAW 264.7 cells. To achieve this, the specific aims of this chapter are:

- To characterise the differentiation of RAW cells by looking at the expression of osteoclastic markers and visual assessment of mature osteoclast formation.

- To analyse the effects of sEV treatment on both the expression of these osteoclast markers, and the formation of mature osteoclasts.

- To assess the effect of sEV treatment on the function of osteoclasts.

7.3   Results

Characterisaiton of RAW Cell Differentiation

RAW 264.7 (RAW) cells are Abelson murine leukaemia virus-transformed macrophage cells, able to differentiate into multinucleated, bone resorbing osteoclasts when treated with RANKL (for overview of osteoclast differentiation see figure 1.7, section 1.3.2.3.1) (Collin-Osdoby & Osdoby, 2012). Before analysing the effects of PC3 sEVs on RAW cells, their capacity to differentiate into mature osteoclasts in our hands was assessed. RAW cells were treated with 25ng/mL RANKL for 8 days. Cells were then stained for tartrate-resistant acid phosphatase (TRAP), a metalloenzyme involved in ROS production (Hirschfeld *et al.*, 2017) and also responsible for increasing osteoclast migration by dephosphorylating OPN (Ek-Rylander *et al.*, 1994), a key protein for binding osteoclasts to the bone matrix. TRAP stained cells were then imaged using a brightfield microscope (figure 7.1). Positive TRAP staining is indicated by a maroon coloured precipitate. Although positive staining appeared to also be seen in undifferentiated cells, cells treated with RANKL were much darker, indicating increased TRAP levels. Most noticeably, within the RANKL treated cells, multiple multinucleated cells were visible, with a substantial cytoplasmic area, typical of successful osteoclastic differentiation.

To further characterise RAW cell differentiation, cells were treated with 1-25ng/mL of RANKL then analysed by qPCR for changes in expression of TRAP and osteoclast-associated immunoglobulin-like receptor (OSCAR) (figure 7.2). OSCAR is an IgG-like receptor and an important costimulatory molecule for osteoclast differentiation via the activation of NFATc1 (Nemeth *et al.*, 2011). OSCAR is also commonly used as a marker of osteoclast differentiation (Kim *et al.*, 2017). RANKL treatment increased the expression of OSCAR (figure 7.2A) and TRAP (figure 7.2B) in a dose dependent manner, reaching significance at 3ng/mL for OSCAR and 1ng/mL for TRAP ($p < 0.05$ for all).
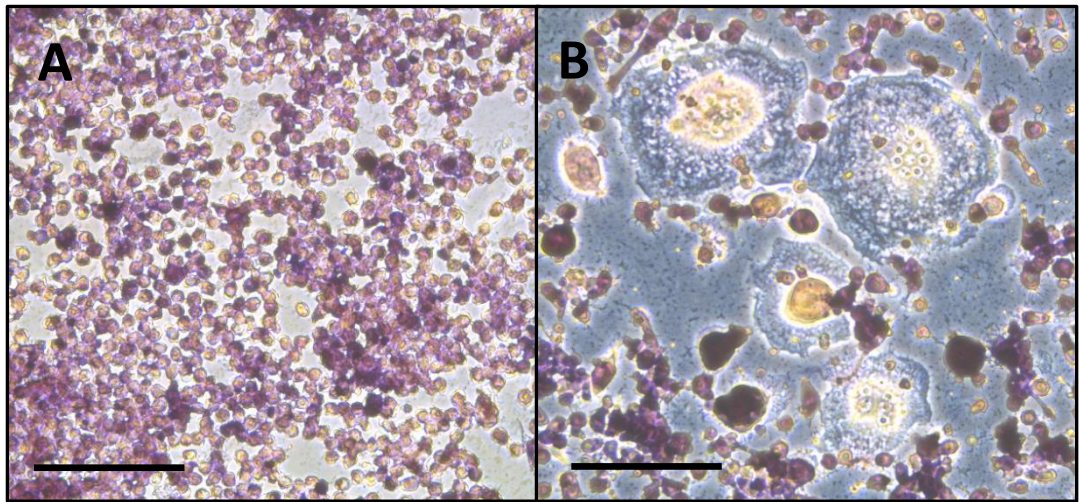
Figure 7.1: Morphology of RAW Cells. 10x magnified brightfield microscopy images of TRAP stained RAW cells grown on 6 well plates for 8 days in either regular DMEM (A) or DMEM + 25ng/mL RANKL (B) Scale Bar: 250μm.

A

O S C A R

B
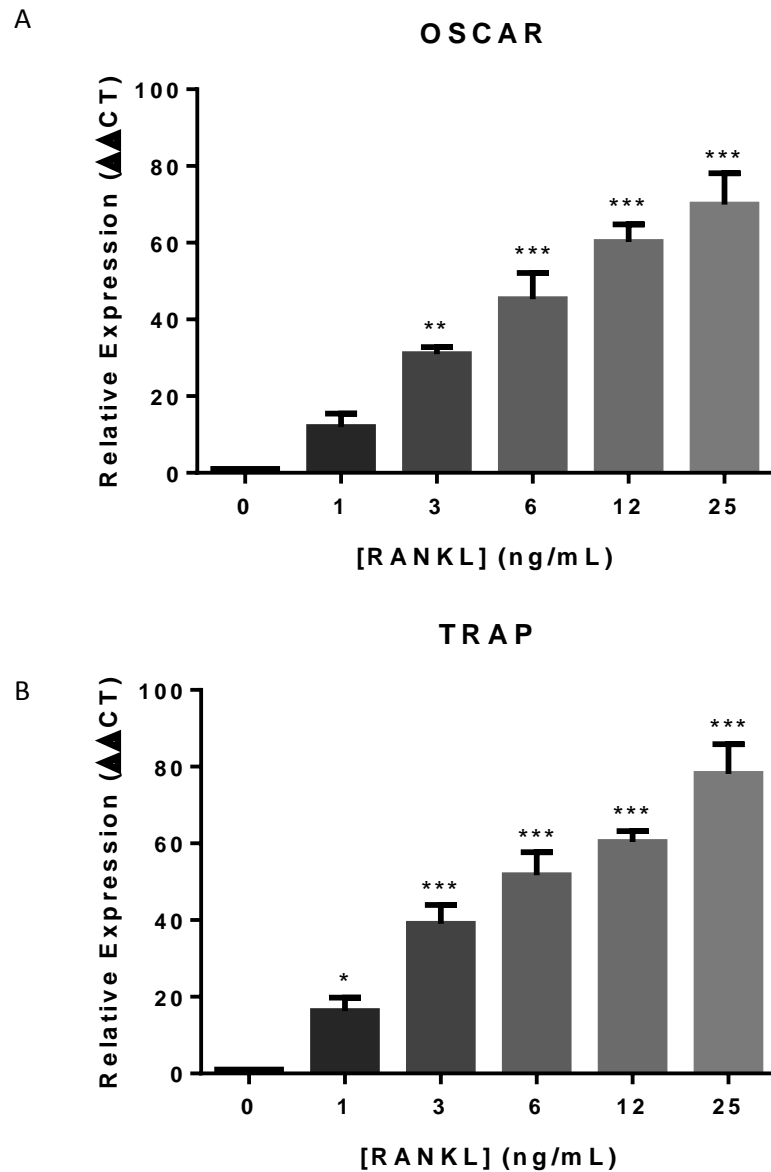
T R A P

Figure 7.2: Expression of Osteoclast Differentiation Genes in RAW Cells Treated with RANKL. Expression of OSCAR (A) and TRAP (B) in RAW cells treated with 0-25ng/mL of RANKL, analysed by qPCR. Graphs show average fold change compared to control +SEM, n=3. Statistical significance assessed by one-way ANOVA using Holm-Sidak multiple comparisons test, *p<0.05, **p<0.01, ***p<0.001.

Differentiation of RAW Cells Treated with PC3 sEVs

To test the effect of PC3 sEVs on RAW cell differentiation, cells were treated with 200µg/mL of sEVs or vehicle in regular or 20ng/mL RANKL supplemented media (figure 7.3). Treatment with sEVs in regular media had no effect on OSCAR expression (figure 7.3A). Addition of RANKL alone caused aa increase in OSCAR expression, mirroring the result seen in figure 7.2A. Treatment with sEVs in RANKL supplemented media caused an increase in OSCAR expression compared to RANKL alone. However, changes in OSCAR expression failed to reach significance although this narrowly failed to reach significance.

sEV treatment in regular media had no effect TRAP expression (figure 7.3B). RANKL treatment alone caused a significant increase in TRAP ($p < 0.05$) and sEV treatment with RANKL induced a small but insignificant increase in TRAP expression compared to RANKL alone.

These results suggest that sEV treatment increases RAW cell differentiation in combination with RANKL but have no effect on differentiation in isolation. However, upon visual inspection, cells treated with RANKL and sEVs appeared to have a much higher rate of cell death/severe abnormality, seen by reduced cell number and multiple floating cells. Cells were imaged using a brightfield microscope (figure 7.4). Untreated cells showed an unchanged, round morphology, and were highly confluent, likely due to no cessation in their proliferation. Cells treated with RANKL alone showed multiple mature osteoclasts. RAW cells treated with sEVs alone showed a similar morphology to untreated cells, but with reduced cell number. Furthermore, a small number of cells showed an elongated and potentially partially differentiated morphology. Cells treated with RANKL and sEVs showed no clear evidence of fused cells, although some cells had appeared to cluster together. There was also substantially less cells compared to all other treatments, indicating either a marked reduction in proliferation, increased cell death or indeed, both.

After witnessing the effect of sEVs in combination with RANKL, which appeared to induce reduced proliferation and differentiation, we assessed the health of the cells using a number of cellular viability assays. A CellTox™ Green Cytotoxicity Assay was used to assess the levels of dead or damaged cells, with binding of the luminescent dye to cellular DNA only occurring in cells with damaged membranes. Compared to an untreated control, treatment with sEVs had no effect on the levels of luminescence, indicating no increase in cell damage/death (figure 7.5A). Addition of RANKL caused a resulted in >4x increase in luminescence (p<0.001) and treatment with sEVs in combination with RANKL, caused a further, significant, 22% increase in luminescence compared to treatment with RANKL (p=0.001) or sEVs (p<0.001) alone.

Reactive oxygen species (ROS) production is another marker of cytotoxicity and excessive ROS production can lead to apoptosis (Lee *et al.*, 2014). Compared to untreated cells, treatment of RAW cells with sEVs alone caused a significant increase in ROS production (p<0.001), and a similar increase in ROS production compared to control cells was seen in RANKL treated cells (p<0.001) (figure 7.5B). Treatment of cells with RANKL and sEVs resulted in an increase in ROS production compared to treatment with sEVs or RANKL alone (p=0.005 for both).

An MTT assay was used in parallel with the cytotoxicity assay, to measure the metabolic activity in these cells, as a marker of cellular function and health. MTT assays measure the production of insoluble purple formazan crystals, which are produced as a result of cellular reductase activity. The level of formazan production is then measured colourimetrically by absorbance, after the purple product is dissolved in DMSO. Thus, MTT assays are utilised as a high throughput measure of cell viability (Riss *et al.*, 2004). As expected, the results of the MTT assay appear to generally oppose those shown in the cytotoxicity assay. Compared to untreated cells, absorbance was significantly reduced by both sEV treatment alone (<0.001)

and treatment with RANKL alone (p<0.001) (figure 7.5C). Absorbance was also significantly reduced in cells treated with RANKL and sEVs compared to sEVs or RANKL alone (p<0.001 for both).

Given the synergistic effects of sEVs + RANKL on their ability to induce both changes in osteoclastic marker expression and changes in cell viability, we hypothesised that sEVs may contain additional RANKL. To test this, we analysed sEV lysate for the presence of RANKL. Western blot of PC3 sEV lysate confirmed the weak presence of PC3 sEV RANKL (figure 7.6), which combined, suggests that sEV RANKL may be involved in PCa sEV signalling to osteoclasts. However, based on the quality of this evidence, significant further work is needed to confirm this.

Finally, to assess the overall effect of RANKL and sEV treatment on RAW cell function, a pit formation assay was performed. RAW cells (30,000/24 well) were seeded on calcium (HA) coated Corning® osteo assay surface plates. After 7 days, cells were removed, and ARS staining was used to visualise the remaining calcium, highlighting the newly formed osteoclast resorbed pits. Control or sEV treated RAW cells in the absence of RANKL resulted in no mature osteoclasts, and therefore no osteoclast pits (figure 7.7A). Treatment with RANKL resulted in a marked induction of differentiation, resulting in the formation of numerous osteoclast pits (figure 7.7B). Cells treated with RANKL and sEVs showed a decreased number of osteoclast pits, indicating a reduction of osteoclastogenesis (figure 7.7B). To quantify the level of osteoclast activity, the total resorbed area for each well was calculated from 3 representative images using ImageJ software. Analysis in this way revealed a significant decrease in total resorbed area for RANKL + sEV treated cells compared to RANKL treated cells (p=0.046) (figure 7.7C).

A

OSCAR

B
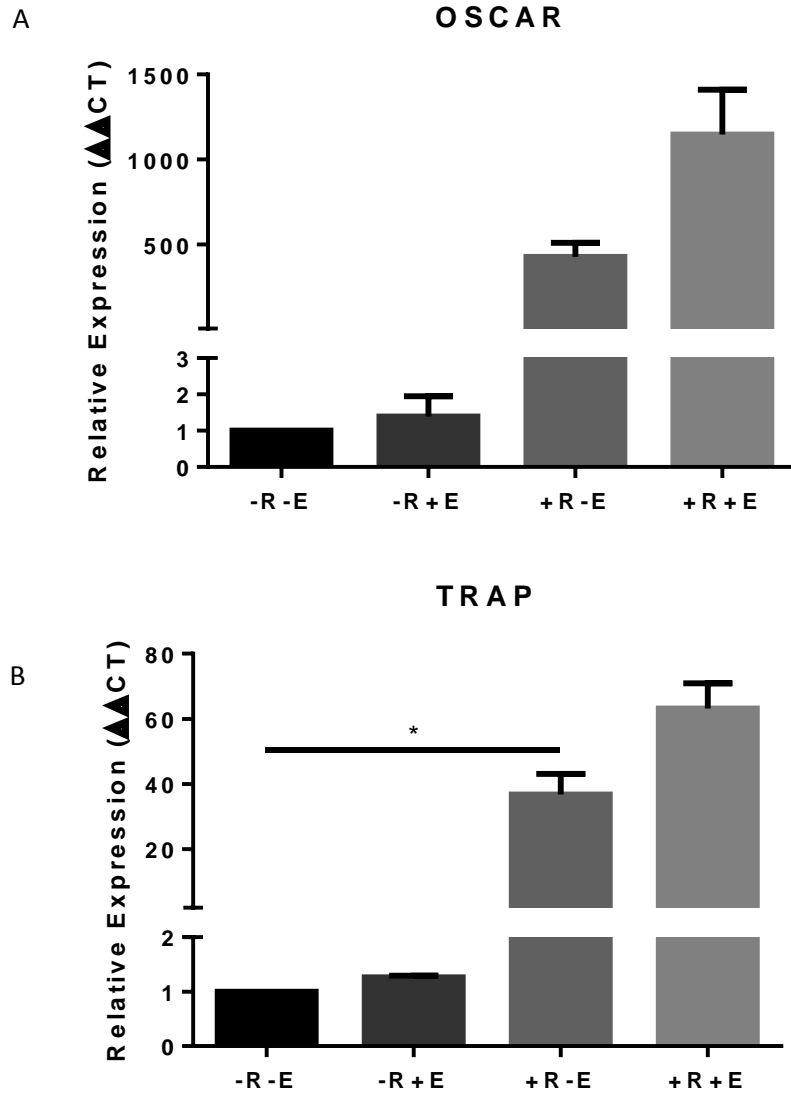
TRAP

Figure 7.3: Expression of Osteoclast Differentiation Genes in RAW Cells Treated with RANKL/sEVs. Expression of OSCAR (A) and TRAP (B) in RAW cells treated with 20ng/mL of RANKL (R) and 200µg/mL of sEVs (E). Graphs show average fold change compared to control +SEM, n=3. Statistical significance assessed by Kruskal-Wallis with Tukey test, *p<0.05, **p<0.01.
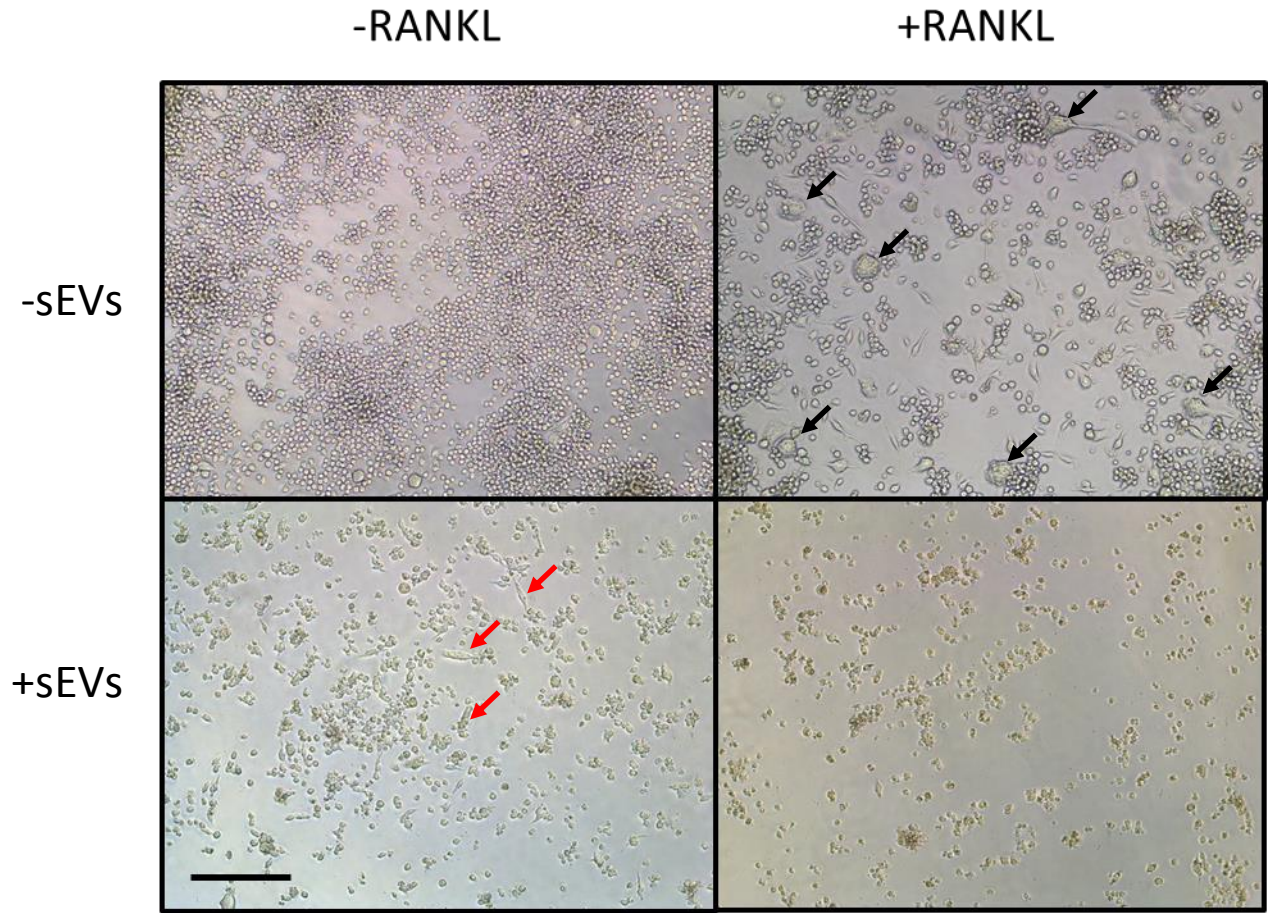
Figure 7.4: Morphology of RAW Cells Treated with RANKL/sEVs. 4x magnified brightfield images of RAW cells treated with 20ng/mL of RANKL and 200μg/mL of sEVs. Black arrows show fused, multinucleated, mature osteoclasts. Red arrow shows elongated cells, similar to those seen in RANKL treated cells. Scale bar: 500μm.
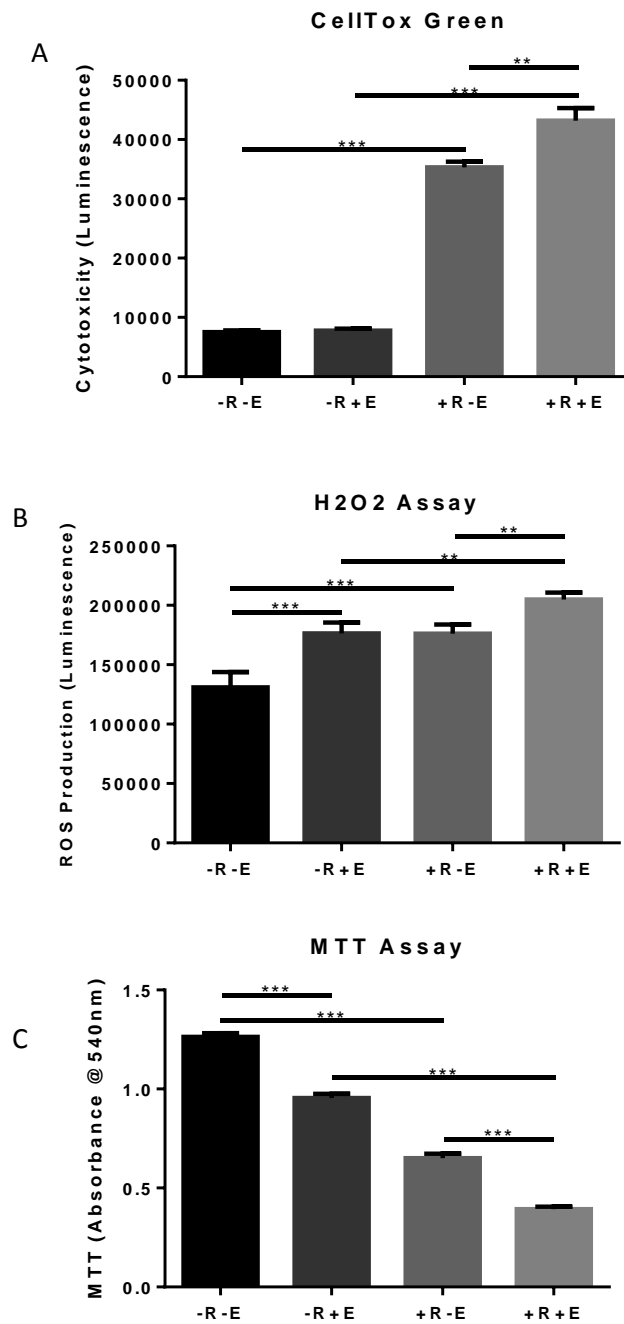
Figure 7.5: Cell Viability Assays on RANKL(R)/sEVs(E) Treated RAW Cells. CellToxGreen assay (A), H_2O_2 assay (B) and MTT assay (C) on RAW cells treated with 20ng/mL of RANKL (R) and 200μg/mL of sEVs (E). Graphs show average fold change compared to control +SEM, n=3. Statistical significance assessed by one-way ANOVA using a Holm-Sidak multiple comparisons test, **p<0.01, ***p<0.001.
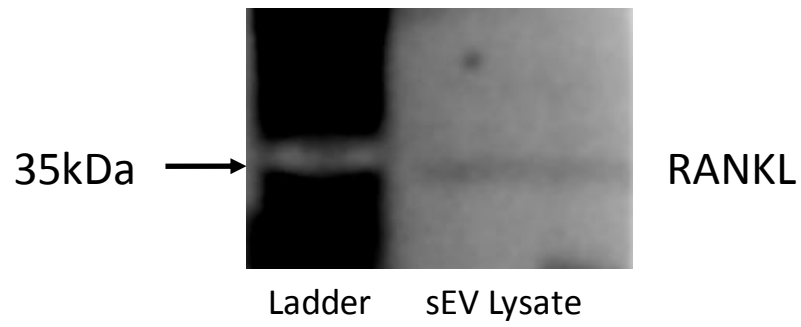
Figure 7.6: RANKL Expression in sEV Protein. Western blot of RANKL in PC3 sEV lysate (20µg).
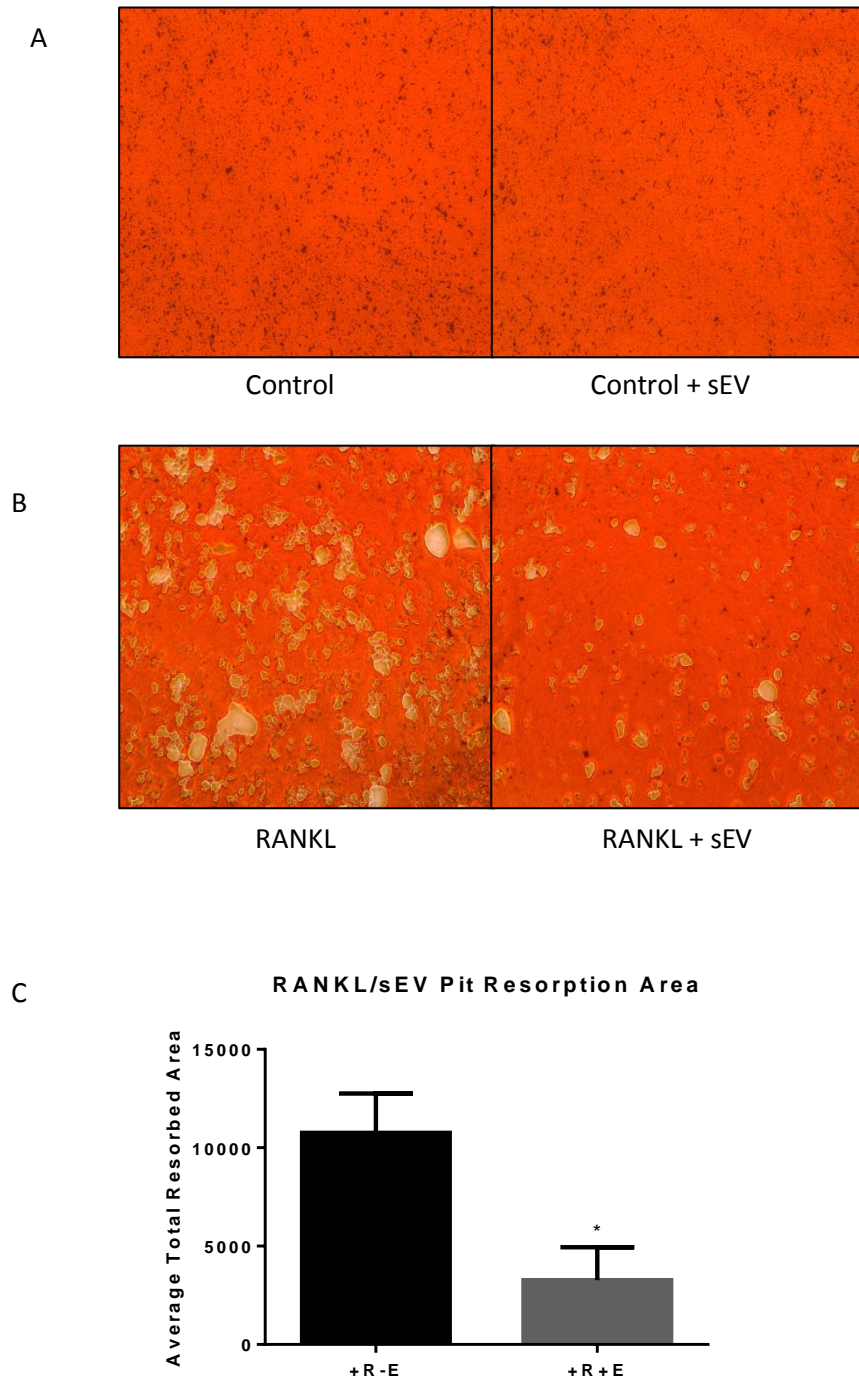
Figure 7.7: Pit Formation Assay on RANKL and sEV Treated RAW Cells. Pit formation assay on RAW cells treated with 20ng/mL of RANKL and 200µg/mL of sEVs. (A) Control and sEV treated cells in the absence of RANKL. (B) Control and sEV treated cells with RANKL. (C) Average resorbed area of control and sEV treated cells with RANKL. Graphs show average +SEM, n=3. Statistical significance assessed by unpaired ttest, *p<0.05.

7.4 Discussion

The balance of osteoclastic and osteoblastic activity in physiology is tightly regulated and is crucial for skeletal repair and mineral homeostasis. The dysregulation of this cycle leads to the osteoblastic and osteoclastic lesions seen in bone metastases. Therefore, after showing that PCa sEV communication drove osteoblastic differentiation, we looked to analyse the effects of this communication on osteoclasts in an osteoclast model system.

RAW 264.7 cells were used to study osteoclast differentiation. Human and mouse osteoclast precursor cells such as macrophages or haematopoietic stem cells can be isolated from bone marrow or peripheral blood to study osteoclastogenesis (Cody *et al.*, 2011; Iwaki *et al.*, 2016; Susa *et al.*, 2004). However, RAW cells are often favoured in osteoclast differentiation studies due to their ease of culture as well as their rapid and reproducible ability to differentiate. Furthermore, RAW cells can effectively differentiate in the absence of macrophage colony stimulating factor (M-CSF) (Vincent *et al.*, 2009), allowing for treatments to be given with only RANKL, thus reducing the collateral cellular effects of additional differentiation supplements. RAW cells have previously been treated with exosomes from human cells including PC3 cells, and actually show markedly increased levels of PC3 exosome uptake compared to numerous human cell lines (Ferguson *et al.*, 2018a).

Osteoclast differentiation is easily characterised visually due to the obvious difference in morphology between osteoclast precursors, and the considerably larger, multinucleated mature osteoclasts. We saw that when RAW cells were treated with 25ng/mL RANKL, multiple multinucleated cells were visible with a vast cytoplasm, typical of mature osteoclasts (Quan *et al.*, 2017). Whereas untreated cells remained small and circular, similar to cells in culture. However, untreated cells did show increased numbers, indicating their proliferation over the 8 day period.

As well as visual assessment of differentiation, genetic markers of osteoclast differentiation were also used. TRAP and OSCAR were the genetic markers used to determine osteoclast differentiation. TRAP and OSCAR are both expressed in mature cells of the osteoclast differentiation pathway but are both also present in macrophages (Doster *et al.*, 2018; Sinningen *et al.*, 2013). After 8 days of culture, the expression of TRAP and OSCAR increased in a dose dependant manner with RANKL treatment. This validates that RANKL treatment for 8 days is able to induce differentiation of RAW cells, and suggests that induction of differentiation may be proportional to the dose of RANKL given. However, it has been shown that multinucleated osteoclast number doesn't necessarily increase dose dependently with RANKL (Nguyen & Nohe, 2017; Song *et al.*, 2018). In these studies, it was seen that mature osteoclast number shows no increase at doses of RANKL >10ng/mL and >30ng/mL respectively. Therefore, as it was unknown whether PC3 sEVs would inhibit or induce osteoclast differentiation, for experiments combining RANKL and sEVs, a dose of 20ng/mL RANKL was used.

Addition of sEVs alone resulted in no increase in OSCAR or TRAP expression, suggesting sEVs alone may be ineffective at stimulating osteoclast differentiation at the high doses used in this study. Conversely, when sEVs were given with RANKL, an increase in OSCAR and TRAP expression was seen. Similar to results seen in osteoblast stimulation, this collectively suggested that sEVs are more effective at synergistically increasing differentiation of osteoclasts with the aid of RANKL, rather than initiating differentiation when given alone.

Given the increase in OSCAR and TRAP expression seen in RAW cells treated with sEVs + RANKL, it was expected that these wells would feature at least as many multinucleated cells as those treated with RANKL. However, upon visual inspection, it was clear that cells treated with sEVs + RANKL had a much higher proportion of floating dead cells. Visual assessment of the cells confirmed a decrease in cell number, consistent with the increased floating cells.

Furthermore, the remaining cells showed no distinct differentiation, collectively indicating that a combination of RANKL and sEVs not only prevents differentiation, but may in fact trigger apoptosis and/or be cytotoxic. Interestingly, when given alone, sEVs appeared to be able to induce very mild differentiation characteristics in some osteoclasts. Although fused cells were not clearly visible, some cells appeared elongated. As some of the RANKL treated cells also appeared elongated, it is possible that this represents cells that may have begun differentiation but have yet to undergo cellular fusion.

As it was now suggested that sEVs + RANKL may affect the health of the RAW cells as well as their ability differentiate, cell viability assays were performed. Cytotoxicity (in the form of dead cell quantification), cell stress (in the form of H_2O_2 production) and cell viability (in the form of cellular metabolism level) were all measured to help build a well-rounded idea of the combined effects of sEVs + RANKL.

When treated with sEVs alone, RAW cells showed no increase in dead cell number, but did show both an increase in cell stress and a decrease in cell metabolism. Combined with qPCR of osteoclastic markers and brightfield images, the data suggests that sEVs alone are not able to induce cell death, but may decrease proliferation and partially induce differentiation.

Treatment of cells with RANKL resulted in a significant increase in both cell death and cell stress, an unexpected result. However, links between osteoclast differentiation and accelerated cell death *in vitro* have been made. For example, Akchurin *et al.* (2008) showed that when stimulated with RANKL, RAW cells produced multinucleated osteoclasts in a cyclical manner, displaying peaks of multinucleated cell number, followed by an increase in apoptosis, which then repeated. Furthermore, Ikeda and Takeshita (2016) found that plating bone marrow macrophages at too high confluency resulted in accelerated osteoclast formation but subsequently an acceleration in osteoclast death. These results may explain

why an increase in cell death and cellular stress can be seen in differentiating RAW cells following treatment with RANKL.

Treatment of RAW cells with sEVs + RANKL resulted in a significant increase in both cell death and cell stress compared to sEVs or RANKL alone. Given the results seen with RANKL alone, this would suggest either a further increase in differentiation or a genuine cytotoxic effect when combining both treatments. However, combining these results with images of sEV + RANKL treated cells, it is clear that treatment of RAW cells with sEVs + RANKL is cytotoxic and results in an increase in cell death. Nevertheless, given the links between differentiation of RAW cells and subsequent apoptosis of these cells, the use of further viability assays, potentially looking at different mechanisms of cell death, may be better at distinguishing between differentiation and cytotoxicity induced cell death.

Although sEV + RANKL treated cells displayed increased cell death, the increased expression of osteoclast markers in these cells would suggest that, despite what microscopy images may show, the surviving cells may have differentiated to a greater extent. This would show a synergistic effect of treatment with sEVs + RANKL. We then showed that PC3 sEVs carried additional RANKL, which may be driving the increased expression of these osteoclastic markers, as human RANKL is shown to be functional in mice (Rinotas *et al.*, 2014).

However, although RANKL has been extensively linked with apoptosis of osteoclasts as well as their differentiation (Bharti & Aggarwal, 2004), this effect is not thought to be dose dependant. Therefore, the cytotoxic effect of sEVs + RANKL is likely not due to excess stimulation from both sEV and soluble RANKL. Instead, regulation of apoptosis by RANKL is controlled by a number of downstream signalling networks within the osteoclasts, such as the PI3K/Akt/mTOR and JNK pathways (Bharti & Aggarwal, 2004). For example, activation of JNK by RANKL signalling may induce apoptosis of osteoclasts through inhibition of anti-apoptotic molecules such as B-cell lymphoma 2 (Bcl-2) (Maundrell *et al.*, 1997) or activation

of apoptotic molecules such as BCL-2-interacting mediator of cell death-extra long (Bim$_{EL}$) (Whitfield *et al.*, 2001). sEVs from multiple cell types, including cancer cells, have been shown to activate JNK (Blackwell *et al.*, 2017; Li *et al.*, 2018b; Yoon *et al.*, 2014). Therefore, it is possible that activation of JNK by sEVs, combined with RANKL treatment, may shift the RANKL signalling pathway in the favour of apoptosis over differentiation. However, significant further analysis of these signalling pathways and the downstream effects is required.

Finally, the effect of these treatments on the overall function of RAW cells was tested. Corning® osteo assay plates are coated with a layer of "inorganic crystalline calcium phosphate coating that mimics living bone material". Upon differentiation, mature multinucleated osteoclasts begin to resorb the calcium phosphate layer, which can then be visualised, aided by staining with ARS. We saw that without RANKL, both control and sEV treated RAW cells formed no pits, indicating that both treatments were ineffective at initiating osteoclastogenesis, at least to the point of mature osteoclast formation. This data matches earlier microscopy images which showed a lack of multinucleated cells in RAW cells treated with sEVs alone. Compared to RANKL treated cells, RANKL + sEV treated RAW cells displayed a significant decrease in activity. Total resorbed area was used to determine osteoclast activity. Also analysing pit number would give details as to the number of cells undergoing differentiation, as opposed to resorption area, which may be a combination of osteoclast number and activity. However, there were difficulties determining the number of individual pits due to the close proximity and fusion of pits, combined with their often irregular shape. ImageJ software was used to automatically determine resorbed area based on a colorimetric threshold, detecting pits based on their lighter appearance. Identical threshold values were used for all images, to reduce variability and bias.

To conclude, the data from this chapter indicates that when given in combination with RANKL, PC3 sEVs reduce the function of RAW cells and may in fact be cytotoxic. However, this treatment is also associated with an increase in the expression of osteoclastic markers. Thus, a number of cellular responses may be occurring. The cytotoxicity witnessed may be associated with an over-activation of the RAW cells, although this process that is as yet not documented. Conversely, there may be 2 signalling pathways initiated, one driving further osteoclast differentiation, potentially as a result of the sEV RANKL, and another initiating cytotoxic cell death, through JNK related pathways discussed previously. Overall, the osteoclastic function of RAW cells was attenuated by sEV treatment, indicating a push towards bone formation rather than resorption.

7.5 Summary of Key Points

sEVs were able to induce increased expression of the osteoclastic markers TRAP and OSCAR in RANKL treated RAW cells, suggesting a pro-osteoclastic effect. However, visual assessment showed an anti-osteoclastic, and potentially cytotoxic effect of this treatment. Cell viability assays also pointed towards a cytotoxic effect of RANKL + sEV treatment. Finally, overall it was shown that RANKL + sEV treatment resulted in a decrease in RAW cell function, assessed by the ability of these cells to resorb bone.

Chapter VIII:

General Discussion

8 General Discussion

Bone metastases are the most common form of secondary tumour associated with PCa. The development of secondary tumours is associated with markedly higher levels of morbidity and mortality compared to primary disease (Sieh *et al.*, 2013; Tangen *et al.*, 2003). Currently, treatment options for skeletal metastases are limited, with bisphosphonates and the anti-RANKL antibody denosumab representing the best existing treatments, both acting to reduce osteoclast activity (Smith *et al.*, 2015; Woodward & Coleman, 2010). Once the secondary tumour has seeded within the bone, growth of the tumour is accompanied by the development of either an osteolytic (most common with metastatic breast cancer) or osteoblastic (most common with metastatic PCa) lesion. These lesions reflect direct changes in the function of osteoblasts and osteoclasts, with the dominance of a particular cell type resulting in excess bone formation or degradation. Given the significant increase in morbidity and mortality with bone metastases vs primary disease, recent studies have focussed on gaining an understanding of both the spread of cells as well as the signalling pathways responsible for altered bone cell function.

Molecular signalling between metastatic cancer cells and bone cells has been extensively examined. A number of well characterised signalling molecules have been implemented in both the function of bone cells and the development of the secondary tumour, such as TGF-β, VEGF, MMPs, ET-1 and many more (Kingsley *et al.*, 2007). However, the lack of available treatment options for metastatic bone disease reflects a difficulty in manipulating these pathways in order to produce a therapeutic benefit. miRNAs have been linked to several classic aspects of cancer development, such as proliferation and apoptosis (Hwang & Mendell, 2006). Furthermore miRNAs have been implemented in the metastasis of certain cancers (Peng & Croce, 2016). sEVs, including exosomes, are significant carriers of miRNAs and are involved in extensive signalling between both nearby and distant cells (Falcone *et*

al., 2015). These sEV miRNAs have been implicated in signalling between PCa cells and bone cells, resulting in changes in the function of these cells that may drive the development of osteolytic/osteoblastic lesions. For example, miR-141-3p from PCa sEVs was shown to increase osteoblast activity and induce osteoblastic lesion development in mice (Ye *et al.*, 2017). Furthermore, inhibiting miRNA activity using antisense oligos is cheap, specific and fast. Thus, miRNA based treatment options have significant potential.

The aim for this study was therefore, to further analyse signalling between PCa cells and bone cells via miRNAs, especially those carried by sEVs. By examining this signalling using a variety of techniques such as next generation sequencing, the hope was to uncover new signalling pathways that may contribute to bone metastatic lesions.

As bone metastases associated with PCa are predominantly osteoblastic, the primary focus of this study was the effect of PCa sEV miRNA signalling on osteoblastogenesis and the associated function of mature osteoblasts. Due to the complexity of *in vivo* models, and the lack of available clinical bone metastatic samples including cadaver-derived samples currently available at Cardiff University, an *in vitro* model was utilised. Before testing the effects of PCa sEVs, a model of osteoblastic differentiation and function was first characterised. 7F2 mouse osteoblasts, treated with osteogenic media, showed reproducible differentiation, culminating in the deposition of hydroxyapatite (HA). Manipulation of this process is a commonly used to study osteoblast differentiation (Gharibi *et al.*, 2016), with the level of HA deposition being an easily and reliably measurable end point. To add validity to the osteoblast differentiation model, the expression levels of key osteoblastic genes are often measured, in tandem with HA staining. Commonly used markers of osteoblast differentiation such as RUNX2 and ALP could not be reproducibly induced in mineralising 7F2 cells in this study. However, 4 other genes, linked with osteogenesis were found to be differentially expressed in mineralising vs non-mineralising 7F2 cells, COL1A1, MMP3, DLX5

and ACVR1. Although we recognise that using mouse osteoblasts as a model of human bone metastases offers a degree of limitation, the ability of human PCa cell xenografts to readily form bone metastases in mice displays a commonality across these two species. Thus, the ease of handling of the 7F2 cell line, combined with its well documented reliable mineralisation (Gharibi *et al.*, 2016) was favoured over a human cell line equivalent.

The ability of PCa cells to induce increased osteoblastogenesis and osteoblast function is well documented (Logothetis & Lin, 2005). However, PC3 cells form primarily osteolytic lesions following metastasis (Dai *et al.*, 2016), and have displayed an ability to reduce the mineralisation of BMSCs (Alsulaiman *et al.*, 2016). Although sub clones of PC3 cell lines have been developed that induce mixed lesions, thus demonstrating that PC3 cells may have the potential to form more than just purely osteolytic lesions (Fradet *et al.*, 2013), the finding that PC3 cells induced an increase in mineralisation in 7F2 cells was interesting. This induction of mineralisation was validated by an associated increase in osteoblast differentiation genes. These findings suggest that PC3 cells may have different effects on osteoblast differentiation depending on cell line. Furthermore, PC3 cells were shown to induce mineralisation of 7F2 cells to a greater extent than DU145 cells, and both induced mineralisation to a greater extent than LNCaP cells. Given the tendency of LNCaP cells to form mixed lesions, as opposed to the osteolytic lesions seen with PC3 and DU145 cells, this pattern of 7F2 cell mineralisation was surprising. Instead, based on these results, it would appear that induction of mineralisation in 7F2 cells is directly linked to the aggressiveness of the PCa cell line. As studies directly comparing the effects of various PCa cell lines on 7F2 mineralisation are lacking, this finding may in fact be novel. Given the aggressiveness of PC3 cells, combined with their ability to induce osteoblastogenesis, this cell line was further explored.

We hypothesised that exported miRNAs from PC3 cells may be involved in this pro-osteoblastic signalling. The various routes of miRNA export, i.e. EVs, HDL molecules and argonaute proteins, are well characterised (Boon & Vickers, 2013), although the exact mechanisms that govern these pathways are still being widely explored. Therefore, confirmation that various miRNAs were significantly raised in PC3 cell conditioned media compared to regular FCS containing media was of little surprise. Differential centrifugation of PC3 cell conditioned media revealed that although most miRNAs are essentially soluble, and in association with small molecules, a fraction are likely associated with small EVs. This result mirrors findings from Dr Alwyn Dart, who showed, using size exclusion chromatography, that a larger portion of miRNA is either free in solution or associated with smaller molecules compared to those associated with EVs.

sEV associated miRNAs are of great interest in the field of intercellular signalling due to their innate ability to protect their miRNA cargo from RNase activity (Koga *et al.*, 2011), a major hurdle in long range RNA based signalling. Furthermore sEVs are shown to be enriched in miRNAs (Goldie *et al.*, 2014) and are shown to selectively package miRNAs (Guduric-Fuchs *et al.*, 2012), also displaying an ability to alter this selective packaging in diseased states (Skog *et al.*, 2008). sEVs also display a more specialised RNA profile than lEVs (also well known for transporting miRNA), containing a greater proportion of small RNAs whilst being absent of rRNA (Crescitelli *et al.*, 2013; Ji *et al.*, 2014).

We therefore looked to isolate PCa sEVs and determine their miRNA content. NGS is frequently used to assess sEV miRNA profiles due to its high resolution and quantitative nature (Liu *et al.*, 2018; Rodriguez *et al.*, 2017). Combining sequencing results from PC3 and DU145 cells allowed for comparisons of miRNA expression across two aggressive PCa cell lines. Furthermore, cellular miRNAs from these cell lines were also sequenced to give insight into the selective packaging that may be at play. A number of miRNAs appeared highly

expressed in both cell lines and their associated sEVs. Let-7a-5p, highly expressed in both cell lines and their sEVs, was shown to be overexpressed in PCa vs non-malignant samples by Kristensen *et al.* (2016), although in general, expression of let-7 miRNAs is reduced in many cancer types (Ghanbari *et al.*, 2015). miR-16-5p, was also shown to be highly expressed in all samples, a surprising finding given that miR-16-5p is often quoted as a tumour suppressor, with overexpression resulting in reduced proliferation and invasion of cancer cells (Qu *et al.*, 2017; Zhang *et al.*, 2018). The high expression of miR-221-3p seen in PC3 samples in this study is consistent with the findings of Galardi *et al.* (2007), which may reflect the proliferative effects of miR-221 targeting of p27^{Kip1} (le Sage *et al.*, 2007).

After validating miRNA sequencing results by qPCR, the levels of highly expressed miRNAs such as miR-16-5p and miR-221-3p as well as miRNAs that showed lower expression were compared between cancerous PC3/DU145 cells and non-cancerous PZ-HPV-7 cells. All cells showed higher expression of miR-16-5p and miR-221 compared to other miRNAs. miR-221 levels were similar in DU145 and PZ-HPV-7 cells. However, high expression of miR-16-5p appeared to be exclusive to the cancerous cell lines. Hessvik *et al.* (2012) found miR-16 to be among the 20 highest expressed miRNAs in PC3 cells. However, miR-16 was not found to be in the 20 highest expressed miRNAs in sEVs. Li *et al.* (2016b) showed that miR-16-5p was highly expressed in drug resistant PC3 and DU145 cells compared to wild types. Furthermore, they showed that miR-16-5p was higher in drug resistant DU145 sEVs compared to wild type sEVs. This further indicates that miR-16-5p expression is correlated with aggressive PCa cells. The high expression of miR-16-5p in PCa cells, combined with the known tumour suppressive characteristics of miR-16, suggest that high expression of miR-16-5p may be crucial for other aspects of PCa development, such as intercellular signalling at primary or secondary sites. This would explain why miR-16-5p levels appear to be high in the sEVs isolated from these cell types. Additionally, the presence of certain tumour suppressor miRNAs in EVs has been hypothesised as a mechanism of reducing their cellular levels, thus increasing a cancer cells

survival (Ohshima *et al.*, 2010). This may offer another explination as to the high levels of miR-16-5p in PC3 cell sEVs.

sEV to cellular ratio calculations for each miRNA suggest that selective packaging may be at play for PC3 cells, with some miRNAs expressed at higher levels in sEVs than cells. DU145 cells show a different packaging pattern, with most miRNAs showing decreased expression in sEVs compared to cells. This suggests that PC3 sEVs may have a more specialised miRNA cargo, and thus these sEVs may represent a greater intercellular signalling potential. Correlation analysis shows that sEV miRNA levels are linked to cellular concentrations, suggesting the process is likely mediated by both cellular concentrations and selective packaging of particular miRNAs. Interestingly, correlation analysis also demonstrated that DU145 cells likely have a less selectively packaged sEV miRNA transcriptome than PC3 cells, mirroring results from ratio analysis.

Although sEVs have been shown previously to protect encapsulated, intraluminal RNA from RNase degradation (Koga *et al.*, 2011), miRNAs within the PC3 sEVs in this study could not be considered as mediators of long range communication without first displaying an ability to survive in an environment displaying RNase activity. Therefore, by showing that PC3 sEV miRNAs were largely protected from RNase activity, we indicate their potential as long range communicators. The small loss of miRNA seen with RNase treatment likely represents miRNAs associated with the sEV surface, especially as sEVs were pre-treated with proteinase K. These extracellular miRNAs may produce slightly misleading data in experiments such as NGS, especially when combined with the potential for contamination of sEV samples with co-isolates. However, the lack of rRNA in our sEV samples is evidence of a high quality, acellular RNA isolation.

Addition of PC3 sEVs augmented 7F2 mineralisation in osteogenic media, confirmed by changes in expression of osteogenic genes. It was then shown that sEVs also induce

differentiation in regular media, and are able to induce mineralisation in the presence of a phosphate source. The ability of sEVs from other PCa cell lines to induce changes in the differentiation and mineralisation of osteoblasts has been demonstrated (Xu *et al.*, 2018a). Furthermore, MVs from PC3 cells can induce osteoblast differentiation (Itoh *et al.*, 2012), indicating that PC3 cells may also have osteoblastic properties, despite their typical osteolytic presentation, further validating the osteoblastic nature of PC3 sEVs seen in this study.

For a deeper understanding of the effects of sEV communication between PC3 and 7F2 cells, sEV treated 7F2 cells were sequenced for their transcriptome. sEVs were given alongside osteogenic supplements, thus detailing the role sEVs play in addition to regular mineralisation, in an attempt to more accurately mimic the conditions of a metastatic lesion. Pathway analysis revealed a number of bone related development and disorder pathways were affected by PC3 sEV treatment. Furthermore, a number of upstream regulators were implicated in the gene changes seen in sEV treated cells. Within these upstream regulators, 7 miRNAs were determined to be involved in this communication, including miR-16-5p. Given the high expression of miR-16-5p in PC3 cells and sEVs, combined with literature evidence suggesting a correlation between miR-16-5p and PCa cell aggressiveness (Hessvik *et al.*, 2012; Li *et al.*, 2016b), miR-16-5p was further explored as a mediator of sEV communication between PC3 and 7F2 cells.

To validate the previous findings, we confirmed both delivery, and increased functionality of miR-16-5p in sEV treated 7F2 cells using qPCR and a miR-16-5p reporter. In an exciting and novel finding, transfection of miR-16-5p alone, resulting in an increase in intracellular 7F2 miR-16-5p levels of 50%, was able to stimulate a significant increase in osteoblast differentiation. Although the change in mineralisation was mild, reflected by a change in only 2 of the 4 osteoblast differentiation genes, this finding highlights a new way of inducing osteoblast differentiation, and therefore may hold clinical significance within the field of

bone metastasis as well as other skeletal related disorders such as osteoporosis. Describing a model in which transfection of a single miRNA can increase osteoblastic function has the potential to inspire a range of clinical therapeutic agents in this area. As discussed, the clinical application of miRNA inhibitors hold great potential. Already, clinical trials involving miRNA inhibitors for conditions such as T-cell lymphoma (Seto *et al.*, 2018) and Hepatitis C infection (van der Ree *et al.*, 2017) are underway. However, as stated, the change in osteoblast function with miR-16-5p transfection was mild compared to sEV treatment. It is therefore recognised that the remaining osteoblast inducing capability of sEVs is either caused by additional miRNAs or by non-miRNA based signalling.

To further explore the mechanism(s) by which miR-16-5p induces osteoblast differentiation, we re-analysed the sEV treated 7F2 sequencing data, specifically looking for altered targets of miR-16-5p. 3 individual miRNA target databases were used to compile a representative list of sequenced miR-16-5p targets. From which 4 genes, related to osteoblast function, and significantly reduced by sEV treatment, were selected; DLL1, PLSCR4, ADRB2 and AXIN2.

A successful reduction in the exzpression of these genes was then confirmed following treatment with miR-16-5p or PCE sEVS, thus validating their potential involvement in the associated osteoblastic signalling. We therefore looked to analyse the effects of the overexpression of these genes on 7F2 differentiation and mineralisation.

AXIN2 knockout has previously been shown to rescue the loss in mineralisation of BMSCs from RUNX2$^{+/-}$ mice, but produced a mild and insignificant increase in mineralisation alone (McGee-Lawrence *et al.*, 2013). This contradicts our own data from 7F2 cells, which indicates that AXIN2 may augment osteoblastogenesis. However, the effect of AXIN2 KO shown by McGee-Lawrence *et al* (2013) was linked to the expression of RUNX2. As discussed, during the characterisation of mineralising 7F2 cells, RUNX2 was not reliably increased during

differentiation. This may explain why AXIN2 appeared to have a different effect in 7F2 cells compared to the other osteoblasts where RUNX2 induction has been reliably confirmed.

The varying expression patterns of PLSCR4 in osteoblastic vs non-osteoblastic osteosarcomas and high vs low bone forming hBMSCs, suggests a role of PLSCR4 in bone formation (Andersen *et al.*, 2015; Kubista *et al.*, 2011). However, the functional role of PLSCR4 expression in osteoblasts is yet to be explored. We present novel data showing a significant reduction in 7F2 mineralisation following PLSCR4 overexpression.

Although not validated by protein overexpression, transcript overexpression of DLL1 and ADRB2 also lead to a decrease in 7F2 mineralisation. DLL1 expression was previously linked to decreased osteoblast differentiation (Muguruma *et al.*, 2017), and thus our findings agree with these results. ADRB2 expression has been linked to osteoblast proliferation (Fu *et al.*, 2005), which is tightly linked to subsequent differentiation. Thus, the reduction in mineralisation seen in ADRB2 overexpressing 7F2 cells may be the result of increased proliferation, subsequently reducing the differentiation potential of these cells. Ma *et al.* (2011) showed that increased ADRB2 expression in osteoblasts is linked to the catabolic bone effects of glucocorticoids, further showing the treatment with the β-blocker propranolol as well as glucocorticoids prevented the loss of bone in mice. Thus, our data, showing reduced mineralisation in ADRB2 overexpression osteoblasts, is in keeping with these results.

The dynamic restructuring of bone is a process reliant on the function of multiple cell types, primarily osteoblasts and osteoclasts. The balance of this process, as well as its aberrance during metastatic lesion formation, crucially depends on the functionality of both cell types. Therefore, the effect of sEVs on osteoclasts was assessed to build a more complete picture of the effects of PCa sEV signalling within the bone microenvironment.

PC3 sEVs in combination with RANKL appeared cytotoxic to RAW cells, with cellular assays confirming an increase in cell stress and death. This effect ultimately lead to a decrease in

osteoclast formation and function. Thus the effects of sEVs appear to be linked to the effects of RANKL signalling in these cells. It has been shown that RANKL can induce apoptosis of osteoclasts, as opposed to differentiation depending on downstream signalling cascades, including JNK activation (Maundrell *et al.*, 1997; Whitfield *et al.*, 2001). sEVs have also displayed an ability to activate JNK (Blackwell *et al.*, 2017; Li *et al.*, 2018b; Yoon *et al.*, 2014), thus based on the current data, sEV activation of JNK coupled with RANKL signalling may shift signalling from pro-osteoclastic to apoptotic. Karlsson *et al.* (2016) also demonstrated that sEVs from murine TRAMP-C1 PCa cells with RANKL impaired the formation of mature osteoclasts from RAW cells, whereas fibroblast sEVs had no effect. However, the levels of apoptotic markers in these cells showed no change with sEV treatment, indicating the reduction of osteoclastogenesis was occurring via another mechanism. Though apoptosis markers are tested, the study makes no mention of witnessing cell death in sEV treated cells. Therefore the action of PCa sEVs from these cells may well be inhibitory, but does not negate that PC3 sEVs may induce apoptosis of RAW cells, although further testing of apoptotic markers and pathways is necessary.

In conclusion, although further assessment of the effects of PC3 sEVs on bone cells, particularly osteoclasts, is required, the combined pro-osteoblastic and anti-osteoclastic nature of PC3 sEVs seen in this thesis mirrors the common osteoblastic presentation of PCa metastatic bone disease. We show that PC3 sEV miR-16-5p is able to induce mineralisation of 7F2 cells and highlight key gene targets that may effect this process (figure 8.1A). We then show that PC3 sEVs reduce the osteoclastogenic signalling of RANKL and may induce apoptosis in these cells (figure 8.1B). However, as PC3 cells form predominantly osteolytic metastatic lesions, further testing of sEVs from other PCa cell types on osteoblasts and osteoclasts may help to build a more substantial picture as to the effects of local sEV signalling between PCa and bone cells within a metastatic lesion.
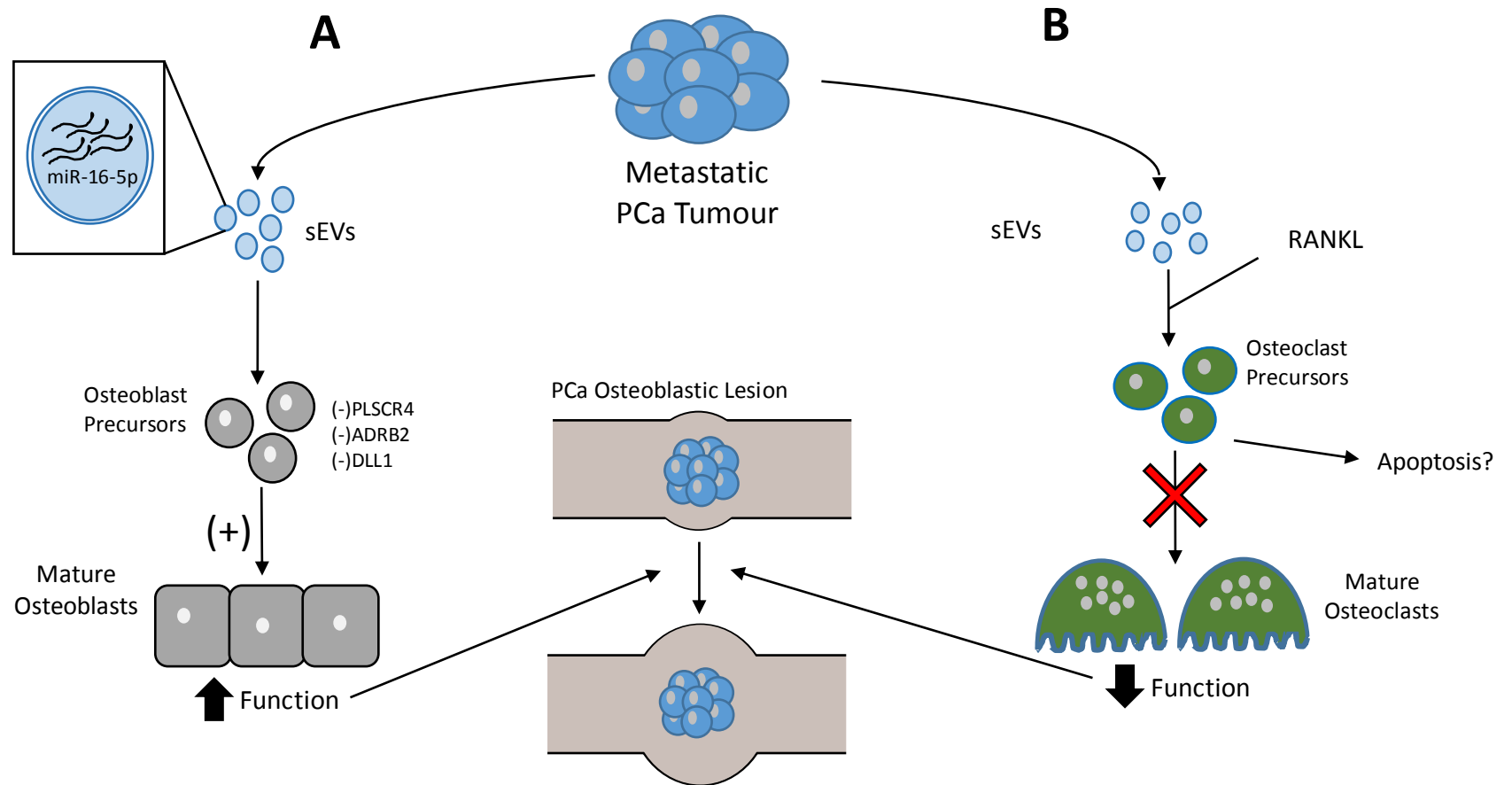
Figure 8.1: Schematic Summary of the Thesis Findings. (A) sEVs from metastatic PCa tumours deliver miR-16-5p to osteoblast precursor cells, reducing their expression of PLSCR4, ADRB2 and DLL1, which contribute to increased osteoblast differentiation and mineralisation. (B) The same sEVs impair RANKL induced differentiation of osteoclast precursors, and may induce apoptosis in these cells. The overall effect of this pro-osteoblastic and anti-osteoclastic signalling suggests that PCa sEVs may contribute to the osteoblastic presentation of PCa metastatic bone lesions.

Future Work

The findings of this project detail mechanisms by which PCa sEVs may induce osteoblastogenesis, as well as highlighting the effect of these same sEVs on osteoclastogenesis, thus highlighting a "double-pronged" effect in driving bone formation. Future work, following on from these findings, should focus on expanding these assays into an *ex vivo* bone model system, which would encompass the multiple PCa, osteoblast and osteoclast cell types and capitulate the full complexity and heterogeneity of cells in this specialised environment. It would also facilitate detailed examination of vesicle-mediated manipulation of the bone niche, prior to the physical landing and engraftment of metastatic cells. This represents an important area of metastasis requiring greater insight, as the effect of EVs on this process has shown recent promise (Peinado *et al.*, 2012). This would build a more representative idea as to the effects of PCa sEV signalling within the metastatic lesion. Furthermore, specific findings within the project, such as the ability of miR-16-5p to induce osteoblast differentiation, and PCa sEVs to alter RANKL signalling in osteoclasts, should be further examined, and the relative importance of vesicles in this complex system should be established

9   <u>**Appendix 1**</u>
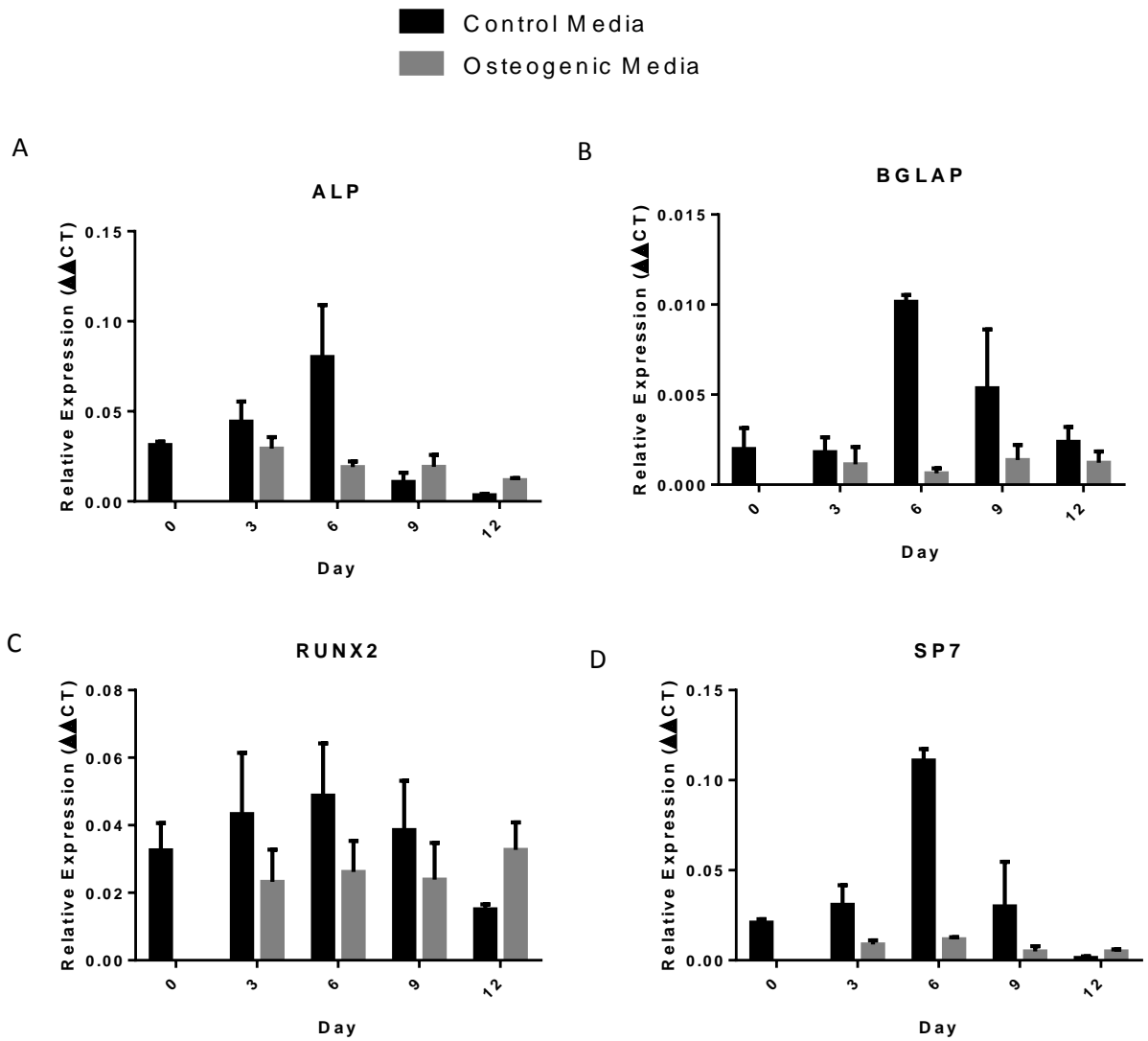
Appendix figure 1: qPCR of additional genes for 7F2 characterisation (unused): (A) ALP expression, (B) BGLAP expression, (C) RUNX2 expression and (D) SP7 expression in cells treated with regular or osteogenic media over a 12 day period. (n=4)

References:

Abdelgawad, M. E., Delaisse, J. M., Hinge, M., Jensen, P. R., Alnaimi, R. W., Rolighed, L., . . . Andersen, T. L. (2016). Early reversal cells in adult human bone remodeling: osteoblastic nature, catabolic functions and interactions with osteoclasts. *Histochem Cell Biol, 145*(6), 603-615. doi:10.1007/s00418-016-1414-y

Abe, E., Mocharla, H., Yamate, T., Taguchi, Y., & Manolagas, S. C. (1999). Meltrin-alpha, a fusion protein involved in multinucleated giant cell and osteoclast formation. *Calcif Tissue Int, 64*(6), 508-515.

Akchurin, T., Aissiou, T., Kemeny, N., Prosk, E., Nigam, N., & Komarova, S. V. (2008). Complex dynamics of osteoclast formation and death in long-term cultures. *PLoS One, 3*(5), e2104. doi:10.1371/journal.pone.0002104

Akduman, B., & Crawford, E. D. (2006). Treatment of localized prostate cancer. *Rev Urol, 8 Suppl 2*, S15-21.

Akech, J., Wixted, J. J., Bedard, K., van der Deen, M., Hussain, S., Guise, T. A., . . . Lian, J. B. (2010). Runx2 association with progression of prostate cancer in patients: mechanisms mediating bone osteolysis and osteoblastic metastatic lesions. *Oncogene, 29*(6), 811-821. doi:10.1038/onc.2009.389

Akers, J. C., Gonda, D., Kim, R., Carter, B. S., & Chen, C. C. (2013). Biogenesis of extracellular vesicles (EV): exosomes, microvesicles, retrovirus-like vesicles, and apoptotic bodies. *J Neurooncol, 113*(1), 1-11. doi:10.1007/s11060-013-1084-8

Al-Qtaitat, A. (2014). A Review of Non-Collagenous Proteins; their Role in Bone. *American Journal of Life Sciences, 2*, 351. doi:10.11648/j.ajls.20140206.14

Alderton, G. K. (2012). Metastasis. Exosomes drive premetastatic niche formation. *Nat Rev Cancer, 12*(7), 447. doi:10.1038/nrc3304

Alexander, M., Hu, R., Runtsch, M. C., Kagele, D. A., Mosbruger, T. L., Tolmachova, T., . . . O'Connell, R. M. (2015). Exosome-delivered microRNAs modulate the inflammatory response to endotoxin. *Nat Commun, 6*, 7321. doi:10.1038/ncomms8321

Alkhateeb, S. S., Alibhai, S. M., Finelli, A., Fleshner, N. E., Jewett, M. A., Zlotta, A. R., & Trachtenberg, J. (2010). Does nerve-sparing radical prostatectomy increase the risk of positive surgical margins and biochemical progression? *Urol Ann, 2*(2), 58-62. doi:10.4103/0974-7796.65107

Allott, E. H., Masko, E. M., & Freedland, S. J. (2013). Obesity and prostate cancer: weighing the evidence. *Eur Urol, 63*(5), 800-809. doi:10.1016/j.eururo.2012.11.013

Alsulaiman, M., Bais, M. V., & Trackman, P. C. (2016). Lysyl oxidase propeptide stimulates osteoblast and osteoclast differentiation and enhances PC3 and

DU145 prostate cancer cell effects on bone in vivo. *J Cell Commun Signal, 10*(1), 17-31. doi:10.1007/s12079-015-0311-9

Ambs, S., Prueitt, R. L., Yi, M., Hudson, R. S., Howe, T. M., Petrocca, F., . . . Croce, C. M. (2008). Genomic profiling of microRNA and messenger RNA reveals deregulated microRNA expression in prostate cancer. *Cancer Res, 68*(15), 6162-6170. doi:10.1158/0008-5472.CAN-08-0144

Ameres, S. L., & Zamore, P. D. (2013). Diversifying microRNA sequence and function. *Nat Rev Mol Cell Biol, 14*(8), 475-488. doi:10.1038/nrm3611

Andersen, R. K., Zaher, W., Larsen, K. H., Ditzel, N., Drews, K., Wruck, W., . . . Kassem, M. (2015). Association between in vivo bone formation and ex vivo migratory capacity of human bone marrow stromal cells. *Stem Cell Res Ther, 6*, 196. doi:10.1186/s13287-015-0188-9

Andersen, T. L., Abdelgawad, M. E., Kristensen, H. B., Hauge, E. M., Rolighed, L., Bollerslev, J., . . . Delaisse, J. M. (2013). Understanding coupling between bone resorption and formation: are reversal cells the missing link? *Am J Pathol, 183*(1), 235-246. doi:10.1016/j.ajpath.2013.03.006

Anderson, H. C., Garimella, R., & Tague, S. E. (2005). The role of matrix vesicles in growth plate development and biomineralization. *Front Biosci, 10*, 822-837.

Andreu, Z., & Yanez-Mo, M. (2014). Tetraspanins in extracellular vesicle formation and function. *Front Immunol, 5*, 442. doi:10.3389/fimmu.2014.00442

Aqil, M., Naqvi, A. R., Mallik, S., Bandyopadhyay, S., Maulik, U., & Jameel, S. (2014). The HIV Nef protein modulates cellular and exosomal miRNA profiles in human monocytic cells. *J Extracell Vesicles, 3*. doi:10.3402/jev.v3.23129

Ardekani, A. M., & Naeini, M. M. (2010). The Role of MicroRNAs in Human Diseases. *Avicenna J Med Biotechnol, 2*(4), 161-179.

Arroyo, J. D., Chevillet, J. R., Kroh, E. M., Ruf, I. K., Pritchard, C. C., Gibson, D. F., . . . Tewari, M. (2011). Argonaute2 complexes carry a population of circulating microRNAs independent of vesicles in human plasma. *Proc Natl Acad Sci U S A, 108*(12), 5003-5008. doi:10.1073/pnas.1019055108

Asagiri, M., & Takayanagi, H. (2007). The molecular understanding of osteoclast differentiation. *Bone, 40*(2), 251-264. doi:10.1016/j.bone.2006.09.023

Atay, S., Banskota, S., Crow, J., Sethi, G., Rink, L., & Godwin, A. K. (2014). Oncogenic KIT-containing exosomes increase gastrointestinal stromal tumor cell invasion. *Proc Natl Acad Sci U S A, 111*(2), 711-716. doi:10.1073/pnas.1310501111

Axmann, R., Bohm, C., Kronke, G., Zwerina, J., Smolen, J., & Schett, G. (2009). Inhibition of interleukin-6 receptor directly blocks osteoclast formation in vitro and in vivo. *Arthritis Rheum, 60*(9), 2747-2756. doi:10.1002/art.24781

Baietti, M. F., Zhang, Z., Mortier, E., Melchior, A., Degeest, G., Geeraerts, A., . . . David, G. (2012). Syndecan-syntenin-ALIX regulates the biogenesis of exosomes. *Nat Cell Biol, 14*(7), 677-685. doi:10.1038/ncb2502

Bang, C., Batkai, S., Dangwal, S., Gupta, S. K., Foinquinos, A., Holzmann, A., . . . Thum, T. (2014). Cardiac fibroblast-derived microRNA passenger strand-enriched exosomes mediate cardiomyocyte hypertrophy. *J Clin Invest, 124*(5), 2136-2146. doi:10.1172/JCI70577

Batson, O. V. (1967). The vertebral system of veins as a means for cancer dissemination. *Prog Clin Cancer, 3*, 1-18.

Bauer, O., Sharir, A., Kimura, A., Hantisteanu, S., Takeda, S., & Groner, Y. (2015). Loss of osteoblast Runx3 produces severe congenital osteopenia. *Mol Cell Biol, 35*(7), 1097-1109. doi:10.1128/MCB.01106-14

Bazzini, A. A., Lee, M. T., & Giraldez, A. J. (2012). Ribosome profiling shows that miR-430 reduces translation before causing mRNA decay in zebrafish. *Science, 336*(6078), 233-237. doi:10.1126/science.1215704

Beg, M. S., Brenner, A. J., Sachdev, J., Borad, M., Kang, Y. K., Stoudemire, J., . . . Hong, D. S. (2017). Phase I study of MRX34, a liposomal miR-34a mimic, administered twice weekly in patients with advanced solid tumors. *Invest New Drugs, 35*(2), 180-188. doi:10.1007/s10637-016-0407-y

Belair, C. D., Paikari, A., Moltzahn, F., Shenoy, A., Yau, C., Dall'Era, M., . . . Blelloch, R. (2015). DGCR8 is essential for tumor progression following PTEN loss in the prostate. *EMBO Rep, 16*(9), 1219-1232. doi:10.15252/embr.201439925

Beno, T., Yoon, Y. J., Cowin, S. C., & Fritton, S. P. (2006). Estimation of bone permeability using accurate microstructural measurements. *J Biomech, 39*(13), 2378-2387. doi:10.1016/j.jbiomech.2005.08.005

Bharti, A. C., & Aggarwal, B. B. (2004). Ranking the role of RANK ligand in apoptosis. *Apoptosis, 9*(6), 677-690. doi:10.1023/B:APPT.0000045780.10463.c6

Bijnsdorp, I. V., Mulder, J., Geldof, A., Koppers-Lalic, D., Pegtel, M., Bakker, A., . . . van Moorselaar, J. (2015). Prostate Cancer Cell Secreted Exosomes Stimulate Osteoclast Formation and Activity. *ECTS Abstracts, 1*, 127.

Bill-Axelson, A., Holmberg, L., Ruutu, M., Garmo, H., Stark, J. R., Busch, C., . . . Investigators, S.-. (2011). Radical prostatectomy versus watchful waiting in early prostate cancer. *N Engl J Med, 364*(18), 1708-1717. doi:10.1056/NEJMoa1011967

Birkedal-Hansen, H., Moore, W. G., Bodden, M. K., Windsor, L. J., Birkedal-Hansen, B., DeCarlo, A., & Engler, J. A. (1993). Matrix metalloproteinases: a review. *Crit Rev Oral Biol Med, 4*(2), 197-250. doi:10.1177/10454411930040020401

Bischoff, F. R., & Gorlich, D. (1997). RanBP1 is crucial for the release of RanGTP from importin beta-related nuclear transport factors. *FEBS Lett, 419*(2-3), 249-254.

Bissig, C., & Gruenberg, J. (2013). Lipid sorting and multivesicular endosome biogenesis. *Cold Spring Harb Perspect Biol, 5*(10), a016816. doi:10.1101/cshperspect.a016816

Blackwell, R. H., Foreman, K. E., & Gupta, G. N. (2017). The Role of Cancer-Derived Exosomes in Tumorigenicity & Epithelial-to-Mesenchymal Transition. *Cancers (Basel), 9*(8). doi:10.3390/cancers9080105

Blades, R. A., Keating, P. J., McWilliam, L. J., George, N. J., & Stern, P. L. (1995). Loss of HLA class I expression in prostate cancer: implications for immunotherapy. *Urology, 46*(5), 681-686; discussion 686-687. doi:10.1016/S0090-4295(99)80301-X

Blair, H. C., Teitelbaum, S. L., Ghiselli, R., & Gluck, S. (1989). Osteoclastic bone resorption by a polarized vacuolar proton pump. *Science, 245*(4920), 855-857.

Blanchard, N., Lankar, D., Faure, F., Regnault, A., Dumont, C., Raposo, G., & Hivroz, C. (2002). TCR activation of human T cells induces the production of exosomes bearing the TCR/CD3/zeta complex. *J Immunol, 168*(7), 3235-3241.

Body, J. J., Coleman, R. E., & Piccart, M. (1996). Use of bisphosphonates in cancer patients. *Cancer Treat Rev, 22*(4), 265-287.

Bonewald, L. F. (2007). Osteocytes as dynamic multifunctional cells. *Ann N Y Acad Sci, 1116*, 281-290. doi:10.1196/annals.1402.018

Boon, R. A., & Vickers, K. C. (2013). Intercellular transport of microRNAs. *Arterioscler Thromb Vasc Biol, 33*(2), 186-192. doi:10.1161/ATVBAHA.112.300139

Boukpessi, T., Menashi, S., Camoin, L., Tencate, J. M., Goldberg, M., & Chaussain-Miller, C. (2008). The effect of stromelysin-1 (MMP-3) on non-collagenous extracellular matrix proteins of demineralized dentin and the adhesive properties of restorative resins. *Biomaterials, 29*(33), 4367-4373. doi:10.1016/j.biomaterials.2008.07.035

Boyce, B. F., & Xing, L. (2008). Functions of RANKL/RANK/OPG in bone modeling and remodeling. *Arch Biochem Biophys, 473*(2), 139-146. doi:10.1016/j.abb.2008.03.018

Boyle, W. J., Simonet, W. S., & Lacey, D. L. (2003). Osteoclast differentiation and activation. *Nature, 423*(6937), 337-342. doi:10.1038/nature01658

Brennecke, J., Stark, A., Russell, R. B., & Cohen, S. M. (2005). Principles of microRNA-target recognition. *PLoS Biol, 3*(3), e85. doi:10.1371/journal.pbio.0030085

Bronner, F. (1992). Bone and calcium homeostasis. *Neurotoxicology, 13*(4), 775-782.

Bruno, I. G., Karam, R., Huang, L., Bhardwaj, A., Lou, C. H., Shum, E. Y., . . . Wilkinson, M. F. (2011). Identification of a microRNA that activates gene expression by repressing nonsense-mediated RNA decay. *Mol Cell, 42*(4), 500-510. doi:10.1016/j.molcel.2011.04.018

Bubendorf, L., Schopfer, A., Wagner, U., Sauter, G., Moch, H., Willi, N., . . . Mihatsch, M. J. (2000). Metastatic patterns of prostate cancer: an autopsy study of 1,589 patients. *Hum Pathol, 31*(5), 578-583.

Buck, A. H., Coakley, G., Simbari, F., McSorley, H. J., Quintana, J. F., Le Bihan, T., . . . Maizels, R. M. (2014). Exosomes secreted by nematode parasites transfer small RNAs to mammalian cells and modulate innate immunity. *Nat Commun, 5*, 5488. doi:10.1038/ncomms6488

Caetano-Lopes, J., Canhao, H., & Fonseca, J. E. (2007). Osteoblasts and bone formation. *Acta Reumatol Port, 32*(2), 103-110.

Capulli, M., Paone, R., & Rucci, N. (2014). Osteoblast and osteocyte: games without frontiers. *Arch Biochem Biophys, 561*, 3-12. doi:10.1016/j.abb.2014.05.003

Cech, T. R., & Steitz, J. A. (2014). The noncoding RNA revolution-trashing old rules to forge new ones. *Cell, 157*(1), 77-94. doi:10.1016/j.cell.2014.03.008

Charhon, S. A., Chapuy, M. C., Delvin, E. E., Valentin-Opran, A., Edouard, C. M., & Meunier, P. J. (1983). Histomorphometric analysis of sclerotic bone metastases from prostatic carcinoma special reference to osteomalacia. *Cancer, 51*(5), 918-924.

Cheloufi, S., Dos Santos, C. O., Chong, M. M., & Hannon, G. J. (2010). A dicer-independent miRNA biogenesis pathway that requires Ago catalysis. *Nature, 465*(7298), 584-589. doi:10.1038/nature09092

Chen, G., Deng, C., & Li, Y. P. (2012). TGF-beta and BMP signaling in osteoblast differentiation and bone formation. *Int J Biol Sci, 8*(2), 272-288. doi:10.7150/ijbs.2929

Chendrimada, T. P., Finn, K. J., Ji, X., Baillat, D., Gregory, R. I., Liebhaber, S. A., . . . Shiekhattar, R. (2007). MicroRNA silencing through RISC recruitment of eIF6. *Nature, 447*(7146), 823-828. doi:10.1038/nature05841

Cheng, L., Montironi, R., Bostwick, D. G., Lopez-Beltran, A., & Berney, D. M. (2012). Staging of prostate cancer. *Histopathology, 60*(1), 87-117. doi:10.1111/j.1365-2559.2011.04025.x

Cheng, L., Sharples, R. A., Scicluna, B. J., & Hill, A. F. (2014). Exosomes provide a protective and enriched source of miRNA for biomarker profiling compared to intracellular and cell-free blood. *J Extracell Vesicles, 3*. doi:10.3402/jev.v3.23743

Chetram, M. A., Don-Salu-Hewage, A. S., & Hinton, C. V. (2011). ROS enhances CXCR4-mediated functions through inactivation of PTEN in prostate cancer cells. *Biochemical and Biophysical Research Communications, 410*(2), 195-200. doi:10.1016/j.bbrc.2011.05.074

Chiang, H. R., Schoenfeld, L. W., Ruby, J. G., Auyeung, V. C., Spies, N., Baek, D., . . . Bartel, D. P. (2010). Mammalian microRNAs: experimental evaluation of novel and previously annotated genes. *Genes Dev, 24*(10), 992-1009. doi:10.1101/gad.1884710

Chim, S. S., Shing, T. K., Hung, E. C., Leung, T. Y., Lau, T. K., Chiu, R. W., & Lo, Y. M. (2008). Detection and characterization of placental microRNAs in maternal plasma. *Clin Chem, 54*(3), 482-490. doi:10.1373/clinchem.2007.097972

Chiosea, S., Jelezcova, E., Chandran, U., Acquafondata, M., McHale, T., Sobol, R. W., & Dhir, R. (2006). Up-regulation of dicer, a component of the MicroRNA machinery, in prostate adenocarcinoma. *Am J Pathol, 169*(5), 1812-1820. doi:10.2353/ajpath.2006.060480

Chiu, Y. H., & Ritchlin, C. T. (2016). DC-STAMP: A Key Regulator in Osteoclast Differentiation. *J Cell Physiol, 231*(11), 2402-2407. doi:10.1002/jcp.25389

Clark, E. L., Coulson, A., Dalgliesh, C., Rajan, P., Nicol, S. M., Fleming, S., . . . Robson, C. N. (2008). The RNA helicase p68 is a novel androgen receptor coactivator involved in splicing and is overexpressed in prostate cancer. *Cancer Res, 68*(19), 7938-7946. doi:10.1158/0008-5472.CAN-08-0932

Clark, E. L., Hadjimichael, C., Temperley, R., Barnard, A., Fuller-Pace, F. V., & Robson, C. N. (2013). p68/DdX5 supports beta-catenin & RNAP II during androgen receptor mediated transcription in prostate cancer. *PLoS One, 8*(1), e54150. doi:10.1371/journal.pone.0054150

Clarke, B. (2008). Normal bone anatomy and physiology. *Clin J Am Soc Nephrol, 3 Suppl 3*, S131-139. doi:10.2215/CJN.04151206

Clouet d'Orval, B., Bortolin, M. L., Gaspin, C., & Bachellerie, J. P. (2001). Box C/D RNA guides for the ribose methylation of archaeal tRNAs. The tRNATrp intron guides the formation of two ribose-methylated nucleosides in the mature tRNATrp. *Nucleic Acids Res, 29*(22), 4518-4529.

Cocucci, E., Racchetti, G., & Meldolesi, J. (2009). Shedding microvesicles: artefacts no more. *Trends Cell Biol, 19*(2), 43-51. doi:10.1016/j.tcb.2008.11.003

Cody, J. J., Rivera, A. A., Liu, J., Liu, J. M., Douglas, J. T., & Feng, X. (2011). A simplified method for the generation of human osteoclasts in vitro. *Int J Biochem Mol Biol, 2*(2), 183-189.

Cohen, R. J., Shannon, B. A., Phillips, M., Moorin, R. E., Wheeler, T. M., & Garrett, K. L. (2008). Central zone carcinoma of the prostate gland: a distinct tumor type with poor prognostic features. *J Urol, 179*(5), 1762-1767; discussion 1767. doi:10.1016/j.juro.2008.01.017

Cole, J. S., & Patchell, R. A. (2008). Metastatic epidural spinal cord compression. *Lancet Neurol, 7*(5), 459-466. doi:10.1016/S1474-4422(08)70089-9

Coleman, R., Body, J. J., Aapro, M., Hadji, P., Herrstedt, J., & Group, E. G. W. (2014). Bone health in cancer patients: ESMO Clinical Practice Guidelines. *Ann Oncol, 25 Suppl 3*, iii124-137. doi:10.1093/annonc/mdu103

Coleman, R. E. (2001). Metastatic bone disease: clinical features, pathophysiology and treatment strategies. *Cancer Treat Rev, 27*(3), 165-176. doi:10.1053/ctrv.2000.0210

Collin-Osdoby, P., & Osdoby, P. (2012). RANKL-mediated osteoclast formation from murine RAW 264.7 cells. *Methods Mol Biol, 816*, 187-202. doi:10.1007/978-1-61779-415-5_13

Crawford, E. D., & DeAntoni, E. P. (1993). PSA as a screening test for prostate cancer. *Urol Clin North Am, 20*(4), 637-646.

Crescitelli, R., Lasser, C., Szabo, T. G., Kittel, A., Eldh, M., Dianzani, I., . . . Lotvall, J. (2013). Distinct RNA profiles in subpopulations of extracellular vesicles: apoptotic bodies, microvesicles and exosomes. *J Extracell Vesicles, 2*. doi:10.3402/jev.v2i0.20677

Cui, D., Zhang, C., Liu, B., Shu, Y., Du, T., Shu, D., . . . Guo, P. (2015). Regression of Gastric Cancer by Systemic Injection of RNA Nanoparticles Carrying both Ligand and siRNA. *Sci Rep, 5*, 10726. doi:10.1038/srep10726

Cui, Y., Luan, J., Li, H., Zhou, X., & Han, J. (2016). Exosomes derived from mineralizing osteoblasts promote ST2 cell osteogenic differentiation by alteration of microRNA expression. *FEBS Lett, 590*(1), 185-192. doi:10.1002/1873-3468.12024

Cunha, G. R., Fujii, H., Neubauer, B. L., Shannon, J. M., Sawyer, L., & Reese, B. A. (1983). Epithelial-mesenchymal interactions in prostatic development. I. morphological observations of prostatic induction by urogenital sinus mesenchyme in epithelium of the adult rodent urinary bladder. *J Cell Biol, 96*(6), 1662-1670.

Dai, J., Hensel, J., Wang, N., Kruithof-de Julio, M., & Shiozawa, Y. (2016). Mouse models for studying prostate cancer bone metastasis. *Bonekey Rep, 5*, 777. doi:10.1038/bonekey.2016.4

Daige, C., Priddy, L., Wiggins, J., Nelligan-Davis, T., Enzler, D., Vadnagara, K., & Brown, D. (2016). MRX34, a liposomal miR-34 mimic and potential first-in-class microRNA therapeutic: activity in animal models of liver cancer. *Journal of Clinical Oncology, 34*(15_suppl), e14076-e14076. doi:10.1200/JCO.2016.34.15_suppl.e14076

Dallas, S. L., Prideaux, M., & Bonewald, L. F. (2013). The osteocyte: an endocrine cell ... and more. *Endocr Rev, 34*(5), 658-690. doi:10.1210/er.2012-1026

Daneshgari, F., Taylor, G. D., Miller, G. J., & Crawford, E. D. (1995). Computer simulation of the probability of detecting low volume carcinoma of the prostate with six random systematic core biopsies. *Urology, 45*(4), 604-609. doi:10.1016/S0090-4295(99)80051-X

Darzacq, X., Jady, B. E., Verheggen, C., Kiss, A. M., Bertrand, E., & Kiss, T. (2002). Cajal body-specific small nuclear RNAs: a novel class of 2'-O-methylation and pseudouridylation guide RNAs. *EMBO J, 21*(11), 2746-2756. doi:10.1093/emboj/21.11.2746

de Groot, A. E., Roy, S., Brown, J. S., Pienta, K. J., & Amend, S. R. (2017). Revisiting Seed and Soil: Examining the Primary Tumor and Cancer Cell Foraging in Metastasis. *Mol Cancer Res, 15*(4), 361-370. doi:10.1158/1541-7786.MCR-16-0436

Del Fattore, A., Teti, A., & Rucci, N. (2012). Bone cells and the mechanisms of bone remodelling. *Front Biosci (Elite Ed), 4*, 2302-2321.

Delaisse, J. M. (2014). The reversal phase of the bone-remodeling cycle: cellular prerequisites for coupling resorption and formation. *Bonekey Rep, 3*, 561. doi:10.1038/bonekey.2014.56

Deneberg, S., Kanduri, M., Ali, D., Bengtzen, S., Karimi, M., Qu, Y., . . . Lehmann, S. (2014). microRNA-34b/c on chromosome 11q23 is aberrantly methylated in chronic lymphocytic leukemia. *Epigenetics, 9*(6), 910-917. doi:10.4161/epi.28603

Denli, A. M., Tops, B. B., Plasterk, R. H., Ketting, R. F., & Hannon, G. J. (2004). Processing of primary microRNAs by the Microprocessor complex. *Nature, 432*(7014), 231-235. doi:10.1038/nature03049

Diederichs, S., & Haber, D. A. (2007). Dual role for argonautes in microRNA processing and posttranscriptional regulation of microRNA expression. *Cell, 131*(6), 1097-1108. doi:10.1016/j.cell.2007.10.032

Djuranovic, S., Nahvi, A., & Green, R. (2012). miRNA-mediated gene silencing by translational repression followed by mRNA deadenylation and decay. *Science, 336*(6078), 237-240. doi:10.1126/science.1215691

Doherty, G. J., & McMahon, H. T. (2009). Mechanisms of endocytosis. *Annu Rev Biochem, 78*, 857-902. doi:10.1146/annurev.biochem.78.081307.110540

Doster, R. S., Rogers, L. M., Gaddy, J. A., & Aronoff, D. M. (2018). Macrophage Extracellular Traps: A Scoping Review. *J Innate Immun, 10*(1), 3-13. doi:10.1159/000480373

Ducy, P., Zhang, R., Geoffroy, V., Ridall, A. L., & Karsenty, G. (1997). Osf2/Cbfa1: a transcriptional activator of osteoblast differentiation. *Cell, 89*(5), 747-754.

Dudas, M., Sridurongrit, S., Nagy, A., Okazaki, K., & Kaartinen, V. (2004). Craniofacial defects in mice lacking BMP type I receptor Alk2 in neural crest cells. *Mech Dev, 121*(2), 173-182. doi:10.1016/j.mod.2003.12.003

Eguchi, T., Watanabe, K., Hara, E. S., Ono, M., Kuboki, T., & Calderwood, S. K. (2013). OstemiR: a novel panel of microRNA biomarkers in osteoblastic and osteocytic differentiation from mesencymal stem cells. *PLoS One, 8*(3), e58796. doi:10.1371/journal.pone.0058796

Ek-Rylander, B., Flores, M., Wendel, M., Heinegard, D., & Andersson, G. (1994). Dephosphorylation of osteopontin and bone sialoprotein by osteoclastic tartrate-resistant acid phosphatase. Modulation of osteoclast adhesion in vitro. *J Biol Chem, 269*(21), 14853-14856.

Elbashir, S. M., Lendeckel, W., & Tuschl, T. (2001). RNA interference is mediated by 21- and 22-nucleotide RNAs. *Genes Dev, 15*(2), 188-200.

Eriksen, E. F., Axelrod, D.W., Melsen, F. (1994). *Bone Histomorphometry*. Raven Press: Raven Press.

Esau, C., Davis, S., Murray, S. F., Yu, X. X., Pandey, S. K., Pear, M., . . . Monia, B. P. (2006). miR-122 regulation of lipid metabolism revealed by in vivo antisense targeting. *Cell Metab, 3*(2), 87-98. doi:10.1016/j.cmet.2006.01.005

Escola, J. M., Kleijmeer, M. J., Stoorvogel, W., Griffith, J. M., Yoshie, O., & Geuze, H. J. (1998). Selective enrichment of tetraspan proteins on the internal vesicles of multivesicular endosomes and on exosomes secreted by human B-lymphocytes. *J Biol Chem, 273*(32), 20121-20127.

Eulalio, A., Huntzinger, E., & Izaurralde, E. (2008). GW182 interaction with Argonaute is essential for miRNA-mediated translational repression and mRNA decay. *Nat Struct Mol Biol, 15*(4), 346-353. doi:10.1038/nsmb.1405

Everts, V., Delaisse, J. M., Korper, W., Jansen, D. C., Tigchelaar-Gutter, W., Saftig, P., & Beertsen, W. (2002). The bone lining cell: its role in cleaning Howship's lacunae and initiating bone formation. *J Bone Miner Res, 17*(1), 77-90. doi:10.1359/jbmr.2002.17.1.77

Falcone, G., Felsani, A., & D'Agnano, I. (2015). Signaling by exosomal microRNAs in cancer. *J Exp Clin Cancer Res, 34*, 32. doi:10.1186/s13046-015-0148-3

Fei, Y., Xiao, L., Doetschman, T., Coffin, D. J., & Hurley, M. M. (2011). Fibroblast growth factor 2 stimulation of osteoblast differentiation and bone formation is mediated by modulation of the Wnt signaling pathway. *J Biol Chem, 286*(47), 40575-40583. doi:10.1074/jbc.M111.274910

Feng, D., Zhao, W. L., Ye, Y. Y., Bai, X. C., Liu, R. Q., Chang, L. F., . . . Sui, S. F. (2010). Cellular internalization of exosomes occurs through phagocytosis. *Traffic, 11*(5), 675-687. doi:10.1111/j.1600-0854.2010.01041.x

Ferguson, S., Kim, S., Lee, C., Deci, M., & Nguyen, J. (2018a). The Phenotypic Effects of Exosomes Secreted from Distinct Cellular Sources: a Comparative Study Based on miRNA Composition. *AAPS J, 20*(4), 67. doi:10.1208/s12248-018-0227-4

Ferguson, S. W., Wang, J., Lee, C. J., Liu, M., Neelamegham, S., Canty, J. M., & Nguyen, J. (2018b). The microRNA regulatory landscape of MSC-derived exosomes: a systems view. *Sci Rep, 8*(1), 1419. doi:10.1038/s41598-018-19581-x

Ferlay, J., Parkin, D. M., & Steliarova-Foucher, E. (2010). Estimates of cancer incidence and mortality in Europe in 2008. *Eur J Cancer, 46*(4), 765-781. doi:10.1016/j.ejca.2009.12.014

Fitzner, D., Schnaars, M., van Rossum, D., Krishnamoorthy, G., Dibaj, P., Bakhti, M., . . . Simons, M. (2011). Selective transfer of exosomes from oligodendrocytes to microglia by macropinocytosis. *J Cell Sci, 124*(Pt 3), 447-458. doi:10.1242/jcs.074088

Florencio-Silva, R., Sasso, G. R., Sasso-Cerri, E., Simoes, M. J., & Cerri, P. S. (2015). Biology of Bone Tissue: Structure, Function, and Factors That Influence Bone Cells. *Biomed Res Int, 2015*, 421746. doi:10.1155/2015/421746

Fradet, A., Sorel, H., Depalle, B., Serre, C. M., Farlay, D., Turtoi, A., . . . Bonnelye, E. (2013). A new murine model of osteoblastic/osteolytic lesions from human androgen-resistant prostate cancer. *PLoS One, 8*(9), e75092. doi:10.1371/journal.pone.0075092

Fu, L., Patel, M. S., Bradley, A., Wagner, E. F., & Karsenty, G. (2005). The molecular clock mediates leptin-regulated bone formation. *Cell, 122*(5), 803-815. doi:10.1016/j.cell.2005.06.028

Fujimoto, R., Higashi, T., Nakamoto, Y., Hara, T., Lyshchik, A., Ishizu, K., . . . Togashi, K. (2006). Diagnostic accuracy of bone metastases detection in cancer patients: comparison between bone scintigraphy and whole-body FDG-PET. *Ann Nucl Med, 20*(6), 399-408.

Fujisawa, R., & Tamura, M. (2012). Acidic bone matrix proteins and their roles in calcification. *Front Biosci (Landmark Ed), 17*, 1891-1903.

Galardi, S., Mercatelli, N., Giorda, E., Massalini, S., Frajese, G. V., Ciafre, S. A., & Farace, M. G. (2007). miR-221 and miR-222 expression affects the proliferation potential of human prostate carcinoma cell lines by targeting p27Kip1. *J Biol Chem, 282*(32), 23716-23724. doi:10.1074/jbc.M701805200

Galindo-Hernandez, O., Villegas-Comonfort, S., Candanedo, F., Gonzalez-Vazquez, M. C., Chavez-Ocana, S., Jimenez-Villanueva, X., . . . Salazar, E. P. (2013). Elevated concentration of microvesicles isolated from peripheral blood in breast cancer patients. *Arch Med Res, 44*(3), 208-214. doi:10.1016/j.arcmed.2013.03.002

Gandaglia, G., Abdollah, F., Schiffmann, J., Trudeau, V., Shariat, S. F., Kim, S. P., . . . Sun, M. (2014). Distribution of metastatic sites in patients with prostate cancer: A population-based analysis. *Prostate, 74*(2), 210-216. doi:10.1002/pros.22742

Gandy, S. Z., Linnstaedt, S. D., Muralidhar, S., Cashman, K. A., Rosenthal, L. J., & Casey, J. L. (2007). RNA editing of the human herpesvirus 8 kaposin transcript eliminates its transforming activity and is induced during lytic replication. *J Virol, 81*(24), 13544-13551. doi:10.1128/JVI.01521-07

Garcia-Roman, J., & Zentella-Dehesa, A. (2013). Vascular permeability changes involved in tumor metastasis. *Cancer Lett, 335*(2), 259-269. doi:10.1016/j.canlet.2013.03.005

Genge, B. R., Cao, X., Wu, L. N., Buzzi, W. R., Showman, R. W., Arsenault, A. L., . . . Wuthier, R. E. (1992). Establishment of the primary structure of the major lipid-dependent Ca2+ binding proteins of chicken growth plate cartilage matrix vesicles: identity with anchorin CII (annexin V) and annexin II. *J Bone Miner Res, 7*(7), 807-819. doi:10.1002/jbmr.5650070710

Ghanbari, R., Mosakhani, N., Sarhadi, V. K., Armengol, G., Nouraee, N., Mohammadkhani, A., . . . Knuutila, S. (2015). Simultaneous Underexpression of let-7a-5p and let-7f-5p microRNAs in Plasma and Stool Samples from Early Stage Colorectal Carcinoma. *Biomark Cancer, 7*(Suppl 1), 39-48. doi:10.4137/BIC.S25252

Gharibi, B., Ghuman, M., & Hughes, F. J. (2016). DDIT4 regulates mesenchymal stem cell fate by mediating between HIF1alpha and mTOR signalling. *Sci Rep, 6*, 36889. doi:10.1038/srep36889

Giles, G. G., Severi, G., English, D. R., McCredie, M. R., Borland, R., Boyle, P., & Hopper, J. L. (2003). Sexual factors and prostate cancer. *BJU Int, 92*(3), 211-216.

Glimcher, M. J. (1984). Recent studies of the mineral phase in bone and its possible linkage to the organic matrix by protein-bound phosphate bonds. *Philos Trans R Soc Lond B Biol Sci, 304*(1121), 479-508. doi:10.1098/rstb.1984.0041

Goldie, B. J., Dun, M. D., Lin, M., Smith, N. D., Verrills, N. M., Dayas, C. V., & Cairns, M. J. (2014). Activity-associated miRNA are packaged in Map1b-enriched exosomes released from depolarized neurons. *Nucleic Acids Res, 42*(14), 9195-9208. doi:10.1093/nar/gku594

Green, D., Mohorianu, I., McNamara, I., Dalmay, T., & Fraser, W. D. (2017). miR-16 is highly expressed in Paget's associated osteosarcoma. *Endocr Relat Cancer, 24*(5), L27-L31. doi:10.1530/ERC-16-0487

Green, L. (1993). Digital rectal examination screening for prostate cancer. *JAMA, 270*(11), 1315; author reply 1315-1316.

Griffiths, S. G., Cormier, M. T., Clayton, A., & Doucette, A. A. (2017). Differential Proteome Analysis of Extracellular Vesicles from Breast Cancer Cell Lines by Chaperone Affinity Enrichment. *Proteomes, 5*(4). doi:10.3390/proteomes5040025

Grigoriadis, A. E., Heersche, J. N., & Aubin, J. E. (1988). Differentiation of muscle, fat, cartilage, and bone from progenitor cells present in a bone-derived clonal cell population: effect of dexamethasone. *J Cell Biol, 106*(6), 2139-2151.

Gruenberg, J., Griffiths, G., & Howell, K. E. (1989). Characterization of the early endosome and putative endocytic carrier vesicles in vivo and with an assay of vesicle fusion in vitro. *J Cell Biol, 108*(4), 1301-1316.

Gu, S., & Kay, M. A. (2010). How do miRNAs mediate translational repression? *Silence, 1*(1), 11. doi:10.1186/1758-907X-1-11

Guduric-Fuchs, J., O'Connor, A., Camp, B., O'Neill, C. L., Medina, R. J., & Simpson, D. A. (2012). Selective extracellular vesicle-mediated export of an overlapping set of microRNAs from multiple cell types. *BMC Genomics, 13*, 357. doi:10.1186/1471-2164-13-357

Guihard, P., Danger, Y., Brounais, B., David, E., Brion, R., Delecrin, J., . . . Blanchard, F. (2012). Induction of osteogenesis in mesenchymal stem cells by activated monocytes/macrophages depends on oncostatin M signaling. *Stem Cells, 30*(4), 762-772. doi:10.1002/stem.1040

Guise, T. A., Mohammad, K. S., Clines, G., Stebbins, E. G., Wong, D. H., Higgins, L. S., . . . Chirgwin, J. M. (2006). Basic mechanisms responsible for osteolytic and osteoblastic bone metastases. *Clin Cancer Res, 12*(20 Pt 2), 6213s-6216s. doi:10.1158/1078-0432.CCR-06-1007

Guo, B. B., Bellingham, S. A., & Hill, A. F. (2016). Stimulating the Release of Exosomes Increases the Intercellular Transfer of Prions. *J Biol Chem, 291*(10), 5128-5137. doi:10.1074/jbc.M115.684258

Guo, D., Li, Q., Lv, Q., Wei, Q., Cao, S., & Gu, J. (2014). MiR-27a targets sFRP1 in hFOB cells to regulate proliferation, apoptosis and differentiation. *PLoS One, 9*(3), e91354. doi:10.1371/journal.pone.0091354

Guo, H., Ingolia, N. T., Weissman, J. S., & Bartel, D. P. (2010). Mammalian microRNAs predominantly act to decrease target mRNA levels. *Nature, 466*(7308), 835-840. doi:10.1038/nature09267

Guo, Y., Sklar, G. N., Borkowski, A., & Kyprianou, N. (1997). Loss of the cyclin-dependent kinase inhibitor p27(Kip1) protein in human prostate cancer correlates with tumor grade. *Clin Cancer Res, 3*(12 Pt 1), 2269-2274.

Gupta, A., & Pulliam, L. (2014). Exosomes as mediators of neuroinflammation. *J Neuroinflammation, 11*, 68. doi:10.1186/1742-2094-11-68

Ha, T. Y. (2011). MicroRNAs in Human Diseases: From Cancer to Cardiovascular Disease. *Immune Netw, 11*(3), 135-154. doi:10.4110/in.2011.11.3.135

Hakeda, Y., Kobayashi, Y., Yamaguchi, K., Yasuda, H., Tsuda, E., Higashio, K., . . . Kumegawa, M. (1998). Osteoclastogenesis inhibitory factor (OCIF) directly inhibits bone-resorbing activity of isolated mature osteoclasts. *Biochem Biophys Res Commun, 251*(3), 796-801. doi:10.1006/bbrc.1998.9523

Hammond, S. M., Bernstein, E., Beach, D., & Hannon, G. J. (2000). An RNA-directed nuclease mediates post-transcriptional gene silencing in Drosophila cells. *Nature, 404*(6775), 293-296. doi:10.1038/35005107

Han, J., Lee, Y., Yeom, K. H., Nam, J. W., Heo, I., Rhee, J. K., . . . Kim, V. N. (2006). Molecular basis for the recognition of primary microRNAs by the Drosha-DGCR8 complex. *Cell, 125*(5), 887-901. doi:10.1016/j.cell.2006.03.043

Han, X., Sterling, H., Chen, Y., Saginario, C., Brown, E. J., Frazier, W. A., . . . Vignery, A. (2000). CD47, a ligand for the macrophage fusion receptor, participates in macrophage multinucleation. *J Biol Chem, 275*(48), 37984-37992. doi:10.1074/jbc.M002334200

Harding, C., Heuser, J., & Stahl, P. (1983). Receptor-mediated endocytosis of transferrin and recycling of the transferrin receptor in rat reticulocytes. *J Cell Biol, 97*(2), 329-339.

Harms, A., Fuehner, T., Warnecke, G., Haverich, A., Gottlieb, J., & Trummer, A. (2015). Epithelial and Erythrocyte Microvesicles From Bronchoalveolar Lavage Fluid Are Elevated and Associated With Outcome in Chronic Lung Allograft Dysfunction. *Transplantation, 99*(11), 2394-2400. doi:10.1097/TP.0000000000000881

Harrington, K. D. (1995). Orthopaedic management of extremity and pelvic lesions. *Clin Orthop Relat Res*(312), 136-147.

Harvey, H. A. (1997). Issues concerning the role of chemotherapy and hormonal therapy of bone metastases from breast carcinoma. *Cancer, 80*(8 Suppl), 1646-1651.

Hayward, S. W., Baskin, L. S., Haughney, P. C., Foster, B. A., Cunha, A. R., Dahiya, R., . . . Cunha, G. R. (1996). Stromal development in the ventral prostate,

anterior prostate and seminal vesicle of the rat. *Acta Anat (Basel), 155*(2), 94-103.

Heindel, W., Gubitz, R., Vieth, V., Weckesser, M., Schober, O., & Schafers, M. (2014). The diagnostic imaging of bone metastases. *Dtsch Arztebl Int, 111*(44), 741-747. doi:10.3238/arztebl.2014.0741

Heino, T. J., Hentunen, T. A., & Vaananen, H. K. (2002). Osteocytes inhibit osteoclastic bone resorption through transforming growth factor-beta: enhancement by estrogen. *Journal of Cellular Biochemistry, 85*(1), 185-197.

Hellwinkel, O. J., Sellier, C., Sylvester, Y. M., Brase, J. C., Isbarn, H., Erbersdobler, A., . . . Wagner, C. (2013). A Cancer-Indicative microRNA Pattern in Normal Prostate Tissue. *Int J Mol Sci, 14*(3), 5239-5249. doi:10.3390/ijms14035239

Heo, I., Ha, M., Lim, J., Yoon, M. J., Park, J. E., Kwon, S. C., . . . Kim, V. N. (2012). Mono-uridylation of pre-microRNA as a key step in the biogenesis of group II let-7 microRNAs. *Cell, 151*(3), 521-532. doi:10.1016/j.cell.2012.09.022

Hessvik, N. P., Phuyal, S., Brech, A., Sandvig, K., & Llorente, A. (2012). Profiling of microRNAs in exosomes released from PC-3 prostate cancer cells. *Biochim Biophys Acta, 1819*(11-12), 1154-1163. doi:10.1016/j.bbagrm.2012.08.016

Hirschfeld, J., White, P. C., Milward, M. R., Cooper, P. R., & Chapple, I. L. C. (2017). Modulation of Neutrophil Extracellular Trap and Reactive Oxygen Species Release by Periodontal Bacteria. *Infect Immun, 85*(12). doi:10.1128/IAI.00297-17

Hodge, K. K., McNeal, J. E., Terris, M. K., & Stamey, T. A. (1989). Random systematic versus directed ultrasound guided transrectal core biopsies of the prostate. *J Urol, 142*(1), 71-74; discussion 74-75.

Holen, I., Croucher, P. I., Hamdy, F. C., & Eaton, C. L. (2002). Osteoprotegerin (OPG) is a survival factor for human prostate cancer cells. *Cancer Res, 62*(6), 1619-1623.

Hong, S. D., Kang, Y., Brenner, A. J., Sachdev, J. C., Ejadi, S., Borad, M. J., . . . Beg, M. S. (2016). MRX34, a liposomal miR-34 mimic, in patients with advanced solid tumors: Final dose-escalation results from a first-in-human phase I trial of microRNA therapy. *Journal of Clinical Oncology, 34*(15_suppl), 2508-2508. doi:10.1200/JCO.2016.34.15_suppl.2508

Horstman, L. L., & Ahn, Y. S. (1999). Platelet microparticles: a wide-angle perspective. *Crit Rev Oncol Hematol, 30*(2), 111-142.

Howard, G. A., Bottemiller, B. L., Turner, R. T., Rader, J. I., & Baylink, D. J. (1981). Parathyroid hormone stimulates bone formation and resorption in organ culture: evidence for a coupling mechanism. *Proc Natl Acad Sci U S A, 78*(5), 3204-3208.

Hu-Lieskovan, S., Heidel, J. D., Bartlett, D. W., Davis, M. E., & Triche, T. J. (2005). Sequence-specific knockdown of EWS-FLI1 by targeted, nonviral delivery of small interfering RNA inhibits tumor growth in a murine model of metastatic

Ewing's sarcoma. *Cancer Res, 65*(19), 8984-8992. doi:10.1158/0008-5472.CAN-05-0565

Hu, W., & Coller, J. (2012). What comes first: translational repression or mRNA degradation? The deepening mystery of microRNA function. *Cell Res, 22*(9), 1322-1324. doi:10.1038/cr.2012.80

Huang, R., Wang, X., Zhou, Y., & Xiao, Y. (2017). RANKL-induced M1 macrophages are involved in bone formation. *Bone Res, 5*, 17019. doi:10.1038/boneres.2017.19

Huang, X., Yuan, T., Tschannen, M., Sun, Z., Jacob, H., Du, M., . . . Wang, L. (2013). Characterization of human plasma-derived exosomal RNAs by deep sequencing. *BMC Genomics, 14*, 319. doi:10.1186/1471-2164-14-319

Hundley, H. A., & Bass, B. L. (2010). ADAR editing in double-stranded UTRs and other noncoding RNA sequences. *Trends Biochem Sci, 35*(7), 377-383. doi:10.1016/j.tibs.2010.02.008

Huotari, J., & Helenius, A. (2011). Endosome maturation. *EMBO J, 30*(17), 3481-3500. doi:10.1038/emboj.2011.286

Huraskin, D., Eiber, N., Reichel, M., Zidek, L. M., Kravic, B., Bernkopf, D., . . . Hashemolhosseini, S. (2016). Wnt/beta-catenin signaling via Axin2 is required for myogenesis and, together with YAP/Taz and Tead1, active in IIa/IIx muscle fibers. *Development, 143*(17), 3128-3142. doi:10.1242/dev.139907

Hwang, H. W., & Mendell, J. T. (2006). MicroRNAs in cell proliferation, cell death, and tumorigenesis. *Br J Cancer, 94*(6), 776-780. doi:10.1038/sj.bjc.6603023

Hwang, P. A., Hung, Y. L., Phan, N. N., Hieu, B. T., Chang, P. M., Li, K. L., & Lin, Y. C. (2016). The in vitro and in vivo effects of the low molecular weight fucoidan on the bone osteogenic differentiation properties. *Cytotechnology, 68*(4), 1349-1359. doi:10.1007/s10616-015-9894-5

Hyenne, V., Labouesse, M., & Goetz, J. G. (2018). The Small GTPase Ral orchestrates MVB biogenesis and exosome secretion. *Small GTPases, 9*(6), 445-451. doi:10.1080/21541248.2016.1251378

Hyytinen, E. R., Thalmann, G. N., Zhau, H. E., Karhu, R., Kallioniemi, O. P., Chung, L. W., & Visakorpi, T. (1997). Genetic changes associated with the acquisition of androgen-independent growth, tumorigenicity and metastatic potential in a prostate cancer model. *Br J Cancer, 75*(2), 190-195.

Ibrahim, T., Flamini, E., Mercatali, L., Sacanna, E., Serra, P., & Amadori, D. (2010). Pathogenesis of osteoblastic bone metastases from prostate cancer. *Cancer, 116*(6), 1406-1418. doi:10.1002/cncr.24896

Iizasa, H., Wulff, B. E., Alla, N. R., Maragkakis, M., Megraw, M., Hatzigeorgiou, A., . . . Nishikura, K. (2010). Editing of Epstein-Barr virus-encoded BART6 microRNAs controls their dicer targeting and consequently affects viral latency. *J Biol Chem, 285*(43), 33358-33370. doi:10.1074/jbc.M110.138362

Ikeda, K., & Takeshita, S. (2016). The role of osteoclast differentiation and function in skeletal homeostasis. *J Biochem, 159*(1), 1-8. doi:10.1093/jb/mvv112

Ishiyama, K., Yashiro, T., Nakano, N., Kasakura, K., Miura, R., Hara, M., . . . Nishiyama, C. (2015). Involvement of PU.1 in NFATc1 promoter function in osteoclast development. *Allergol Int, 64*(3), 241-247. doi:10.1016/j.alit.2015.01.006

Itoh, T., Ito, Y., Ohtsuki, Y., Ando, M., Tsukamasa, Y., Yamada, N., . . . Akao, Y. (2012). Microvesicles released from hormone-refractory prostate cancer cells facilitate mouse pre-osteoblast differentiation. *J Mol Histol, 43*(5), 509-515. doi:10.1007/s10735-012-9415-1

Iwaki, F., Amano, H., & Ohura, K. (2016). Nicorandil inhibits osteoclast differentiation in vitro. *Eur J Pharmacol, 793*, 14-20. doi:10.1016/j.ejphar.2016.10.034

Iwasaki, S., Kawamata, T., & Tomari, Y. (2009). Drosophila argonaute1 and argonaute2 employ distinct mechanisms for translational repression. *Mol Cell, 34*(1), 58-67. doi:10.1016/j.molcel.2009.02.010

Iwasaki, S., Kobayashi, M., Yoda, M., Sakaguchi, Y., Katsuma, S., Suzuki, T., & Tomari, Y. (2010). Hsc70/Hsp90 chaperone machinery mediates ATP-dependent RISC loading of small RNA duplexes. *Mol Cell, 39*(2), 292-299. doi:10.1016/j.molcel.2010.05.015

Jakymiw, A., Lian, S., Eystathioy, T., Li, S., Satoh, M., Hamel, J. C., . . . Chan, E. K. (2005). Disruption of GW bodies impairs mammalian RNA interference. *Nat Cell Biol, 7*(12), 1267-1274. doi:10.1038/ncb1334

Jansen, F., Yang, X., Proebsting, S., Hoelscher, M., Przybilla, D., Baumann, K., . . . Werner, N. (2014). MicroRNA expression in circulating microvesicles predicts cardiovascular events in patients with coronary artery disease. *J Am Heart Assoc, 3*(6), e001249. doi:10.1161/JAHA.114.001249

Jenjaroenpun, P., Kremenska, Y., Nair, V. M., Kremenskoy, M., Joseph, B., & Kurochkin, I. V. (2013). Characterization of RNA in exosomes secreted by human breast cancer cell lines using next-generation sequencing. *PeerJ, 1*, e201. doi:10.7717/peerj.201

Ji, H., Chen, M., Greening, D. W., He, W., Rai, A., Zhang, W., & Simpson, R. J. (2014). Deep sequencing of RNA from three different extracellular vesicle (EV) subtypes released from the human LIM1863 colon cancer cell line uncovers distinct miRNA-enrichment signatures. *PLoS One, 9*(10), e110314. doi:10.1371/journal.pone.0110314

Jimenez-Andrade, J. M., Bloom, A. P., Stake, J. I., Mantyh, W. G., Taylor, R. N., Freeman, K. T., . . . Mantyh, P. W. (2010). Pathological sprouting of adult nociceptors in chronic prostate cancer-induced bone pain. *J Neurosci, 30*(44), 14649-14656. doi:10.1523/JNEUROSCI.3300-10.2010

Jimenez-Wences, H., Martinez-Carrillo, D. N., Peralta-Zaragoza, O., Campos-Viguri, G. E., Hernandez-Sotelo, D., Jimenez-Lopez, M. A., . . . Fernandez-Tilapa, G. (2016). Methylation and expression of miRNAs in precancerous lesions and

cervical cancer with HPV16 infection. *Oncol Rep, 35*(4), 2297-2305. doi:10.3892/or.2016.4583

Jorgensen, M., Baek, R., Pedersen, S., Sondergaard, E. K., Kristensen, S. R., & Varming, K. (2013). Extracellular Vesicle (EV) Array: microarray capturing of exosomes and other extracellular vesicles for multiplexed phenotyping. *J Extracell Vesicles, 2*. doi:10.3402/jev.v2i0.20920

Juvvuna, P. K., Khandelia, P., Lee, L. M., & Makeyev, E. V. (2012). Argonaute identity defines the length of mature mammalian microRNAs. *Nucleic Acids Res, 40*(14), 6808-6820. doi:10.1093/nar/gks293

Kamiya, N., Kaartinen, V. M., & Mishina, Y. (2011). Loss-of-function of ACVR1 in osteoblasts increases bone mass and activates canonical Wnt signaling through suppression of Wnt inhibitors SOST and DKK1. *Biochem Biophys Res Commun, 414*(2), 326-330. doi:10.1016/j.bbrc.2011.09.060

Kanellopoulou, C., Muljo, S. A., Kung, A. L., Ganesan, S., Drapkin, R., Jenuwein, T., . . . Rajewsky, K. (2005). Dicer-deficient mouse embryonic stem cells are defective in differentiation and centromeric silencing. *Genes Dev, 19*(4), 489-501. doi:10.1101/gad.1248505

Kang, B. J., Jeun, M., Jang, G. H., Song, S. H., Jeong, I. G., Kim, C. S., . . . Lee, K. H. (2015). Diagnosis of prostate cancer via nanotechnological approach. *Int J Nanomedicine, 10*, 6555-6569. doi:10.2147/IJN.S91908

Kapinas, K., & Delany, A. M. (2011). MicroRNA biogenesis and regulation of bone remodeling. *Arthritis Res Ther, 13*(3), 220. doi:10.1186/ar3325

Karimi, N., Cvjetkovic, A., Jang, S. C., Crescitelli, R., Hosseinpour Feizi, M. A., Nieuwland, R., . . . Lasser, C. (2018). Detailed analysis of the plasma extracellular vesicle proteome after separation from lipoproteins. *Cell Mol Life Sci, 75*(15), 2873-2886. doi:10.1007/s00018-018-2773-4

Karlsson, T., Lundholm, M., Widmark, A., & Persson, E. (2016). Tumor Cell-Derived Exosomes from the Prostate Cancer Cell Line TRAMP-C1 Impair Osteoclast Formation and Differentiation. *PLoS One, 11*(11), e0166284. doi:10.1371/journal.pone.0166284

Katahira, J., & Yoneda, Y. (2011). Nucleocytoplasmic transport of microRNAs and related small RNAs. *Traffic, 12*(11), 1468-1474. doi:10.1111/j.1600-0854.2011.01211.x

Katoh, T., Sakaguchi, Y., Miyauchi, K., Suzuki, T., Kashiwabara, S., Baba, T., & Suzuki, T. (2009). Selective stabilization of mammalian microRNAs by 3' adenylation mediated by the cytoplasmic poly(A) polymerase GLD-2. *Genes Dev, 23*(4), 433-438. doi:10.1101/gad.1761509

Kawamata, T., & Tomari, Y. (2010). Making RISC. *Trends Biochem Sci, 35*(7), 368-376. doi:10.1016/j.tibs.2010.03.009

Keaveny, T. M., Morgan, E. F., Niebur, G. L., & Yeh, O. C. (2001). Biomechanics of trabecular bone. *Annu Rev Biomed Eng, 3*, 307-333. doi:10.1146/annurev.bioeng.3.1.307

Keller, E. T., & Brown, J. (2004). Prostate cancer bone metastases promote both osteolytic and osteoblastic activity. *Journal of Cellular Biochemistry, 91*(4), 718-729. doi:10.1002/jcb.10662

Kim, B. J., Lee, Y. S., Lee, S. Y., Park, S. Y., Dieplinger, H., Ryu, S. H., . . . Kim, G. S. (2012). Afamin secreted from nonresorbing osteoclasts acts as a chemokine for preosteoblasts via the Akt-signaling pathway. *Bone, 51*(3), 431-440. doi:10.1016/j.bone.2012.06.015

Kim, J. M., Lee, J. H., Lee, G. S., Noh, E. M., Song, H. K., Gu, D. R., . . . Lee, Y. R. (2017). Sophorae Flos extract inhibits RANKL-induced osteoclast differentiation by suppressing the NF-kappaB/NFATc1 pathway in mouse bone marrow cells. *BMC Complement Altern Med, 17*(1), 164. doi:10.1186/s12906-016-1550-x

Kim, Y. K., & Kim, V. N. (2007). Processing of intronic microRNAs. *EMBO J, 26*(3), 775-783. doi:10.1038/sj.emboj.7601512

Kingsley, L. A., Fournier, P. G., Chirgwin, J. M., & Guise, T. A. (2007). Molecular biology of bone metastasis. *Mol Cancer Ther, 6*(10), 2609-2617. doi:10.1158/1535-7163.MCT-07-0234

Kiriakidou, M., Tan, G. S., Lamprinaki, S., De Planell-Saguer, M., Nelson, P. T., & Mourelatos, Z. (2007). An mRNA m7G cap binding-like motif within human Ago2 represses translation. *Cell, 129*(6), 1141-1151. doi:10.1016/j.cell.2007.05.016

Klotz, L. (2013). Prostate cancer overdiagnosis and overtreatment. *Curr Opin Endocrinol Diabetes Obes, 20*(3), 204-209. doi:10.1097/MED.0b013e328360332a

Knerr, K., Ackermann, K., Neidhart, T., & Pyerin, W. (2004). Bone metastasis: Osteoblasts affect growth and adhesion regulons in prostate tumor cells and provoke osteomimicry. *Int J Cancer, 111*(1), 152-159. doi:10.1002/ijc.20223

Koberle, V., Pleli, T., Schmithals, C., Augusto Alonso, E., Haupenthal, J., Bonig, H., . . . Piiper, A. (2013). Differential stability of cell-free circulating microRNAs: implications for their utilization as biomarkers. *PLoS One, 8*(9), e75184. doi:10.1371/journal.pone.0075184

Koga, Y., Yasunaga, M., Moriya, Y., Akasu, T., Fujita, S., Yamamoto, S., & Matsumura, Y. (2011). Exosome can prevent RNase from degrading microRNA in feces. *J Gastrointest Oncol, 2*(4), 215-222. doi:10.3978/j.issn.2078-6891.2011.015

Komori, T. (2006). Regulation of osteoblast differentiation by transcription factors. *Journal of Cellular Biochemistry, 99*(5), 1233-1239. doi:10.1002/jcb.20958

Koppers-Lalic, D., Hackenberg, M., Bijnsdorp, I. V., van Eijndhoven, M. A. J., Sadek, P., Sie, D., . . . Pegtel, D. M. (2014). Nontemplated nucleotide additions distinguish the small RNA composition in cells from exosomes. *Cell Rep, 8*(6), 1649-1658. doi:10.1016/j.celrep.2014.08.027

Kornak, U., Kasper, D., Bosl, M. R., Kaiser, E., Schweizer, M., Schulz, A., . . . Jentsch, T. J. (2001). Loss of the ClC-7 chloride channel leads to osteopetrosis in mice and man. *Cell, 104*(2), 205-215.

Kosaka, N., Iguchi, H., Hagiwara, K., Yoshioka, Y., Takeshita, F., & Ochiya, T. (2013). Neutral sphingomyelinase 2 (nSMase2)-dependent exosomal transfer of angiogenic microRNAs regulate cancer cell metastasis. *J Biol Chem, 288*(15), 10849-10859. doi:10.1074/jbc.M112.446831

Koutsilieris, M. (1993). Osteoblastic metastasis in advanced prostate cancer. *Anticancer Res, 13*(2), 443-449.

Koutsilieris, M. (1995). Skeletal metastases in advanced prostate cancer: cell biology and therapy. *Crit Rev Oncol Hematol, 18*(1), 51-64.

Koutsilieris, M., & Polychronakos, C. (1992). Proteinolytic activity against IGF-binding proteins involved in the paracrine interactions between prostate adenocarcinoma cells and osteoblasts. *Anticancer Res, 12*(3), 905-910.

Kowal, J., Tkach, M., & Thery, C. (2014). Biogenesis and secretion of exosomes. *Curr Opin Cell Biol, 29*, 116-125. doi:10.1016/j.ceb.2014.05.004

Kristensen, H., Thomsen, A. R., Haldrup, C., Dyrskjot, L., Hoyer, S., Borre, M., . . . Sorensen, K. D. (2016). Novel diagnostic and prognostic classifiers for prostate cancer identified by genome-wide microRNA profiling. *Oncotarget, 7*(21), 30760-30771. doi:10.18632/oncotarget.8953

Krutzfeldt, J., Rajewsky, N., Braich, R., Rajeev, K. G., Tuschl, T., Manoharan, M., & Stoffel, M. (2005). Silencing of microRNAs in vivo with 'antagomirs'. *Nature, 438*(7068), 685-689. doi:10.1038/nature04303

Kubista, B., Klinglmueller, F., Bilban, M., Pfeiffer, M., Lass, R., Giurea, A., . . . Singer, C. F. (2011). Microarray analysis identifies distinct gene expression profiles associated with histological subtype in human osteosarcoma. *Int Orthop, 35*(3), 401-411. doi:10.1007/s00264-010-0996-6

Kudo, O., Sabokbar, A., Pocock, A., Itonaga, I., Fujikawa, Y., & Athanasou, N. A. (2003). Interleukin-6 and interleukin-11 support human osteoclast formation by a RANKL-independent mechanism. *Bone, 32*(1), 1-7.

Kumar, B., & Lupold, S. E. (2016). MicroRNA expression and function in prostate cancer: a review of current knowledge and opportunities for discovery. *Asian J Androl, 18*(4), 559-567. doi:10.4103/1008-682X.177839

Lamparski, H. G., Metha-Damani, A., Yao, J. Y., Patel, S., Hsu, D. H., Ruegg, C., & Le Pecq, J. B. (2002). Production and characterization of clinical grade exosomes derived from dendritic cells. *J Immunol Methods, 270*(2), 211-226.

Lasser, C., Eldh, M., & Lotvall, J. (2012). Isolation and characterization of RNA-containing exosomes. *J Vis Exp*(59), e3037. doi:10.3791/3037

Laulagnier, K., Grand, D., Dujardin, A., Hamdi, S., Vincent-Schneider, H., Lankar, D., . . . Record, M. (2004). PLD2 is enriched on exosomes and its activity is correlated to the release of exosomes. *FEBS Lett, 572*(1-3), 11-14. doi:10.1016/j.febslet.2004.06.082

Laxman, N., Mallmin, H., Nilsson, O., & Kindmark, A. (2016). miR-203 and miR-320 Regulate Bone Morphogenetic Protein-2-Induced Osteoblast Differentiation by Targeting Distal-Less Homeobox 5 (Dlx5). *Genes (Basel), 8*(1). doi:10.3390/genes8010004

le Sage, C., Nagel, R., Egan, D. A., Schrier, M., Mesman, E., Mangiola, A., . . . Agami, R. (2007). Regulation of the p27(Kip1) tumor suppressor by miR-221 and miR-222 promotes cancer cell proliferation. *EMBO J, 26*(15), 3699-3708. doi:10.1038/sj.emboj.7601790

Lee, Y., Ahn, C., Han, J., Choi, H., Kim, J., Yim, J., . . . Kim, V. N. (2003a). The nuclear RNase III Drosha initiates microRNA processing. *Nature, 425*(6956), 415-419. doi:10.1038/nature01957

Lee, Y., Schwarz, E., Davies, M., Jo, M., Gates, J., Wu, J., . . . Lieberman, J. R. (2003b). Differences in the cytokine profiles associated with prostate cancer cell induced osteoblastic and osteolytic lesions in bone. *J Orthop Res, 21*(1), 62-72. doi:10.1016/S0736-0266(02)00095-5

Lehr, J. E., & Pienta, K. J. (1998). Preferential adhesion of prostate cancer cells to a human bone marrow endothelial cell line. *J Natl Cancer Inst, 90*(2), 118-123.

Leitzmann, M. F., Platz, E. A., Stampfer, M. J., Willett, W. C., & Giovannucci, E. (2004). Ejaculation frequency and subsequent risk of prostate cancer. *JAMA, 291*(13), 1578-1586. doi:10.1001/jama.291.13.1578

Leung, A. K., Calabrese, J. M., & Sharp, P. A. (2006). Quantitative analysis of Argonaute protein reveals microRNA-dependent localization to stress granules. *Proc Natl Acad Sci U S A, 103*(48), 18125-18130. doi:10.1073/pnas.0608845103

Leung, A. K. L. (2015). The Whereabouts of microRNA Actions: Cytoplasm and Beyond. *Trends Cell Biol, 25*(10), 601-610. doi:10.1016/j.tcb.2015.07.005

Levaot, N., Ottolenghi, A., Mann, M., Guterman-Ram, G., Kam, Z., & Geiger, B. (2015). Osteoclast fusion is initiated by a small subset of RANKL-stimulated monocyte progenitors, which can fuse to RANKL-unstimulated progenitors. *Bone, 79*, 21-28. doi:10.1016/j.bone.2015.05.021

Li, D., Liu, J., Guo, B., Liang, C., Dang, L., Lu, C., . . . Zhang, G. (2016a). Osteoclast-derived exosomal miR-214-3p inhibits osteoblastic bone formation. *Nat Commun, 7*, 10872. doi:10.1038/ncomms10872

Li, J., Yang, X., Guan, H., Mizokami, A., Keller, E. T., Xu, X., . . . Zhang, J. (2016b). Exosome-derived microRNAs contribute to prostate cancer chemoresistance. *Int J Oncol, 49*(2), 838-846. doi:10.3892/ijo.2016.3560

Li, M., Zeringer, E., Barta, T., Schageman, J., Cheng, A., & Vlassov, A. V. (2014). Analysis of the RNA content of the exosomes derived from blood serum and urine and its potential as biomarkers. *Philos Trans R Soc Lond B Biol Sci, 369*(1652). doi:10.1098/rstb.2013.0502

Li, P., Kaslan, M., Lee, S. H., Yao, J., & Gao, Z. (2017). Progress in Exosome Isolation Techniques. *Theranostics, 7*(3), 789-804. doi:10.7150/thno.18133

Li, S., Jiang, J., Yang, Z., Li, Z., Ma, X., & Li, X. (2018a). Cardiac progenitor cellderived exosomes promote H9C2 cell growth via Akt/mTOR activation. *Int J Mol Med, 42*(3), 1517-1525. doi:10.3892/ijmm.2018.3699

Li, X., Wang, S., Zhu, R., Li, H., Han, Q., & Zhao, R. C. (2016c). Lung tumor exosomes induce a pro-inflammatory phenotype in mesenchymal stem cells via NFkappaB-TLR signaling pathway. *J Hematol Oncol, 9*, 42. doi:10.1186/s13045-016-0269-y

Li, Y., Fan, L., Liu, S., Liu, W., Zhang, H., Zhou, T., . . . Jin, Y. (2013). The promotion of bone regeneration through positive regulation of angiogenic-osteogenic coupling using microRNA-26a. *Biomaterials, 34*(21), 5048-5058. doi:10.1016/j.biomaterials.2013.03.052

Li, Y., & Kowdley, K. V. (2012). MicroRNAs in common human diseases. *Genomics Proteomics Bioinformatics, 10*(5), 246-253. doi:10.1016/j.gpb.2012.07.005

Li, Y., Xiu, F., Mou, Z., Xue, Z., Du, H., Zhou, C., . . . Zhou, H. (2018b). Exosomes derived from Toxoplasma gondii stimulate an inflammatory response through JNK signaling pathway. *Nanomedicine (Lond), 13*(10), 1157-1168. doi:10.2217/nnm-2018-0035

Lichtenstein, P., Holm, N. V., Verkasalo, P. K., Iliadou, A., Kaprio, J., Koskenvuo, M., . . . Hemminki, K. (2000). Environmental and heritable factors in the causation of cancer--analyses of cohorts of twins from Sweden, Denmark, and Finland. *N Engl J Med, 343*(2), 78-85. doi:10.1056/NEJM200007133430201

Liegeois, S., Benedetto, A., Garnier, J. M., Schwab, Y., & Labouesse, M. (2006). The V0-ATPase mediates apical secretion of exosomes containing Hedgehog-related proteins in Caenorhabditis elegans. *J Cell Biol, 173*(6), 949-961. doi:10.1083/jcb.200511072

Lin, S. L., Chang, D., Wu, D. Y., & Ying, S. Y. (2003). A novel RNA splicing-mediated gene silencing mechanism potential for genome evolution. *Biochem Biophys Res Commun, 310*(3), 754-760.

Ling, H., Fabbri, M., & Calin, G. A. (2013). MicroRNAs and other non-coding RNAs as targets for anticancer drug development. *Nat Rev Drug Discov, 12*(11), 847-865. doi:10.1038/nrd4140

Lingel, A., Simon, B., Izaurralde, E., & Sattler, M. (2004). Nucleic acid 3'-end recognition by the Argonaute2 PAZ domain. *Nat Struct Mol Biol, 11*(6), 576-577. doi:10.1038/nsmb777

Liu, B., Yu, H. M., & Hsu, W. (2007). Craniosynostosis caused by Axin2 deficiency is mediated through distinct functions of beta-catenin in proliferation and differentiation. *Dev Biol, 301*(1), 298-308. doi:10.1016/j.ydbio.2006.10.018

Liu, J., Carmell, M. A., Rivas, F. V., Marsden, C. G., Thomson, J. M., Song, J. J., . . . Hannon, G. J. (2004). Argonaute2 is the catalytic engine of mammalian RNAi. *Science, 305*(5689), 1437-1441. doi:10.1126/science.1102513

Liu, N., Abe, M., Sabin, L. R., Hendriks, G. J., Naqvi, A. S., Yu, Z., . . . Bonini, N. M. (2011). The exoribonuclease Nibbler controls 3' end processing of

microRNAs in Drosophila. *Curr Biol, 21*(22), 1888-1893. doi:10.1016/j.cub.2011.10.006

Liu, W., Xu, C., Zhao, H., Xia, P., Song, R., Gu, J., . . . Liu, Z. (2015). Osteoprotegerin Induces Apoptosis of Osteoclasts and Osteoclast Precursor Cells via the Fas/Fas Ligand Pathway. *PLoS One, 10*(11), e0142519. doi:10.1371/journal.pone.0142519

Liu, X., Jin, D. Y., McManus, M. T., & Mourelatos, Z. (2012). Precursor microRNA-programmed silencing complex assembly pathways in mammals. *Mol Cell, 46*(4), 507-517. doi:10.1016/j.molcel.2012.03.010

Liu, X., Yuan, W., Yang, L., Li, J., & Cai, J. (2018). miRNA Profiling of Exosomes from Spontaneous Hypertensive Rats Using Next-Generation Sequencing. *J Cardiovasc Transl Res*. doi:10.1007/s12265-017-9784-7

Lodes, M. J., Caraballo, M., Suciu, D., Munro, S., Kumar, A., & Anderson, B. (2009). Detection of cancer with serum miRNAs on an oligonucleotide microarray. *PLoS One, 4*(7), e6229. doi:10.1371/journal.pone.0006229

Logothetis, C. J., & Lin, S. H. (2005). Osteoblasts in prostate cancer metastasis to bone. *Nat Rev Cancer, 5*(1), 21-28. doi:10.1038/nrc1528

Lotinun, S., Kiviranta, R., Matsubara, T., Alzate, J. A., Neff, L., Luth, A., . . . Baron, R. (2013). Osteoclast-specific cathepsin K deletion stimulates S1P-dependent bone formation. *J Clin Invest, 123*(2), 666-681. doi:10.1172/JCI64840

Lotvall, J., Hill, A. F., Hochberg, F., Buzas, E. I., Di Vizio, D., Gardiner, C., . . . Thery, C. (2014). Minimal experimental requirements for definition of extracellular vesicles and their functions: a position statement from the International Society for Extracellular Vesicles. *J Extracell Vesicles, 3*, 26913. doi:10.3402/jev.v3.26913

Lowe, C., Yoneda, T., Boyce, B. F., Chen, H., Mundy, G. R., & Soriano, P. (1993). Osteopetrosis in Src-deficient mice is due to an autonomous defect of osteoclasts. *Proc Natl Acad Sci U S A, 90*(10), 4485-4489.

Lu, S. Y., Li, M., & Lin, Y. L. (2014). Mitf regulates osteoclastogenesis by modulating NFATc1 activity. *Exp Cell Res, 328*(1), 32-43. doi:10.1016/j.yexcr.2014.08.018

Luu, H. N., Lin, H. Y., Sorensen, K. D., Ogunwobi, O. O., Kumar, N., Chornokur, G., . . . Di Pietro, G. (2017). miRNAs associated with prostate cancer risk and progression. *BMC Urol, 17*(1), 18. doi:10.1186/s12894-017-0206-6

Luzio, J. P., Pryor, P. R., & Bright, N. A. (2007). Lysosomes: fusion and function. *Nat Rev Mol Cell Biol, 8*(8), 622-632. doi:10.1038/nrm2217

Lytle, J. R., Yario, T. A., & Steitz, J. A. (2007). Target mRNAs are repressed as efficiently by microRNA-binding sites in the 5' UTR as in the 3' UTR. *Proc Natl Acad Sci U S A, 104*(23), 9667-9672. doi:10.1073/pnas.0703820104

Ma, J. B., Ye, K., & Patel, D. J. (2004). Structural basis for overhang-specific small interfering RNA recognition by the PAZ domain. *Nature, 429*(6989), 318-322. doi:10.1038/nature02519

Ma, J. B., Yuan, Y. R., Meister, G., Pei, Y., Tuschl, T., & Patel, D. J. (2005). Structural basis for 5'-end-specific recognition of guide RNA by the A. fulgidus Piwi protein. *Nature, 434*(7033), 666-670. doi:10.1038/nature03514

Ma, Y., Nyman, J. S., Tao, H., Moss, H. H., Yang, X., & Elefteriou, F. (2011). beta2-Adrenergic receptor signaling in osteoblasts contributes to the catabolic effect of glucocorticoids on bone. *Endocrinology, 152*(4), 1412-1422. doi:10.1210/en.2010-0881

Ma, Y. L., Cain, R. L., Halladay, D. L., Yang, X., Zeng, Q., Miles, R. R., . . . Onyia, J. E. (2001). Catabolic effects of continuous human PTH (1--38) in vivo is associated with sustained stimulation of RANKL and inhibition of osteoprotegerin and gene-associated bone formation. *Endocrinology, 142*(9), 4047-4054. doi:10.1210/endo.142.9.8356

Macfarlane, L. A., & Murphy, P. R. (2010). MicroRNA: Biogenesis, Function and Role in Cancer. *Curr Genomics, 11*(7), 537-561. doi:10.2174/138920210793175895

Maisano, R., Pergolizzi, S., & Cascinu, S. (2001). Novel therapeutic approaches to cancer patients with bone metastasis. *Crit Rev Oncol Hematol, 40*(3), 239-250.

Maniataki, E., & Mourelatos, Z. (2005). A human, ATP-independent, RISC assembly machine fueled by pre-miRNA. *Genes Dev, 19*(24), 2979-2990. doi:10.1101/gad.1384005

Mari, M., Bujny, M. V., Zeuschner, D., Geerts, W. J., Griffith, J., Petersen, C. M., . . . Geuze, H. J. (2008). SNX1 defines an early endosomal recycling exit for sortilin and mannose 6-phosphate receptors. *Traffic, 9*(3), 380-393. doi:10.1111/j.1600-0854.2007.00686.x

Marras, F., & Leali, P. T. (2016). The role of drugs in bone pain. *Clin Cases Miner Bone Metab, 13*(2), 93-96. doi:10.11138/ccmbm/2016.13.2.093

Martin, B. R., Burr, D., Sharkey, N., & Fyhrie, D. (2015). *Skeletal Tissue Mechanics*.

Mathivanan, S., & Simpson, R. J. (2009). ExoCarta: A compendium of exosomal proteins and RNA. *Proteomics, 9*(21), 4997-5000. doi:10.1002/pmic.200900351

Mathonnet, G., Fabian, M. R., Svitkin, Y. V., Parsyan, A., Huck, L., Murata, T., . . . Sonenberg, N. (2007). MicroRNA inhibition of translation initiation in vitro by targeting the cap-binding complex eIF4F. *Science, 317*(5845), 1764-1767. doi:10.1126/science.1146067

Matic, I., Matthews, B. G., Wang, X., Dyment, N. A., Worthley, D. L., Rowe, D. W., . . . Kalajzic, I. (2016). Quiescent Bone Lining Cells Are a Major Source of Osteoblasts During Adulthood. *Stem Cells, 34*(12), 2930-2942. doi:10.1002/stem.2474

Matsuo, K., & Irie, N. (2008). Osteoclast-osteoblast communication. *Arch Biochem Biophys, 473*(2), 201-209. doi:10.1016/j.abb.2008.03.027

Maundrell, K., Antonsson, B., Magnenat, E., Camps, M., Muda, M., Chabert, C., . . . Arkinstall, S. (1997). Bcl-2 undergoes phosphorylation by c-Jun N-terminal kinase/stress-activated protein kinases in the presence of the constitutively active GTP-binding protein Rac1. *J Biol Chem, 272*(40), 25238-25242.

Maxson, M. E., & Grinstein, S. (2014). The vacuolar-type H(+)-ATPase at a glance - more than a proton pump. *J Cell Sci, 127*(Pt 23), 4987-4993. doi:10.1242/jcs.158550

Mayer-Kuckuk, P., Gade, T. P., Buchanan, I. M., Doubrovin, M., Ageyeva, L., Bertino, J. R., . . . Banerjee, D. (2005). High-resolution imaging of bone precursor cells within the intact bone marrow cavity of living mice. *Mol Ther, 12*(1), 33-41. doi:10.1016/j.ymthe.2005.02.018

Mbalaviele, G., Chen, H., Boyce, B. F., Mundy, G. R., & Yoneda, T. (1995). The role of cadherin in the generation of multinucleated osteoclasts from mononuclear precursors in murine marrow. *J Clin Invest, 95*(6), 2757-2765. doi:10.1172/JCI117979

McGee-Lawrence, M. E., Li, X., Bledsoe, K. L., Wu, H., Hawse, J. R., Subramaniam, M., . . . Westendorf, J. J. (2013). Runx2 protein represses Axin2 expression in osteoblasts and is required for craniosynostosis in Axin2-deficient mice. *J Biol Chem, 288*(8), 5291-5302. doi:10.1074/jbc.M112.414995

McHugh, K. P., Hodivala-Dilke, K., Zheng, M. H., Namba, N., Lam, J., Novack, D., . . . Teitelbaum, S. L. (2000). Mice lacking beta3 integrins are osteosclerotic because of dysfunctional osteoclasts. *J Clin Invest, 105*(4), 433-440. doi:10.1172/JCI8905

McKelvey, K. J., Powell, K. L., Ashton, A. W., Morris, J. M., & McCracken, S. A. (2015). Exosomes: Mechanisms of Uptake. *J Circ Biomark, 4*, 7. doi:10.5772/61186

Misra, D. N. (1992). Reaction of Alizarin Red-S with Hydroxyapatite - Stoichiometry and Surface Effect. *Colloids and Surfaces, 66*(3), 181-187. doi:Doi 10.1016/0166-6622(92)80191-4

Mohler, J. L., Kantoff, P. W., Armstrong, A. J., Bahnson, R. R., Cohen, M., D'Amico, A. V., . . . National Comprehensive Cancer, N. (2014). Prostate cancer, version 2.2014. *J Natl Compr Canc Netw, 12*(5), 686-718.

Montecalvo, A., Larregina, A. T., Shufesky, W. J., Stolz, D. B., Sullivan, M. L., Karlsson, J. M., . . . Morelli, A. E. (2012). Mechanism of transfer of functional microRNAs between mouse dendritic cells via exosomes. *Blood, 119*(3), 756-766. doi:10.1182/blood-2011-02-338004

Montessuit, C., Bonjour, J. P., & Caverzasio, J. (1995). Expression and regulation of Na-dependent P(i) transport in matrix vesicles produced by osteoblast-like cells. *J Bone Miner Res, 10*(4), 625-631. doi:10.1002/jbmr.5650100416

Moore, S., Kuhrik, M., Kuhrik, N., & Shea, L. (1992). Screening for prostate cancer: PSA blood test, rectal examination, and ultrasound. *Urol Nurs, 12*(3), 106-107.

Morgan, E. F., Barnes, G. L., & Einhorn, T. A. (2013). *The Bone Organ System. Form and Function*.

Morris, D. C., Masuhara, K., Takaoka, K., Ono, K., & Anderson, H. C. (1992). Immunolocalization of alkaline phosphatase in osteoblasts and matrix vesicles of human fetal bone. *Bone Miner, 19*(3), 287-298.

Mortazavi, A., Williams, B. A., McCue, K., Schaeffer, L., & Wold, B. (2008). Mapping and quantifying mammalian transcriptomes by RNA-Seq. *Nat Methods, 5*(7), 621-628. doi:10.1038/nmeth.1226

Most, D., Leiter, C., Blednov, Y. A., Harris, R. A., & Mayfield, R. D. (2016). Synaptic microRNAs Coordinately Regulate Synaptic mRNAs: Perturbation by Chronic Alcohol Consumption. *Neuropsychopharmacology, 41*(2), 538-548. doi:10.1038/npp.2015.179

Msaouel, P., Pissimissis, N., Halapas, A., & Koutsilieris, M. (2008). Mechanisms of bone metastasis in prostate cancer: clinical implications. *Best Pract Res Clin Endocrinol Metab, 22*(2), 341-355. doi:10.1016/j.beem.2008.01.011

Muguruma, Y., Hozumi, K., Warita, H., Yahata, T., Uno, T., Ito, M., & Ando, K. (2017). Maintenance of Bone Homeostasis by DLL1-Mediated Notch Signaling. *J Cell Physiol, 232*(9), 2569-2580. doi:10.1002/jcp.25647

Mulcahy, L. A., Pink, R. C., & Carter, D. R. (2014). Routes and mechanisms of extracellular vesicle uptake. *J Extracell Vesicles, 3*. doi:10.3402/jev.v3.24641

Muralidharan, A., & Smith, M. T. (2013). Pathobiology and management of prostate cancer-induced bone pain: recent insights and future treatments. *Inflammopharmacology, 21*(5), 339-363. doi:10.1007/s10787-013-0183-7

Nabhan, J. F., Hu, R., Oh, R. S., Cohen, S. N., & Lu, Q. (2012). Formation and release of arrestin domain-containing protein 1-mediated microvesicles (ARMMs) at plasma membrane by recruitment of TSG101 protein. *Proc Natl Acad Sci U S A, 109*(11), 4146-4151. doi:10.1073/pnas.1200448109

Naguibneva, I., Ameyar-Zazoua, M., Polesskaya, A., Ait-Si-Ali, S., Groisman, R., Souidi, M., . . . Harel-Bellan, A. (2006). The microRNA miR-181 targets the homeobox protein Hox-A11 during mammalian myoblast differentiation. *Nat Cell Biol, 8*(3), 278-284. doi:10.1038/ncb1373

Nakanishi, K. (2016). Anatomy of RISC: how do small RNAs and chaperones activate Argonaute proteins? *Wiley Interdiscip Rev RNA, 7*(5), 637-660. doi:10.1002/wrna.1356

Nakashima, K., Zhou, X., Kunkel, G., Zhang, Z., Deng, J. M., Behringer, R. R., & de Crombrugghe, B. (2002). The novel zinc finger-containing transcription factor osterix is required for osteoblast differentiation and bone formation. *Cell, 108*(1), 17-29.

Nakata, S., Nakano, K., Takahashi, H., Shimizu, K., Higashi, H., & Ohki, K. (2005). [A case of prostate cancer diagnosed pathologically by bone metastatic site biopsy]. *Nihon Hinyokika Gakkai Zasshi, 96*(4), 507-510.

Nelson, W. G., De Marzo, A. M., & Isaacs, W. B. (2003). Prostate cancer. *N Engl J Med, 349*(4), 366-381. doi:10.1056/NEJMra021562

Nemeth, K., Schoppet, M., Al-Fakhri, N., Helas, S., Jessberger, R., Hofbauer, L. C., & Goettsch, C. (2011). The role of osteoclast-associated receptor in osteoimmunology. *J Immunol, 186*(1), 13-18. doi:10.4049/jimmunol.1002483

Nguyen, J., & Nohe, A. (2017). Factors that Affect the Osteoclastogenesis of RAW264.7 Cells. *J Biochem Anal Stud, 2*(1). doi:10.16966/2576-5833.109

NHS. (2014). Symptoms - Prostate cancer.   Retrieved from https://www.nhs.uk/conditions/prostate-cancer/symptoms/

Nudelman, F., Pieterse, K., George, A., Bomans, P. H., Friedrich, H., Brylka, L. J., . . . Sommerdijk, N. A. (2010). The role of collagen in bone apatite formation in the presence of hydroxyapatite nucleation inhibitors. *Nat Mater, 9*(12), 1004-1009. doi:10.1038/nmat2875

O'Brien, E. A., Williams, J. H., & Marshall, M. J. (2001). Osteoprotegerin is produced when prostaglandin synthesis is inhibited causing osteoclasts to detach from the surface of mouse parietal bone and attach to the endocranial membrane. *Bone, 28*(2), 208-214.

O'Dowd, G. J., Veltri, R. W., Orozco, R., Miller, M. C., & Oesterling, J. E. (1997). Update on the appropriate staging evaluation for newly diagnosed prostate cancer. *J Urol, 158*(3 Pt 1), 687-698.

Ohshima, K., Inoue, K., Fujiwara, A., Hatakeyama, K., Kanto, K., Watanabe, Y., . . . Mochizuki, T. (2010). Let-7 microRNA family is selectively secreted into the extracellular environment via exosomes in a metastatic gastric cancer cell line. *PLoS One, 5*(10), e13247. doi:10.1371/journal.pone.0013247

Olivares-Navarrete, R., Sutha, K., Hyzy, S. L., Hutton, D. L., Schwartz, Z., McDevitt, T., & Boyan, B. D. (2012). Osteogenic differentiation of stem cells alters vitamin D receptor expression. *Stem Cells Dev, 21*(10), 1726-1735. doi:10.1089/scd.2011.0411

Orom, U. A., Nielsen, F. C., & Lund, A. H. (2008). MicroRNA-10a binds the 5'UTR of ribosomal protein mRNAs and enhances their translation. *Mol Cell, 30*(4), 460-471. doi:10.1016/j.molcel.2008.05.001

Ostrowski, M., Carmo, N. B., Krumeich, S., Fanget, I., Raposo, G., Savina, A., . . . Thery, C. (2010). Rab27a and Rab27b control different steps of the exosome secretion pathway. *Nat Cell Biol, 12*(1), 19-30; sup pp 11-13. doi:10.1038/ncb2000

Ottewell, P. D. (2016). The role of osteoblasts in bone metastasis. *J Bone Oncol, 5*(3), 124-127. doi:10.1016/j.jbo.2016.03.007

Paget, S. (1989). The distribution of secondary growths in cancer of the breast. 1889. *Cancer Metastasis Rev, 8*(2), 98-101.

Park, J. C., & Eisenberger, M. A. (2015). Advances in the Treatment of Metastatic Prostate Cancer. *Mayo Clin Proc, 90*(12), 1719-1733. doi:10.1016/j.mayocp.2015.10.010

Park, J. H., Lee, N. K., & Lee, S. Y. (2017). Current Understanding of RANK Signaling in Osteoclast Differentiation and Maturation. *Mol Cells, 40*(10), 706-713. doi:10.14348/molcells.2017.0225

Parker, J. S., Roe, S. M., & Barford, D. (2005). Structural insights into mRNA recognition from a PIWI domain-siRNA guide complex. *Nature, 434*(7033), 663-666. doi:10.1038/nature03462

Parolini, I., Federici, C., Raggi, C., Lugini, L., Palleschi, S., De Milito, A., . . . Fais, S. (2009). Microenvironmental pH is a key factor for exosome traffic in tumor cells. *J Biol Chem, 284*(49), 34211-34222. doi:10.1074/jbc.M109.041152

Pegtel, D. M., Cosmopoulos, K., Thorley-Lawson, D. A., van Eijndhoven, M. A., Hopmans, E. S., Lindenberg, J. L., . . . Middeldorp, J. M. (2010). Functional delivery of viral miRNAs via exosomes. *Proc Natl Acad Sci U S A, 107*(14), 6328-6333. doi:10.1073/pnas.0914843107

Peinado, H., Aleckovic, M., Lavotshkin, S., Matei, I., Costa-Silva, B., Moreno-Bueno, G., . . . Lyden, D. (2012). Melanoma exosomes educate bone marrow progenitor cells toward a pro-metastatic phenotype through MET. *Nat Med, 18*(6), 883-891. doi:10.1038/nm.2753

Peng, S., Gao, D., Gao, C., Wei, P., Niu, M., & Shuai, C. (2016). MicroRNAs regulate signaling pathways in osteogenic differentiation of mesenchymal stem cells (Review). *Mol Med Rep, 14*(1), 623-629. doi:10.3892/mmr.2016.5335

Peng, Y., & Croce, C. M. (2016). The role of MicroRNAs in human cancer. *Signal Transduct Target Ther, 1*, 15004. doi:10.1038/sigtrans.2015.4

Pepe, P., & Aragona, F. (2011). PCA3 score vs PSA free/total accuracy in prostate cancer diagnosis at repeat saturation biopsy. *Anticancer Res, 31*(12), 4445-4449.

Petersen, C. P., Bordeleau, M. E., Pelletier, J., & Sharp, P. A. (2006). Short RNAs repress translation after initiation in mammalian cells. *Mol Cell, 21*(4), 533-542. doi:10.1016/j.molcel.2006.01.031

Place, R. F., Li, L. C., Pookot, D., Noonan, E. J., & Dahiya, R. (2008). MicroRNA-373 induces expression of genes with complementary promoter sequences. *Proc Natl Acad Sci U S A, 105*(5), 1608-1613. doi:10.1073/pnas.0707594105

Pollen, J. J., Gerber, K., Ashburn, W. L., & Schmidt, J. D. (1981). Nuclear bone imaging in metastatic cancer of the prostate. *Cancer, 47*(11), 2585-2594.

Pratt, A. J., & MacRae, I. J. (2009). The RNA-induced silencing complex: a versatile gene-silencing machine. *J Biol Chem, 284*(27), 17897-17901. doi:10.1074/jbc.R900012200

Proff, P., & Romer, P. (2009). The molecular mechanism behind bone remodelling: a review. *Clin Oral Investig, 13*(4), 355-362. doi:10.1007/s00784-009-0268-2

Pugh, C. W., & Ratcliffe, P. J. (2003). Regulation of angiogenesis by hypoxia: role of the HIF system. *Nat Med, 9*(6), 677-684. doi:10.1038/nm0603-677

Qin, J., Ke, J., Xu, J., Wang, F., Zhou, Y., Jiang, Y., & Wang, Z. (2015). Downregulation of microRNA-132 by DNA hypermethylation is associated with cell invasion in colorectal cancer. *Onco Targets Ther, 8*, 3639-3648. doi:10.2147/OTT.S91560

Qu, Y., Liu, H., Lv, X., Liu, Y., Wang, X., Zhang, M., . . . Li, H. (2017). MicroRNA-16-5p overexpression suppresses proliferation and invasion as well as triggers apoptosis by targeting VEGFA expression in breast carcinoma. *Oncotarget, 8*(42), 72400-72410. doi:10.18632/oncotarget.20398

Quan, J., Du, Q., Hou, Y., Wang, Z., & Zhang, J. (2017). Utilization of E-cadherin by monocytes from tumour cells plays key roles in the progression of bone invasion by oral squamous cell carcinoma. *Oncol Rep, 38*(2), 850-858. doi:10.3892/or.2017.5749

Raggatt, L. J., & Partridge, N. C. (2010). Cellular and molecular mechanisms of bone remodeling. *J Biol Chem, 285*(33), 25103-25108. doi:10.1074/jbc.R109.041087

Raucci, A., Bellosta, P., Grassi, R., Basilico, C., & Mansukhani, A. (2008). Osteoblast proliferation or differentiation is regulated by relative strengths of opposing signaling pathways. *J Cell Physiol, 215*(2), 442-451. doi:10.1002/jcp.21323

Reddi, K. K., & Holland, J. F. (1976). Elevated serum ribonuclease in patients with pancreatic cancer. *Proc Natl Acad Sci U S A, 73*(7), 2308-2310.

Rennebeck, G., Martelli, M., & Kyprianou, N. (2005). Anoikis and survival connections in the tumor microenvironment: is there a role in prostate cancer metastasis? *Cancer Res, 65*(24), 11230-11235. doi:10.1158/0008-5472.CAN-05-2763

Reponen, P., Sahlberg, C., Munaut, C., Thesleff, I., & Tryggvason, K. (1994). High expression of 92-kD type IV collagenase (gelatinase B) in the osteoclast lineage during mouse development. *J Cell Biol, 124*(6), 1091-1102.

Riches, A., Campbell, E., Borger, E., & Powis, S. (2014). Regulation of exosome release from mammary epithelial and breast cancer cells - a new regulatory pathway. *Eur J Cancer, 50*(5), 1025-1034. doi:10.1016/j.ejca.2013.12.019

Rinotas, V., Niti, A., Dacquin, R., Bonnet, N., Stolina, M., Han, C. Y., . . . Douni, E. (2014). Novel genetic models of osteoporosis by overexpression of human RANKL in transgenic mice. *J Bone Miner Res, 29*(5), 1158-1169. doi:10.1002/jbmr.2112

Riss, T. L., Moravec, R. A., Niles, A. L., Duellman, S., Benink, H. A., Worzella, T. J., & Minor, L. (2004). Cell Viability Assays. In G. S. Sittampalam, N. P. Coussens, K. Brimacombe, A. Grossman, M. Arkin, D. Auld, C. Austin, J. Baell, B. Bejcek, J. M. M. Caaveiro, T. D. Y. Chung, J. L. Dahlin, V. Devanaryan, T. L. Foley, M. Glicksman, M. D. Hall, J. V. Haas, J. Inglese, P. W. Iversen, S. D. Kahl, S. C. Kales, M. Lal-Nag, Z. Li, J. McGee, O. McManus, T. Riss, O. J. Trask, Jr., J. R.

Weidner, M. J. Wildey, M. Xia, & X. Xu (Eds.), *Assay Guidance Manual*. Bethesda (MD).

Rivas, F. V., Tolia, N. H., Song, J. J., Aragon, J. P., Liu, J., Hannon, G. J., & Joshua-Tor, L. (2005). Purified Argonaute2 and an siRNA form recombinant human RISC. *Nat Struct Mol Biol, 12*(4), 340-349. doi:10.1038/nsmb918

Robb, G. B., & Rana, T. M. (2007). RNA helicase A interacts with RISC in human cells and functions in RISC loading. *Mol Cell, 26*(4), 523-537. doi:10.1016/j.molcel.2007.04.016

Robledo, R. F., Rajan, L., Li, X., & Lufkin, T. (2002). The Dlx5 and Dlx6 homeobox genes are essential for craniofacial, axial, and appendicular skeletal development. *Genes Dev, 16*(9), 1089-1101. doi:10.1101/gad.988402

Rodriguez, A., Griffiths-Jones, S., Ashurst, J. L., & Bradley, A. (2004). Identification of mammalian microRNA host genes and transcription units. *Genome Res, 14*(10A), 1902-1910. doi:10.1101/gr.2722704

Rodriguez, M., Bajo-Santos, C., Hessvik, N. P., Lorenz, S., Fromm, B., Berge, V., . . . Llorente, A. (2017). Identification of non-invasive miRNAs biomarkers for prostate cancer by deep sequencing analysis of urinary exosomes. *Mol Cancer, 16*(1), 156. doi:10.1186/s12943-017-0726-4

Roudier, M. P., Corey, E., True, L. D., Hiagno, C. S., Ott, S. M., & Vessell, R. L. (2004). Histological, immunophenotypic and histomorphometric characterization of prostate cancer bone metastases. *Cancer Treat Res, 118*, 311-339.

Ruby, J. G., Jan, C. H., & Bartel, D. P. (2007). Intronic microRNA precursors that bypass Drosha processing. *Nature, 448*(7149), 83-86. doi:10.1038/nature05983

Rutkovskiy, A., Stenslokken, K. O., & Vaage, I. J. (2016). Osteoblast Differentiation at a Glance. *Med Sci Monit Basic Res, 22*, 95-106.

Ryan, B., Joilin, G., & Williams, J. M. (2015). Plasticity-related microRNA and their potential contribution to the maintenance of long-term potentiation. *Frontiers in Molecular Neuroscience, 8*. doi:ARTN 4

10.3389/fnmol.2015.00004

Ryoo, H. M., Hoffmann, H. M., Beumer, T., Frenkel, B., Towler, D. A., Stein, G. S., . . . Lian, J. B. (1997). Stage-specific expression of Dlx-5 during osteoblast differentiation: involvement in regulation of osteocalcin gene expression. *Mol Endocrinol, 11*(11), 1681-1694. doi:10.1210/mend.11.11.0011

Sakr, W. A., Haas, G. P., Cassin, B. F., Pontes, J. E., & Crissman, J. D. (1993). The frequency of carcinoma and intraepithelial neoplasia of the prostate in young male patients. *J Urol, 150*(2 Pt 1), 379-385.

Salem, S., Salahi, M., Mohseni, M., Ahmadi, H., Mehrsai, A., Jahani, Y., & Pourmand, G. (2011). Major dietary factors and prostate cancer risk: a prospective multicenter case-control study. *Nutr Cancer, 63*(1), 21-27. doi:10.1080/01635581.2010.516875

Santarelli, D. M., Beveridge, N. J., Tooney, P. A., & Cairns, M. J. (2011). Upregulation of dicer and microRNA expression in the dorsolateral prefrontal cortex Brodmann area 46 in schizophrenia. *Biol Psychiatry, 69*(2), 180-187. doi:10.1016/j.biopsych.2010.09.030

Sarahrudi, K., Hora, K., Heinz, T., Millington, S., & Vecsei, V. (2006). Treatment results of pathological fractures of the long bones: a retrospective analysis of 88 patients. *Int Orthop, 30*(6), 519-524. doi:10.1007/s00264-006-0205-9

Schaefer, A., Jung, M., Mollenkopf, H. J., Wagner, I., Stephan, C., Jentzmik, F., . . . Jung, K. (2010). Diagnostic and prognostic implications of microRNA profiling in prostate carcinoma. *Int J Cancer, 126*(5), 1166-1176. doi:10.1002/ijc.24827

Schirle, N. T., & MacRae, I. J. (2012). The crystal structure of human Argonaute2. *Science, 336*(6084), 1037-1040. doi:10.1126/science.1221551

Schweitzer, J. K., & D'Souza-Schorey, C. (2004). Finishing the job: cytoskeletal and membrane events bring cytokinesis to an end. *Exp Cell Res, 295*(1), 1-8. doi:10.1016/j.yexcr.2003.12.023

Selvaggi, G., & Scagliotti, G. V. (2005). Management of bone metastases in cancer: a review. *Crit Rev Oncol Hematol, 56*(3), 365-378. doi:10.1016/j.critrevonc.2005.03.011

Seto, A. G., Beatty, X., Lynch, J. M., Hermreck, M., Tetzlaff, M., Duvic, M., & Jackson, A. L. (2018). Cobomarsen, an oligonucleotide inhibitor of miR-155, co-ordinately regulates multiple survival pathways to reduce cellular proliferation and survival in cutaneous T-cell lymphoma. *Br J Haematol, 183*(3), 428-444. doi:10.1111/bjh.15547

Shang, J., & Gao, X. (2014). Nanoparticle counting: towards accurate determination of the molar concentration. *Chem Soc Rev, 43*(21), 7267-7278. doi:10.1039/c4cs00128a

Sharma, S. M., Bronisz, A., Hu, R., Patel, K., Mansky, K. C., Sif, S., & Ostrowski, M. C. (2007). MITF and PU.1 recruit p38 MAPK and NFATc1 to target genes during osteoclast differentiation. *J Biol Chem, 282*(21), 15921-15929. doi:10.1074/jbc.M609723200

Shi, B., Gao, H., Zhang, T., & Cui, Q. (2016). Analysis of plasma microRNA expression profiles revealed different cancer susceptibility in healthy young adult smokers and middle-aged smokers. *Oncotarget, 7*(16), 21676-21685. doi:10.18632/oncotarget.7866

Shiirevnyamba, A., Takahashi, T., Shan, H., Ogawa, H., Yano, S., Kanayama, H., . . . Uehara, H. (2011). Enhancement of osteoclastogenic activity in osteolytic prostate cancer cells by physical contact with osteoblasts. *Br J Cancer, 104*(3), 505-513. doi:10.1038/sj.bjc.6606070

Sieh, W., Lichtensztajn, D. Y., Nelson, D. O., Cockburn, M., West, D. W., Brooks, J. D., & Chang, E. T. (2013). Treatment and Mortality in Men with Localized Prostate Cancer: A Population-Based Study in California. *Open Prost Cancer J, 6*, 1-9.

Simmons, M. N., Berglund, R. K., & Jones, J. S. (2011). A practical guide to prostate cancer diagnosis and management. *Cleve Clin J Med, 78*(5), 321-331. doi:10.3949/ccjm.78a.10104

Sinningen, K., Rauner, M., Goettsch, C., Al-Fakhri, N., Schoppet, M., & Hofbauer, L. C. (2013). Monocytic expression of osteoclast-associated receptor (OSCAR) is induced in atherosclerotic mice and regulated by oxidized low-density lipoprotein in vitro. *Biochem Biophys Res Commun, 437*(2), 314-318. doi:10.1016/j.bbrc.2013.06.074

Skliar, M., Chernyshev, V. S., Belnap, D. M., Sergey, G. V., Al-Hakami, S. M., Bernard, P. S., . . . Rachamadugu, R. (2018). Membrane proteins significantly restrict exosome mobility. *Biochem Biophys Res Commun, 501*(4), 1055-1059. doi:10.1016/j.bbrc.2018.05.107

Skog, J., Wurdinger, T., van Rijn, S., Meijer, D. H., Gainche, L., Sena-Esteves, M., . . . Breakefield, X. O. (2008). Glioblastoma microvesicles transport RNA and proteins that promote tumour growth and provide diagnostic biomarkers. *Nat Cell Biol, 10*(12), 1470-1476. doi:10.1038/ncb1800

Skowronek, J. (2013). Low-dose-rate or high-dose-rate brachytherapy in treatment of prostate cancer - between options. *J Contemp Brachytherapy, 5*(1), 33-41. doi:10.5114/jcb.2013.34342

Smith, M. R., Coleman, R. E., Klotz, L., Pittman, K., Milecki, P., Ng, S., . . . Fizazi, K. (2015). Denosumab for the prevention of skeletal complications in metastatic castration-resistant prostate cancer: comparison of skeletal-related events and symptomatic skeletal events. *Ann Oncol, 26*(2), 368-374. doi:10.1093/annonc/mdu519

Sobel, R. E., & Sadar, M. D. (2005). Cell lines used in prostate cancer research: a compendium of old and new lines--part 1. *J Urol, 173*(2), 342-359. doi:10.1097/01.ju.0000141580.30910.57

Soki, F. N., Park, S. I., & McCauley, L. K. (2012). The multifaceted actions of PTHrP in skeletal metastasis. *Future Oncol, 8*(7), 803-817. doi:10.2217/fon.12.76

Sommerfeldt, D. W., & Rubin, C. T. (2001). Biology of bone and how it orchestrates the form and function of the skeleton. *Eur Spine J, 10 Suppl 2*, S86-95. doi:10.1007/s005860100283

Song, C., Yang, X., Lei, Y., Zhang, Z., Smith, W., Yan, J., & Kong, L. (2018). Evaluation of efficacy on RANKL induced osteoclast from RAW264.7 cells. *J Cell Physiol*. doi:10.1002/jcp.27852

Song, J., Ouyang, Y., Che, J., Li, X., Zhao, Y., Yang, K., . . . Yuan, W. (2017). Potential Value of miR-221/222 as Diagnostic, Prognostic, and Therapeutic Biomarkers for Diseases. *Front Immunol, 8*, 56. doi:10.3389/fimmu.2017.00056

Stenbeck, G. (2002). Formation and function of the ruffled border in osteoclasts. *Semin Cell Dev Biol, 13*(4), 285-292.

Stewart, A. F. (2005). Clinical practice. Hypercalcemia associated with cancer. *N Engl J Med, 352*(4), 373-379. doi:10.1056/NEJMcp042806

Sugawara, Y., Suzuki, K., Koshikawa, M., Ando, M., & Iida, J. (2002). Necessity of enzymatic activity of alkaline phosphatase for mineralization of osteoblastic cells. *Jpn J Pharmacol, 88*(3), 262-269.

Sugimoto, K., Miyata, Y., Nakayama, T., Saito, S., Suzuki, R., Hayakawa, F., . . . Naoe, T. (2016). Fibroblast Growth Factor-2 facilitates the growth and chemo-resistance of leukemia cells in the bone marrow by modulating osteoblast functions. *Sci Rep, 6*, 30779. doi:10.1038/srep30779

Sun, W., Zhao, C., Li, Y., Wang, L., Nie, G., Peng, J., . . . Li, Y. (2016). Osteoclast-derived microRNA-containing exosomes selectively inhibit osteoblast activity. *Cell Discov, 2*, 16015. doi:10.1038/celldisc.2016.15

Susa, M., Luong-Nguyen, N. H., Cappellen, D., Zamurovic, N., & Gamse, R. (2004). Human primary osteoclasts: in vitro generation and applications as pharmacological and clinical assay. *J Transl Med, 2*(1), 6. doi:10.1186/1479-5876-2-6

Suva, L. J., Washam, C., Nicholas, R. W., & Griffin, R. J. (2011). Bone metastasis: mechanisms and therapeutic opportunities. *Nat Rev Endocrinol, 7*(4), 208-218. doi:10.1038/nrendo.2010.227

Svensson, K. J., Christianson, H. C., Wittrup, A., Bourseau-Guilmain, E., Lindqvist, E., Svensson, L. M., . . . Belting, M. (2013). Exosome uptake depends on ERK1/2-heat shock protein 27 signaling and lipid Raft-mediated endocytosis negatively regulated by caveolin-1. *J Biol Chem, 288*(24), 17713-17724. doi:10.1074/jbc.M112.445403

Swarthout, J. T., D'Alonzo, R. C., Selvamurugan, N., & Partridge, N. C. (2002). Parathyroid hormone-dependent signaling pathways regulating genes in bone cells. *Gene, 282*(1-2), 1-17.

Szatanek, R., Baj-Krzyworzeka, M., Zimoch, J., Lekka, M., Siedlar, M., & Baran, J. (2017). The Methods of Choice for Extracellular Vesicles (EVs) Characterization. *Int J Mol Sci, 18*(6). doi:10.3390/ijms18061153

Szatanek, R., Baran, J., Siedlar, M., & Baj-Krzyworzeka, M. (2015). Isolation of extracellular vesicles: Determining the correct approach (Review). *Int J Mol Med, 36*(1), 11-17. doi:10.3892/ijmm.2015.2194

Szewczyk, K. A., Fuller, K., & Chambers, T. J. (2013). Distinctive subdomains in the resorbing surface of osteoclasts. *PLoS One, 8*(3), e60285. doi:10.1371/journal.pone.0060285

Tai, S., Sun, Y., Squires, J. M., Zhang, H., Oh, W. K., Liang, C. Z., & Huang, J. (2011). PC3 is a cell line characteristic of prostatic small cell carcinoma. *Prostate, 71*(15), 1668-1679. doi:10.1002/pros.21383

Takeshita, S., Fumoto, T., Matsuoka, K., Park, K. A., Aburatani, H., Kato, S., . . . Ikeda, K. (2013). Osteoclast-secreted CTHRC1 in the coupling of bone resorption to formation. *J Clin Invest, 123*(9), 3914-3924. doi:10.1172/JCI69493

Tang, Y. T., Huang, Y. Y., Zheng, L., Qin, S. H., Xu, X. P., An, T. X., . . . Wang, Q. (2017). Comparison of isolation methods of exosomes and exosomal RNA from cell

culture medium and serum. *Int J Mol Med, 40*(3), 834-844. doi:10.3892/ijmm.2017.3080

Tangen, C. M., Faulkner, J. R., Crawford, E. D., Thompson, I. M., Hirano, D., Eisenberger, M., & Hussain, M. (2003). Ten-year survival in patients with metastatic prostate cancer. *Clin Prostate Cancer, 2*(1), 41-45.

Tannock, I. F., de Wit, R., Berry, W. R., Horti, J., Pluzanska, A., Chi, K. N., . . . Investigators, T. A. X. (2004). Docetaxel plus prednisone or mitoxantrone plus prednisone for advanced prostate cancer. *N Engl J Med, 351*(15), 1502-1512. doi:10.1056/NEJMoa040720

Tay, Y., Zhang, J., Thomson, A. M., Lim, B., & Rigoutsos, I. (2008). MicroRNAs to Nanog, Oct4 and Sox2 coding regions modulate embryonic stem cell differentiation. *Nature, 455*(7216), 1124-1128. doi:10.1038/nature07299

Terris, M. K., & Stamey, T. A. (1991). Determination of prostate volume by transrectal ultrasound. *J Urol, 145*(5), 984-987.

The Lab Depot, I. (2018). CELLine Bioreactors. Retrieved from https://www.labdepotinc.com/p-60670-celline-bioreactors.php

Thery, C., Zitvogel, L., & Amigorena, S. (2002). Exosomes: composition, biogenesis and function. *Nat Rev Immunol, 2*(8), 569-579. doi:10.1038/nri855

Thompson, D. L., Lum, K. D., Nygaard, S. C., Kuestner, R. E., Kelly, K. A., Gimble, J. M., & Moore, E. E. (1998). The derivation and characterization of stromal cell lines from the bone marrow of p53-/- mice: new insights into osteoblast and adipocyte differentiation. *J Bone Miner Res, 13*(2), 195-204. doi:10.1359/jbmr.1998.13.2.195

Tian, T., Zhu, Y. L., Zhou, Y. Y., Liang, G. F., Wang, Y. Y., Hu, F. H., & Xiao, Z. D. (2014). Exosome uptake through clathrin-mediated endocytosis and macropinocytosis and mediating miR-21 delivery. *J Biol Chem, 289*(32), 22258-22267. doi:10.1074/jbc.M114.588046

Tondravi, M. M., McKercher, S. R., Anderson, K., Erdmann, J. M., Quiroz, M., Maki, R., & Teitelbaum, S. L. (1997). Osteopetrosis in mice lacking haematopoietic transcription factor PU.1. *Nature, 386*(6620), 81-84. doi:10.1038/386081a0

Trajkovic, K., Hsu, C., Chiantia, S., Rajendran, L., Wenzel, D., Wieland, F., . . . Simons, M. (2008). Ceramide triggers budding of exosome vesicles into multivesicular endosomes. *Science, 319*(5867), 1244-1247. doi:10.1126/science.1153124

Trams, E. G., Lauter, C. J., Salem, N., Jr., & Heine, U. (1981). Exfoliation of membrane ecto-enzymes in the form of micro-vesicles. *Biochim Biophys Acta, 645*(1), 63-70.

Troen, B. R. (2004). The role of cathepsin K in normal bone resorption. *Drug News Perspect, 17*(1), 19-28.

Tsui, N. B., Ng, E. K., & Lo, Y. M. (2002). Stability of endogenous and added RNA in blood specimens, serum, and plasma. *Clin Chem, 48*(10), 1647-1653.

Tsuzuki, S., Park, S. H., Eber, M. R., Peters, C. M., & Shiozawa, Y. (2016). Skeletal complications in cancer patients with bone metastases. *Int J Urol, 23*(10), 825-832. doi:10.1111/iju.13170

Turchinovich, A., Samatov, T. R., Tonevitsky, A. G., & Burwinkel, B. (2013). Circulating miRNAs: cell-cell communication function? *Front Genet, 4*, 119. doi:10.3389/fgene.2013.00119

Udagawa, N., Takahashi, N., Akatsu, T., Tanaka, H., Sasaki, T., Nishihara, T., . . . Suda, T. (1990). Origin of osteoclasts: mature monocytes and macrophages are capable of differentiating into osteoclasts under a suitable microenvironment prepared by bone marrow-derived stromal cells. *Proc Natl Acad Sci U S A, 87*(18), 7260-7264.

Ueda, Y., Higuchii, Y., Hashimoto, T., Mitsui, Y., Maruyamai, T., Kondou, N., . . . Shima, H. (2007). [Prostate cancer diagnosed through the biopsy of the bone metastatic lesion; a case report]. *Hinyokika Kiyo, 53*(5), 327-330.

Valadi, H., Ekstrom, K., Bossios, A., Sjostrand, M., Lee, J. J., & Lotvall, J. O. (2007). Exosome-mediated transfer of mRNAs and microRNAs is a novel mechanism of genetic exchange between cells. *Nat Cell Biol, 9*(6), 654-659. doi:10.1038/ncb1596

Valencia, K., Luis-Ravelo, D., Bovy, N., Anton, I., Martinez-Canarias, S., Zandueta, C., . . . Lecanda, F. (2014). miRNA cargo within exosome-like vesicle transfer influences metastatic bone colonization. *Mol Oncol, 8*(3), 689-703. doi:10.1016/j.molonc.2014.01.012

Vali, R., Loidl, W., Pirich, C., Langesteger, W., & Beheshti, M. (2015). Imaging of prostate cancer with PET/CT using (18)F-Fluorocholine. *Am J Nucl Med Mol Imaging, 5*(2), 96-108.

van Bezooijen, R. L., Roelen, B. A., Visser, A., van der Wee-Pals, L., de Wilt, E., Karperien, M., . . . Lowik, C. W. (2004). Sclerostin is an osteocyte-expressed negative regulator of bone formation, but not a classical BMP antagonist. *J Exp Med, 199*(6), 805-814. doi:10.1084/jem.20031454

van der Ree, M. H., de Vree, J. M., Stelma, F., Willemse, S., van der Valk, M., Rietdijk, S., . . . Reesink, H. W. (2017). Safety, tolerability, and antiviral effect of RG-101 in patients with chronic hepatitis C: a phase 1B, double-blind, randomised controlled trial. *Lancet, 389*(10070), 709-717. doi:10.1016/S0140-6736(16)31715-9

van Niel, G., Charrin, S., Simoes, S., Romao, M., Rochin, L., Saftig, P., . . . Raposo, G. (2011). The tetraspanin CD63 regulates ESCRT-independent and -dependent endosomal sorting during melanogenesis. *Dev Cell, 21*(4), 708-721. doi:10.1016/j.devcel.2011.08.019

van Niel, G., Raposo, G., Candalh, C., Boussac, M., Hershberg, R., Cerf-Bensussan, N., & Heyman, M. (2001). Intestinal epithelial cells secrete exosome-like vesicles. *Gastroenterology, 121*(2), 337-349.

Vanneste, B. G., Van Limbergen, E. J., van Lin, E. N., van Roermund, J. G., & Lambin, P. (2016). Prostate Cancer Radiation Therapy: What Do Clinicians Have to Know? *Biomed Res Int, 2016*, 6829875. doi:10.1155/2016/6829875

VanWijk, M. J., VanBavel, E., Sturk, A., & Nieuwland, R. (2003). Microparticles in cardiovascular diseases. *Cardiovasc Res, 59*(2), 277-287.

Vasudevan, S., & Steitz, J. A. (2007). AU-rich-element-mediated upregulation of translation by FXR1 and Argonaute 2. *Cell, 128*(6), 1105-1118. doi:10.1016/j.cell.2007.01.038

Vasudevan, S., Tong, Y., & Steitz, J. A. (2007). Switching from repression to activation: microRNAs can up-regulate translation. *Science, 318*(5858), 1931-1934. doi:10.1126/science.1149460

Verze, P., Cai, T., & Lorenzetti, S. (2016). The role of the prostate in male fertility, health and disease. *Nat Rev Urol, 13*(7), 379-386. doi:10.1038/nrurol.2016.89

Vickers, K. C., Palmisano, B. T., Shoucri, B. M., Shamburek, R. D., & Remaley, A. T. (2011). MicroRNAs are transported in plasma and delivered to recipient cells by high-density lipoproteins. *Nat Cell Biol, 13*(4), 423-433. doi:10.1038/ncb2210

Viguet-Carrin, S., Garnero, P., & Delmas, P. D. (2006). The role of collagen in bone strength. *Osteoporos Int, 17*(3), 319-336. doi:10.1007/s00198-005-2035-9

Villarroya-Beltri, C., Gutierrez-Vazquez, C., Sanchez-Cabo, F., Perez-Hernandez, D., Vazquez, J., Martin-Cofreces, N., . . . Sanchez-Madrid, F. (2013). Sumoylated hnRNPA2B1 controls the sorting of miRNAs into exosomes through binding to specific motifs. *Nat Commun, 4*, 2980. doi:10.1038/ncomms3980

Vincent, C., Kogawa, M., Findlay, D. M., & Atkins, G. J. (2009). The generation of osteoclasts from RAW 264.7 precursors in defined, serum-free conditions. *J Bone Miner Metab, 27*(1), 114-119. doi:10.1007/s00774-008-0018-6

Volinia, S., Calin, G. A., Liu, C. G., Ambs, S., Cimmino, A., Petrocca, F., . . . Croce, C. M. (2006). A microRNA expression signature of human solid tumors defines cancer gene targets. *Proc Natl Acad Sci U S A, 103*(7), 2257-2261. doi:10.1073/pnas.0510565103

Wang, R., & Brattain, M. G. (2007). The maximal size of protein to diffuse through the nuclear pore is larger than 60kDa. *FEBS Lett, 581*(17), 3164-3170. doi:10.1016/j.febslet.2007.05.082

Wang, T., & Xu, Z. (2010). miR-27 promotes osteoblast differentiation by modulating Wnt signaling. *Biochem Biophys Res Commun, 402*(2), 186-189. doi:10.1016/j.bbrc.2010.08.031

Wang, X., Xu, X., Ma, Z., Huo, Y., Xiao, Z., Li, Y., & Wang, Y. (2011). Dynamic mechanisms for pre-miRNA binding and export by Exportin-5. *RNA, 17*(8), 1511-1528. doi:10.1261/rna.2732611

Webber, J., & Clayton, A. (2013). How pure are your vesicles? *J Extracell Vesicles, 2*. doi:10.3402/jev.v2i0.19861

Weber, J. A., Baxter, D. H., Zhang, S., Huang, D. Y., Huang, K. H., Lee, M. J., . . . Wang, K. (2010). The microRNA spectrum in 12 body fluids. *Clin Chem, 56*(11), 1733-1741. doi:10.1373/clinchem.2010.147405

Welton, J. L., Webber, J. P., Botos, L. A., Jones, M., & Clayton, A. (2015). Ready-made chromatography columns for extracellular vesicle isolation from plasma. *J Extracell Vesicles, 4*, 27269. doi:10.3402/jev.v4.27269

Westholm, J. O., Ladewig, E., Okamura, K., Robine, N., & Lai, E. C. (2012). Common and distinct patterns of terminal modifications to mirtrons and canonical microRNAs. *RNA, 18*(2), 177-192. doi:10.1261/rna.030627.111

Whitfield, J., Neame, S. J., Paquet, L., Bernard, O., & Ham, J. (2001). Dominant-negative c-Jun promotes neuronal survival by reducing BIM expression and inhibiting mitochondrial cytochrome c release. *Neuron, 29*(3), 629-643.

Willms, E., Johansson, H. J., Mager, I., Lee, Y., Blomberg, K. E., Sadik, M., . . . Vader, P. (2016). Cells release subpopulations of exosomes with distinct molecular and biological properties. *Sci Rep, 6*, 22519. doi:10.1038/srep22519

Wisenbaugh, E. S., Andrews, P. E., Ferrigni, R. G., Schild, S. E., Keole, S. R., Wong, W. W., & Vora, S. A. (2014). Proton beam therapy for localized prostate cancer 101: basics, controversies, and facts. *Rev Urol, 16*(2), 67-75.

Woodward, E. J., & Coleman, R. E. (2010). Prevention and treatment of bone metastases. *Curr Pharm Des, 16*(27), 2998-3006.

Wu, C. J., & Lu, L. F. (2017). MicroRNA in Immune Regulation. *Curr Top Microbiol Immunol, 410*, 249-267. doi:10.1007/82_2017_65

Xie, Q., Wang, Z., Bi, X., Zhou, H., Wang, Y., Gu, P., & Fan, X. (2014). Effects of miR-31 on the osteogenesis of human mesenchymal stem cells. *Biochem Biophys Res Commun, 446*(1), 98-104. doi:10.1016/j.bbrc.2014.02.058

Xu, Q., Cui, Y., Luan, J., Zhou, X., Li, H., & Han, J. (2018a). Exosomes from C2C12 myoblasts enhance osteogenic differentiation of MC3T3-E1 pre-osteoblasts by delivering miR-27a-3p. *Biochem Biophys Res Commun, 498*(1), 32-37. doi:10.1016/j.bbrc.2018.02.144

Xu, R., Rai, A., Chen, M., Suwakulsiri, W., Greening, D. W., & Simpson, R. J. (2018b). Extracellular vesicles in cancer - implications for future improvements in cancer care. *Nat Rev Clin Oncol, 15*(10), 617-638. doi:10.1038/s41571-018-0036-9

Yagi, M., Miyamoto, T., Sawatani, Y., Iwamoto, K., Hosogane, N., Fujita, N., . . . Suda, T. (2005). DC-STAMP is essential for cell-cell fusion in osteoclasts and foreign body giant cells. *J Exp Med, 202*(3), 345-351. doi:10.1084/jem.20050645

Yamaguchi, A., Ishizuya, T., Kintou, N., Wada, Y., Katagiri, T., Wozney, J. M., . . . Yoshiki, S. (1996). Effects of BMP-2, BMP-4, and BMP-6 on osteoblastic differentiation of bone marrow-derived stromal cell lines, ST2 and MC3T3-G2/PA6. *Biochem Biophys Res Commun, 220*(2), 366-371. doi:10.1006/bbrc.1996.0411

Yan, Y., Tang, D., Chen, M., Huang, J., Xie, R., Jonason, J. H., . . . Chen, D. (2009). Axin2 controls bone remodeling through the beta-catenin-BMP signaling pathway in adult mice. *J Cell Sci, 122*(Pt 19), 3566-3578. doi:10.1242/jcs.051904

Yang, Z., Jakymiw, A., Wood, M. R., Eystathioy, T., Rubin, R. L., Fritzler, M. J., & Chan, E. K. (2004). GW182 is critical for the stability of GW bodies expressed during the cell cycle and cell proliferation. *J Cell Sci, 117*(Pt 23), 5567-5578. doi:10.1242/jcs.01477

Ye, L., Kynaston, H. G., & Jiang, W. G. (2007). Bone metastasis in prostate cancer: molecular and cellular mechanisms (Review). *Int J Mol Med, 20*(1), 103-111.

Ye, Y., Li, S. L., Ma, Y. Y., Diao, Y. J., Yang, L., Su, M. Q., . . . Hao, X. K. (2017). Exosomal miR-141-3p regulates osteoblast activity to promote the osteoblastic metastasis of prostate cancer. *Oncotarget, 8*(55), 94834-94849. doi:10.18632/oncotarget.22014

Yeh, C. C., Su, Y. H., Lin, Y. J., Chen, P. J., Shi, C. S., Chen, C. N., & Chang, H. I. (2015). Evaluation of the protective effects of curcuminoid (curcumin and bisdemethoxycurcumin)-loaded liposomes against bone turnover in a cell-based model of osteoarthritis. *Drug Des Devel Ther, 9*, 2285-2300. doi:10.2147/DDDT.S78277

Yekta, S., Shih, I. H., & Bartel, D. P. (2004). MicroRNA-directed cleavage of HOXB8 mRNA. *Science, 304*(5670), 594-596. doi:10.1126/science.1097434

Yoneda, T., Hiasa, M., Nagata, Y., Okui, T., & White, F. (2015). Contribution of acidic extracellular microenvironment of cancer-colonized bone to bone pain. *Biochim Biophys Acta, 1848*(10 Pt B), 2677-2684. doi:10.1016/j.bbamem.2015.02.004

Yoo, N. J., Hur, S. Y., Kim, M. S., Lee, J. Y., & Lee, S. H. (2010). Immunohistochemical analysis of RNA-induced silencing complex-related proteins AGO2 and TNRC6A in prostate and esophageal cancers. *APMIS, 118*(4), 271-276. doi:10.1111/j.1600-0463.2010.02588.x

Yoon, Y. J., Kim, D. K., Yoon, C. M., Park, J., Kim, Y. K., Roh, T. Y., & Gho, Y. S. (2014). Egr-1 activation by cancer-derived extracellular vesicles promotes endothelial cell migration via ERK1/2 and JNK signaling pathways. *PLoS One, 9*(12), e115170. doi:10.1371/journal.pone.0115170

Yu, X., Odenthal, M., & Fries, J. W. (2016). Exosomes as miRNA Carriers: Formation-Function-Future. *Int J Mol Sci, 17*(12). doi:10.3390/ijms17122028

Yuan, Q., Jiang, Y., Zhao, X., Sato, T., Densmore, M., Schuler, C., . . . Lanske, B. (2014). Increased osteopontin contributes to inhibition of bone mineralization in FGF23-deficient mice. *J Bone Miner Res, 29*(3), 693-704. doi:10.1002/jbmr.2079

Yuen, H. F., Chiu, Y. T., Chan, K. K., Chan, Y. P., Chua, C. W., McCrudden, C. M., . . . Chan, K. W. (2010). Prostate cancer cells modulate osteoblast mineralisation and osteoclast differentiation through Id-1. *Br J Cancer, 102*(2), 332-341. doi:10.1038/sj.bjc.6605480

Zakian, K. L., Eberhardt, S., Hricak, H., Shukla-Dave, A., Kleinman, S., Muruganandham, M., . . . Koutcher, J. A. (2003). Transition zone prostate cancer: metabolic characteristics at 1H MR spectroscopic imaging--initial results. *Radiology, 229*(1), 241-247. doi:10.1148/radiol.2291021383

Zanotti, S., Smerdel-Ramoya, A., Stadmeyer, L., Durant, D., Radtke, F., & Canalis, E. (2008). Notch inhibits osteoblast differentiation and causes osteopenia. *Endocrinology, 149*(8), 3890-3899. doi:10.1210/en.2008-0140

Zaorsky, N. G., Davis, B. J., Nguyen, P. L., Showalter, T. N., Hoskin, P. J., Yoshioka, Y., . . . Horwitz, E. M. (2017). The evolution of brachytherapy for prostate cancer. *Nat Rev Urol, 14*(7), 415-439. doi:10.1038/nrurol.2017.76

Zernecke, A., Bidzhekov, K., Noels, H., Shagdarsuren, E., Gan, L., Denecke, B., . . . Weber, C. (2009). Delivery of microRNA-126 by apoptotic bodies induces CXCL12-dependent vascular protection. *Sci Signal, 2*(100), ra81. doi:10.1126/scisignal.2000610

Zhang, B., Chen, H., Zhang, L., Dakhova, O., Zhang, Y., Lewis, M. T., . . . Xin, L. (2014). A dosage-dependent pleiotropic role of Dicer in prostate cancer growth and metastasis. *Oncogene, 33*(24), 3099-3108. doi:10.1038/onc.2013.281

Zhang, H., Kolb, F. A., Jaskiewicz, L., Westhof, E., & Filipowicz, W. (2004). Single processing center models for human Dicer and bacterial RNase III. *Cell, 118*(1), 57-68. doi:10.1016/j.cell.2004.06.017

Zhang, H., Yang, K., Ren, T., Huang, Y., Tang, X., & Guo, W. (2018). miR-16-5p inhibits chordoma cell proliferation, invasion and metastasis by targeting Smad3. *Cell Death Dis, 9*(6), 680. doi:10.1038/s41419-018-0738-z

Zhang, J., Li, S., Li, L., Li, M., Guo, C., Yao, J., & Mi, S. (2015). Exosome and exosomal microRNA: trafficking, sorting, and function. *Genomics Proteomics Bioinformatics, 13*(1), 17-24. doi:10.1016/j.gpb.2015.02.001

Zhang, J., Liu, X., Li, H., Chen, C., Hu, B., Niu, X., . . . Wang, Y. (2016). Exosomes/tricalcium phosphate combination scaffolds can enhance bone regeneration by activating the PI3K/Akt signaling pathway. *Stem Cell Res Ther, 7*(1), 136. doi:10.1186/s13287-016-0391-3

Zhang, Y., Wu, L., Wang, Y., Zhang, M., Li, L., Zhu, D., . . . Zen, K. (2012). Protective role of estrogen-induced miRNA-29 expression in carbon tetrachloride-induced mouse liver injury. *J Biol Chem, 287*(18), 14851-14862. doi:10.1074/jbc.M111.314922

Zhao, P., Xiao, L., Peng, J., Qian, Y. Q., & Huang, C. C. (2018). Exosomes derived from bone marrow mesenchymal stem cells improve osteoporosis through promoting osteoblast proliferation via MAPK pathway. *Eur Rev Med Pharmacol Sci, 22*(12), 3962-3970. doi:10.26355/eurrev_201806_15280

Zhu, F., Friedman, M. S., Luo, W., Woolf, P., & Hankenson, K. D. (2012). The transcription factor osterix (SP7) regulates BMP6-induced human osteoblast differentiation. *J Cell Physiol, 227*(6), 2677-2685. doi:10.1002/jcp.23010

Zhu, H., Zhou, Y., Castillo-Gonzalez, C., Lu, A., Ge, C., Zhao, Y. T., . . . Zhang, X. (2013). Bidirectional processing of pri-miRNAs with branched terminal loops by Arabidopsis Dicer-like1. *Nat Struct Mol Biol, 20*(9), 1106-1115. doi:10.1038/nsmb.2646

Zhu, W. E. I., Gehron Robey, P., & Boskey, A. (2008). *The Regulatory Role of Matrix Proteins in Mineralization of Bone* (Vol. 2).

Zoni, E., van der Horst, G., van de Merbel, A. F., Chen, L., Rane, J. K., Pelger, R. C., . . . van der Pluijm, G. (2015). miR-25 Modulates Invasiveness and Dissemination of Human Prostate Cancer Cells via Regulation of alphav- and alpha6-Integrin Expression. *Cancer Res, 75*(11), 2326-2336. doi:10.1158/0008-5472.CAN-14-2155